CRANFIELD UNIVERSITY

V E SANDERSON

TURBULENCE MODELLING OF TURBULENT BUOYANT JETS AND COMPARTMENT FIRES

SCHOOL OF MECHANICAL ENGINEERING

PhD THESIS

CRANFIELD UNIVERSITY

SCHOOL OF MECHANICAL ENGINEERING

PhD THESIS

Academic Year 1998-2000

V E SANDERSON

Turbulence modelling of turbulent buoyant jets and compartment fires

Supervisor: Dr P A Rubini

February 2001

This thesis is submitted in partial fulfilment of the requirements for the degree of Doctor of Philosophy

Abstract

Turbulent buoyant jets are a major feature in fire hazards. The solution of the Reynolds Averaged Navier-Stokes (RANS) equations through computational fluid dynamic (CFD) techniques allow such flows to be simulated. The use of Reynolds averaging requires an empirical model to close the set of equations, this is known as the turbulence model. This thesis undertakes to investigate linear and nonlinear approaches to turbulence modelling and to apply the knowledge gained to the simulation of compartment fires. The principle contribution of this work is the re-analysis of the standard k-ε turbulence model and the implementation and application of more sophisticated models as applied to thermal plumes.

Validation in this work, of the standard k-ε model against the most recent experimental data, counters the established view that the model is inadequate for the simulation of buoyant flows. Examination of previous experimental data suggests that the measurements were not taken in the self-similar region resulting in misleading comparisons with published numerical solutions. This is a significant conclusion that impacts of the general approach taken to modelling turbulence in this field.

A number of methods for modelling the Reynolds stresses and the turbulent scalar fluxes have been considered and, in some cases for the first time, are applied to non-isothermal flows. The relative influence of each model has been assessed enabling its performance to be gauged. The results from this have made a valuable contribution to the knowledge in the field and have enabled the acquired experience to be applied to the simulation of compartment fires.

The overall conclusion drawn from this thesis is that for the simulation of compartment fires, the most appropriate approach with current computational resources, is still the buoyancy corrected standard k-ε model. However, the turbulence scalar flux should be modelled by the generalised gradient diffusion hypothesis (GGDH) rather than the eddy-diffusivity assumption.

Acknowledgements

I would like to express my thanks to my supervisor Dr. Philip Rubini and to Professor Moss for the guidance and advise through the course of this work.

I am grateful to my parents Michael and Mariana Sanderson for their unending encouragement and support.

The careful and helpful reading of the various drafts of this thesis by my aunt and uncle, Carolyn and Richard Yeates is greatly appreciated.

Finally, Robert Percy must be acknowledged for providing much required distraction.

Table of Contents

Table of Contents ..... **i**

Nomenclature ..... **v**

Greek v

Subscripts v

Superscripts v

Abbreviations ..... **v**

1. INTRODUCTION **5**

2. TURBULENT BUOYANT JETS **5**

2.1 Introduction 5

2.2 Physical Theory of Buoyant Jets 5

2.2.1 Introduction 5

2.2.2 Characteristic Non-Dimensional Numbers 5

2.2.3 General Physical Characteristics 5

2.2.4 Decay Laws 5

2.3 Experimental Data 5

2.3.1 Line Plumes 5

2.3.2 Axisymmetric Plumes 5

2.4 Closure 5

3. GOVERNING EQUATIONS **5**

3.1 Introduction 5

3.2 Governing Equations 5

3.3 Reynolds Equations 5

3.4 Implicit Algebraic Stress Modelling (ASM) 5

3.5 Eddy-viscosity Models 5

3.5.1 Linear Eddy-viscosity 5
3.5.2 Nonlinear Eddy-viscosity 5
3.6 Turbulent Kinetic Energy Transport Equation 5
3.6.1 Modelled Form of Turbulent Kinetic Energy Equation 5
3.6.2 Turbulent Buoyant Production (G_k) 5
3.7 Transport Equation for Dissipation of Turbulent Kinetic Energy 5
3.8 Transport Equation for the Rate of Dissipation per unit Turbulent Kinetic Energy 5
3.9 Two-Equation Turbulence Models 5
3.10 Closure 5

4. NUMERICAL STUDIES OF TURBULENT BUOYANT JETS 5
4.1 Introduction 5
4.2 Numerical Simulations of Natural Convective Flows 5
4.2.1 Two-Equations Models 5
4.2.2 Low Reynolds Number Flows 5
4.2.3 Coefficients 5
4.2.4 Turbulent Heat Flux ($\overline{\rho u_i^{"}\theta}$) and Turbulent Scalar Flux ($\overline{\rho u_i^{"}\phi^{"}}$) 5
4.2.5 Modelling of Reynolds Stresses 5
4.2.6 Higher Order Models 5
4.3 Numerical Simulations Compartment Fire 5
4.4 Closure 5

5. NUMERICAL IMPLEMENTATION 5
5.1 Introduction 5
5.2 Curvilinear Non-Orthogonal Coordinate System 5
5.3 Transformed Governing Equations 5
5.4 Finite Volume Method 5
5.5 Discretised Equations 5
5.6 Treatment of Convective and Diffusive Terms 5
5.6.1 Transport Terms for General Scalar Transport Equation 5

5.6.2 Transport Terms for Momentum Transport Equation 5
5.7 Treatment of Source Terms 5
5.8 Generalised Gradient Diffusion Hypothesis (GGDH) Diffusion Model 5
5.9 Nonlinear Eddy-Viscosity models 5
5.9.1 Quadratic Model 5
5.9.2 Cubic Model 5
5.10 Closure 5

6. VALIDATION OF BUOYANT JETS PREDICTED WITH STANDARD *K-ε* MODEL 5
6.1 Introduction 5
6.2 Simulated Plumes 5
6.2.1 Plane Pure Plume 5
6.2.2 Plane Buoyant Jet 5
6.2.3 Axisymmetric Buoyant Jet 5
6.3 Comparison of Standard k-ε Model Predictions against Experimental Data 5
6.3.1 Spreading Rate 5
6.3.2 Mean Velocity and Scalar Fields 5
6.3.3 Turbulent Characteristics 5
6.4 Closure 5

7. SIMULATIONS OF BUOYANT JETS WITH SELECTED TURBULENCE MODELS 5
7.1 Introduction 5
7.2 Alternative Two Equation Models 5
7.2.1 High Reynolds Number (HRN) Models 5
7.2.2 Low Reynolds Number (LRN) Models 5
7.3 Turbulent Buoyancy Models 5
7.3.1 Buoyancy Correction in the ε-equation 5
7.3.2 Ceiling Layers 5
7.4 Scalar Diffusion Models 5
7.5 Nonlinear Eddy-Viscosity Models 5

7.5.1 Speziale's Quadratic Model 5
7.5.2 Craft's Cubic Eddy-viscosity Model 5
7.6 Closure 5

8. NUMERICAL MODELLING OF COMPARTMENT FIRES 5
8.1 Introduction 5
8.2 Steckler Compartment 5
8.3 Atrium 5
8.4 Closure 5

9. CONCLUSIONS AND FURTHER WORK 5
9.1 Conclusions 5
9.2 Further Work 5

APPENDIX A. VALIDATION 5
A.1 Introduction 5
A.2 Channel flow simulations by two-equation turbulence models 5
High Reynolds Number (HRN) Models 5
Low Reynolds Number (LRN) Model 5
Nonlinear Models 5
A.3 Closure 5

APPENDIX B. COMPUTATIONAL GRIDS 5

APPENDIX C. INFLUENCE OF 'LEDGE' ON FLOW FIELD 5

REFERENCES 5

Nomenclature

a – coefficient in discretised equations

B – buoyancy flux

B_i^j – coefficient to transformed differential equations

B_u,B_ρ - axial decay constants

b_i^j – discretised form of transformation factors

b –half width

Δc – excess concentration

C – coefficient

C_j – convective term in general transport equation

C_p – Specific heat at constant pressure

C_μ - closure coefficient

$C_{\varepsilon 1}$,$C_{\varepsilon 2}$,$C_{\varepsilon 3}$ – closure coefficient in the dissipation of turbulent kinetic energy transport equation

$C_{\omega 1}$,$C_{\omega 2}$,$C_{\omega 3}$ – closure coefficient in the rate of dissipation of turbulent kinetic energy transport equation

CD – cross derivative

D_j – diffusion term in general scalar transport equation, in tensor notation

d – inlet diameter or width

E – Term in k-ε model

e – dissipation of turbulent kinetic energy

f – mixture fraction

f_μ,f_1,f_2 – damping coefficient associated with low Reynolds number turbulence model

F_j – flux term in general transport equation

Fr – Froude number

g – acceleration due to gravity

Gr – Grashof number

G_k – buoyant production of turbulent kinetic energy

h – enthalpy

k – turbulent kinetic energy: constant in Gaussian property profile curves

ℓ - length scale

M – momentum

ND – normal derivative

P_k – shear production of turbulent kinetic energy

J – Jacobian of coordinate transformation

p – pressure

$p^{'}$ – pressure fluctuation

Q – heat flux

Re – Reynolds number

Re_t –turbulent Reynolds number

S – source term

s_{ij} – instantaneous strain rate tensor

$\overline{S}_{ij}$ – mean strain rate tensor

$\widetilde{S}_{ij}$ – mean strain rate tensor

T – mean temperature

T_{ij} – transformed stress tensor

q_j – transformed flux vector

t – time

t_{ij} – viscous stress tensor

U – velocity

$\overline{U}_i$ - mean velocity in tensor notation

$\widetilde{U}_i$ - Favre averaged velocity in tensor notation

u_i – instantaneous velocity in tensor notation

$u_i^{'}$ - fluctuating velocity in tensor notation

$u_i^{''}$ - Favre fluctuating velocity in tensor notation

$-\rho\overline{u_i^{''}u_j^{''}}$ - Reynolds stress tensor ($\overline{\tau}_{ij}$)

$-\overline{\rho u_i^{''}\phi^{''}}$ - turbulent scalar flux tensor ($\widetilde{\tau}_{ij}$)

W – weight deficit

w - rate of dissipation of turbulent kinetic energy

x,y,z – Cartesian co-ordinates

x_i – Cartesian co-ordinate in tensor notation

y – height in plume

ΔT – excess temperature

Greek

ϑ - velocity scale

α - Cartesian components of a dual natural base vector

β - volumetric expansion coefficient

β_i^j - coordinate transformation factors

δ_{ij} – Kronecker delta

ε - dissipation of turbulent kinetic energy

ϕ - general term for a scalar

$\phi_i^{'}$ - fluctuating velocity in tensor notation

$\phi_i^{''}$ - Favre fluctuating velocity in tensor notation

η - dimensionless distance

μ - laminar dynamic viscosity

μ_{eff} – effective dynamic viscosity

μ_t – turbulent dynamic viscosity

ν - laminar kinematic viscosity

θ - temperature fluctuation

ρ - density

σ - Prandtl/Schmidt number: universal constant in self-similar relationships

$\bar{\tau}_{ij}$ – Reynolds stress tensor $\bar{\tau}_{ij} = -\overline{\rho u_i^{'} u_j^{'}}$

$\tilde{\tau}_{ij}$ – Favre-averaged Reynolds stress tensor $\tilde{\tau}_{ij} = -\overline{\rho u_i^{''} u_j^{''}}$

τ_w – surface shear stress

ω - dissipation of turbulent kinetic energy

ξ_i – computational coordinate system in tenser notation ($\xi_I = (\xi,,\eta,\zeta)$)

Γ - turbulent diffusivity

Ω_{ij} – vorticity tensor

Subscripts

$_{\phi}$ - with reference to a scalar

$_{a}$ – ambient condition

$_{B}$ –bottom cell centre

$_{b}$ – bottom face of grid cell

$_{CD}$ – cross derivative

$_{cont}$ – with reference to the continuity equation

$_{E}$ – east cell centre

$_{e}$ – east face of grid cell

$_{f}$ – face of grid cell

$_{h}$ – with reference to enthalpy

$_{l}$ – laminar condition

$_{mom}$ – related to the momentum transport equation

$_{N}$ – north cell centre

$_{n}$ – north face of grid cell; with reference to the cell centre of cells neighbouring cell of interest

$_{ND}$ – normal derivative

$_{o}$ – initial condition

$_{p}$ – with reference to the cell centre cell of interest

$_{S}$ south cell centre

$_{s}$ - south face of grid cell

$_{T}$ - top cell centre

$_{t}$ – top face of grid cell; turbulent condition

$_{W}$ – west cell centre

$_{w}$ – west face of grid cell

Superscripts

^{o} – previous timestep

‘ – fluctuating component: constant component of source term

‘’ – Favre fluctuating component: coefficient associated with scalar in source term

Abbreviations

AFM – Algebraic flux model

ASM – Algebraic stress model

CFD – Computational Fluid Dynamics

DNS – direct numerical simulation

DTF – Dai, Tseng and Faeth (1994, 1995a, 1995b)

GGDH – generalised gradient diffusion hypothesis

HRN – High Reynolds number

HRR – heat release rate

JLkε - Jones and Launder (1973) k-ε model

KL - Kotsovinos and List (1977)

LDA – laser Doppler anemometer

LES – large eddy simulations

LIF – laser induced fluorescence

LRN – Low Reynolds number

LSkε – Launder and Sharma (1974) k-ε model

RC – Ramaprian and Chandrasekhara (1989)

RNG – Renormalisation Group

RSM – Reynolds stress model

RSM – Reynolds stress model

SG – Shabbir and George (1994)

SIMPLEC – semi-implicit method for pressure linked equations - consistent

SIP – Strongly implicit procedure

SMC – single moment closure

SOFIE – Simulation of fires in enclosures

Stkε - Standard k-ε model

TDMA – tri-diagonal matrix algorithm

CHAPTER 1

Introduction

A fire within a compartment can create a complex fluid flow structure driven by buoyant forces. The nature of the containment of a fire and its heat release rate affect this complexity. The hot plume that rises from a fire develops into a form that has the same properties as a non-combusting turbulent buoyant jet. Knowledge gained from the study of non-combusting turbulent buoyant jets can thus be applied to investigations of fire plumes and the more complex flows that form in compartments.

In this thesis, the numerical simulation of such flows is undertaken using computational fluid dynamics (CFD) methods. CFD is a procedure for numerically solving the equations governing fluid flow. A given fluid flow of interest that is defined by its dimensions and the conditions at its boundaries can be numerically simulated. The governing equations for fluid flow are the continuity equation combined with the Navier-Stokes equations. However, in practice, their complexity renders them difficult to solve using current methods and computational power, except in the simplest of cases. Statistical averaging of these equations reduces their

complexity and gives the Reynolds time-averaged or density weighted-average Navier-Stokes equations. The averaged equation has a similar form to the Navier-Stokes equation, but introduces an "unknown" into the equation that is referred to as the Reynolds or turbulent stress. The method used to represent these unknowns is turbulence modelling. Similar equations can be solved concurrently to describe, for example, the temperature field. These equations also contain a term (analogous to the Reynolds stress) known as the scalar turbulent flux that becomes apparent in the derivation from the instantaneous equations. Additional sub-models can also be incorporated into the calculation to model processes such as combustion and radiation.

The industry standard k-ε turbulence model employs the Boussinesq assumption combined with two transport equations for the turbulent kinetic energy (k) and the dissipation of turbulent kinetic energy (ε). This model has been successfully applied to a vast variety of both isothermal and non-isothermal flows. In the case of turbulent buoyant jets, this modelling procedure has a number of acknowledged inadequacies. The major one is an underprediction of the spreading rate.

The purpose of the current work was to investigate the influence of the turbulence model on the solution of turbulent buoyant jets with the aim of establishing a recommended turbulence modelling approach for compartment fire simulations. The quality of the prediction using the standard k-ε turbulence model was validated against existing experimental data. Alternative turbulence models were then implemented and the quality of their prediction was assessed against the standard turbulence model and the existing experimental data.

Chapter 2 presents the established theory associated with buoyant jets and reports on experimental studies of buoyant jets. The governing equations required in the simulations of buoyant jets are introduced in chapter 3. This includes a discussion of the various levels of turbulence models and details those models that have been implemented in the current work. Previous numerical studies of natural convective

type flows are reviewed in chapter 4. These are categorised by the turbulence model used in each simulation in order to assess the level of understanding in this area of CFD. The numerical implementation of the governing equations of flow, turbulence and scalar equations is discussed in chapter 5. Chapter 6 presents the three turbulent buoyant jets simulated in the current work and details the preliminary simulations undertaken to ensure the reliability of their solutions. Comparison of the mean field predicted for each of the turbulent buoyant jets is made with existing experimental data. The turbulence characteristics of only one of the turbulent buoyant jets has been validated against experimental data due to the limited availability of reliable measurements. Chapter 7 compares predictions made by the newly implemented models against those of the experimental data and the standard k-ε model predictions.

The experience gained in the prediction of the turbulent buoyant jets is then applied in the simulation of a compartment fire, in chapter 8. Two compartment fires were considered, the Steckler compartment and an atrium based on the Steckler compartment. The Steckler compartment is an experimental rig in which measurements of developed flow and temperature fields were made. Atria are becoming a common feature of commercial building and, due to the larger development region for the fire plume in an atrium, buoyant aspects of the turbulence models may have a more significant influence on the flow in the atrium. The simulations of the atrium enable a comparison of relative influence of the model of interest in the two scenarios.

The work undertaken for this thesis consisted of the application of a variety of turbulence models to the simulation of turbulent buoyant jets and the subsequent application of successful models to compartment fire simulations. The experience gained through examination of the quality of the results enabled a confident recommendation of the necessary complexity of turbulence modelling to achieve a good prediction of the mean flow and scalar fields in compartment fires.

CHAPTER 2

Turbulent Buoyant Jets

2.1 Introduction

Turbulent buoyant jets are a common feature of both natural and engineering flows. They can lead to complex flow scenarios such as those often observed in compartment fires. The basic theory associated with the ideal buoyant jet has become well established through analyses of the governing equations and experimental research.

Section 2.2 summarises the established theories of buoyant jets. The recognised characteristics and normalised numbers used to describe buoyant jets, together with the established correlations of their properties, are also presented in the section. Section 2.3 reviews the literature of the experimental work on buoyant jets in two sections, according to their source geometry. Section 2.3.1 covers plane (or line) buoyant jets and section 2.3.2 axisymmetric buoyant jets. An assessment of the relative quality of the datasets was made to identify those suitable for use in the validation of numerical simulations.

2.2 Physical Theory of Buoyant Jets

2.2.1 Introduction

The following section considers the physical theory of ideal buoyant jets. A buoyant jet can be considered as a flow of very low Mach number that issues into an ambient fluid of a different density with its axis parallel to the gravity vector. Buoyant jets are free shear flows, remote from walls in the streamwise direction.

The limiting cases of buoyant jets are pure plumes and pure jets. Pure plumes are initiated solely by a heat source and are driven by a buoyant force. Pure jets are driven by momentum with no buoyant force. This thesis only considers those buoyant jets with a buoyant influence. Figure 2-1 summarises the characteristics of both a pure plume and a buoyant jet.

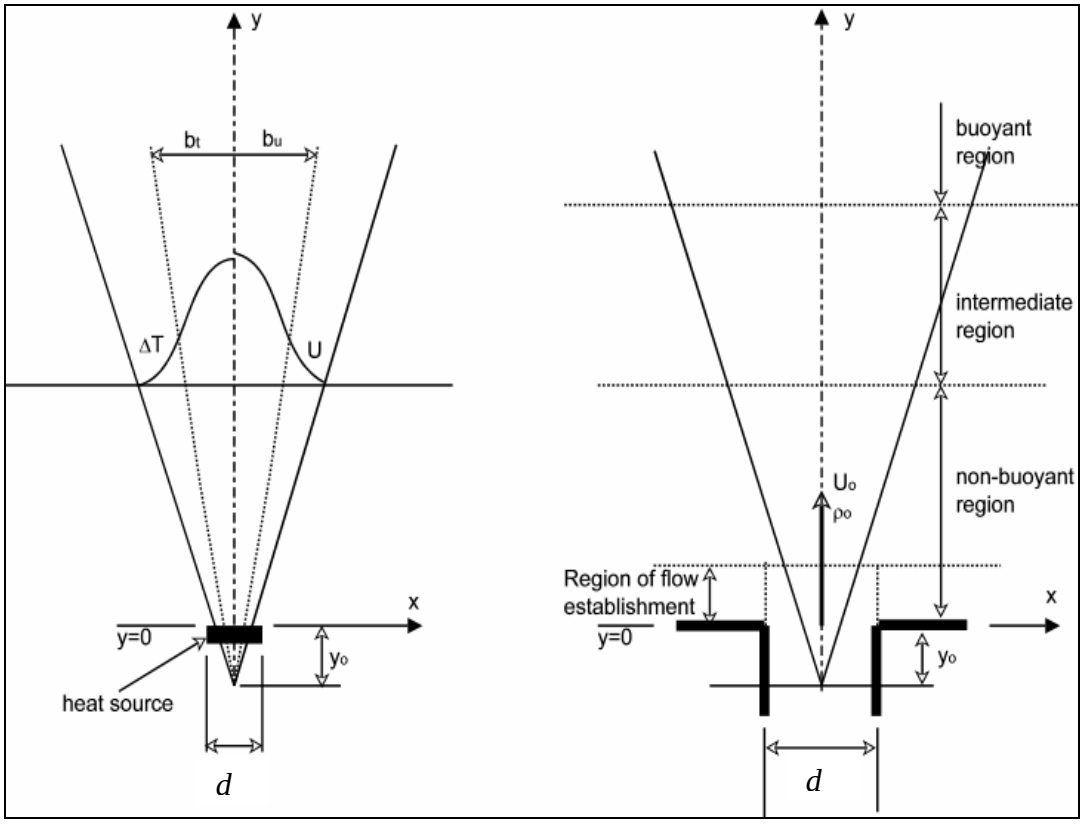

Figure 2-1: Schematic of the basic properties of a pure plume (left) and a buoyant jet (right)

Figure 2-1 (left) shows a typical pure plume that is generated by a heat source with no initial momentum. Heat is transferred to the fluid from this heat source and causes a density difference in the fluid adjacent to the heat source. This, in turn, causes a buoyancy driven momentum in the vertical direction. The plume is initially laminar but undergoes transition to become turbulent. The point of transition is dependent on the initial conditions.

Figure 2-1 (right) shows a typical buoyant jet. Unlike the pure plume, this has an initial momentum. Most buoyant jets of engineering interest are turbulent. They may have a small transitional region of flow, shown in figure 2-1 (right), as the region of establishment. As with pure plumes, the size of this region depends on the initial conditions. The turbulent region of the buoyant jet is recognised as consisting of three sections:

The non-buoyant region that is adjacent to the discharge and is dominated by momentum force and that acts as a pure jet;

The intermediate region where both the momentum forces and the buoyant forces have influence;

The buoyant region that is completely dominated by the buoyant forces and acts as a pure plume.

2.2.2 Characteristic Non-Dimensional Numbers

The characteristics of both the pure plumes and buoyant jets are dependent largely on the strength of the inlet forces and the ambient conditions. Non-dimensional parameters, the Reynolds (Re) and Grashof (Gr) numbers, describe these initial conditions. Hence these numbers give an indication of whether the flow will be laminar or turbulent and when transition will occur.

The Reynolds number is the ratio of inertial to viscous forces, and for initial conditions is defined as:

$$\mathrm{Re} = \frac{U_o d}{\nu} \qquad 2.1$$

The Grashof number is the ratio of buoyant forces to viscous forces:

$$\mathrm{Gr} = \frac{g(\rho_a - \rho_o)d^3}{\rho_o \nu^2} \qquad 2.2$$

The Reynolds and Grashof numbers represent the absolute magnitude of the inlet inertia and buoyancy forces. The ratio of these forces, the Froude number (Fr), determines the character of the flow:

$$\mathrm{Fr} = \frac{M_o U_o}{W_o d} \qquad 2.3$$

The definition of the Froude number adopted here is taken from Chen and Rodi (1980), this varies from the common definition which is the square root of equation 2.3. The momentum (M) and weight (W) deficit can be defined at any height in the plume by the following expressions:

$$M = 2\int_0^\infty \rho U^2 (\pi x)^j dx \qquad 2.4$$

$$W = 2g\int_0^\infty (\rho_a - \rho) U (\pi x)^j dx \qquad 2.5$$

where j=0 for plane jets and j=1 for axisymmetric jets. In the case of an ideal gas, the following relationship can be assumed:

$$\frac{\rho_a - \rho}{\rho} = \frac{T - T_a}{T_a} \qquad 2.6$$

This allows the weight deficit to be defined in terms of the heat flux (Q):

$$W = \frac{Qg}{C_p T_a} \qquad 2.7$$

where:

$$Q = 2\int_0^\infty C_p \rho (T - T_a) U (\pi x)^j \, dx \qquad 2.8$$

2.2.3 General Physical Characteristics

Ideal buoyant jets of differing geometry, and initial conditions have some properties that are generally common; this enables direct comparison between non-similar plumes.

Figure 2-1 demonstrates how a plume-type flow is characterised by a column of fluid that expands laterally through entrainment. Entrainment is the process by which the surrounding ambient fluid is mixed into the plume. A time-averaged representation of a plume has a sharp straight boundary that separates the plume from the surrounding environment. An instantaneous representation, however, reveals the plume boundary to be highly irregular, consisting of a series of eddies that engulf ambient fluid into the plume.

From early observations of entrainment, it was suggested that the local centreline velocity was proportional to the entrained velocity (Morton, Taylor and Turner (1956)). The proportionality constant, known as the 'entrainment coefficient', was regarded as a universal constant. This is now considered a primitive assumption as it has been found that the entrainment coefficient is dependent on the local character of the flow. Various proposals have been made for the calculation of the entrainment coefficient; these are discussed in, for example, Turner (1973) and Chen and Rodi (1980).

Plume-type flows are considered to exhibit similarity or to become self-similar (also known as self-preservation). This occurs at a point remote from the source where the properties of the plume become independent of the source. In this region, scalar and velocity profiles can be normalised to enable comparison between plumes with

different properties. The scalar and velocity cross-stream profiles are generalised in terms of a Gaussian curve such that:

$$\frac{\overline{U}}{\overline{U}_o} = e^{-k_u \eta^2} \qquad 2.9$$

$$\frac{\overline{T} - \overline{T}_a}{\overline{T}_o - \overline{T}_a} = e^{-k_T \eta^2} \qquad 2.10$$

where η is the non-dimensional cross-stream distance and *k* is a constant.

Similarity analysis requires that the plume spread linearly. It is thus possible to define a quantity that is a measure of this spread either in terms of the scalar or velocity field. The spreading rate is defined as:

$$K = b / H \qquad 2.11$$

where K is spreading rate; b is characteristic width; H is height at which characteristic width is calculated. The characteristic width is defined as the width of the plume where the considered quantity is a fraction of the maximum. This fraction is commonly half; hence, the characteristic width is generally referred to as the half width. An alternative fraction, which is used with reference to axisymmetric plumes, is e^{-1}.

The consideration of practical plumes has led to the concept of a virtual or ideal origin. This is demonstrated in figure 2-1 as the ideal origin if the plume originates from a point source. The concept appeared in early papers for the experimental analysis of laminar plumes (Forstrom and Sparrow (1967)) in order that algebraic relationships proposed for the similarity region of the plumes fitted to experimental results. Validity of this concept has been questioned in subsequent papers (Collins and Williams (1954) and Yosinobu et al (1979)), however it is still often used.

2.2.4 Decay Laws

Chen and Rodi (1980) derived the conditions for the existence of self-similarity and the analysis led to the so-called decay laws. These laws describe the variation of the centreline velocity, temperature/concentration and density with height in the self-similar region. The scaled form of the decay laws enabled general application to buoyant jets. The scaling parameters for length velocity and buoyant force are defined in the equations below:

$$x = d\mathrm{Fr}^{2/(3+j)}\left(\frac{\rho_o}{\rho_a}\right)^{1/(3+j)} y_S \qquad 2.12$$

$$U = U_o\mathrm{Fr}^{-(1+j)/(3+j)}\left(\frac{\rho_o}{\rho_a}\right)^{1/(3+j)} U_S \qquad 2.13$$

$$g(\rho_a - \rho) = g(\rho_a - \rho_o)U_o\mathrm{Fr}^{-(1+j)/(3+j)}\left(\frac{\rho_o}{\rho_a}\right)^{-(2+j)/(3+j)} g_S \qquad 2.14$$

where j is equal to 0 for plane plumes and 1 for axisymmetric plumes and y represents the height in the plume.

The decay laws defined in terms of these scaling parameters in the self–similar region of a buoyant jet are:

$$U_S = B_u\left(\frac{\rho_o}{\rho_a}\right)^{-1/3} y_S^{-j/3} \qquad 2.15$$

$$g_S = B_\rho\left(\frac{\rho_o}{\rho_a}\right)^{1/3} y_S^{-(2j+3)/3} \qquad 2.16$$

In order to eliminate the dependence on ρ_o/ρ_a it is assumed that the density field is uniform hence ρ_o/ρ_a=1. This assumption also enables the laws to be applied to temperature and concentration, in addition to density, since the relationship between excess density and excess temperature/concentration can be approximated as:

$$\frac{\Delta\rho}{\Delta\rho_o} \approx \frac{\Delta c}{\Delta c_o}\frac{\rho_a}{\rho_o} \qquad 2.17$$

2.3 Experimental Data

The intention of early researchers, undertaking experimental studies on plumes, was to collate data for the verification of similarity relationships discussed in the previous section. Schmidt (1941) and Rouse, Yih and Humphreys (1952) found, independently, the experimental data agreed reasonably well with the proposed similarity relationships. Unfortunately, at this time the apparatus was primitive compared to present instrumentation, thus the experimental error could be expected to be large.

More recently, work has been aimed at providing data for validation of numerical simulations. Chen and Rodi (1980) conducted a review of all the experimental studies available for vertical buoyant jets. Comparison of the various studies enabled assessment of the quality of the experimental data and suggestions for the most reliable values to be used in validation. List (1982) also conducted a review of experimental studies for turbulent jets and plumes.

The following sections review published experimental studies concerning buoyant jets. The studies have been categorised in terms of geometric characteristics of buoyant jets: line (or plane) or axisymmetric buoyant jets. A line plume is a two-dimensional plume that is formed by a long thin heat source. An axisymmetric plume is formed by a circular heat source of finite diameter that, theoretically, is a point heat source.

2.3.1 Line Plumes

A considerable amount of work has been undertaken with relation to laminar line plumes (e.g. Brodowicz and Kierkus (1966), Forstrom and Sparrow (1967), Schorr and Gebhart (1970), Collins and Williams (1954), Noto (1989), Yosinobu et al

(1979)). These studies, although not of direct interest to the current work, have lead to consideration of some important factors such as the virtual origin (section 2.2) and the 'swaying' of the plume. The plume source was generally an electrical wire heated by resistance. The swaying phenomenon that can effect experimental measurements, occurs when the plume sways longitudinally over the source and meanders along the length of the source. This appears to be the result of outside environmental influences (Noto (1989)).

Plumes created by density difference or by fires are concerned with the turbulent region of the plume. This is of direct interest to the present work, since the initial intention is to use a turbulent plume as a base case against which solutions from different turbulent models can be compared.

Rouse et al (1952) worked on both plane and axisymmetric plumes created by a fire, to provide a better understanding of natural convection for meteorologists. With no prior knowledge, they closely mirrored the work conducted in Germany by Schmidt (1941).

The theoretical analysis of Rouse et al (1952) proposed integral equations for momentum diffusion and energy. The experimental work measured both temperature and velocity. Temperature was measured by a hot wire and velocity by an anemometer. Reasonably good agreement was found between the theoretical and experimental work.

Lee and Emmons (1961) measured the temperature field above line fires of acetone and methanol. This allowed the effect of the surroundings on the radiative loss of flames with different luminance to be investigated. The averaged temperature measurements were taken along lines parallel to the channel burner by a piece of resistance wire. The non-luminous methanol flame was unaffected by a change in the material of the plates adjacent to the flame, since radiation was unimportant. The luminous acetone flame showed that the radiative heat loss to the surroundings

was low with asbestos side plates and high with aluminium plates. The results from the temperature measurements in the natural convection plume above the fire agreed well with the plume theory.

Kotsovinos and List (1977) and Kotsovinos (1977) (future reference of these works will only refer to Kotsovinos) conducted extensive studies of turbulent buoyant line plumes. A number of experiments with exit Froude numbers ranging from 1.4 to 17,000 were performed. The plume was generated by the discharge of heated water into a tank containing water of uniformly cooler temperature. Velocity, temperature and heat flux were measured and their time-averages and root mean square deviation computed. Temperature was measured by thermistors and velocity by forward scattering/reference beam laser Doppler anemometry (LDA).

Gaussian fits of the non-dimensionalised velocity and temperature profiles were in reasonable agreement with those proposed by Rouse at al (1952) and Lee and Emmons (1961). Kotsovinos gave the first reported measurements of turbulence statistics for a line plume and, in later reviews, there was considerable discussion about their validity. The review of Chen and Rodi (1980) questioned the validity of the turbulence statistics. In comparison with other experiments for axisymmetric plumes, the turbulence measurements, in particular the turbulence longitudinal heat flux, appear to be too high. A later review by List (1982) gave a detailed defence of Kotsovinos's study and an informative summary of the conclusions. The subsequent study by Ramaprian and Chandrasekhara (1983) upheld the concerns of Chen and Rodi. Similar results were found except for the turbulent longitudinal heat flux.

Ramaprian and Chandrasekhara (1983, 1985 and 1989) investigated plumes that were produced in a similar manner to Kotsovinos. A non-buoyant jet was also investigated to provide a comparison. The measurements of velocity were taken using a two-point LDA, rather than single-point LDA used by Kotsovinos. Therefore, they were able to measure the cross-stream turbulent fluxes in addition to

the longitudinal turbulent fluxes. A microresistance thermometer was used to measure the instantaneous temperature excess.

Ramaprian and Chandrasekhara (1983) drew three main conclusions from their study. Firstly, they confirmed that all plane buoyant jets reach a universal asymptotic state in respect of both mean and turbulent properties. However, in general, their mean velocity values were greater than those found by Kotsovinos. Secondly, the buoyancy of the system was found to increase the turbulent fluxes significantly. As mentioned previously, the order of this increase was significantly smaller than that found by Kotsovinos and in line with the proposal of Chen and Rodi (1980). Finally, the increased production of turbulent shear stress and buoyancy, in the central region of the plume, resulted in the sustenance and enhancement of the turbulence in the plume.

Sangras et al (1998) ran a set of experiments with a helium/air source issuing into an unstratified air environment at normal temperature and pressure. This work was a continuation of experiments on axisymmetric plumes (Dai, Tseng and Faeth (1994), (1995(a)), (1995(b))). Measurements of the mean and fluctuating mixture fraction were taken using laser induced iodine fluorescence and extensive comparisons were made with previous experimental studies on line plumes. It was proposed that measurements taken in these previous studies were too close to the source and hence in a region that was not yet self-similar. The half width in the lower region of the plume considered by Sangras et al (1998) were comparable to values reported in earlier studies at the highest point at which measurements had been taken. They found the half width became smaller in the higher regions of the plume. A second reason given for the broader plumes in earlier studies is the method of scaling used. The buoyancy force is often used as a scaling factor; earlier work estimated this value from experimental results, whereas the current study is able to calculate the value from the initial conditions. The lack of quality measurements of the turbulent contribution to the buoyancy force, in the earlier studies, could have resulted in an underestimation of this value, hence leading to a broader profile than is correct.

Sangras et al (1998) also found the measurement of fluctuating quantities varied considerably from earlier studies, in that a maximum was observed at the centreline. The profile of the fluctuating mixture fraction, taken across the plume, was found in earlier studies to dip at the centreline. This result is comparable with those found in non-buoyant jets (Papanicolaou and List (1988)) and early stages of axisymmetric buoyant jets (Dai et al (1994)). The dip in non-buoyant jets appears because the shear turbulence production at this point is small. Although the buoyant plume has a similar mean flow cross-stream profile to non-buoyant jets, the effects of buoyancy provides a mechanism for turbulent production near the central plane of the plume.

Verripoulos and Papailiou (1994) studied a methanol line fire. The main purpose of the experiments was to increase understanding of the turbulent transport processes that govern the flow around a line fire, through flow visualisation. The mean temperature field and the turbulent temperature fluctuations, above the fire, were also considered. Hot wire probes measured the temperatures. The Gaussian fit to their lateral mean temperature profile, in the self-similar region, was in close agreement with that proposed by Chen and Rodi (1980). Verripoulos and Papailou showed the on-axis variation of the turbulent temperature intensity of a fire plume to be slightly different to that of an ordinary (non-fire) plume. In a fire plume there is a decay of turbulence intensity in the initial stages of development, whereas in conventional plumes, there is an increase with height that becomes constant in the self-similar region. The decay is explained by the presence of large hot structures that are periodically shed from the flames in the plume. Subsequent downstream decay of these structures, caused by the mixing action of the entrainment vortices, results in a gradual increase of the turbulence intensity, until a constant value is reached in the self-similar region. The non-dimensional intensity distribution suggests that self-similarity is reached at 15 diameters above the source. A flat region is observed in the distribution, around the axis, similar to that reported by Kotsovinos (1977) that is attributed to the buoyant production of turbulence. Consideration of the turbulent transport process reveals a double structure. This

comprises large entrainment eddies, which transfer ambient air into the centre of the plume and a background of nearly isotropic turbulence that is destroyed by the presence of the entrained buoyant vortices.

A considerable amount of work has been undertaken for reactive plumes. Li and Bilger (1996) give a good summary. Although this type of plume is not of direct relevance to the current work, some interesting conclusions have been achieved. Li and Bilger studied both reactive and non-reactive line plumes, for the purpose of comparison. The reactants were nitrogen-oxide and ozone, in an ambient air environment. The plume created can be considered to be similar to a fire plume, since there is a core region near the source in which the reaction is dominant, an intermittent stage and then the diffusive plume. The results showed that the spreading rate of the plume is dominated by turbulent mixing with the chemical reaction having little effect. However, the chemical reactions had a strong effect on the decay of mean reactant concentration. Similarity solutions are not possible for the reactive scalars since they do not achieve a self-similar state. The gradient model for diffusivity was assessed and found to work well in the far field. Earlier papers found the turbulent diffusivities to be considerably different for reactive and non-reactive scalars. The Li and Bilger paper, however, found these comparable.

2.3.2 Axisymmetric Plumes

There are a great deal more experimental studies concerning axisymmetric plumes than line plumes, due to the relative ease of sustaining an axisymmetric plume. Line plumes have a tendency to lose their 2-dimensional form at some distance from the source and take on the characteristics of an axisymmetric plume. The large amount of data permits a more discerning assessment of axisymmetric plumes. The following discussion will be restricted only to the most reliable data. The choice of this data has been guided by the reviews of Chen and Rodi (1980) and List (1982).

Chen and Rodi cited four references for axisymmetric turbulent buoyant self-similar plumes: Rouse et al (1952), Schmidt (1941), George et al (1977), Nakagome and

Hirata (1976). Of these, Rouse et al (1957) and George et al (1977) were credited with greatest consistency. The apparatus used by Rouse et al (1957) was criticised for being primitive because an anemometer was used for velocity measurements. The apparatus of Schmidt (1941) were also thought to be primitive "since hot wire anemometer measurements were probably inaccurate for the early 1940's". The experiments of Nakagome and Hirata (1976) were considered inaccurate because their plume was shown not to be axisymmetric. However, useful data were extracted from these experiments that allowed scaling laws and similarity constants to be proposed with confidence.

Work involving George et al (1977) has identified the sensitivity of plumes to the surrounding conditions. Beuther (1980) and Beuther and George (1982) demonstrated the significant effects that even a slightly stratified ambient environment has on the flow and noted how this had not been monitored in most previous experiments. Shabbir and George (1994) showed how the presence of screens around the source could affect the plume. These screens were often employed to minimise external disturbances.

A wide-ranging review of experimental data by List (1982) suggested that inconsistencies in previous work resulted, mainly, from two factors. First, there was substantial uncertainty as to whether measurements had been taken in the transitional or self-similar region, leading to some suspicion of the accuracy of proposed similarity laws. Secondly, none of these studies equated the integrated buoyancy flux to the source buoyancy flux. The buoyancy flux, which appears directly in the similarity relations, was obtained in these studies by integrating the measured temperature and velocity profiles. This could result in an error since the probes used, hot wires, did not have the ability to resolve flow reversals believed to be present at the outer edge of the flow.

The latter of these two factors was addressed by Shabbir and George (1994). The balance of the mean buoyancy and momentum equations was determined. The

imbalance found was said to represent the error in the measurements. These balances also identified the dominant transport processes. The momentum balance showed that the buoyancy force was as large as the transport of turbulent shear stress. This buoyancy force led to larger velocity gradients in buoyant plumes than in jets and resulted in an increased production of turbulent energy through the production term in the turbulent kinetic energy equation.

The first of the factors identified by List (1982), (i.e. that previous experimental measurements had been taken before the plume was fully self-similar), as the cause of inconsistencies in previous experimental work, was supported by Dai et al (1994, 1995a, 1995b). This series of papers that investigated buoyant turbulent plumes experimentally, with the distinct emphasis on measurements being taken in the self-similar region. The plumes were produced using carbon dioxide and sulphur hexafluoride in still air. The test rig was designed to minimise room disturbances. Measurements of the mixture fraction were taken by iodine laser induced fluorescence (LIF) and of velocity by laser velocimetry. The measurements gave a comprehensive set of data, for both mean and fluctuating quantities, against which numerical models could be compared. Initially, the mixture fraction was considered, then the velocity and, finally, the higher order turbulent characteristics.

The measurements of both mean streamwise velocity and mixture fraction distribution, by Dai et al (1994, 1995a), were found to be 40% and 30%, respectively, narrower than reported in previous work. In addition, scaled values near the axis were found to be larger. The velocity measurements also revealed that the entrainment rate was smaller. The authors suggested that this difference arose because the measurements in previous experiments had not been taken in the self-similar region.

Measurements of mixture fraction and velocity fluctuations by Dai et al (1995b), produced some interesting results. The radial profiles produced by the velocity fluctuations were found to be comparable to those of non-buoyant jets. That is, the

profile exhibited a dip in the region near the axis and a tendency towards isotropic behaviour near the edge of the flow. The mixture fraction fluctuations profile for the buoyant plume, however, did not exhibit this dip, in contrast to the non-buoyant turbulent jet, and, instead, displayed a maximum at the axis. The authors suggested that this maximum was responsible for the large radiation fluctuation levels observed in the near over-fire regions of fire plumes. Measurements of the streamwise turbulent fluxes were also found to be quite large near the axis in the turbulent buoyant plume. They suggested that this behaviour, combined with the rapid decay of mean mixture fraction, was a strong source of production of scalar fluctuations. These were probably responsible for the large values of mixture fraction fluctuation intensities observed near the axis of round self-preserving buoyant turbulent plumes. Measurements of the velocity/mixture fraction statistics revealed more details of the transport processes within the similarity region of a turbulent plume. The streamwise turbulent fluxes of mass and momentum exhibit counter gradient diffusion. Although this was small compared with radial fluxes, it raises concerns about the use of simple gradient diffusion hypotheses often used in modelling the flow. In addition, constants used in the radial diffusion approximation were shown to vary across the flow.

2.4 Closure

Buoyant jets can be considered as the simplest example of natural convective flows. A considerable body of works exists aimed at understanding and algebraically describing buoyant jets. This chapter has outlined the physical theory of buoyant jets and described the characteristics, non-dimensional numbers and relationships used in the description of their flow.

A review of the experimental work on buoyant jets, categorised by their source geometry, has been presented. Suitable datasets, for each geometry, were identified for the validation of the numerical simulations of buoyant jets. The chosen dataset in each case was the most recently published data. Considerable variation exists between the measurements in different studies. It has been found that, with the

increased sophistication of experimental methods and more reliable apparatus, data has been taken at distances further from the source. This has resulted in the measured profiles of velocity and temperature, or mixture fraction, having a lesser spreading rate.

CHAPTER 3

Governing Equations

3.1 Introduction

The continuity and Navier-Stokes equations provide a description of the instantaneous flow field. These are a set of complex, partial differential equations that require simplification or manipulation before they can be practically solved. The adoption of computational fluid dynamic methods in the current work requires that these equations be averaged. The averaging process introduces a turbulent term that includes the Reynolds stresses into the governing flow equations; these are defined by a turbulence model.

The solution of a mean scalar field introduces an additional averaged transport equation into the calculations. This equation includes a term analogous to the Reynolds stresses and is known as the turbulent scalar flux.

This chapter presents the equations governing fluid flow and turbulence. The transport equations for instantaneous and average fluid flow are presented in section 3.**2**. A discussion of different approaches to turbulence modelling, such as Reynolds

stress modelling (RSM), algebraic stress modelling (ASM) and eddy viscosity models is given in sections 3.3, 3.4 and 3.5, respectively. The turbulent scalar flux is discussed in section 3.**Error! Bookmark not defined.** with reference to both the eddy-diffusivity model and the generalised gradient diffusion hypothesis (GGDH) model. The transport equations for the turbulent quantities of turbulent kinetic energy (k), dissipation of turbulent kinetic energy (ε) and rate of dissipation of turbulent kinetic energy (ω) are summarised individually sections 3.6, 3.7 and 3.8, respectively. In section 3, combinations of the transport equations of the turbulence quantities are presented as the two-equations turbulence models that are implemented in the current work.

3.2 Governing Equations

The equations that govern fluid flow are the continuity equation and the Navier-Stokes equations. These can be derived through consideration of the conservation of mass and Newton's second law applied to an infinitesimally small volume. The full derivation is given in many CFD textbooks (e.g. Versteeg and Malalasekera (1995)). The equations are specified below in a conservative form:

$$\frac{\partial \rho}{\partial t} + \frac{\partial (\rho u_i)}{\partial x_i} = 0 \qquad 3.1$$

$$\frac{\partial (\rho u_i)}{\partial t} + \frac{\partial (\rho u_i u_j)}{\partial x_j} = -\frac{\partial p}{\partial x_i} + \frac{\partial t_{ij}}{\partial x_j} + S_{mom} \qquad 3.2$$

This work is confined to the consideration of Newtonian fluids. Sir Isaac Newton (1642-1727) defined such fluids as those in which the shear stress is proportional to the time rate of strain, i.e. velocity gradients. This has been shown to be true, experimentally, for all gases and many liquids. The viscous stress tensor, t_{ij}, was thus defined by Stokes (1851):

$$t_{ij} = 2\mu s_{ij} - \frac{2}{3}\frac{\partial u_k}{\partial x_k}\delta_{ij} \qquad 3.3$$

$$s_{ij} = \frac{1}{2}\left(\frac{\partial u_i}{\partial x_j} + \frac{\partial u_j}{\partial x_i}\right) \qquad 3.4$$

An exact equation can also be derived, for energy transfer by application of the conservation of energy to an infinitesimally small volume:

$$\frac{\partial(\rho h)}{\partial t} + \frac{\partial(\rho u_j h)}{\partial x_j} = \frac{\partial}{\partial x_j}\left(\Gamma_h \frac{\partial h}{\partial x_j}\right) + S_h \qquad 3.5$$

Comparison of the momentum and energy transport equations reveals the two have a similar form. This can be generalised to represent the transport of any conserved variable, ϕ, in a fluid. The generalised form of the equations, known as the general scalar transport equation, is shown below together with the physical representation of the terms:

$$\underbrace{\frac{\partial(\rho\phi)}{\partial t}}_{\text{transient term}} + \underbrace{\frac{\partial(\rho u_j \phi)}{\partial x_j}}_{\text{convective term}} = \underbrace{\frac{\partial}{\partial x_j}\left(\Gamma_\phi \frac{\partial \phi}{\partial x_j}\right)}_{\text{diffusive term}} + \underbrace{S_\phi}_{\text{source term}} \qquad 3.6$$

A typical turbulent flow contains eddies with a wide range of length scales ranging from the very small dissipative eddy to very large eddies based on the limits of the fluid domain. An eddy is an area of swirling fluid with a characteristic dimension known as the turbulence length scale. A continuous spectrum is observed in the transport of the kinetic energy, from the mean flow to the large scale eddies, through the eddies of decreasing length scale. The kinetic energy is dissipated from the smallest eddies into heat through molecular action.

The exact solution of these equations, known as direct numerical simulation (DNS), requires resolution of all the eddies both spatially and temporally. This is a substantial computational task for all but the simplest small-scale flows.

Some solutions by DNS have appeared for simple low Reynolds number flows. These have no practical use for industrialists but provide a useful tool for the examination of the predictive capabilities of turbulence models. DNS is confined more by the capabilities of modern computers than the methodologies involved in the solution of the equations.

Large eddy simulation (LES) is an alternative to the DNS. This concept relies on the observation that turbulence consists of a continuous spectrum of scales. LES aims to solve the Navier-Stokes equations for the largest eddies in a spectrum and model the smallest. Thereby eliminating the requirement for small-scale temporal and spatial resolution.

A description of the mean flow characteristics is generally sufficient for engineering purposes. As such, statistical methods have been developed whereby the instantaneous value is decomposed into a fluctuating and a mean component. This approach was first suggested by Osborne Reynolds (1842-1912), who derived the time-averaged form of the Navier Stokes equation, to give the Reynolds-averaged equations defined below:

$$\bar{\phi}(x_i,t) = \lim_{T\to\infty} \frac{1}{T} \int_0^T \phi(x_i,t)dt \qquad 3.7$$

and

$$\phi = \bar{\phi} + \phi' \qquad 3.8$$

For incompressible flows, the substitution of equation 3.8 into the instantaneous governing equations (equation 3.1 and 3.2) and subsequent time-averaging yields the Reynolds-averaged Navier Stokes equations, given below:

$$\frac{\partial\left(\rho\bar{U}_i\right)}{\partial x_i} = 0 \qquad 3.9$$

$$\frac{\partial\left(\rho\bar{U}_i\right)}{\partial t} + \frac{\partial\left(\rho\bar{U}_j\bar{U}_i\right)}{\partial x_j} = -\frac{\partial\bar{p}}{\partial x_i} + \frac{\partial}{\partial x_j}\left(2\mu\bar{S}_{ij} - \rho\overline{u_i'u_j'}\right) + \bar{S}_{mom} \qquad 3.10$$

$$\frac{\partial(\rho\bar{\phi})}{\partial t}+\frac{\partial(\rho\bar{U}_j\bar{\phi})}{\partial x_j}=\frac{\partial}{\partial x_j}\left(\frac{\mu}{\sigma_l}\frac{\partial\bar{\phi}}{\partial x_j}-\rho\overline{u_j'\phi'}\right)+\bar{S}_\phi \qquad 3.11$$

$$\bar{S}_{ij}=\frac{1}{2}\left(\frac{\partial\bar{U}_i}{\partial x_j}+\frac{\partial\bar{U}_j}{\partial x_i}\right) \qquad 3.12$$

The time-averaged momentum equations and the Navier-Stokes equations have a similar form except for the third term on the right hand side of the former. This term is the spatial derivative of the Reynolds or turbulent stresses ($\bar{\tau}_{ij}=-\rho\overline{u_j'u_i'}$.) A similar term referred to as the turbulent scalar flux (-$\rho\overline{u_j'\phi'}$), exists in the general scalar transport equation. A turbulence model is required for closure of the equations through the modelling of the Reynolds stress and turbulence flux.

The above equations were derived for isothermal incompressible flow. However, the flows of interest in the current work are non-isothermal, where fluctuations of density are non-negligible. The averaging process described above, when applied to variable density flows, introduces a number of further averaged correlations including the density fluctuation terms. The additional correlations also require modelling leading to a far more complex solution procedure.

Consideration of the Favre-averaged (density-weighted averaged) values rather then the time-average values avoids this complexity. The Favre average variable is defined below:

$$\tilde{\phi}(x_i,t)=\frac{1}{\bar{\rho}}\lim_{T\to\infty}\int_0^T\rho(x_i,t)\phi(x_i,t)dt \qquad 3.13$$

and

$$\phi=\tilde{\phi}+\phi'' \qquad 3.14$$

The Favre-averaged form of the governing equations is:

$$\frac{\partial \overline{\rho}}{\partial t} + \frac{\partial \left(\overline{\rho} \widetilde{U}_i \right)}{\partial x_i} = 0 \qquad 3.15$$

$$\frac{\partial \left(\overline{\rho} \widetilde{U}_i \right)}{\partial t} + \frac{\partial \left(\overline{\rho} \widetilde{U}_j \widetilde{U}_i \right)}{\partial x_j} = -\frac{\partial \overline{p}}{\partial x_i} + \frac{\partial}{\partial x_j} \left(2\mu \widetilde{S}_{ij} - \overline{\rho u_i'' u_j''} \right) + \widetilde{S}_{mom} \qquad 3.16$$

$$\frac{\partial \left(\overline{\rho} \widetilde{\phi} \right)}{\partial t} + \frac{\partial \left(\overline{\rho} \widetilde{U}_j \widetilde{\phi} \right)}{\partial x_j} = \frac{\partial}{\partial x_j} \left(\frac{\mu}{\sigma_l} \frac{\partial \widetilde{\phi}}{\partial x_j} - \overline{\rho u_j'' \phi''} \right) + \widetilde{S}_{\phi} \qquad 3.17$$

$$\widetilde{S}_{ij} = \frac{1}{2} \left(\frac{\partial \widetilde{U}_i}{\partial x_j} + \frac{\partial \widetilde{U}_j}{\partial x_i} \right) \qquad 3.18$$

3.3 Reynolds Equations

An exact equation for the time-averaged and the Favre-averaged shear stresses can be derived from a similar procedure. The Navier-Stokes equations are multiplied by the fluctuating component and the mean of the product is taken. The derivation is detailed in, for example Wilcox (1994). The Reynolds-averaged form is given below:

$$\frac{\partial \overline{\tau}_{ij}}{\partial t} + \overline{U}_k \frac{\partial \overline{\tau}_{ij}}{\partial x_k} = -\overline{\tau}_{ik} \frac{\partial \overline{U}_j}{\partial x_k} - \overline{\tau}_{jk} \frac{\partial \overline{U}_i}{\partial x_k} + \varepsilon_{ij} - \Pi_{ij} + \frac{\partial}{\partial x_k} \left[-\nu \frac{\partial \overline{\tau}_{ij}}{\partial x_k} + C_{ijk} \right] + G_{ij} \qquad 3.19$$

$$\Pi_{ij} = \overline{p' \left(\frac{\partial u_i'}{\partial x_j} + \frac{\partial u_j'}{\partial x_i} \right)} \qquad 3.20$$

$$\varepsilon_{ij} = 2\mu \overline{\frac{\partial u_i'}{\partial x_k} \frac{\partial u_j'}{\partial x_k}} \qquad 3.21$$

$$C_{ijk} = \rho \overline{u_i' u_j' u_k'} + \overline{p' u_i'} \delta_{jk} + \overline{p' u_j'} \delta_{ik} \qquad 3.22$$

$$G_{ij} = -\beta \overline{\rho} \left(g_i \overline{u_j' \theta} + g_j \overline{u_j' \theta} \right)$$

The Favre-averaged Reynolds stress tensor ($\widetilde{\tau}_{ij} = -\overline{\rho u_i'' u_j''}$) is given;

$$\frac{\partial \tilde{\tau}_{ij}}{\partial t} + \tilde{U}_k \frac{\partial \tilde{\tau}_{ij}}{\partial x_k} = -\tilde{\tau}_{ik} \frac{\partial \tilde{U}_j}{\partial x_k} - \tilde{\tau}_{jk} \frac{\partial \tilde{U}_i}{\partial x_k} + \varepsilon_{ij} - \Pi_{ij} + \frac{\partial}{\partial x_k}\left[-\overline{\left(t_{kj} u_i^{"} + t_{ki} u_j^{"} \right)} + C_{ijk} \right] + u_i^{"} \frac{\partial \overline{p}}{\partial x_j} + u_j^{"} \frac{\partial \overline{p}}{\partial x_i} \qquad 3.23$$

where

$$\Pi_{ij} = \overline{p' \left(\frac{\partial u_i^{"}}{\partial x_j} + \frac{\partial u_j^{"}}{\partial x_i} \right)} \qquad 3.24$$

$$\varepsilon_{ij} = \overline{t_{kj} \frac{\partial u_i^{"}}{\partial x_k} + t_{ki} \frac{\partial u_j^{"}}{\partial x_k}} \qquad 3.25$$

$$C_{ijk} = \overline{\rho u_i^{"} u_j^{"} u_k^{"}} + \overline{p' u_i^{"}} \delta_{jk} + \overline{p' u_j^{"}} \delta_{ik} \qquad 3.26$$

The closure of the governing equations by the Reynolds stress tensor is considered to be the highest level of closure at this level of modelling. Closure of the averaged Navier-Stokes equations by the Reynolds stress tensor is known as Reynolds Stress Modelling (RSM).

RSM has been applied to natural convection type flows by, for example, Peeters and Henkes (1992), Chen (1996), Saunders, Sarh and Gokalp (1997), Murakami, Kato and Ooka (1994) and Malin and Younis (1990). Although these models have shown improvement over subsequently discussed simpler models, they require considerably more computational effort. In addition, several of the terms in the equations must be modelled and, within the literature, there is still considerable discussion regarding the quality and accuracy of the models used. Hence, for a large or complex simulation scenario RSM is still, at present, unproven.

3.4 Implicit Algebraic Stress Modelling (ASM)

The next level of modelling is to simplify the Reynolds stress tensor to an algebraic relationship. This is known as implicit Algebraic Stress Modelling (ASM), as opposed to explicit algebraic stress models that can be defined as nonlinear eddy-viscosity relationships with coefficients that are functions of the strain and vorticity invariants. The transport equations are reduced to algebraic relationships by neglecting terms not relevant to the flow of interest and modelling other terms where necessary. This type of modelling has had some success as a balance between the complexity, lack of economy and the accuracy of the RSM. Detailed descriptions of the turbulent stress and flux transport equations are given in both Hossain and Rodi (1982) and Launder (1996). These authors give an informative discussion of the assumptions, made by themselves and by others, for second order closure and the simplifications made to form the ASM.

Hossain and Rodi proposed that the Reynolds stress tensor be modelled by equation 3.27 rather than a transport equation.

$$\overline{u_i' u_j'} = \frac{2}{3}\delta_{ij}k + \frac{k}{\varepsilon}\frac{(1-C_3)\left(P_{ij} - \frac{2}{3}\delta_{ij}P\right)}{C_1 + (P + G/\varepsilon - 1)} + \frac{k}{\varepsilon}\frac{(1-C_3)\left(G_{ij} - \frac{2}{3}\delta_{ij}G\right)}{C_1 + (P + G/\varepsilon - 1)} \qquad 3.27$$

$$P_{ij} = \overline{u_i' u_j'}\frac{\partial \overline{U}_i}{\partial x_j};\ P = \tfrac{1}{2}P_{kk} \qquad 3.28$$

$$G_{ij} = -\beta\left(g_i \overline{u_j'\theta} + g_j \overline{u_i'\theta}\right);\ G = \tfrac{1}{2}G_{kk} \qquad 3.29$$

where, C_1 = 3.0; C_2 = 0.5; C_3 = 0.5; g is the gravitational tensor; G_{ij} represents the buoyant production/destruction of the Reynolds Stress tensor.

An intimate knowledge of the physical relevance of each term in the transport equations is important, in order that modelling assumptions and simplifications will not have an adverse affect on the quality of the final solution. The earlier models relied on the experience and depth of knowledge of the modeller, since there was nothing against which to compare the predicted budgets of the turbulent transport equations. More recently, improvements in experimental techniques have enabled prediction of turbulent quantities. In addition, some direct numerical simulations

(DNS) of simple natural convection type flows have been published, as discussed by Dol et al (1997). The results of the experimental data and DNS can be used to estimate the importance of each of the terms in the transport equations, as well as how they interact and, hence, the validity of the modelling assumptions can be judged. Recent work by Dol et al (1997) conducted a "term-by-term comparison of the modelled terms [of the heat flux and temperature variance transport equations] against DNS data". They concluded that most available models poorly reproduce the DNS for the corresponding terms in the exact equations. Despite this, second moment closure models perform reasonably in reproducing mean flow parameters and turbulent statistics.

Gibson and Launder (1976, 1978) are usually credited with the first non-isothermal algebraic stress/flux model. There have also been several successful attempts to apply ASM models to the prediction of plumes (Chen and Rodi (1975), Tamanini (1978), Chen and Chen (1979), Hossain and Rodi (1982), Bergstrom, Strong and Stubley (1990), Shabbir and Taulbee (1990), Pereira and Rocha (1993), Martynenko and Korovkin (1994). Unlike the Gibson and Launder model, many ASM models for buoyant flows make the assumption of equilibrium, i.e. that the local rate of production equals the local rate of dissipation and hence the transport effects can be neglected. This assumption is justified by the argument that the rate at which the flows evolve is so slow that the turbulent transport is negligible.

Work by Bergstrom et al (1990) and Shabbir and Taulbee (1990) did not assume the flow to be in equilibrium. The former authors concluded that it was an unreasonable assumption based on the transport balance for turbulent kinetic energy. The comparison of their simulated results against experimental data showed that "it is clear that the net transport term C_k-D_k [convection - diffusion] is not negligible in the plume. Convection, associated with the entrainment of ambient non-turbulent fluid into the plume, acts to limit the outward transport of turbulent kinetic energy at the edge. Diffusion acts to transport the turbulent kinetic energy away from the area of maximum production…". Shabbir and Taulbee (1990) also looked at the

relevance of the equilibrium assumption as part of a wider investigation into the closure formulations used in ASM models. They concluded that the non-equilibrium version of the equations "did improve the prediction for the vertical heat flux and temperature variance but the comparison [with experimental data] for radial heat flux and shear stress became worse". No consensus has been reached on this subject, as subsequent papers are inconsistent in the inclusion of this equilibrium assumption. Bergstrom et al (1990) also noted that previous models had used the thin shear layer approximation that had been shown, experimentally, to be an unsuitable assumption for vertical buoyant jets (Ramaprian et al (1983) and Kotsovinos (1977)). They did not make this assumption themselves.

The representation of temperature variance also differs between the published models listed above, either the full transport equation for temperature variance was solved or a simplified version that neglects convection and diffusion was used. However, the main point of contention concerning the solution of temperature variance is the determination of the coefficient used in either solution method. Investigation by Shabbir and Taulbee showed that good agreement with experimental values, in some previous studies, was achieved through a large overprediction in temperature variance that results from the inaccurate determination of values for the coefficients.

Hanjalic and co-workers (1993, 1994, 1996) have done much work in the development of ASM for prediction of non-isothermal flows. They note that the ASM model for isothermal flows is obsolete, since intensive research of the RSM model for isothermal flows, has shown it to be a fairly reliable alternative to the k-ε model. The justification for developing the ASM for non-isothermal flows is, partly, a consequence of the immature stage of reliability of the equivalent modelling assumptions and, partly, as hypothesised by Dol et al (1997), that the thermal convection offers a decisive advantage at this level of approximation because of the strong coupling between the velocity and temperature field.

3.5 Eddy-viscosity Models

3.5.1 Linear Eddy-viscosity

The most common method used to describe the Reynolds stresses is the eddy viscosity model. This model is based on the presumption that there is an analogy between the viscous and Reynolds stresses, such that a relationship similar to that proposed by Stokes, equation 3.3, could be used to describe the Reynolds stress. This similarity in the behaviour can be observed experimentally. Boussinesq (1877) proposed the relationship below for time-averaged flows in which the Reynolds stresses are described in terms of the mean strain rates, S_{ij}, and an eddy viscosity, μ_t.

$$-\rho\overline{u_i' u_j'} = \mu_t \bar{S}_{ij} \qquad 3.30$$

This was later generalised and, for compressible flows in the Favre averaged form, as follows:

$$-\overline{\rho u_i'' u_j''} = \underbrace{\mu_t \tilde{S}_{ij}}_{1} - \delta_{ij}\left(\underbrace{\frac{1}{3}\mu_t \frac{\partial \tilde{U}_k}{\partial x_k}}_{2} + \frac{2}{3}\underbrace{\bar{\rho} k}_{3}\right) \qquad 3.31$$

By virtue of continuity term 2 becomes zero for incompressible flows. Term 3 is included to ensure the trace of the Reynolds stresses is not zero.

Dimensional consideration of the eddy-viscosity reveals that it consists of a velocity (ϑ) and a length scale (ℓ) and a dimensionless constant (C), such that:

$$\mu_t = C\bar{\rho}\vartheta\ell \qquad 3.32$$

The numerous models proposed to represent the eddy-viscosity are classified in terms of complexity. The classification system refers to the number of transport equations applied to the solution of the eddy-viscosity. The first models were zero-equation models. These models assumed the eddy-viscosity to be a function of position only. Prandtl (1925) proposed the mixing length hypothesis:

$$\mu_t = \bar{\rho}\ell_m^2\left|\frac{\partial \bar{U}}{\partial y}\right| \qquad 3.33$$

where ℓ_m is the mixing length described by some algebraic relationship and is multiplied by the significant velocity scale. This model had limited success in the prediction of simple flows, but the lack of a general description of ℓ_m and the fact that only a single velocity gradient at a single position was considered, restricted its value severely.

Subsequent developments lead to a description of the eddy-viscosity in which both the velocity and length scales were modelled as transport equations. These models were referred to as two-equations models. This approach allowed for a general description of turbulence in which effects of transport of mean flow, diffusion, production and dissipation of turbulence were accounted for.

Prandtl (1945) and Kolmogorov (1942) proposed that the velocity scale should be modelled as turbulent kinetic energy (k). This has generally been used in subsequent models. The description of the length scale is more subjective and has varied through proposed models. Launder and Spalding (1972) documented the early development in the modelling of the eddy-viscosity model and the various descriptions of the length scale.

The industry standard model is the k-ε model (Harlow and Nakayama (1968), Jones and Launder (1972)) where the eddy-viscosity model is defined as:

$$\mu_t = \bar{\rho}C_\mu \frac{k^2}{\varepsilon} \qquad 3.34$$

The linear eddy-viscosity model has been used with considerable success to predict a wide variety of flows. However, it has a number of well-documented limitations, such as the failure to predict flows with sudden changes in strain rate, streamline curvature effects and swirling flows. The linear model is dependent on the mean

flow field only that, in the case of sudden changes in strain rate, is inappropriate. The normal Reynolds stress anisotropy is also generally badly represented by the linear model. The anisotropy is dependent on the normal mean velocity gradients that are commonly small in the relevant flow, such as plumes, resulting in Reynolds stresses that are approximately equal. These are two examples of where the linear eddy-viscosity model is limited, a discussion of these and further deficiencies is given in Wilcox (1994).

3.5.2 Nonlinear Eddy-viscosity

Nonlinear eddy-viscosity models offer a compromise between second moment closure and linear eddy-viscosity. As has been mentioned, the linear eddy-viscosity model is inadequate for many types of flow. Second moment closure methods (e.g. Reynolds stress models) are comparatively much more computationally expensive and, in complex flows, such as those of interest in the current work, suffer from numerical instabilities. The nonlinear models are still relatively 'new' and their capabilities in buoyant-type flows have not been established. They have been shown to offer an improvement over the linear models in terms of prediction of anisotropy of normal stress and sensitivity to secondary strains, in strongly convective type flows.

The first attempts at the development of a nonlinear model appeared in the early seventies but were not transformed into realistic alternatives to the linear model until the next decade. Speziale (1987) noted that these models had been developed in a "somewhat preliminary fashion" and, as such, "could not be considered to be generally applicable". Pope's (1975) paper employed a number of physical arguments to bound the capability of the model and hence the number of quantities needed to determine the Reynolds stresses. The result of these arguments was to propose that $a_{ij}=a_{ij}(\mathbf{s},\boldsymbol{\omega})$ where a_{ij} was the normalised Reynolds stresses and $\mathbf{s}$ and $\boldsymbol{\omega}$ were representations of the normalised rates of strain and vorticity, respectively. From this proposal, a general stress-strain relation was deduced, "by applying dimensional analysis, imposing invariance under coordinate transformation and

exploiting the tensor properties of U_{ij} [mean velocity] and $\overline{u_i' u_j'}$ [Reynolds stresses]". Statistical methods have also been used to develop nonlinear models; Yoshizawa (1984) used Kraichnan Direct-Iteration Approximation (DIA) formalism.

Since the 1980's interest in nonlinear models has increased and many variants have been proposed (e.g. Speziale (1987), Shih et al. (1993), Craft, Launder and Suga (1993), Lien and Leschziner (1994), Myong and Kasagi (1990), Park and Sung (1995), Yoshizawa (1984) Rubinstein and Barton (1990), Aspley and Leschziner (1998)). A number of these were based on the theory of Pope. The most popular of these have proved to be the Speziale (1987) model (referred to as Speziale's model) and the Craft et al (1993) model (referred to as Craft's model) at various stages of its development. The subsequent discussion concentrates on these two models.

Speziale's model was developed with the intention of broadening the range of applicability of the linear model. The form of the model was inspired by the established similarities between mean turbulent flow of a Newtonian fluid and the laminar flow of a visoelastic fluid. Within the constraint of general coordinate and dimensional invariance, realisabilty and material frame-indifference in the limit of two-dimensional turbulence, Speziale proposed the following quadratic model:

$$\tau_{ij} = -\frac{2}{3}\bar{\rho}k\delta_{ij} + 2C_\mu \frac{k^2}{\varepsilon}\bar{S}_{ij} + 4C_D C_\mu^2 \frac{k^3}{\varepsilon^2}\left(\overset{\cdots}{S}_{ij} - \frac{1}{3}\overset{\cdots}{S}_{kk}\delta_{ij} + \bar{S}_{ik}\bar{S}_{kj} - \frac{1}{3}\bar{S}_{kl}\bar{S}_{kl}\delta_{ij}\right) \qquad 3.35$$

$$\overset{\cdots}{S}_{ij} = \frac{\partial \bar{S}_{ij}}{\partial t} + \bar{U}_k \frac{\partial \bar{S}_{ij}}{\partial x_k} - \frac{\partial \bar{U}_i}{\partial x_k}\bar{S}_{kj} - \frac{\partial \bar{U}_j}{\partial x_k}\bar{S}_{ki} \qquad 3.36$$

$\overset{\cdots}{S}_{ij}$ is the frame-indifferent Oldroyd derivative and C_D=1.68.

Although this model was derived using the principles of continuum mechanics, it claims to be a 'special case' of the more complex nonlinear eddy-viscosity model obtained by Yoshizawa (1984) using Kraichnan's DIA formalism. This model was tested on channel and duct flows and later on a backwards-facing step (Thangam and

Speziale (1992)). The predictions for flows in a square duct correctly show secondary circulations that are observed physically but are beyond the capabilities of the linear model. Predictions of flow over a backwards-facing step showed an improvement over the linear model, in the reattachment length. Lien and Leschziner (1994) tested Speziale's model on a backstep and compared it to a range of other two-equation models and second moment closure models. They found that the model returns a reattachment length similar to that of the standard model but that a secondary recirculation was also predicted. However, it should be noted that the simulations neglected certain terms from Speziale's model. In the current study, a variant of Speziale's model was also tested in which it was combined with the RNG (Renormalisation Group) (section 3.**9**) model. This proved more successful in returning an improved reattachment length compared to the nonlinear model. Rubinstein and Barton (1990) and Mompean (1998) have also successfully combined Speziale's model with the RNG model.

Apsley and Leschziner (1998) proposed a new cubic model. It was tested against Speziale's model on an aerofoil, a diffuser and a backstep. Generally, Speziale's model offered an improvement over the linear models, as well as giving a better prediction than the cubic model for backstep flow. The poor quality of turbulence predictions by the new cubic model over a backstep was considered to be a result of the manner in which the C_μ was sensitised to the strain invariant.

Hwang, Zhu, Massaudi and Ekmann (1993) applied Speziale's model to swirling combustor flow. This study did not find a great improvement in the predictions of the nonlinear model over those of the linear model. It was suggested that this could be a result of using the coefficient proposed by Speziale (1987), optimised for simple shear flows, or that the numerics of their code were of insufficient quality. Later papers have suggested that a cubic model may be more appropriate in swirling flows.

The work done by Craft and colleagues has led to the development of a cubic eddy-viscosity relationship. In its most developed form, it is combined with a LRN (low Reynolds number) k-ε model and a third transport equation for an anisotropy parameter of the stress field, in addition to the coefficients' becoming functions of the stress invariant. The stimulus for the model came from a number of sources: firstly, the computational difficulties found with the ASM models that were previously considered as the main option between linear eddy-viscosity and full second moment closure; secondly, it was observed that, although previously proposed nonlinear models had a similar form, their coefficients varied considerably; thirdly, a cubic model had not previously been derived. The reason given for developing a cubic model was that, although quadratic models can represent turbulent stress anisotropy, they have no effect on the mean velocity of swirling flows or on the flow with streamline curvature.

The cubic nonlinear model was defined as follows:

$$\begin{aligned}\tau_{ij} = & -\frac{2}{3}\overline{\rho}k\delta_{ij} + \mu_t \overline{S}_{ij} \\ & - C_1\mu_t \frac{k}{\varepsilon}\left(\overline{S}_{ik}\overline{S}_{kj} - \frac{1}{3}\overline{S}_{kl}\overline{S}_{kl}\delta_{ij}\right) \\ & - C_2\mu_t \frac{k}{\varepsilon}\left(\overline{\Omega}_{ik}\overline{S}_{kj} - \overline{\Omega}_{jk}\overline{S}_{ki}\right) \\ & - C_3\mu_t \frac{k}{\varepsilon}\left(\overline{\Omega}_{ik}\overline{\Omega}_{jk} - \frac{1}{3}\overline{\Omega}_{kl}\overline{\Omega}_{kl}\delta_{ij}\right) \\ & - C_4\mu_t \frac{k^2}{\varepsilon^2}\left(\overline{S}_{ki}\overline{\Omega}_{lj} - \overline{S}_{kj}\overline{\Omega}_{li} - \frac{2}{3}\overline{S}_{km}\overline{\Omega}_{lm}\delta_{ij}\right)\overline{S}_{kl} \\ & - C_5\mu_t \frac{k^2}{\varepsilon^2}\overline{S}_{ij}\overline{S}_{kl}\overline{S}_{kl} + C_6\mu_t \frac{k^2}{\varepsilon^2}\overline{\Omega}_{ij}\overline{\Omega}_{kl}\overline{\Omega}_{kl}\end{aligned} \qquad 3.37$$

where:

$$\overline{\Omega}_{ij} = \frac{\partial \overline{U}_i}{\partial x_j} - \frac{\partial \overline{U}_j}{\partial x_i} \qquad 3.38$$

It was proposed that the coefficients should be:

C_1=-0.1; C_2=0.1; C_3=0.26; C_4=-10C_μ^2; C_5=-5 C_μ^2; C_6=5 C_μ^2

These were determined through consideration of flow with homogeneous shear, swirling shear and streamline curvature. A functional form of C_μ is used in order that it is still valid in situations where the assumption of local equilibrium is not valid:

$$C_\mu = \frac{0.3}{1+0.35S^{1.5}}\left[1-\exp\left\{\frac{-0.36}{\exp(-0.75S)}\right\}\right] \qquad 3.39$$

$$\text{where } S \equiv \frac{k}{\varepsilon}\sqrt{\frac{1}{2}\left(\frac{\partial \overline{U}_i}{\partial x_j}+\frac{\partial \overline{U}_j}{\partial x_i}\right)^2} \qquad 3.40$$

Craft's model was further developed in order to address deficiencies in near wall regions. It was proposed that introducing a dependence on the second invariant of a_{ij} into the damping functions enabled 'strongly individual variations of components of $\overline{u_i' u_j'}$ to be realistically captured'.

The model was tested on channel flows, impinging jets and the flow around a turbine blade. It performed well and showed an improvement over linear models. However, a defect was found in the simulation of convex surfaces, which was attributed to the values of coefficients.

3.6 Turbulent Kinetic Energy Transport Equation

The equation for turbulent kinetic energy, *k*, can be derived by taking the trace of the Reynolds stresses equation, resulting in the following equation for incompressible flows:

$$\frac{\partial(\overline{\rho}k)}{\partial t}+\underbrace{\frac{\partial\left(\overline{\rho}\overline{U}_j k\right)}{\partial x_j}}_{C_k} = \underbrace{\overline{\tau}_{ij}\frac{\partial \overline{U}_i}{\partial x_j}}_{P_k}+\underbrace{\frac{\partial}{\partial x_j}\left(\mu\frac{\partial k}{\partial x_j}-\overline{\rho}\overline{u_i' u_i' u_j'}-\overline{p' u_j'}\right)}_{D_k} \qquad 3.41$$
$$-\underbrace{\beta g_i \overline{u_i'\theta}}_{G_k}-\overline{\rho}\varepsilon$$

where ε is the dissipation of turbulent kinetic energy per unit mass and is defined below:

$$\varepsilon = \nu \overline{\frac{\partial u_i'}{\partial x_k} \frac{\partial u_i'}{\partial x_k}} \tag{3.42}$$

The non-isothermal Favre averaged form of the *k*-equation is defined as follows:

$$\frac{\partial(\bar{\rho}k)}{\partial t} + \underbrace{\frac{\partial\left(\bar{\rho}\tilde{u}_j k\right)}{\partial x_j}}_{C_k} = \underbrace{\tilde{\tau}_{ij}\frac{\partial \tilde{u}_i}{\partial x_j}}_{P_k} + \underbrace{\frac{\partial}{\partial x_j}\left(\overline{t_{ji}u_i''} - \overline{\rho u_j'' \tfrac{1}{2}u_i''u_i''} - \overline{p'u_j''}\right)}_{D_k} - \underbrace{\beta g_i \overline{u_i''\theta}}_{G_k} - \overline{u_i''}\frac{\partial P}{\partial x_i} + \overline{p'\frac{\partial u_i''}{\partial x_i}} - \bar{\rho}\varepsilon \tag{3.43}$$

where:

$$\bar{\rho}\varepsilon = \overline{t_{ji}\frac{\partial u_i''}{\partial x_j}} \tag{3.44}$$

The general forms of both the incompressible and non-isothermal forms of the equations are similar to the general transport equation. The terms on the right hand side of the equations require more explanation. The two equations will be explained in common, reference to velocity will be made in a general sense but should be recognised as time-averaged or Favre-averaged in the incompressible and non-isothermal equations respectively.

The first term is the shear production of turbulent kinetic energy, P_k, represents the transfer of kinetic energy to turbulent eddies from the mean flow. The second term that appears in different forms in the two equations, represents the molecular diffusion. The third term is a triple correlation and represents the turbulence transported through the fluid by the turbulent eddies. The fourth term is the pressure diffusion term. This represents the transport correlation between pressure and velocity fluctuations. The last term is common between both equations and is the dissipation of turbulent kinetic energy. Physically, it represents the turbulence diffused on a molecular scale from the smallest eddies to viscosity.

The additional terms in the compressible form, pressure-work and pressure-dilation, arise as a result of the density fluctuations.

3.6.1 Modelled Form of Turbulent Kinetic Energy Equation

The current work is concerned with compressible flow at low velocity, and, for this reason, it has been assumed that the time-averaged form of the turbulent kinetic energy equation combined with Favre-averaged velocities is sufficient. The modelled form of the *k*-equations simplifies the complex correlations in order that they can be modelled. The form of the modelled equation is as follows:

$$\frac{\partial(\overline{\rho}k)}{\partial t}+\frac{\partial\left(\overline{\rho}\widetilde{U}_j k\right)}{\partial x_j}=\underbrace{\tau_{ij}\frac{\partial\widetilde{U}_i}{\partial x_j}}_{P_k}+\frac{\partial}{\partial x_j}\left(\mu\frac{\partial k}{\partial x_j}-\tfrac{1}{2}\overline{\rho u_j'' u_i'' u_i''}-\overline{p' u_j''}\right)+\underbrace{\beta g_i \overline{u_i'' \theta}}_{G_k}-\overline{\rho}\varepsilon \qquad 3.45$$

Turbulent transport is generally modelled in an analogy to molecular transport by a gradient diffusion relationship. In section 3.**Error! Bookmark not defined.** an alternative method of modelling the turbulent diffusion was introduced. The pressure diffusion term is generally considered as a part of this analogy:

$$\tfrac{1}{2}\overline{\rho u_j'' u_i'' u_i''}+\overline{p' u_j''}=-\frac{\mu_t}{\sigma_k}\frac{\partial k}{\partial x_j} \qquad 3.46$$

The final term, the turbulent buoyancy production, is considered in the following section.

3.6.2 Turbulent Buoyant Production (G_k)

The temperature velocity correlation in the G_k term has been traditionally modelled with the eddy-diffusivity model, as shown below:

$$-\rho\overline{u_i'\theta} = \underbrace{\frac{\mu_t}{\sigma_T}}_{\Gamma_T}\frac{\partial T}{\partial x_i} \qquad 3.47$$

Defined by the eddy-diffusivity model, G_k is only a function of the streamwise mean temperature gradient. This assumption is inadequate for many flows. For example, in a simple 2-dimensional plume, the streamwise temperature gradient variations are small compared to the cross-stream variations. The shortcoming was addressed by Ince and Launder (1989) through the application of the generalised gradient diffusion hypothesis (GGDH), first proposed by Daly and Harlow (1970), which is defined by:

$$\overline{u_i'\theta} = -C_T\frac{k}{\varepsilon}\overline{u_i'u_j'}\frac{\partial T}{\partial x_j} \qquad 3.48$$

It can be seen that this equation takes all the components of temperature gradient into consideration. This method has since been successfully used in a number of published studies (e.g. Henkes and Hoogendoorn (1992)), in which the Reynolds stress term was modelled by the linear eddy-viscosity relationship (equation 3.**31**). In the current work, the Reynolds stress tensor in the GGDH has also been modelled by a hybrid relationship and a cubic nonlinear eddy-viscosity relationship.

Davidson (1990) proposed a more complex model for the turbulent buoyancy production. In this, a hybrid of an ASM and *k*-ε model was proposed to model the turbulent production of turbulent kinetic energy. The ASM representation of the Reynolds Stress, given in equation 3.27, is reduced and combined with the standard eddy-viscosity relationship. The total Reynolds stress is:

$$\overline{u_i'u_j'} = \left(\overline{u_i'u_j'}\right)_{k-\varepsilon} + \left(\overline{u_i'u_j'}\right)_{ASM} \qquad 3.49$$

Where:

$$\left(\rho\overline{u_i'u_j'}\right)_{k-\varepsilon} = -\mu_t\bar{S}_{ij} + \frac{2}{3}\delta_{ij}\rho k \qquad 3.50$$

$$\left(\rho\overline{u_i'u_j'}\right)_{ASM} = \rho\frac{k}{\varepsilon}\frac{(1-c_3)\left(G_{ij} - \frac{2}{3}\delta_{ij}G\right)}{c_1 + (P+G/\varepsilon - 1)} \qquad 3.51$$

$$G_{ij} = -\beta\left(g_i\overline{u_j'\theta} + g_j\overline{u_i'\theta}\right);\ G = \tfrac{1}{2}G_{kk} \qquad 3.52$$

$$\rho\overline{u_i'\theta} = -\Gamma_T\frac{\partial T}{\partial x_i} \qquad 3.53$$

Thus, in this model, the production of turbulent kinetic energy is modelled in the same way as for the standard model, and a more complex representation of buoyant production of turbulent kinetic energy is used.

3.7 Transport Equation for Dissipation of Turbulent Kinetic Energy

The popularity of the ε-equation to represent the length scale, in the standard k-ε model, results from the early success of the model. ε appears directly in the k-equation and an exact equation from ε can be derived and is given below:

$$\begin{aligned}\bar{\rho}\frac{\partial\varepsilon}{\partial t} + \bar{\rho}\frac{\partial\bar{U}_j\varepsilon}{\partial x_j} = &-2\mu\left[\overline{u_{i,k}'u_{j.k}'} + \overline{u_{k,i}'u_{k,j}'}\right]\frac{\partial\bar{U}_i}{\partial x_j} - 2\mu\overline{u_k'u_{i,j}'}\frac{\partial^2\bar{U}_i}{\partial x_k\partial x_j}\\ &- 2\mu\overline{u_{i,k}'u_{i,m}'u_{i,m}'} - 2\nu\overline{p_{,m}'u_{j,m}'}\\ &+ \frac{\partial}{\partial x_j}\left[\mu\frac{\partial\varepsilon}{\partial x_j} - \mu\overline{u_j'u_{i,m}'u_{i,m}'} - 2\nu\overline{p_{,m}'u_{j,m}'}\right]\end{aligned} \qquad 3.54$$

The comma in the tensor subscripts denotes a spatial derivative. This equation is highly complex and contains a number of double and triple correlations that must be modelled to achieve a solvable equation. The general modelled form of this equation is given below:

$$\frac{\partial(\bar{\rho}\varepsilon)}{\partial t}+\frac{\partial\left(\bar{\rho}\tilde{U}_j\varepsilon\right)}{\partial x_j}=C_{\varepsilon 1}\frac{\varepsilon}{k}\tilde{\tau}_{ij}\frac{\partial\tilde{U}_i}{\partial x_j}+\frac{\partial}{\partial x_j}\left(\left(\mu+\frac{\mu_t}{\sigma_\varepsilon}\right)\frac{\partial\varepsilon}{\partial x_j}\right) \qquad 3.55$$
$$-C_{\varepsilon 2}\bar{\rho}\frac{\varepsilon^2}{k}-C_{\varepsilon 3}\beta g_i\overline{u_i''\theta}$$

This form of the equation is very similar to the modelled *k*-equation (equation 3.45).

From the discussions of Rodi (1993) and various other authors, it becomes apparent that the addition of a buoyancy term in the dissipation equation is a contentious issue. Markatos et al. (1982) adopted the form of the dissipation equation suggested by Rodi i.e. the form given above. They were not satisfied with the physical basis for this and conducted a parametric study on the value of the buoyancy coefficient ($C_{\varepsilon 3}$). The results showed that the addition of the buoyancy term in the dissipation equation had a minimal effect on the solution. In later studies (Markatos and Pericleous (1984)), the buoyancy term in the dissipation equation was completely omitted on the grounds that there was no physical basis for its inclusion. Others (e.g. Heindel et al. (1994) and Henkes and Hoogendoorn (1990)) also found that the form of the buoyancy term in the turbulent dissipation equation makes little difference to the final solution

3.8 Transport Equation for the Rate of Dissipation per unit Turbulent Kinetic Energy

The historical development of the *k*-ω model has been summarised by Wilcox (1991). Although the *k*-ω model was first proposed some time prior to the *k*-ε model (Kolmogorov (1942)), it never achieved the same status, apparently because early formulations were flawed and did not have the general applicability of the latter.

The standard form of the *k*-ω model (Wilcox (1994)) is now considered to be superior to *k*-ε models for the prediction of near-wall or low Reynolds number flow, and for flow with adverse pressure gradients. The main advantages of the *k*-ω model, in such situations, arise from its greater computational robustness.

The general modelled form of the ω equations are given below:

$$\frac{\partial(\bar{\rho}\omega)}{\partial t}+\frac{\partial\left(\bar{\rho}\tilde{U}_i\omega\right)}{\partial x_j}=\frac{\partial}{\partial x_j}\left[\left(\mu+\frac{\mu_t}{\sigma_\omega}\right)\frac{\partial\omega}{\partial x_j}\right]+C_{\omega 1}\frac{\omega}{k}P_k+C_{\omega 3}\frac{\omega}{k}G_k-C_{\omega 2\omega}\bar{\rho}\omega^2 \qquad 3.56$$

3.9 Two-Equation Turbulence Models

In the previous three sections, the transport equations of the turbulent quantities that are fundamental to two-equation turbulence models were presented. This section presented the various combinations of these that form the two-equation models considered in this work. Table 3-1 summarises the references and abbreviations for the considered two-equation models

Model	Model reference	Abbreviation	Model type
Standard k-ε model		Stkε	HRN
Low Reynolds Number k-ε model	Jones and Launder (1973)	JLkε	LRN
	Launder and Sharma (1974)	LSkε	LRN
Renormalisation Group k-ε model	Yakhot and Smith (1992)	RNG	HRN/LRN
Standard k-ω model	Wilcox (1994)	Stkw	LRN
Transformed k-ε model	Menter (1992)	Trke	HRN

Table 3-1: Summary of references and abbreviations for considered two-equation models

General form of k-ε model is given below and table 3.2 summarises the differences between the various models.

$$\frac{\partial(\bar{\rho}k)}{\partial t}+\frac{\partial\left(\bar{\rho}\tilde{U}_j k\right)}{\partial x_j}=\underbrace{\tilde{\tau}_{ij}\frac{\partial\tilde{U}_i}{\partial x_j}}_{P_k}+\frac{\partial}{\partial x_j}\left(\left(\mu+\frac{\mu_t}{\sigma_k}\right)\frac{\partial k}{\partial x_j}\right)+\underbrace{\beta g_i\frac{\mu_t}{\sigma_T}\frac{\partial T}{\partial x_j}}_{G_k}-\bar{\rho}\hat{\varepsilon} \qquad 3.57$$

$$\hat{\varepsilon}=\varepsilon+D$$

$$\frac{\partial(\bar{\rho}\varepsilon)}{\partial t}+\frac{\partial\left(\bar{\rho}\tilde{U}_j\varepsilon\right)}{\partial x_j}=C_{\varepsilon 1}f_1\frac{\varepsilon}{k}(P_k+G_k)+\frac{\partial}{\partial x_j}\left(\left(\mu+\frac{\mu_t}{\sigma_\varepsilon}\right)\frac{\partial\varepsilon}{\partial x_j}\right) \qquad 3.58$$
$$-C_{\varepsilon 2}f_2\bar{\rho}\frac{\varepsilon^2}{k}+E$$

$$\mu_t=\bar{\rho}C_\mu f_\mu\frac{k^2}{\varepsilon};\ \mathrm{Re}_t=\frac{\bar{\rho}k^2}{\mu_t\varepsilon} \qquad 3.59$$

Model	D	C_μ	$C_{\varepsilon 1}$	$C_{\varepsilon 2}$	σ_k	σ_ε	σ_θ
Stkε	0	.09	1.44	1.92	1.0	1.3	0.7
JLkε	$\frac{2\mu_t}{\bar{\rho}}\left(\frac{\partial\sqrt{k}}{\partial x_i}\right)^2$	.09	1.44	1.92	1.0	1.3	0.7
LSkε	$\frac{2\mu_t}{\bar{\rho}}\left(\frac{\partial\sqrt{k}}{\partial x_i}\right)^2$	.09	1.44	1.92	1.0	1.3	0.7
RNG	0	.0085	$1.42-\frac{\eta\left(1-\eta/\eta_0\right)}{1+\beta\eta^3}$ *	1.68	0.7179	0.7179	0.7

Model	f_μ	f_1	F_2	E
Stkε	1.0	1.0	1.0	0
JLkε	$exp[-2.5/(1+Re_t/50)]$	1.0	$1.0-0.3exp(-Re_t)$	$2\frac{\mu\mu_t}{\bar{\rho}}\left(\frac{\partial^2\tilde{U}_i}{\partial x_k\partial x_j}\right)^2$
LSkε	$exp[-3.4/(1+Re_t/50)^2]$	1.0	$1.0-0.3exp(-Re_t)$	$2\frac{\mu\mu_t}{\bar{\rho}}\left(\frac{\partial^2\tilde{U}_i}{\partial x_k\partial x_j}\right)^2$
RNG	1.0	1.0	1.0	0.0

Table 3-22: Summary of coefficients, damping functions and additional terms for considered two equation turbulence models

* η_0=4.38 and β=0.012

The values of the coefficients used in the current work are the standard values, given below:

C_μ=0.09; σ_k=1.0; σ_ε=1.3; $C_{1\varepsilon}$=1.44; $C_{2\varepsilon}$=1.92

C_μ and $C_{\varepsilon 1}$ were determined through consideration of experimental data in boundary layer flow when equilibrium is assumed. Similarly, $C_{\varepsilon 2}$ was determined from experimental data of grid or isotropic turbulence. The values of σ_k and σ_ε were evaluated through optimisation. Launder and Spalding (1972) has described the

determination of these constants in detail. Many alternative values for these have been proposed in the literature. The coefficients that have the largest effect on simulation results tend to be $C_{\varepsilon 1}$, σ_k and σ_ε (Patel, Rodi and Scheuerer (1985), Nam and Bill (1993)). The values of the coefficients used in the current work have been shown to have considerable general applicability and, as such, are retained here in preference to optimising the values for each different simulation.

The summary of differences between the high and low Reynolds number model, given in Table 3-2, shows the added complexity of the JLkε/LSkε models. Damping functions (f_μ, f_1, f_2), based on the turbulence Reynolds number, Re_t, were introduced to sensitise the model to low Reynolds number characteristics of near-wall flows. Unlike many LRN models (e.g. Lam and Bremhorst (1981)), the damping terms are not dependent on the distance from a boundary. Thus the JLkε/LSkε models should be sensitised to low Reynolds number regions of flows other than boundary layers, such as those experienced by plumes.

Additional source terms are also added to the k and ε equations in the JL/LS k-ε models. The D term (the additional term in the k-equation) is a 'fix' in order that the value of ε, considered to be isotropic dissipation, can be set to zero at the wall. The argument for this was that there was a definite numerical advantage in being able to define ε to be zero at solid boundaries. The D term can be derived from an analysis of total dissipation at the wall (Jones and Launder (1972)). The E term in the ε equation has no physical basis; it was introduced in order that the computed peak turbulence in the boundary layer was in accord with experimental results. Patel et al. (1985) give a detailed discussion of the effects and capabilities of the various functions and coefficients which have been proposed in conjunction with these and other low Reynolds number models.

Yakhot and Orszag (1986) derived the k-ε model through RNG theory and achieved equations that were very similar to the standard k-ε model. The RNG k-ε generally implemented in current codes is a revised version (Yakhot and Smith (1992)).

Renormalisation procedures originated from quantum field theory. Zhou et al. (1997) give an informative discussion on the background and theory involved in RNG theory with a history of its application to turbulence. A general description of RNG theory was given by McComb (1985):

'In the context of fluid turbulence, renormalisation group may be seen as a systematic way of progressively eliminating the effect of the smallest eddies; then the next smallest eddies; and so on: and replacing their mean effect by an effective turbulent viscosity. In other words, the molecular kinematic viscosity of the fluid becomes renormalised by the collective interaction of the turbulent viscosity.'

The RNG model is now an established model that has been tested on a wide range of flows and shown generally to give an improvement over the standard k-ε model. Further development has led to the successful combination of RNG k-ε model and nonlinear eddy viscosity models (Barton et al. (1991), Ashworth (1994), Mompean (1998)).

The general modelled form of the k-ω equation is given below and the differences between the models is given in table 3-3.

$$\frac{\partial(\overline{\rho}k)}{\partial t}+\frac{\partial\left(\overline{\rho}\widetilde{U}_j k\right)}{\partial x_j}=\underbrace{\tau_{ij}\frac{\partial\widetilde{U}_i}{\partial x_j}}_{P_k}+\frac{\partial}{\partial x_j}\left(\left(\mu+\frac{\mu_t}{\sigma_k}\right)\frac{\partial k}{\partial x_j}\right)+\underbrace{\beta g_i\frac{\mu_t}{\sigma_T}\frac{\partial T}{\partial x_j}}_{G_k}-\overline{\rho}k\omega \quad 3.60$$

$$\frac{\partial(\overline{\rho}\omega)}{\partial t}+\frac{\partial\left(\overline{\rho}\widetilde{U}_i\omega\right)}{\partial x_j}=\frac{\partial}{\partial x_j}\left[\left(\mu+\frac{\mu_t}{\sigma_\varpi}\right)\frac{\partial\omega}{\partial x_j}\right]+C_{\omega1}\frac{\omega}{k}(P_k+G_k)-C_{\omega2}\overline{\rho}\omega^2+E \quad 3.61$$

$$\mu_t=\overline{\rho}f_\mu\frac{k}{\omega} \quad 3.62$$

$$\mathrm{Re}_t=\frac{\overline{\rho}k}{\mu_t\omega} \quad 3.63$$

Model	α	β_k	β_ω	σ_k	σ_ω	E
Standard k-ω	0.5317	0.09	0.0750	2	2	0.0
Transformed k-ε	0.4403	0.09	0.0828	1.0	1.168	$2\bar{\rho}\sigma_{\omega 2}\frac{1}{\omega}\frac{\partial k}{\partial x_j}\frac{\partial \omega}{\partial x_j}$ *

Table 3-33: Definition of coefficients and additional source terms in k-ω model

* Referred to as cross-diffusion term (*CD*)

The major disadvantage of the standard formulation of the k-ω model (Wilcox (1994)) compared to the k-ε models, is that it is highly dependent on freestream values of ω. Menter (1992) addressed this problem by deriving the ω equation through the transformation of the ε equation. This transformed ε-equation contained an additional cross-diffusion term, '*E*' (table 3-3). The simulations with this transformed model did not exhibit the same inadequacies as the standard formulation. This led to the development of Menter's blended model (Menter (1992)), which included the advantageous features of both the k-ε and the k-ω models. A blending function was introduced as a multiplier to the cross-diffusion term, which increases the influence of the latter with distance from the boundary. The model, thus, effectively switches between the k-ε and k-ω models.

3.10 Closure

The equations that govern the flow and scalar field were presented in this chapter in both their instantaneous and averaged form. The derivation of the averaged form from the instantaneous equation introduces additional terms that are defined by the turbulence models. These are known as the Reynolds stresses in the flow equations and the turbulence scalar flux in the scalar equations.

A discussion of turbulence models has been undertaken with the turbulence models categorised in terms of their complexity. In addition, details of the models implemented in this work are considered.

CHAPTER 4

Numerical Studies of Turbulent Buoyant Jets

4.1 Introduction

This chapter undertakes to review the literature associated with the numerical simulations of natural convective flows and compartment fires. The scope of the review has been expanded beyond the narrow confines of turbulent buoyant jets to natural convective flows in general due to the large amount of work that has been undertaken in this area. This literature review has been arranged by the turbulence models used in the simulations in order to gauge the current level of experience of turbulence modelling in this field. The review of compartment fire simulations is a more general discussion to establish an understanding of the current level of turbulence modelling used in this field.

The initial part of this literature survey focuses on reported natural convection simulations that use turbulence models of comparable complexity to the standard k-ε model. Section 4.2.1 considers literature that utilised alternatives to the k and ε

terms. Low Reynolds number (LRN) models are discussed in section 4.2.2. These models have a similar form to the standard k-ε model but include damping functions to account for LRN flows. Section 4.2.3 reports on the simulations that adopt different coefficients from those that are used with the standard k-ε model.

Application of more complex turbulence models than the standard k-ε model that uses a linear representation of the Reynolds stresses and scalar fluxes is discussed. Section 4.2.4 considers work that has adopted algebraic relationships for individual scalar fluxes; these models are known as algebraic flux models (AFM). These relationships are derived from the transport equations for the scalar fluxes. Section 4.2.4 reviews application of the comparative models for the Reynolds Stresses, known as algebraic stress models (ASM). Finally, section 4.2.6 summarises the limited work published on the applications of higher order turbulence models and representations of such flows. Section 4.3 outline literature published concerning the simulations of compartment fire using CFD techniques.

4.2 Numerical Simulations of Natural Convective Flows

4.2.1 Two-Equations Models

The standard k-ε model is by far the most common turbulence model, although alternatives to these two quantities have been considered. The k-equation is consistently solved for buoyant flows, although alternatives have been considered for other flow types. The dependent variable, which is solved by the second or complementary equations, is often taken to be ε, although a number of alternatives have been proposed (Launder and Spalding (1972)). The popularity of the ε-equation derives from the fact that it appears in the k-equation directly and that it has seen considerable success in its applications. Malin and Spalding (1984) also suggested that this was due to all other dependent variables requiring a near-wall correction term.

In the field of buoyant flows, only two alternatives appear to have been considered. Malin and Spalding (1984) proposed a k-W equation where W is the time mean square of vorticity fluctuation. It was suggested that this model could be a serious competitor to the k-ε equation. However, for free shear flows, it has not been shown to have any particular advantages.

Peng et al (1996, 1997,1999) applied a k-ω model to isothermal and non-isothermal enclosure flows. Peng et al (1996) discussed the advantages of the standard k-ω model (Wilcox (1988)). It does not require damping functions to solve for near wall flows and can either be integrated up to the wall or be combined with wall functions. The lack of damping functions is computationally advantageous since it eliminates the need to solve additional, sometimes complex, terms. Later papers (Peng et al (1997), (1999)) used a modified form of the standard k-ω model (Wilcox (1994)) that included damping functions for application to transitional boundary layers. The simulation of cavities with differentially heated walls (buoyant cavities) has become a standard test case of turbulent models applied to buoyant flows. One of the recognised difficulties in predicting this flow is achieving a grid independent solution. This has often been attributed to the dependence of the onset of transition on the near wall grid density (Henkes and Hoogendoorn (1992)). However, Peng et al (1999) established that the grid dependence is the result of the buoyant turbulent production term when modelled by the eddy diffusivity relationship. A damping function was proposed for this buoyancy term that eliminated this problem. It was also concluded that a model of greater complexity such as the generalised gradient diffusion model would also overcome this problem.

The solution of the ω-equation for LRN flows, such as the buoyant cavity or plume type flows, offers the advantage that ω possesses a solution as k approaches zero. Peng et al (1996) suggested that the k-ω model was thus better able to capture the LRN wall distant flow in buoyant cavities, unlike the LRN k-ε models which predict relaminarisation throughout the cavity (Davidson (1990)).

Despite encouraging results from the k-ω model, the standard k-ε model remains by far the most popular model in most types of flow prediction in CFD.

4.2.2 Low Reynolds Number Flows

The standard k-ε model was developed for application to high Reynolds number (HRN) convective flows. Wall functions are employed to compensate for near wall flows, which are characterised by LRN highly viscous properties.

Wall functions are algebraic relationships that describe the flow in the region adjacent to the wall (boundary layer). The boundary layer is characterised by steep property gradients and hence requires a fine grid to resolve the details of the flow. Wall functions are used to provide a bridge between the wall (solid boundary) and the high Reynolds number region of flow, so that this region does not need to be solved numerically. This method has shown great universality in a wide range of situation, and gives acceptable results for many purposes.

The standard wall functions are derived through consideration of experimental data for forced convection boundary layers. These wall functions have been widely employed in the prediction of both non-isothermal and isothermal flows. However, as pointed out by Hanjalic (1994), the standard wall functions are not appropriate for buoyant flows because they employ the friction velocity as the velocity scale, which, in buoyant flows, is not directly relevant. Hanjalic goes on to discuss, at length, the problems of using wall functions for buoyant flows. Those authors who have used the standard wall functions for buoyant flows (e.g. Markatos and Pericleous (1984), Ooze et al. (1986), Henkes and Hoogendoorn (1990)) have found that they tend to overpredict wall heat transfer and consideration must be given to the near wall grid density.

Thermal wall functions have been proposed (e.g. George and Capp (1979)) but these have only had limited success. Ince and Launder (1989) found the temperature boundary layer prediction in a buoyant cavity was in accord with George and Capp's

wall functions but the velocity boundary layer prediction was not; this was attributed to the low Rayleigh number. Hanjalic (1994) gives a detailed explanation of the inadequacy of George and Capp and other thermal wall functions.

The problems associated with the use of wall functions in buoyant flows have prompted the recommendation that the use of LRN turbulent models is preferable (e.g. To and Humphrey (1986) and Henkes and Hoogendoorn (1990))

LRN k-ε models enable the boundary layer to be solved directly. This type of model was originally developed for isothermal flat plate flows. The LRN effects are accounted for by the inclusion of molecular viscosity in the diffusion terms. In addition, for k-ε type models, the coefficients become a function of some measure of turbulence that introduces a damping effect in areas of low turbulence. Certain models also include these additional source terms.

The use of LRN models in isothermal flows is now well established in the literature. A well-quoted reference that assesses the capabilities of various proposed LRN models for non-isothermal, flat plate flows is Patel, Rodi and Scheuerer (1985). Proposed damping functions in the LRN models can be split broadly into two categories: those that have some dependence on distance from a wall (e.g. Lam and Bremhorst (1981)), and those that do not (e.g. Jones and Launder (1972)).

Buoyant type flows, like displacement ventilation, say, are often characterised by regions of low turbulence, remote from the walls, as well as the viscous boundary layer. Hence, it is preferable to adopt a model that is not dependent on a parameter associated with distance from the wall. For this reason, as well as the fact that the Jones and Launder model is one of the best regarded and well established models, many studies (Henkes and Hoogendoorn) of such flows have adopted it or its later incarnations: Launder and Sharma (1974), Ince and Launder (1989, 1995). The Lam and Bremhorst (1994) model has also been used (Chen (1995), Abib and Jaluria (1995)) in some calculations. However, it has been suggested that all the LRN k-ε

models, developed for boundary layer predictions, are inappropriate for LRN wall distant flow (Davidson (1990)).

Henkes and Hoogendoorn (1989) compared simulations by the most popular LRN turbulence models for a heated vertical plate. Both Patel et al (1985) and Henkes and Hoogendoorn (1989) identified the same three models performing best: Jones and Launder (1972), Lam and Bremhorst (1981) and Chein (1980). Betts and Dafa'Alla (1986) found the Jones and Launder model performed best in tall buoyant cavity predictions.

Simulations of buoyancy flows with LRN models have not been wholly successful. There tends to be considerable variation between the results of different studies. The standard test case for this type of model is generally a buoyant cavity (Henkes and Hoogendoorn (1992)). It is common to gain multiple solutions for a single problem (e.g. Henkes et al. (1991), Heindel et al 1994)), although this has also been observed experimentally (Jaluria and Gebhart (1974)). The critical Rayleigh number also appears to show a dependency on turbulence model (Heindel et al (1994), Ooze et al (1986)).

The LRN models mentioned previously in this section were all developed with the aim of predicting the boundary layer in highly convective flows. This has prompted some authors to propose LRN models specifically developed for buoyant flows (To and Humphrey (1986), Murakami et al (1996), Tannos et al. (1978, 1989), Hwang and Lin (1999), Davidson (1990)).

LRN models have been widely tested in buoyant cavity simulations with limited success. However, the arguments used for their adoption, to enable LRN characteristics of flow remote from a wall to be predicted, can be applied equally for the simulation of plume type flows.

4.2.3 Coefficients

The standard k-ε model includes six coefficients (section 3.9). One appears in the k-equation (σ_k), four appear in the ε-equation ($C_{\varepsilon 1}$, $C_{\varepsilon 2}$, $C_{\varepsilon 3}$, σ_ε) and one in the eddy-viscosity relationship (C_μ). σ_ϕ is the Prandtl-Schmidt number and appears in all scalar transport equations which use a gradient type description to model diffusion.

The coefficients for the standard model are all constant (Launder and Spalding (1974)). They have been shown to have good universality in a wide range of situations. However, the values were developed for convective flat plate flow and their application to flows significantly different from this scenario cannot be expected to be valid.

It is generally accepted (Martynenko and Korovkin (1994) and Tamanini (1978)) that the standard value of the coefficient $C_{\varepsilon 2}$ can lead to an overprediction of spreading rate for forced round jets and that a smaller value appears to improve the prediction. For buoyant jets, however, Tamanini (1978) suggested the standard value was suitable, because the velocity decay is slower. It is also noted that good agreement can still be reached by using a non-standard value of $C_{\varepsilon 2}$ and compensating by changing the coefficient correlated with turbulent buoyant production.

The standard value of $C_{\varepsilon 2}$ that produced excessive spreading in a forced jet led Chen and Chao (1997) to suggest that modification to both C_μ and $C_{\varepsilon 2}$ was appropriate. Their results showed a drastic effect on the predictions of a buoyant turbulent plume and a displacement ventilation system in an enclosure. The alteration in these coefficients resulted in the velocity and temperature spreading rates, for the plume, being overpredicted rather than underpredicted. Similarly, the centreline values for velocity and temperature were underpredicted rather than overpredicted. The velocity, temperature, and concentration in the displacement ventilation calculation were also affected by the modification of the coefficient values. The non-standard

values appear to return a slightly worse result, although this is hard to judge due to the poor quality of experimental data.

Nam and Bill (1993) undertook simulations of thermal plumes above pool fires and heptane spray fires. They postulated that C_μ and σ_h would have the most significant effect on the predicted spreading rate of the plume. Increasing the value of C_μ would reduce the peak values while increasing diffusion. A lower σ_h for enthalpy would increase the temperature width and lower temperature whilst having little affect on the velocity field. Nam and Bill ran numerous simulations until the results produced the best fit with the experimental data and hence a significant improvement over the prediction using the standard coefficients. The paper also considered the effect on ceiling jets, a general conclusion being that reasonable predictions were achieved. However, inadequate experimental data render comparison to the turbulence models unproductive.

Despite the work done to optimise the coefficients, many studies still opt to use the standard values. There are two main arguments for this. First, optimising the values for a specific type of flow may limit their applicability to other flows. Second, changing a coefficient may improve the overall prediction, but this may be the result of one term over-compensating for an inadequate prediction of another.

4.2.3.1 Functional Coefficients

Experimental investigations into the values of some coefficients have revealed that they can rarely be expected to be constant across a flow field. The introduction of functionality into the coefficients can make their values more appropriate and responsive to variations in the flows.

Section 4.4.2 discusses LRN turbulence models. These models have functional coefficients in order that the LRN effects can be taken into account.

Rodi (1972) proposed empirical corrections to compensate for the overprediction in the spreading rate of an axisymmetric forced jet. This correction made two coefficients (C_μ, $C_{\varepsilon 2}$ functions of velocity gradient. The correction was later adopted for use in buoyant axisymmetric jets (e.g. Hossain and Rodi (1982), Shabbir and Taulbee (1990)).

Consideration of algebraic stress and flux model led Sini and Dekeyser (1987) to postulate that the characteristic underprediction of the spread rate in plumes resulted from the lack of the influence of buoyancy on the Reynolds stress and turbulent heat flux. Through purely empirical deduction, they proposed that the eddy viscosity coefficient (C_μ) should be a function of the exit Froude number rather than a constant. The prediction of the spread rate and decay laws compared favourably with experimental values and ASM predictions. However, the centreline velocity prediction was still high, as was the temperatures at the plume edge. The latter discrepancy is attributed to the use of an unsteady elliptical model because the temperature increase was weak at the edges due to transient recirculations. Other authors, who experienced the same discrepancy at the plume edge, have suggested it to be a result of poor experimental data in this region (Malin and Spalding (1984)). The Sini and Dekeyser (1987) model was later adopted successfully by Sini and Dekeyser (1989), Moses, Sini and Dekeyser (1992) and Martynenko and Korovkin (1992).

The Renormalisation Group (RNG) k-ε model (Yakhot and Orszag (1989)) has the same general form as the standard k-ε model but has a functional coefficient for $C_{\varepsilon 1}$ in addition to different values for the other coefficients. This is not a plume specific functionality, but rather the model was developed through the derivation of the k-ε model by RNG techniques. The functionality of the coefficient in this model is thus general to all flows and has gained considerable popularity. This model has been applied to buoyancy-influenced flows by Craig, De Kock and Snyman (1999), Chen (1995) and Chen and Chao (1997). Chen (1995) compared the capabilities of five different k-ε models applied to natural, forced and mixed convection. The RNG

model was recommended in the conclusions as the model that gave consistently good results compared to other models that lacked such generality.

Chen and Chao (1997) considered a buoyant plume and a natural convective displacement ventilation system. The RNG model gave very similar results to the standard k-ε model for the plume, hence underpredicting the spreading rate. Compared to the more complex RSM model, the solutions were far worse. The predictions, by the RNG and standard models, for the velocity and temperature in the displacement ventilation system were similar. However, the RNG model appears to return a better prediction of contaminant concentrations in the room.

4.2.3.2 $C_{\varepsilon 3}$ coefficient

The $C_{\varepsilon 3}$ coefficient is correlated to the buoyant production of turbulence term in the complementary equation. This coefficient deserves special consideration due to the variations in its value in different studies. In this section, only the coefficient is considered; the models used for the buoyant production term (G_k) are discussed in section 4.4.4.

The inclusion of the G_k term in the ε-equation was described as a logical assumption by Hossain and Rodi (1982), since it does not appear in the derivation. Hanjalic and Vasic (1993b) suggest its inclusion was physically correct since in pure buoyant generation of turbulence, like a stagnant fluid heated from below, this is the only remaining source of ε.

Hossain and Rodi (1982) argued that the value of the coefficient was dependent on the orientation of a shear layer. Rodi (1979) proposed a functional relationship for the coefficient based on the Richardson flux. The Richardson flux was defined such that the coefficient varied depending on whether the shear layer was vertical or horizontal.

Markatos et al. (1982) adopted this functional form of the coefficient for their simulations of smoke flows in enclosures. Concerns about the constant multiplied by the Richardson number led them to conduct a parametric study for this value. This showed the inclusion of the G_k term with varying values of $C_{\varepsilon 3}$ had no significant effect. In some subsequent studies (Markatos and Pericleous (1984)), the buoyancy term in the ε-equation was neglected.

Heindel et al. (1994) studied natural convection in enclosures. They also stated that the value of $C_{\varepsilon 3}$ made little difference to their study. However, they did not neglect the term but adopted the Henkes et al. (1991) proposal that $C_{\varepsilon 3}=tanh|v/u|$, where v is the streamwise velocity and u is the cross-stream velocity.

Snider and Andrews (1996) determined a value for $C_{\varepsilon 3}$ from an approximate analytical self-similar solution and then with an accurate numerical solution. Simulations of shear and buoyancy driven mixing layers gave successful predictions using this value of $C_{\varepsilon 3}$. However, the value is problem specific and involved a complex derivation procedure.

4.2.4 Turbulent Heat Flux ($\overline{\rho u_i'' \theta}$) and Turbulent Scalar Flux ($\overline{\rho u_i'' \phi''}$)

4.2.4.1 Introduction

The turbulent heat flux is the correlation of density and velocity and temperature fluctuations. It appears in the buoyant production of turbulence term of the *k-ε* model, in addition to the diffusion term of the transport equation for temperature. Higher order turbulence models may include this term in the model for Reynolds stresses.

An analogous term is the turbulent scalar flux term that, rather than being an averaged velocity temperature fluctuation correlation, is an averaged velocity scalar

fluctuation correlation. The correlation appears in the diffusion term of the relevant scalar transport equation.

The following discussion considers models for these flux terms in order of increasing complexity.

4.2.4.2 Eddy Diffusivity Relationship

This relationship defines the turbulent scalar or heat flux as being proportional to the mean gradient of scalar or temperature gradient respectively it is the most commonly used representation of the turbulent heat and scalar fluxes.

The standard k-ε model includes no contribution from buoyancy. Applying this to the simulations of a plume led to a solution in which the spread rate of the plume is underpredicted (Hossain and Rodi (1982)). A buoyancy production term does appear in the exact equation for turbulent kinetic energy but it was neglected from the original model as it was developed for isothermal flows. Hossain and Rodi incorporated this term into their k-ε model and modelled the turbulent heat flux with the eddy-diffusivity relationship. The inclusion of this term led to a significant widening of the plume profile, although the radial property profiles were still narrow compared with experiment.

The budget of the various terms in the turbulent kinetic energy transport equation has been considered by a number of authors (Malin and Spalding (1984), Sini and Dekeyser (1987)). It revealed that the turbulent buoyancy term modelled with the eddy-diffusivity relationship gave a negative contribution towards the edge of the plume. This is considered physically incorrect since experimental data indicate the term should always be positive.

The budget also predicts a value for the term that is much smaller than that found from experiments. This underprediction is considered a direct result of the inadequacy of the eddy-diffusivity model. For a plume-type flow, the eddy-

diffusivity model only takes account of the vertical mean temperature gradients, whereas the dominant gradients are in the cross-stream direction.

4.2.4.3 Generalised Gradient Diffusion Hypothesis (GGDH)

Ince and Launder (1989, 1995) proposed the use of the GGDH to model the heat flux. This takes account of both cross-stream and streamwise temperature gradients. Accounting for the cross-stream gradients overcomes the major inadequacy associated with the eddy-diffusivity model. In addition, an influence from the Reynolds stresses introduced. Ince and Launder successfully applied this model to differentially heated cavities and it has since been adopted in a number of studies.

The GGDH can also be used to define the turbulent scalar flux terms that appear in the diffusion term. This level of modelling was originally confined to second order turbulence modelling. Recently it has been employed at a two-equation modelling level (e.g. Davidson (1990)).

4.2.4.4 Algebraic Flux Model (AFM)

The next level of complexity, after the GGDH, is the use of an AFM. This model is derived from the transport equation for heat flux. The transport equation is simplified, through neglect of and modelling of various terms, to an algebraic relationship.

This approach has drawn considerable interest in the field of buoyant flows but the models have not yet reached a mature and reliable state (Chen and Rodi (1975), Tamanini (1978), Chen and Chen (1979), Hossain and Rodi (1982), Bergstrom, Strong and Stubley (1990), Shabbir and Taulbee (1990), Pereira and Rocha (1993), Martynenko and Korovkin (1994)). Discrepancies exist between the various published studies that have adopted this model. Despite this, Hanjalic (1994) argued that AFM was the most appropriate level of modelling for buoyant type flows. This conclusion was achieved by consideration of the question '… whether and to what

extent, the specific organisation of turbulent structures, preferential scales and other structural peculiarities affect the statistically averaged quantities, and, if they do, can those effects be adequately accounted for by mathematical tools employed by single point closure methods?'. Hanjalic argued that, since some success had already been claimed in dealing with this non-standard behaviour when using higher order modelling schemes, rather than k-ε models and the eddy-viscosity/diffusivity relationship, this was the minimum level of complexity suitable for buoyant flows. However, the solution of the full transport equations for Reynolds stresses and turbulent heat flux was still perceived as too complex and involving too many modelling uncertainties. The AFM was thus seen as the best compromise between the inadequate eddy-diffusivity models and the overly complex solution of the transport equations.

Many of the AFMs have a similar form and drawn on earlier studies such as Gibson and Launder (1976). Authoritative work by Hossain and Rodi (1982) and Hanjalic (1994) and Dol et al (1997) give detailed insights into the various assumptions and models used for AFM.

There are a number of factors that vary between AFMs, the most significant of which are: whether the equilibrium assumption is invoked; the number of transport equations solved, that is, whether transport equations for temperature fluctuation and dissipation of temperature fluctuation are solved; and the value of the coefficients in the model.

Equilibrium Assumptions

The local equilibrium assumption implies that the rate at which the flow develops is slow enough that turbulent transport is negligible. Physically, this is interpreted as the effects of convection and diffusion balancing and hence being neglected. For the *k*-equations, the production and dissipation terms balance. For heat flux and Reynolds stress transport equations, the sum of production and pressure correlation terms balance the molecular destruction terms.

Bergstrom, Strong and Stubley (1990) applied a non-equilibrium model to a vertically buoyant vertical jet. This paper identifies that previous studies have generally invoked the equilibrium approximations. Consideration of the budget of *k* reveals that the equilibrium assumption is inappropriate. The production-dissipation balance is non-negligible. 'Therefore, although the equilibrium models succeed in predicting most of the mean flow behaviour, the turbulence model is inconsistent.' (Bergstrom et al.). These authors found that unlike previous studies (e.g. Hossain and Rodi (1982)) that also introduced the thin shear layer approximation and solved the resultant equations parabolically, the mean flow prediction was realistic. Bergstrom et al. did not invoke the thin shear layer approximation and solved the equations elliptically. Reasonable predictions for turbulence were returned.

The thin shear layer approximation assumes all the derivatives for statistically-averaged quantities in the streamwise direction are much smaller than those in the cross-stream direction and can be neglected from the calculations. This type of assumption is numerically advantageous since the equations are parabolic rather than elliptical. Physically, this means there is no influence from the downstream flow. 'Haroutunian and Launder (1986) have shown that the application of the thin shear layer approximation leads to significant errors in computing the turbulence character of vertical plume' (Pereira and Rocha (1993)).

A recent study by Shabbir and Taulbee (2000) considered the experimental budgets of heat fluxes and Reynolds stresses for an axisymmetric buoyant jet. Consideration of these budgets led the authors to conclude that the equilibrium assumption was suitable for the heat flux but not for the Reynolds stresses. This is contrary to the suggestion of Tamanini (1978) who suggested the equilibrium assumption was appropriate to the Reynolds stresses and not the heat flux.

Temperature Fluctuations

Early papers (e.g. Gibson and Launder (1976)) adopted a generalised gradient type relationship for temperature fluctuation. The justification for this was 'temperature fluctuation appears in a less prominent position in the model than do turbulent kinetic energy and dissipation of turbulent kinetic energy'. Many later papers adopted the same relationship although the value of the coefficient has been found to vary between 1.6 (e.g. Gibson and Launder) and 0.7 (e.g. Peeters and Henkes (1992)). Hanjalic (1994) reported that experimental data have shown that this coefficient cannot be considered a constant.

Hanjalic gave a detailed review of the various models that have been used in the simulations of buoyant flows. The question of whether a transport equation should be solved for temperature fluctuations or whether a gradient-type relationship is adequate was addressed. The gradient-type relationship had been found to be surprisingly successful in certain flow types but was less successful in more complex types of buoyant flow, such as high aspect ratio cavities with differentially heated walls. To improve generality, Hanjalic proposes that solution of the full transport equation is necessary. Other papers (e.g. Pereira and Rocha (1993), Hanjalic, Kenjeres and Durst (1996)) have adopted the full transport equations in calculations.

ε_T

Hanjalic (1994) interpreted ε_T as 'the rate of thermal variance which is being transferred through the thermal turbulence spectrum towards the finer scales where it will ultimately be dissipated under the action of molecular forces, it is obvious that this cascading process will be controlled not only by the dynamics of thermal turbulence, but also by mechanical turbulence'. This term appears in the transport equations for temperature fluctuation and in the AFM, but it is normally neglected from the latter. Hence, the modelling of ε_T generally only becomes an issue when the transport equation for temperature fluctuation is modelled.

The most common method of modelling this term is to take advantage of the time scale ratio ($R=\tau_T/\tau$: the ratio of thermal timescale to mechanical timescale). Substitution of this term into the steady-state transport equation for temperature fluctuation, where the equilibrium assumption has been made, results in the GGDH definition of temperature fluctuation. Buoyant jet simulations, in the literature, are found to have a value of R that varies considerably (Shabbir and Taulbee (1990)). This variation of R reflects the uncertainty in the modelling of this term with a values since it has been shown to vary depending on the flow type and even within a given flow, e.g. plumes (Shabbir and Taulbee). A variety of functional relationships has been proposed to represent this term. These have generally been concerned with near wall flows (Dol et al (1997)).

More generality and better predictions could be achieved through modelling a transport equation for ε_T. Pereira and Rocha (1993) have taken this approach for buoyant jets and Hanjalic et al. (1996) for a partitioned two-dimensional cavity. However, the modelling of this equation is not well tested. Variations are apparent between studies, predominantly in the values of the coefficients adopted.

4.2.5 Modelling of Reynolds Stresses

4.2.5.1 Introduction

The Reynolds stresses appear in the averaged momentum equations and turbulent shear production term. They can appear in the scalar diffusion term, depending on the model employed. The Reynolds stresses are the correlation of fluctuating velocities and density. Physically, the term represents a stress on the fluid.

As has been mentioned previously in this chapter, the standard model of the eddy-viscosity relationship is characterised by the underprediction of spreading rate. Hossain and Rodi (1982) suggested that this could be explained by the lack of influence of buoyancy on the eddy-viscosity relationship. This conclusion was supported by a number of other studies that introduced some buoyant influence into

the eddy-viscosity relationship. However, these changes generally involve changing the values of coefficients (Nam and Bill (1993)) or introducing some functionality to the coefficient (Sini and Dekeyser (1987)). These ad hoc changes tend to be plume specific and offer no general advantage.

4.2.5.2 Algebraic Stress Models (ASM)

The ASM is a more complex alternative to the eddy-viscosity model, however it has still gained considerable popularity. This model is analogous to the AFM in that an algebraic relationship is derived from the transport equations through a series of assumptions and models. All those studies that used an ASM also adopted an AFM.

The ASM/AFM approach has shown improvements in the spreading rate (Hossain and Rodi (1982)). The direct effect of the ASM on plume predictions, however, has not been assessed since those studies that include an ASM model also include a variety of other factors.

The basic form of the ASM is generally consistent between the various studies. Variations between studies do appear in the values of the coefficients and the use of the equilibrium assumptions.

4.2.5.3 Hybrid Model

Davidson (1990) proposed a hybrid model, which combined the eddy-viscosity relationship and the ASM. Effectively, this model is the eddy-viscosity model summed with a non-isotropic part due to buoyancy taken from the ASM. Davidson quotes two disadvantages of the ASM model as reasoning for developing the hybrid approach: firstly, that the ASM models are computationally more expensive; and secondly, they are much less stable. This model was originally developed for application to buoyant cavities but has since been adopted for plume type flows (Yan and Holmstedt (1998), Liu and Wen (1999)). The results for both a plane and axisymmetric plume offered by Yan and Holmstedt showed a considerable widening

of the plume over the buoyancy corrected standard k-ε model. Comparisons of the k calculations between this model and previous ASM model yield reasonably good agreement. A GGDH model was also included for turbulent buoyant production, which makes it hard to judge whether the improvements in spreading rate prediction were a result of the hybrid model or the improved buoyant turbulent production model.

4.2.6 Higher Order Models

The continuous increase in available computing power enables ever more complex models to be solved practically. Approaches such as Reynolds stress modelling, direct numerical simulation and large eddy simulations are not yet common for buoyant flows, but studies are now being undertaken in this field.

The RSM approach solves the full transport equations for the turbulence quantities that appear in the averaged governing equations. Although this method has the obvious disadvantage of computational expense, it facilitates a far more accurate representation of the turbulence field. Some studies of buoyant flows using RSM have been undertaken: Chen (1996) considered room air motion; Peeters and Henkes (1992) considered boundary layers on heated vertical plates; Malin and Younis (1990) considered turbulent buoyant plumes; and Saunders, Sarh and Gökalp (1997) consider the variable density effects in an isothermal jet. All these papers show that the RSM is essential to gain an accurate prediction of the turbulence field, but predictions of the mean fields by the RSM and simpler models are similar.

Direct numerical simulations (DNS) solve the instantaneous governing equations directly, thereby eliminating the need for a turbulence model. These models become very computationally expensive since it is necessary to resolve all the eddy-scales in the flow down to the dispersive level, thus requiring a very small grid. A number of studies have been undertaken for buoyant flows. These have generally been aimed at providing details of turbulence structure, for which experimental methods are unreliable. The details for DNS can then be used to assess the quality of predictions

returned by less complex turbulence models (Dol et al. (1997)). DNS for buoyant simulations tend to be concerned with buoyant-cavity type flows (e.g. Xin and Le Quéré (1995)). Dol et al. summarises a number of other studies. Xin and Le Quéré (1995) make comparisons between DNS and standard k-ε prediction in buoyant cavities. Although no direct comparison is made, clear differences are seen in mean and turbulent predictions. The authors conclude that utilisation of a low Reynolds number model or RSM is necessary.

Large eddy simulation (LES) is based on solving the exact equations for large-scale turbulence and modelling the small-scale turbulence. A number of studies using LES on atmospheric smoke flows have been reported (e.g. McGrattan et al. (1998), Baum et al. (1999)).

4.3 Numerical Simulations Compartment Fire

The requirement for an ability to predict compartment fires can be realised on two levels. Firstly, to enable fire safety engineers to design buildings that offer maximum possible protection in the event of a fire (Cox (1994)). Secondly, as a tool for fire scientists to improve and confirm their knowledge of the physical characteristics and possibly chemical processes involved in compartment fires (e.g. Abib and Jaluria (1995)).

The prediction of the characteristics of a compartment fire through mathematical descriptions is called deterministic modelling. This can broadly be considered in two categories: zone modelling and field modelling. Zone modelling divides a fire environment into zones. The zone is a region of characteristic flow, for example the fire plume or ceiling layer. Each zone is considered as a thermodynamic control volume to which the conservation laws are applied in the full differential or a reduced form. Zone models are the most popular method within the industrial fire engineering community due to their simplicity and low running cost. However, they require a user of considerable experience to break down an environment into zones and then ensure that there is adequate interaction between the various zones.

Despite inadequacies, this approach is well established and has a proven track record.

Field models adopted the principles of CFD to solve the velocity and temperature fields and can be combined with sub-models to describe other physical processes such as combustion, fire spread, soot formation and radiation. They remove the many of the limitations and crudity of zone models but are considerably more expensive and more common as a research tool. However, their future potential to provide a detailed picture a compartment fire from ignition to extinction ensures continuing interest and research. At their present level of development, field models are capable of reliably providing a detailed description of velocity and temperature field for a stationary fire.

A broad introduction into deterministic modelling for compartment fires is give by Kumar (1983) and Cox (1994).

The neglect of a combustion and radiation model is common among published studies on field models; modelling both these processes is complex and expensive. A fixed heat release rate (HRR) can be used to represent the heat input from a fire. Radiative loss can be taken into account by reducing the HRR by an assumed percentage. The subsequent discussion will refer to this approach as basic field modelling.

Chow (1995a), Rho and Ryou (1999) modelled atria using both basic field and zone models. Atria are a common feature of many modern buildings, however prescribed safety guidance for this type of enclosure generally lacks good scientific basis. Deterministic modelling enables the risk to a building from fire to be assessed and studied. A safe building design can be produced based on modelled results. Both studies achieved similar solutions from zone and field models in terms of the layer height. The advantage of the field model is that it provides a more detailed picture of the thermal and velocity field. It is, however, more expensive.

The comparison of simulation results to experimental data is referred to as a validation process. It is important as the capabilities of the models are tested and it is demonstrated, to the wider community, that realistic predictions are possible. Unfortunately, the expense involved in experimental studies means only a limited amount of data is available for validation. Data sets are generally confined to temperature and velocity measurements in a simple cavity.

Chow (1995a) studied the temperature and velocity field predictions by a field and zone model for a series of experimental scenarios. The first of these scenarios (Steckler et al. (1982)) has also been used in a number of other studies (e.g. Hadjisophocleous and Cacambouras (1993)). The Steckler compartment consisted of a compartment (2.8 x 2.8 x 2.18 m) with a single opening of varying size. Measurements of velocity and temperature were taken in the opening for a 62.9 kW methane fire at various locations within the compartment. Chow (1995a) ran simulations for a door (1.0 x 1.8 m) with the fire source opposite against the back wall.

The replication of the experimental conditions for the simulation of the Steckler compartment require the pressure field to be prescribed at the door, these measurements were not available. This was avoided in the majority of simulations by extending the computational domain outside the compartment, in effect including a corridor outside the compartment. Simulation and experimental results were compared at the doorway, Chow showed both the field and zone models returned good results. Chow and Yin (1999) considered the influence of different definitions for the ambient boundary. A large hall (30 x 30 m) with a centrally located fire with a varying heat release rate was considered. The results showed that variation in the calculation method for the ambient boundary had a notably affect on the simulations.

Kerrison et al. (1994) and Mawhinney et al. (1994) considered the Steckler cavity with the fire in a number of locations around the cavity. They found that predictions

with the fire adjacent to a wall or in the corner were worse than those remote from the wall. Among the reasons given for this was the treatment of the wall boundary conditions. The experimental walls were insulated with asbestos that prompted the authors to use adiabatic (perfectly insulated) wall conditions. Allowing for wall heat transfer would improve the predictions. Chow (1995b) also models a 40 kW corner fire and found the temperatures were underpredicted but no details of the boundary conditions are given so it is hard to reach any conclusions about this result.

The second experiment simulated by Chow (1995b), was a two-room structure (total length 7.0 x 3.45 x 2.17 m) (Nakaya, Tanaka and Yoshida (1986)). The end distant from the fire had an opening (1.8 x 1.8 m) and the two rooms were partitioned by a door (1.6 x 0.89 m). A propane burner was located centrally in the burn room (length 3.55 m), HRR of 86 kW, 170 kW, 340 kW and 600 kW were considered. The results from Chows' simulations from both the field and zone models get progressively worse as the HRR increases. In general, although the trends were well predicted, the actually values of temperature were not, by either the zone or field model.

The solution stability for the higher heat release rates was not found to be good by Chow. This was addressed by gradually increasing the HRR in the simulations. The problem of stability and speed of convergence are a major considerations in field modelling and careful consideration of initial condition can often substantially increase stability and reduce require computational time and hence expense. The developments in techniques that are able to improve the solution procedure are of considerable interest. One approach is to use group solvers. This technique localises the major numerical effort to regions of the computational domain with the most significant processes (Ewer et al. (1999)).

A second, 2-room simulation by Chow (1995b) with a fire of 250 kW was based on the experiments of Hagglund (1992). The quality of the results was found to be dependent on the configuration of external vents. The predicted temperatures

returned by the lesser-ventilated scenarios were overpredicted. The experimenter also compared the experimental data against field model simulations and was reported as having achieved good predictions.

The ventilation of compartments has been a dominant feature of other studies. Sanderson et al (1999) simulated the Steckler cavity with an opening of varying size. The temperature became progressively more overpredicted with the reduction in ventilation area, when a basic field model was employed. However, the inclusion of a radiation model in the simulations resulted in good predictions compared to the experimental data.

A study by Sinai (1999) was also concerned with ventilation. A complex 2-storey building (overall dimensions 17.3 x 9.0 x 5.0 m) with a heptane fire was simulated. The fire was located on the second floor, which was a balcony surrounding the whole building. There were also a number of partial walls. Unlike Chows' simulations, combustion and radiation models were employed in addition to conjugate heat transfer. Simulations initially assumed the building was completely sealed. Conventional stratification, as observed in the experiments, was predicted for this case as the pyrolysis was linked to thermal radiation, however the fire diminished as oxygen was consumed. Leakages (openings to the ambient environment) were introduced to the calculation by a crude method. An experimentally estimated global leakage was divided between various leakage points. The observed stratification collapsed in this case. With the leakage points defined more accurately, the stratification was observed and a reasonable prediction of the trends in temperature with time was predicted.

The modelling of combustion has been the subject of considerable research effort but is generally considered in the context of small-scale flame simulations (Someya (1993)) which will not be discussed here. However, their inclusion in compartment fires makes possible a description of the distribution of the chemical species involved in the combustion process. This is of great interest since smoke and carbon

monoxide are the major contributors to fatalities in fires. Further, the future of field modelling of fires is the ability to predict actual compartment fires accounting for fire spread over building contents, for which a combustion model is essential. Lewis et al. (1997) demonstrated the inclusion of a combustion model, rather that a prescribed heat source, can improve the prediction of compartment fires. The combustion model improves the description of the heat source, since it becomes spatially distributed.

Luo and Beck (1994) and Luo et al. (1997) have considered simulations of a multi-room building as a validation exercise. Luo and Beck (1994) considered a propane burner (300 kW) and considered a field model that included a sub-model for radiation and combustion. The field model prediction compared well with both experimental and zone model predictions for both transient and steady state fires. There was a slight improvement in the prediction of chemical species by the field model compared to the zone model. Further, it is concluded that for an accurate prediction of radiative flux, radiation from soot must be accounted for and the effects of the gaseous combustion products should be included in the gas absorption coefficient.

Luo et al. (1997) considered a similar multi-room experimental rig but for a flashover fire for which polyurethane mattresses were burnt. In addition to the combustion and radiation modelling, a simple fire spread model was used. The simple model enabled the mass and heat release rate to be predicted rather than providing prescribed values, unlike zone models. Both the field and the zone model return reasonable estimates. The field models gave better predictions in the burn room, whereas the zone model gave better predictions in the adjoining rooms. The over-prediction of temperature by the field model in the adjoining rooms is attributed to the gas phase combustion model.

The simulation of compartment fire using basic field models is now a well-regarded procedure in both the research and industrial communities. General popularity

among fire safety engineers for the procedure will increase as the computational costs of simulations decrease. There are a number of important aspects that must be considered during simulations that have been highlighted in the preceding discussion: boundary conditions, initial conditions, correct description of ventilation and adequate account of radiation.

4.4 Closure

This chapter provided a literature review of papers concerned with the simulation of natural convective flows and combusting fire simulations. The scope of the review was governed by the interest of the current work. The broad subject of natural convective flows was considered, rather than being limited to buoyant jets, due to the large body of relevant literature in the field and the limited number of papers considering buoyant jets.

The review of numerical studies of natural convective flows was presented by the category of turbulence model used in the study. At the level of 2-equation modelling, the underprediction of the spreading rate of a buoyant jet is a recognised limitation. Alternatives to the standard k-ε model that have been considered appear to offer no improvement in prediction, although an advantage in computational stability is noted (section 4.2.1). The application of low Reynolds number (LRN) models to buoyant cavity type flows is common although success has been limited, with considerable variation between studies. The most established LRN model is the Launder and Sharma model, the main advantage of this, in the application to buoyant flow, is that the damping functions are not solely applicable to near wall flows (section 4.2.2).

The coefficients of the standard k-ε models (section 4.2.3) have been subject to considerable variability in terms of both value and functionality. The majority of work in this field has been to develop flow specific coefficients that can reduce the generality of the model. However, the RNG model that adopts a functional value for

one of the model coefficient was derived in general terms and, as such, could offer benefit in the prediction of all flows.

A substantial number of publications exist concerning the modelling of the turbulent temperature flux. These demonstrate that there are still inconsistencies between studies concerning aspects of the modelling (section 4.2.4). The higher order modelling of the Reynolds stresses (section 4.2.5) has not been so intensively studied in direct relation to natural convective flows. However, the mentioned underprediction in spreading rate is often considered to be a result of a lack of buoyant influence in the linear eddy-viscosity relationship. This has led to the use of algebraic stress models (ASM) that take account of buoyancy. A limited number of studies with the Reynolds stress model (RSM) and models of higher complexity have been undertaken. The conclusion of studies of the RSM was that they only have a significant influence on the turbulent field. Models of higher complexity are not practically applicable but have use in the provision of validation data.

The review of published studies of compartment fire simulations demonstrated that the use of basic field models for stationary fires is now a well-regarded procedure, although the computational expense can still be prohibitive. The main points of concern in many studies is for there to be good description of boundary condition and for adequate account to be taken of the radiative heat loss.

CHAPTER 5

Numerical Implementation

5.1 Introduction

This chapter presents the procedures followed in the implementation of the models discussed in chapter 3. The current work uses an existing research code, SOFIE (Simulation of Fires in Enclosures) (Rubini (1999)), as an established base into which the models could be introduced. SOFIE is a finite volume code that utilises a curvilinear, non-orthogonal, co-ordinate system. The finite volume method is a procedure in which the solution domain is divided into a number of finite volumes to form a grid or mesh. The nomenclature used to describe the grid in this report is given in figure 5-1. The equations governing fluid flow are integrated over each control volume, approximated and discretised to produce a set of linear equations. The discretisation process reduces the derivatives, in the governing equations, to a series of differences applied over the control volumes. The resulting set of linearly algebraic equations relates the fluid properties of local cells. Boundary conditions are specified for a solution domain and thus are accounted for in the equations relevant to the boundary control volumes. The set of linear algebraic equations is solved iteratively to achieve a prediction of the overall flow and thermal field.

The concepts required to transform the governing equations into the curvilinear co-ordinate system are presented in section 5.2 and the transformed governing equations are given in section 5.3. The application of the finite volume method to the governing equation is discussed in section 5.4 and the general form to which they are reduced for storage and solution is detailed in section 5.5. The treatment of the various terms of the transport equation during the implementation can have a significant effect on the stability and convergence of the solution. Sections 5.6 and section 5.7 detail the methods adopted in the implementation of the convection and diffusion terms and the source term, respectively. The treatment of the generalised gradient diffusion hypothesis (GGDH) model in its application to the diffusion term of the scalar transport equations is considered in section 5.8. The implementation of the nonlinear eddy-viscosity models is discussed in section 5.9.

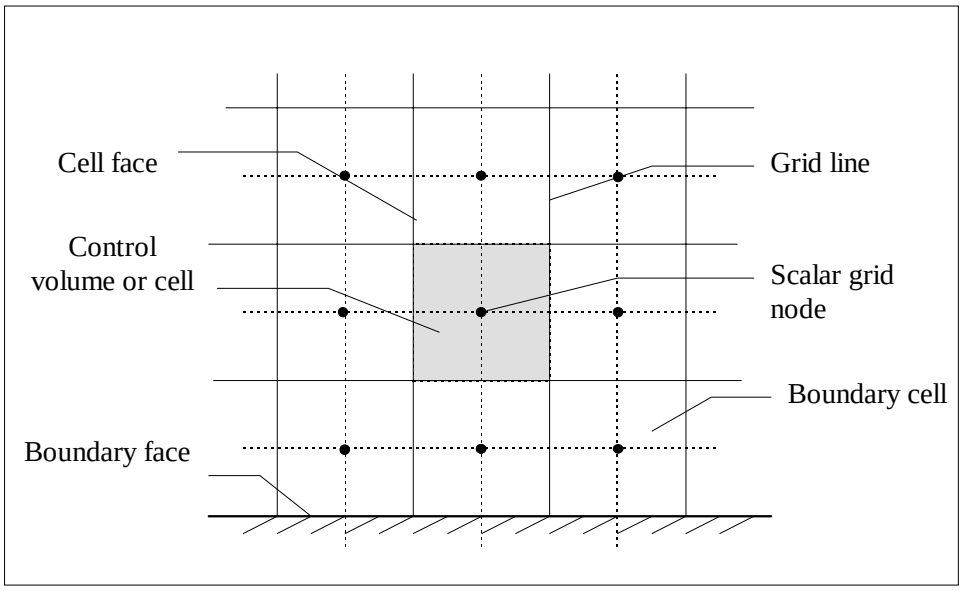

Figure 5-1: Grid nomenclature.

5.2 Curvilinear Non-Orthogonal Coordinate System

The curvilinear non-orthogonal coordinate system allows the grid to be fitted to a non-uniform geometry that allows for a better representation of the flow features than a regular orthogonal grid. Figure 5-2 (left) gives an example of such a geometry in 2-dimensions. The boundary grid line is chosen such that ξ_i = constant at the boundary and the grid lines intersect at arbitrary angles. The solution of the governing equations in physical space (figure 5-2 (left)) is possible, but complex. The complexity arises because of the discretisation and interpolations being conducted on distorted cells. Although the area, volume, and base vectors in the equations have a physical representation, they can be complex and have nonlinear descriptions.

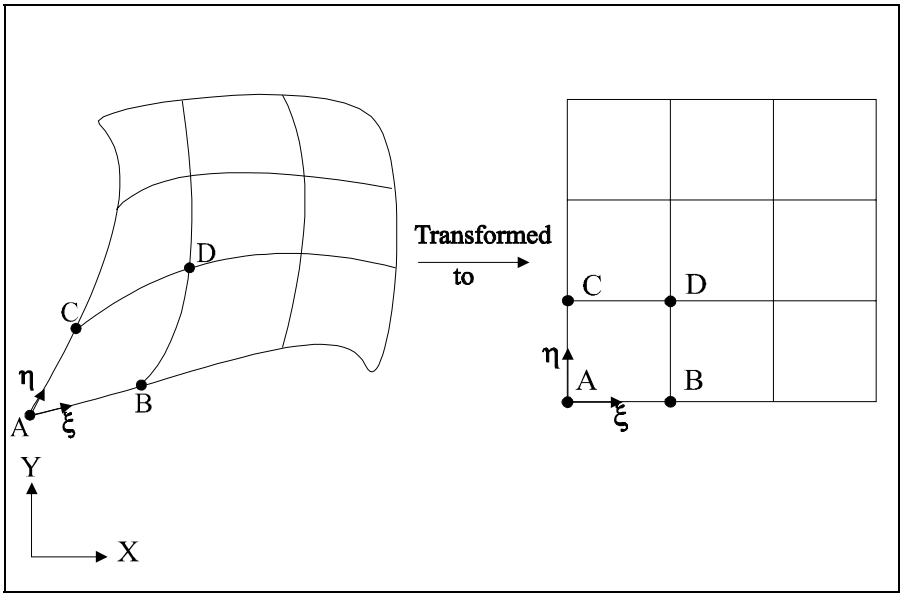

Figure 5-2: Example of a two-dimensional grid transformation

This problem is overcome by transforming the grid to a regular orthogonal grid in computational space (figure 5-2 (right)). This transformation is demonstrated in figure 5-2. The curvilinear coordinate system in the physical plane is mapped to the regular orthogonal grid (transformed grid) in computational space. All grids are transformed in this manner, in addition to axisymmetric grids. A one to one mapping exists between the physical space (described in terms of x_i=(x,y,z)) and

computational plane space (described in terms of $\xi_i=(\xi,\eta,\zeta)$). That is, referring to figure 5-2, the points A,B,C,D on the physical grid can be directly related to points A,B,C,D on the computational grid.

The governing equations are thus transformed into computational space. The discretisation can then be conducted on a regular, linear grid. It should be noted, however, that the transformation procedure could introduce some complex curvature terms.

The derivation of the transformation will not be given here in detail, full details can be found in Peric (1985). The basic transformation can be associated with the chain rule:

$$\frac{\partial \phi}{\partial x_i} = \frac{\partial \xi_j}{\partial x_i}\frac{\partial \phi}{\partial \xi_j} = \alpha_i^j \frac{\partial \phi}{\partial \xi_j} \qquad 5.1$$

The α_i^j term is referred to as the metric coefficient. For ease of manipulation the metric is used in the following form, this is sometimes called the inverse transformation:

$$\alpha_i^j = \frac{1}{\mathrm{J}}\beta_i^j \qquad 5.2$$

Where:

$$\beta_1^l = \frac{\partial x_2}{\partial \xi_m}\frac{\partial x_3}{\partial \xi_n} - \frac{\partial x_2}{\partial \xi_n}\frac{\partial x_3}{\partial \xi_m}$$
$$\beta_2^l = \frac{\partial x_1}{\partial \xi_m}\frac{\partial x_3}{\partial \xi_n} - \frac{\partial x_1}{\partial \xi_n}\frac{\partial x_3}{\partial \xi_m} \qquad 5.3$$
$$\beta_3^l = \frac{\partial x_1}{\partial \xi_m}\frac{\partial x_2}{\partial \xi_n} - \frac{\partial x_1}{\partial \xi_n}\frac{\partial x_2}{\partial \xi_m}$$

$$\mathrm{J} = \det(\beta_i^j) \qquad 5.4$$

In CFD applications derivatives are approximated numerically by taking differences over adjacent cells, hence:

$$\frac{1}{\mathrm{J}}\beta_i^j \approx \frac{1}{\mathrm{J}} b_i^j \qquad 5.5$$

Expansion of equation 3.5 for $\beta_1{}^1$ gives:

$$\beta_1^1 \approx \frac{1}{\delta\xi_1\delta\xi_3}\left[\left(\delta x_2\right)_2\left(\delta x_3\right)_3 - \left(\delta x_2\right)_3\left(\delta x_3\right)_2\right] = \frac{1}{\delta\xi_1\delta\xi_3} b_1^1 \qquad 5.6$$

Where:

$$\begin{aligned}
\left(\delta x_2\right)_2 &= (x_{2_N} - x_{2_S}) \\
\left(\delta x_3\right)_3 &= (x_{3_T} - x_{3_B}) \\
\left(\delta x_2\right)_3 &= (x_{2_t} - x_{2_b}) \\
\left(\delta x_3\right)_2 &= (x_{3_n} - x_{3_s})
\end{aligned} \qquad 5.7$$

The transformed grid is defined with grid cell dimensions of unity. This has a distinct computational advantage, since, the term $\partial\xi_I$=1, effectively disappears from the calculation.

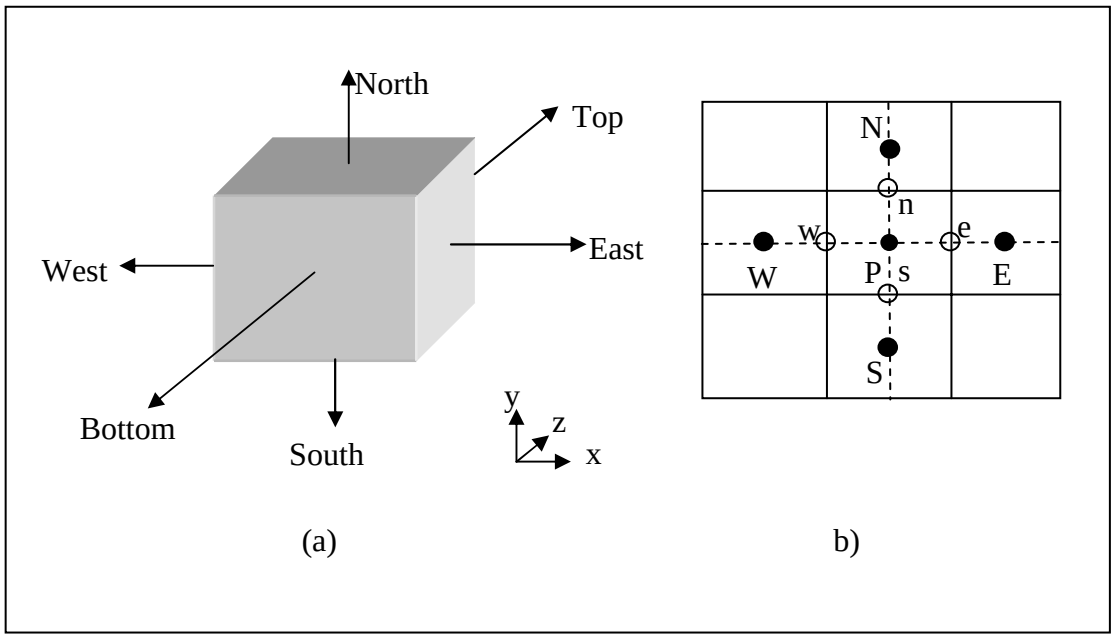

Figure 5-3: (a) 3-dimensional view of a single cell with directional nomenclature. (b) 2-dimensional view of cell connectivity. Capital letters represent cell centres and lower case represent faces.

The following discussions include the expansion of the equations over a typical cell, the nomenclature used to describe this typical cell and the adjacent cells is based on points of a compass, with top and bottom for the third dimension. Figure 5-3 shows this nomenclature.

5.3 Transformed Governing Equations

The transformation procedure presented in the previous section is applied to the governing equations (equations 3.15 to 3.17), giving:

$$\frac{\partial \overline{\rho}}{\partial t} + \frac{1}{\mathrm{J}} \frac{\partial}{\partial \xi_\beta} \left(\overline{\rho} \widetilde{U}_j \beta_j^\beta \right) = S_{cont} \qquad 5.8$$

$$\frac{\partial \left(\rho \widetilde{U}_i \right)}{\partial t} + \frac{1}{\mathrm{J}} \frac{\partial}{\partial \xi_\beta} \left(\overline{\rho} \widetilde{U}_j \widetilde{U}_i - T_{ij} \right) \beta_j^\beta = S_{mom} \qquad 5.9$$

$$\frac{\partial \left(\overline{\rho} \widetilde{\phi} \right)}{\partial t} + \frac{1}{\mathrm{J}} \frac{\partial}{\partial \xi_\beta} \left(\overline{\rho} \widetilde{U}_j \phi - q_j \right) \beta_j^\beta = S_\phi \qquad 5.10$$

Where:

$$T_{ij} = -p\delta_{ij} - \frac{1}{\mathrm{J}} \left(\mu + \mu_t \right) \left(\frac{\partial \widetilde{U}_i}{\partial \xi_n} \beta_j^n + \frac{\partial \widetilde{U}_j}{\partial \xi_m} \beta_i^m \right) \qquad 5.11$$

$$q_j = \Gamma_\phi \frac{\partial \widetilde{\phi}}{\partial \xi_n} . \frac{1}{\mathrm{J}} \beta_j^n \qquad 5.12$$

5.4 Finite Volume Method

The basis of the finite volume method is the integration of the governing equations over the control volumes. The integrated equations are discretised, resulting in a system of linear, interrelated equations. These can be solved iteratively to gain a prediction of the whole flow field and other scalars under consideration.

In this section, the procedure used to discretise the general scalar transport equation is considered. The following discussion is restricted to the turbulence quantities although the general methods can be applied to any scalar. The general scalar transport equation given in equation 5.10, is presented here in a more compact form:

$$\frac{\partial\left(\bar{\rho}\tilde{\phi}\right)}{\partial t} + div(Trans_{\phi}) = S_{\phi} \qquad 5.13$$

Where:

$$Trans_{\phi} = \frac{1}{\mathrm{J}}\left(\bar{\rho}\tilde{U}_j\tilde{\phi} - q_j\right)\beta_j^{\beta} \qquad 5.14$$

Equation 5.13 is integrated over a general control volume (*c.v.*), to give:

$$\int_{c.v.} \frac{\partial\left(\bar{\rho}\tilde{\phi}\right)}{\partial t} dV + \int_{c.v.} div(Trans_{\phi}) dV = \int_{c.v} S_{\phi} dV \qquad 5.15$$

The Gauss Divergence Theorem[1] is applied to give:

$$\int_{c.v.} \frac{\partial\left(\bar{\rho}\tilde{\phi}\right)}{\partial t} dV + \int_{s.a.} Trans_{\phi}.\vec{\mathrm{n}} dA = \int_{c.v} S_{\phi} dV \qquad 5.16$$

The left-hand side of the equation is then discretised, giving:

$$\frac{\bar{\rho}_P\tilde{\phi}_P - \bar{\rho}_P^o\tilde{\phi}_P^o}{\delta t} dV_P + Trans_{\phi}.A|_e - Trans_{\phi}.A|_w + Trans_{\phi}.A|_n - Trans_{\phi}.A|_s + Trans_{\phi}.A|_t - Trans_{\phi}.A|_b = \int_{c.v.} S_{\phi}.dV \qquad 5.17$$

[1] The Gauss divergence theorem states:

$$\int_{c.v} div\vec{V} dV = \int_{s.a} \vec{\mathrm{n}}.\vec{\mathrm{V}} dA$$

This can be interpreted physically as the integral of the divergence of a vector **v** over a volume (*V*) and is equal to the component of **v** in the direction normal to the surface (**n** is the unit vector normal to the surface) which bounds the volume summed over the entire bounding surface *A*.

The superscript '*o*' represents the previous time-step in a transient calculation. The transient term is not considered in detail in the current work.

5.5 Discretised Equations

The prediction of the flow field is achieved through the iterative solution of the discretised equations; hence, the equations must be reduced to a convenient form for numerical manipulation. The form used is shown below in equation 5.18,

$$a_p \phi_p = \sum_n a_n \phi_n + S_p \qquad 5.18$$

'*a*' represents the coefficient multiplying the scalar, ϕ, for the control volume under consideration ($_p$) and the neighbouring control volumes ($_n$). S_p represents the source term.

The coefficients in equation 5.18 are generally derived from the convection and diffusion terms (section 5.6). The source terms include all those terms that differentiate the various scalar equations, and as such can include terms that are functions of the relevant scalar.

The source term is generally treated as two components, as shown below:

$$S_p = S_p^{'} + S_p^{''} \phi_p \qquad 5.19$$

Where $S^{'}$ is the constant component and $S^{''}$ is a coefficient of the scalar. The value of the scalar in equation 5.19 is assumed to be constant over the control volume. This procedure is known as source term linearisation and is adopted to improve the stability and convergence of the solution.

Equation 5.19 is incorporated into equation 5.18, to give

$$\underbrace{\left(a_p - S_p^{''}\right)}_{term\ 1} \phi_p = \underbrace{\sum_n a_n \phi_n}_{term\ 2} + \underbrace{S_p^{'}}_{term\ 3} \qquad 5.20$$

There are four basic rules that were proposed by Patankar (1980) to promote a stable physical solution.

Rule 1: Consistency at control-volume faces. A flux across a face common to two adjacent control volumes must be represented by the same expression in the relevant discretised equation.

Rule 2: Positive coefficients. There is an influence from a neighbouring grid point on the scalar as a given point, as seen in equation 5.18. Hence, an increase in the scalar at one grid point will lead to an increase in the neighbouring grid points. Thus, the coefficients in equation 5.18 must have the same sign.

Rule 3: Negative-slope linearisation of the source term. The S'' term must be less than or equal to zero in order to prevent term 1 in equation 5.20 becoming negative, hence, ensuring compliance with rule 2.

Rule 4: Sum of the neighbouring coefficients. In the case of a governing differential equation only containing derivatives of the dependent variables, the coefficient a_P, must equal the sum of the neighbouring coefficients. Hence $a_p = \Sigma a_n$

An equation of the form given in equation 5.20 and exists for each internal node and of a similar form for each boundary node. The difference arises from the incorporation of the boundary conditions into the equations.

There are a number of different algorithms that can be applied to the solution of equation 5.20. The details of the algorithm shall not be discussed in detail here. The methods used in the current work were TDMA (Tri-Diagonal Matrix Algorithm) (Versteeg and Malalasekera (1995)) or SIP (Strongly Implicit Procedure) (Stone (1968)). These methods can be subject to numerical instability, it is thus important to arrange the equations in the most stable possible form.

5.6 Treatment of Convective and Diffusive Terms

The last section presented the general form of the equations to be solved. The focus in this section is the treatment of the convection and diffusion terms to define them in this general form. Initially in the general scalar transport equation is considered and then the momentum transport equations.

5.6.1 Transport Terms for General Scalar Transport Equation

Equation 5.10 defined the transport terms for a general scalar and, from equation 5.17, it has been shown that these terms must be evaluated at a given face ($_f$), hence:

$$Trans_{\phi}\Big|_f = \frac{1}{\mathrm{J}}\left(\rho\tilde{U}_j\tilde{\phi} - q_j\right)\beta_j^{\beta}\Big|_f \qquad 5.21$$

Consider first the convective term (C_j). This can be represented as a flux term (F_j) multiplied by the scalar, to be evaluated at a given face ($_f$):

$$C_{\mathrm{j}}\Big|_f = \left(\overline{\rho}\tilde{U}_j\beta_j^{\beta}\tilde{\phi}\right)_f = F_{\mathrm{j}}\Big|_f\tilde{\phi}_f \qquad 5.22$$

The expansion of this term on, for example, the east ($_e$) face of a cell gives:

$$C_{\mathrm{j}}\Big|_e = \underbrace{\rho_e\left(\tilde{U}_1\beta_1^1 + \tilde{U}_2\beta_2^1 + \tilde{U}_3\beta_3^1\right)_e}_{F_j|_e}\tilde{\phi}_e. \qquad 5.23$$

SOFIE uses a co-located system for storing data. For this, all the velocity and scalar quantities are stored at the cell centres but the fluxes are stored at the cell faces.

The diffusion term (D_j) is defined by:

$$D_j\Big|_f = q_j\beta_j^{\beta}\Big|_f = \frac{\Gamma_{\phi}}{\sigma_t}\frac{\partial\tilde{\phi}}{\partial\xi_{\mu}}\beta_j^{\mu}\beta_j^{\beta}\Big|_f = \frac{\Gamma_{\phi}}{\sigma_t}\frac{\partial\tilde{\phi}}{\partial\xi_{\mu}}B_{\mu}^{\beta}\Big|_f \qquad 5.24$$

Expansion of this term leads to a normal (*ND*) and a cross derivative (*CD*) component, such that:

$$D_j = D_{ND} + D_{CD} = \frac{\Gamma_\phi}{\mathrm{J}} \frac{\partial \tilde{\phi}}{\partial \xi_\mu} B_\mu^\mu + \frac{\Gamma_\phi}{\mathrm{J}} \frac{\partial \tilde{\phi}}{\partial \xi_\mu} B_\mu^\beta \Big|_{\mu \neq \beta} \qquad 5.25$$

In common with the convective term, this must be evaluated at each face of each cell. The derivatives components are evaluated at the face by using differencing techniques. As an example, the east face is considered here:

$$\begin{aligned} \left. \frac{\partial \tilde{\phi}}{\partial \xi_1} \right|_e &= \frac{\tilde{\phi}_P - \tilde{\phi}_E}{\delta \xi_{1_e}} \\ \left. \frac{\partial \tilde{\phi}}{\partial \xi_2} \right|_e &= \frac{\tilde{\phi}_{ne} - \tilde{\phi}_{se}}{\delta \xi_{2_e}} \\ \left. \frac{\partial \tilde{\phi}}{\partial \xi_3} \right|_e &= \frac{\tilde{\phi}_{te} - \tilde{\phi}_{be}}{\delta \xi_{3_e}} \end{aligned} \qquad 5.26$$

The normal derivative $\partial\phi/\partial\xi_i$ is calculated by central differencing, using the nodal values. The cross derivative terms require differencing of the face values, which are calculate from averaging of stored nodal values.

The resulting terms are:

$$D_j = \frac{\Gamma_\phi}{\mathrm{J}} \Big|_e \tilde{\phi}_P B_1^1 - \frac{\Gamma_\phi}{\mathrm{J}} \Big|_e \tilde{\phi}_E B_1^1 + \frac{\Gamma_\phi}{\mathrm{J}} \Big|_e \left[\left(\tilde{\phi}_{ne} - \tilde{\phi}_{se} \right) B_1^2 + \left(\tilde{\phi}_{te} - \tilde{\phi}_{be} \right) B_1^3 \right] \qquad 5.27$$

In section 5.5, the form of the equation to be solved was presented. The convective, diffusive and source terms are now shown, for the east face component only, in terms of this equation:

$$\begin{aligned} a_e &= \mathrm{F_e} - \frac{\Gamma_\phi}{\mathrm{J}} B_1^1 \Big|_e \\ S &= \frac{\Gamma_\phi}{\mathrm{J}} \Big|_e \left[\left(\tilde{\phi}_{ne} - \tilde{\phi}_{se} \right) B_1^2 + \left(\tilde{\phi}_{ne} - \tilde{\phi}_{se} \right) B_1^3 \right] \end{aligned} \qquad 5.28$$

5.6.2 Transport Terms for Momentum Transport Equation

The transport terms of the momentum equation (equation 5.9) are also evaluated at a face ($_f$):

$$Trans_{velocity}\Big|_f = \frac{1}{\mathrm{J}}\left(\bar{\rho}\tilde{U}_j\tilde{U}_i - T_{ij}\right)\beta_j^{\beta}\Big|_f \qquad 5.29$$

Where:

$$T_{ij} = \bar{p}\delta_{ij} - \frac{1}{\mathrm{J}}\mu\left(\frac{\partial\tilde{U}_i}{\partial\xi_m}\beta_j^m + \frac{\partial\tilde{U}_j}{\partial\xi_n}\beta_i^n\right) \qquad 5.30$$

The expanded form of equation 5.29 can be written as:

$$\begin{aligned} Trans\big|_{velocity} &= \frac{1}{\mathrm{J}}\left(\underbrace{\bar{\rho}\tilde{U}_j\beta_j^{\beta}}_{F_j\big|_f}.\tilde{U}_i + \frac{1}{\mathrm{J}}(\mu+\mu_t)\left[\frac{\partial\tilde{U}_i}{\partial\xi_m}B_m^{\beta} + \underbrace{\frac{\partial\tilde{U}_j}{\partial\xi_n}\beta_i^n}_{w_{ji}}\beta_j^{\beta}\right] + \bar{p}\delta_{ij}\beta_j^{\beta}\right)\Big|_f \\ &= \frac{1}{\mathrm{J}}\left(F_j\big|_f\tilde{U}_i + \underbrace{\frac{\mu+\mu_t}{\mathrm{J}}\left(\frac{\partial\tilde{U}_i}{\partial\xi_m}B_m^m\right)}_{ND}\right)\Big|_f \\ &\quad + \frac{1}{\mathrm{J}}\left(\underbrace{\frac{\mu+\mu_t}{\mathrm{J}}\left(\underbrace{\frac{\partial\tilde{U}_i}{\partial\xi_m}}_{d\tilde{U}_{i,m}}B_m^{\beta}\right)\Big|_{m\neq\beta}}_{CD} + \frac{\mu+\mu_t}{\mathrm{J}}w_{ji}\beta_j^{\beta} + \bar{p}\delta_{ij}\beta_j^{\beta}\right)_f \end{aligned} \qquad 5.31$$

As was the case for the general scalar equation, the diffusion term is decomposed into a normal-derivative and a cross-derivative term. However, unlike the scalar equation, there is an additional set of gradient terms to be calculated.

The flux term F_j is treated in the same way as for the general scalar in equation 5.23.

The velocity derivative in computational space, $dU_{i,m}$, is calculated and stored at a cell centre, for example the calculation for the *U*-component gives:

$$\begin{aligned} d\tilde{U}_{1,1} &= \frac{\tilde{U}_W - \tilde{U}_E}{2} \\ d\tilde{U}_{1,2} &= \frac{\tilde{U}_N - \tilde{U}_S}{2} \\ d\tilde{U}_{1,3} &= \frac{\tilde{U}_T - \tilde{U}_B}{2} \end{aligned} \qquad 5.32$$

The difference of these stored values is taken to find a face value as is shown in equation 5.33.

Considering equation 5.31 for the *u*-component of velocity and for the east face of a control volume gives:

$$\begin{aligned} Trans\big|_{velocity} &= \frac{1}{\mathrm{J}}\left(F_j\big|_e \left(\tilde{U}_p - \tilde{U}_E\right) + \frac{\mu+\mu_t}{\mathrm{J}}\left(\left(\tilde{U}_P - \tilde{U}_E\right)B_1^1\right)\right) \\ &+ \frac{1}{\mathrm{J}}\left(\begin{array}{l} \frac{\mu+\mu_t}{\mathrm{J}}\left(d\tilde{U}_{1,2}\big|_P - d\tilde{U}_{1,2}\big|_E\right)B_2^1 \\ + \frac{\mu+\mu_t}{\mathrm{J}}\left(d\tilde{U}_{1,3}\big|_P - d\tilde{U}_{1,3}\big|_E\right)B_3^1 \\ + \frac{\mu+\mu_t}{\mathrm{J}}\left(w_{11}\beta_1^1\big|_e + w_{21}\beta_2^1\big|_e + w_{31}\beta_3^1\big|_e\right) + (\bar{p}_P - \bar{p}_E)\beta_1^1 \end{array} \right) \end{aligned} \qquad 5.33$$

The face velocity derivatives were calculated explicitly and then multiplied by face values of the effective viscosity and Jacobian. The form of this equation to be solved for the east face components only is:

$$\begin{aligned} a_{\mathrm{e}} &= F_e - \frac{\mu+\mu_t}{\mathrm{J}}B_1^1\Big|_e \\ \mathrm{S} &= \frac{\mu+\mu_t}{\mathrm{J}}\Big|_e \left[\begin{array}{l} \left(d\tilde{U}_{1,2}\big|_P - d\tilde{U}_{1,3}\big|_E\right)B_2^1 + \left(d\tilde{U}_{1,3}\big|_P - d\tilde{U}_{1,3}\big|_E\right)B_2^1 \\ + w_{11}\beta_1^1 + w_{21}\beta_2^1 + w_{31}\beta_3^1 \end{array} \right] \\ &\quad + (\bar{p}_P - \bar{p}_E)\beta_1^1 \end{aligned} \qquad 5.34$$

5.7 Treatment of Source Terms

The treatment of the source terms in a scalar transport equation can be of considerable importance to the speed of convergence and the stability of a solution. In this section, the implementations of the source terms of the turbulent transport equations are considered.

The source terms in the *k*-equation can be described physically as a turbulent production by shear stress (P_k), turbulent production by buoyancy forces (G_k) and dissipation of turbulent kinetic energy ($-\rho\varepsilon$). The source terms of the standard and RNG k-ε model are:

$$S_k = P_k + G_k - \rho\varepsilon \qquad 5.35$$

$$S_\varepsilon = C_{\varepsilon 1}\frac{\varepsilon}{k}P_k + C_{\varepsilon 3}G_k - C_{\varepsilon 2}\rho\frac{\varepsilon^2}{k} \qquad 5.36$$

For the LRN k-ε model the source terms are:

$$S_k = P_k + G_k - \rho\varepsilon \qquad 5.37$$

$$S_\varepsilon = C_{\varepsilon 1}\frac{\varepsilon}{k}P_k + C_{\varepsilon 3}G_k - C_{\varepsilon 2}\rho\frac{\varepsilon^2}{k} + E \qquad 5.38$$

For the transformed k-ω model the source terms are:

$$S_k = P_k + G_k - \rho k\omega \qquad 5.39$$

$$S_\varepsilon = C_{\omega 1}\omega P_k + C_{\omega 3}G_k - C_{\omega 2}\rho k\omega^2 + CD \qquad 5.40$$

The transformed turbulent shear production term is defined as:

$$P_k = \frac{\mu_t}{\mathrm{J}^2}\left(\frac{\partial\tilde{U}_i}{\partial\xi_n}\beta_j^n + \frac{\partial\tilde{U}_j}{\partial\xi_m}\beta_i^m\right)\left(\frac{\partial\tilde{U}_i}{\partial\xi_\alpha}\beta_i^\alpha\right) \qquad 5.41$$

The source terms are linearised, as was discussed in section 5.5. Table 5-4 summarises the linearised form of source terms for the k-ε models and Table 5-5 for the k-ω model to give:

	Source terms			
Model	$S_k^{'}$	$S_k^{''}$	$S_\varepsilon^{'}$	$S_\varepsilon^{''}$
Standard and RNG k-ε	$G_k + P_k$	$-\frac{\rho_p \varepsilon_p}{k_p}$	$C_1 \frac{\varepsilon_p}{k_p} P_k$	$C_2 \frac{\rho_p \varepsilon_p}{k_p}$
LRN k-ε	$G_k + P_k$	$-\frac{\rho_p \varepsilon_p}{k_p} - \frac{D}{k_p}$	$C_1 f_1 \frac{\varepsilon_p}{k_p} P_k + E$	$C_2 f_2 \frac{\rho_p \varepsilon_p}{k_p}$

Table 5-4: Source terms for the k-ε turbulent models in linearised form

	Source terms			
Model	$S_k^{'}$	$S_k^{''}$	$S_\omega^{'}$	$S_\omega^{''}$
k-ω	$G_k + P_k$	$-\frac{\rho_p \varepsilon_p}{k_p}$	$C_1 \frac{\varepsilon_p}{k_p} P_k$	$C_2 \frac{\rho_p \varepsilon_p}{k_p}$

Table 5-5: Source terms for the k-ω turbulent model in linearised form

5.8 Generalised Gradient Diffusion Hypothesis (GGDH) Diffusion Model

The method of implementation adopted for the GGDH diffusion model (section 3.**Error! Bookmark not defined.**) was optimised to enable simplicity within the existing structure of the code.

Implementation of the eddy-diffusion model was presented in the context of the whole transport equation in section 5.6. In order to retain the existing code structure with the implementation of the GGDH model, an effective viscosity was introduced. Consider the diffusion term, D_j, for a given scalar, ϕ:

$$D_j = \frac{1}{\mathrm{J}} \frac{\partial}{\partial \xi_\beta} \left(\frac{\mu}{\sigma_l} \frac{\partial \phi}{\partial \xi_n} \frac{1}{\mathrm{J}} \beta_j^n - \overline{\rho u_j^{''} \phi^{''}} \right) \beta_j^\beta \qquad 5.42$$

The inclusion of the eddy-diffusion model in this term results in:

$$D_j = \frac{1}{\mathrm{J}}\frac{\partial}{\partial \xi_\beta}\left(\left(\frac{\mu}{\sigma_l}+\frac{\mu_t}{\sigma_\phi}\right)\frac{\partial \phi}{\partial \xi_n}\frac{1}{\mathrm{J}}\beta_j^n\right)\beta_j^\beta \qquad 5.43$$

For the GGDH model this term is represented by:

$$\begin{aligned} D_j &= \frac{1}{\mathrm{J}}\frac{\partial}{\partial \xi_\beta}\left(\frac{\mu}{\sigma_l}\frac{\partial \phi}{\partial \xi_n}\frac{1}{\mathrm{J}}\beta_j^n + C_\phi \frac{k}{\varepsilon}\overline{u_j^{"}u_k^{"}}\frac{\partial \phi}{\partial \xi_l}\frac{1}{\mathrm{J}}\beta_k^l\right)\beta_j^\beta \\ &= \frac{1}{\mathrm{J}}\frac{\partial}{\partial \xi_\beta}\left(\underbrace{\left(\frac{\mu}{\sigma_l}+\mu_{eff}\right)\frac{\partial \phi}{\partial \xi_n}\frac{1}{\mathrm{J}}\beta_j^n}_{\text{term 1}} + \underbrace{\mu_{eff}\frac{\partial \phi}{\partial \xi_l}\frac{1}{\mathrm{J}}\beta_k^l\Big|_{k\neq j}}_{\text{term 2}}\right)\beta_j^\beta \end{aligned} \qquad 5.44$$

Where:

$$\mu_{eff} = C_\phi \frac{k}{\varepsilon}\overline{\rho u_j^{"}u_k^{"}} \qquad 5.45$$

The treatment of the term 1 remains the same as for the eddy-diffusion model and terms 2 is incorporated into the source terms. Hence, the effective viscosity, μ_{eff}, replaces the μ_t/σ_ϕ term in the standard calculation.

The Reynolds stress tensor, which appears in the GGDH diffusion model, has been defined by the linear and cubic nonlinear eddy-viscosity (section 3.5) in addition to the hybrid relationship (section 3.6.2). The definition for the effective viscosity with each of these models is given below.

Linear eddy-viscosity model:

$$\mu_{eff} = C_\phi \frac{k}{\varepsilon}\left(-\mu_t S_{ij} + \tfrac{2}{3}k\delta_{ij}\right) \qquad 5.46$$

Cubic eddy-viscosity model:

$$\mu_{eff} = C_\phi \frac{k}{\varepsilon}\left(\begin{array}{l} -\mu_t \bar{S}_{ij} + \frac{2}{3}\rho k \delta_{ij} \\ + c_1 \mu_t \frac{k}{\varepsilon}\left(\bar{S}_{ik}\bar{S}_{kj} - \frac{1}{3}\bar{S}_{kl}\bar{S}_{kl}\delta_{ij}\right) \\ + c_2 \mu_t \frac{k}{\varepsilon}\left(\bar{\Omega}_{ik}\bar{S}_{kj} - \bar{\Omega}_{jk}\bar{S}_{ki}\right) \\ + c_3 \mu_t \frac{k}{\varepsilon}\left(\bar{\Omega}_{ik}\bar{\Omega}_{jk} - \frac{1}{3}\bar{\Omega}_{kl}\bar{\Omega}_{kl}\delta_{ij}\right) \\ + c_4 \mu_t \frac{k^2}{\varepsilon^2}\left(\bar{S}_{ki}\bar{\Omega}_{lj} - \bar{S}_{kj}\bar{\Omega}_{li} - \frac{2}{3}\bar{S}_{km}\bar{\Omega}_{lm}\delta_{ij}\right)\bar{S}_{kl} \\ + c_5 \mu_t \frac{k^2}{\varepsilon^2}\bar{S}_{ij}\bar{S}_{kl}\bar{S}_{kl} + c_6 \mu_t \frac{k^2}{\varepsilon^2}\bar{\Omega}_{ij}\bar{\Omega}_{kl}\bar{\Omega}_{kl} \end{array}\right) \qquad 5.47$$

Hybrid model:

$$\mu_{eff} = C_\phi \frac{k}{\varepsilon}\left(-\mu_t S_{ij} + \tfrac{2}{3}k\delta_{ij}\right) + \rho\frac{k}{\varepsilon}\left(\frac{1-C_3}{C_1}\right)\left(G_{ij} - \tfrac{2}{3}\delta_{ij}G\right) \qquad 5.48$$

where;

$$\rho G_{ij} = \beta \frac{\mu_t}{\sigma_T}\left(g_i \frac{\beta_j^m}{J}\frac{\partial T}{\partial \xi_m} + \frac{\beta_i^n}{J}\frac{\partial T}{\partial \xi_n}\right) \qquad 5.49$$

5.9 Nonlinear Eddy-Viscosity models

This section presents the implementation of the nonlinear models discussed in section 3.5.2. The nonlinear eddy-viscosity model appears both in the momentum equations, in the diffusion term, and in the turbulence equations, in the shear production term.

5.9.1 Quadratic Model

The transformed quadratic nonlinear model is given below:

$$\tau_{ij} = \underbrace{-\frac{2}{3}k\delta_{ij} + 2C_\mu \frac{k^2}{\varepsilon}\bar{S}_{ij}}_{\text{linear component}} + \underbrace{4C_D C_\mu^2 \frac{k^3}{\varepsilon^2}\left[\ddot{\bar{S}}_{ij} - \frac{1}{3}\ddot{\bar{S}}_{kk}\delta_{ij} + \bar{S}_{ik}\bar{S}_{kj} - \frac{1}{3}\bar{S}_{kl}\bar{S}_{kl}\delta_{ij}\right]}_{\text{quadratic component}} \qquad 5.50$$

where:

$$\bar{S}_{ij} = \frac{1}{2J}\left(\underbrace{\beta_j^l \frac{\partial \tilde{U}_i}{\partial \xi_l}}_{w_{ij}} + \underbrace{\beta_i^l \frac{\partial \tilde{U}_j}{\partial \xi_l}}_{w_{ji}} \right) \qquad 5.51$$

$$\dddot{\bar{S}}_{ij} = \underbrace{\frac{\partial \bar{S}_{ij}}{\partial t}}_{\text{term 1}} + \underbrace{\tilde{U}_k \frac{1}{J} \beta_k^l \frac{\partial \bar{S}_{ij}}{\partial \xi_l}}_{\text{term 2}} - \underbrace{\frac{1}{2J^2} w_{ik}\left(w_{kj} + w_{jk}\right)}_{\text{term 3}} - \underbrace{\frac{1}{2J^2} w_{jk}\left(w_{ki} + w_{ik}\right)}_{\text{term 4}} \qquad 5.52$$

In the current work, term 1 has been neglect since only steady state solutions are been considered.

The implementation of the nonlinear eddy-viscosity model in the momentum diffusion term required the determination of the spatial derivative of equation 5.50. The implementation of the linear component remained the same as the linear eddy-viscosity model and the nonlinear terms were included as the source terms. The spatial derivative of the nonlinear term was evaluated, by the component value being calculated at the cell face and then the difference being taken over a cell. Direct calculation of the second derivative in term 2 was avoided by calculating and storing the convective term ($\tilde{U}_k \tilde{S}_{ij}$) at the cell centre. The derivative of this quantity at the cell face was then approximated through differencing of these stored values

The inclusion of the nonlinear term in the turbulent production term requires that they be evaluated at a cell centre and then multiplied by the relevant velocity vector.

5.9.2 Cubic Model

The implementation of the cubic model was more complex than that of the quadratic. The method followed for the quadratic model, where the additional nonlinear terms in the velocity diffusion term were added to the source, was found to

be unstable in the current model. The principle of an effective viscosity was used for the implementation of the cubic model. The nonlinear terms multiplied by the normal derivative are included in the effective viscosity term, as an additional component of the sum of laminar and turbulent viscosities of the linear eddy-viscosity model. These terms are solved as part of the coefficient matrix. The remaining terms are portioned into the source term. The cubic nonlinear relationship was given in equation 3.37. The transformed version of this model can be written in the form give in equation 5.53.

The linear source term incorporates the cross-derivative term of the linear eddy-viscosity, the treatment of which was discussed earlier (section 5.6.6). The components of the nonlinear source term are evaluated and stored at the cell centres. The spatial derivative required in the evaluation of the diffusion term is then approximated using central differencing.

The turbulent shear production was incorporated in the nonlinear model by the same procedure as the quadratic model.

$$\tau_{ij} = \frac{1}{J}\frac{\partial}{\partial x_p}$$

$$\left\{\left[\left(\frac{\mu+\mu_t}{J}\right.\right.\right.$$
$$-C_1\frac{2k}{\varepsilon}\frac{\mu_t}{J^2}w_{jj}$$
$$-C_2\frac{2k}{\varepsilon}\frac{\mu_t}{J^2}w_{jj}$$
$$+C_4\frac{2k^2}{\varepsilon^2}\frac{\mu_t}{J^3}\left(w_{jk}w_{jk}-w_{jk}w_{kj}\right)$$
$$-C_5\frac{k^2}{\varepsilon^2}\frac{\mu_t}{J^3}\left(w_{kl}^2+w_{lk}^2+2w_{kl}w_{lk}\right)$$
$$\left.\left.\left.-C_6\frac{k^2}{\varepsilon^2}\frac{\mu_t}{J^3}\left(w_{kl}^2+w_{lk}^2-2w_{kl}w_{lk}\right)\right)\right]\frac{\partial\tilde{U}_i}{\partial x_m}B_p^m\right| \text{effective viscosity}$$

$$\frac{\mu+\mu_t}{J}w_{ji}\beta_j^p-\frac{2}{3}\rho k\delta_{ij}\Big| \text{linear source term}$$

$$-C_1\frac{k}{\varepsilon}\frac{\mu_t}{J^2}\left(w_{ik}\left(w_{jk}+w_{kj}\right)\Big|_{k\neq j}+w_{ki}\left(w_{jk}+w_{kj}\right)-\frac{1}{3}S_{kl}S_{kl}\delta_{ij}\right)\beta_j^p$$
$$-C_2\frac{k}{\varepsilon}\frac{\mu_t}{J^2}\left(2w_{ik}w_{jk}\Big|_{k\neq j}+2w_{kj}w_{ki}\right)\beta_j^p$$
$$-C_3\frac{k}{\varepsilon}\frac{\mu_t}{J^2}\left(\left(w_{ik}w_{jk}-w_{ik}w_{kj}\right)\Big|_{k\neq j}+w_{ki}w_{kj}-w_{ki}w_{jk}-\frac{1}{3}\Omega_{lk}\Omega_{kl}\delta_{ij}\right)\beta_j^p$$
$$-C_4\frac{k^2}{\varepsilon^2}\frac{\mu_t}{J^3}\left(\begin{array}{l} w_{ki}\left(w_{lj}-w_{jl}\right)\left(w_{kl}+w_{lk}\right)+w_{li}\left(w_{kj}+w_{jk}\right)\left(w_{kl}+w_{lk}\right) \\ w_{ik}\left(w_{lj}-w_{jl}\right)\left(w_{kl}+w_{lk}\right)\Big|_{k\neq l}+w_{il}\left(w_{kj}+w_{jk}\right)\left(w_{kl}+w_{lk}\right)\Big|_{l\neq j}\end{array}\right)\beta_j^p \Big| \text{nonlinear source term}$$
$$-C_5\frac{k^2}{\varepsilon^2}\frac{\mu_t}{J^3}\left(w_{ji}\left(w_{kl}^2+w_{lk}^2+2w_{kl}w_{lk}\right)\right)\beta_j^p$$
$$\left.-C_6\frac{k^2}{\varepsilon^2}\frac{\mu_t}{J^3}\left(w_{ji}\left(w_{kl}^2+w_{lk}^2-2w_{kl}w_{lk}\right)\right)\beta_j^p\right\}$$

5.53

5.10 Closure

The research-based CFD code SOFIE was adopted as the base code into which models were implemented for the current work. SOFIE is a finite volume code that solves the governing equations in a curvilinear coordinate system. This chapter introduced and presented the methods used in the implementation of the governing equations and turbulence models.

The implementation of the models has a significant effect of the stability and rate of convergence of a solution. Thus, the governing equations are manipulated into a form that maximises the stability. This chapter presents the implementation of all the models considered in the current work and measures taken to optimise the stability.

CHAPTER 6

Validation of Buoyant Jets Predicted with Standard k-ε Model

6.1 Introduction

Three different turbulent buoyant jets were considered to assess the effect of variations in the turbulence models: These were a pure plane plume, a plane buoyant jet, and an axisymmetric buoyant jet. The choice of these three cases derived, firstly, from the usefulness of the validation process and, secondly, from the capabilities of SOFIE in undertaking such simulations.

All the simulations in the current work were undertaken using SOFIE. A hybrid discretisation scheme was adopted with a TDMA solver for the momentum and scalar transport equations. The SIMPLEC algorithm was adopted for the pressure correction scheme and SIP was used for the pressure solver. The convergence criterion was based on a mass residual of $1x10^{-3}$.

This chapter makes a detailed comparison of the turbulent buoyant jets modelled with the standard k-ε model and recent experimental data. Sections 6.2.1 to 6.2.3 define the three considered buoyant jets: the plane pure plume, the plane buoyant jet and the axisymmetric buoyant jet, respectively. In addition, the preliminary simulations undertaken to ensure confidence in the reported solutions are summarised. Section 6.3 makes a critical comparison between the simulation results and the experimental data. An overall comparison between all the buoyant jets and a number of experimental studies is made by consideration of their spreading rates (section 6.3.1). The spreading rate was defined in section 2.2. The mean flow and scalar fields are presented in section 6.3.2 for each buoyant jet together with a critical consideration of the experimental data. Finally, the predicted and experimental turbulent characteristics are compared for the axisymmetric buoyant jet, as this represented a reliable dataset (section 6.3.3).

6.2 Simulated Plumes

6.2.1 Plane Pure Plume

Figure 6-2 shows the solution domain of the pure plane plume. The plume was generated by a 54.5 W heat source of width 40mm. The plume can be regarded as an 'ideal case' and is geometrically the simplest possible scenario. The simplicity of this case was thought to be computationally advantageous.

The plane plume has a line of symmetry, parallel with the gravity vector, along the centreline; hence, only half the domain was modelled with a mirror or symmetry boundary defined at this boundary. It is assumed that no flow crosses a mirror boundary, hence the normal velocity is set to zero and all scalar variables are defined with zero gradients. A small ledge was introduced on the upper boundary to prevent a large recirculation (appendix B). The effect of variations in both horizontal and vertical ledge sizes was considered. The base adjacent to the inlet was solid and assumed to be adiabatic. The remaining boundaries were constant pressure

boundaries. This type of boundary is utilised where the exact flow details are unknown but the pressure is known.

The overall size of the solution domain was subject to a domain independence exercise. Domain dimensions were varied in width between 1 and 12.1 metres (m) and in height between 1 and 6.0 m. These variations were found to affect both the stability of the solution and the results. A domain of dimensions 3.5x4.5 m with a ledge covering approximately 55% of the upper surface was found to be the most suitable. Table 6-1 gives a sample of the test domains considered to demonstrate the effect of domain size.

The grid dependence of the solution was considered in terms of both the total number of cells and the stretch of the grid. The spreading rate and cross-stream velocity profiles are given in table 6-2 and figure 6-1. The difference between the coarse and medium density grids is significant, whereas the difference between the medium and fine grids are minimal.

Turbulent boundary conditions were required to be specified at the free boundaries; the chosen values were open to interpretation. The influence of their values was assessed in a series of tests in which the turbulent viscosity was altered at the free boundary by varying the turbulent length scale ($\ell = k^{3/2}/\varepsilon$) (table 6-3).

This comparison suggested that the boundary conditions should be defined such that the effective viscosity at the boundary approaches the laminar viscosity. Hence, the flow entering the domain can physically be considered to be laminar. The two smaller length scales vary by an order of magnitude but yield a turbulent viscosity with a similar magnitude to the laminar viscosity and very similar spreading rates. The majority of experiments have been concerned with plumes issuing into still, ambient environments. Thus the definition of laminar conditions at these boundaries

is appropriate for the replication of experimental conditions.

Width (m)	Height (m)	Velocity spreading rate	Temperature spreading rate
3.25	4.5	0.0812	0.0833
1.76	2.25	0.0794	0.0806
0.885	1.175	0.0716	0.0719

Table 6-1: Effect of domain size on spreading rate of plane pure plume.

Grid	Grid density (nx x ny)	Velocity spreading rate	Temperature spreading rate
Coarse	57 x 57	0.0808	0.0815
Medium	117 x 165	0.0835	0.0851
Fine	147 x 185	0.0846	0.0859

Table 6-2: Effect of grid density on spreading rate of plane pure plume.

Length scale	Velocity spreading rate	Temperature spreading rate	Turbulent viscosity
1	0.0835	0.0851	2.14×10^{-3}
0.01	0.0812	0.0833	2.33×10^{-5}
0.001	0.0812	0.0831	2.26×10^{-5}

Table 6-3: Effect of the turbulent boundary condition at the free boundary of the pure plane plume on the spreading rates and turbulent viscosity.

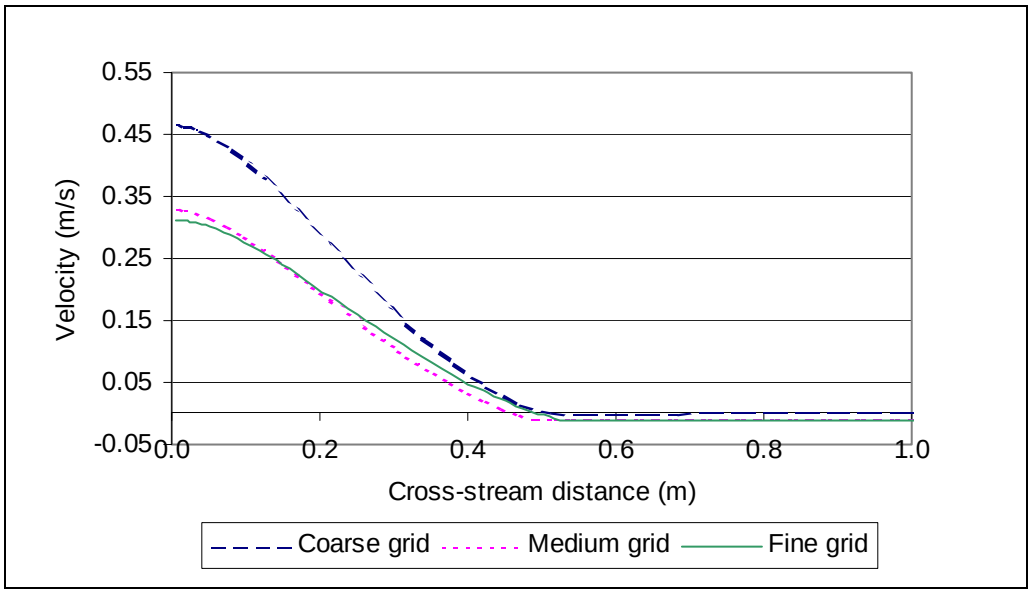

Figure 6-1: Mean velocity cross-stream profiles of the pure plane plume predicted on grids on different density.

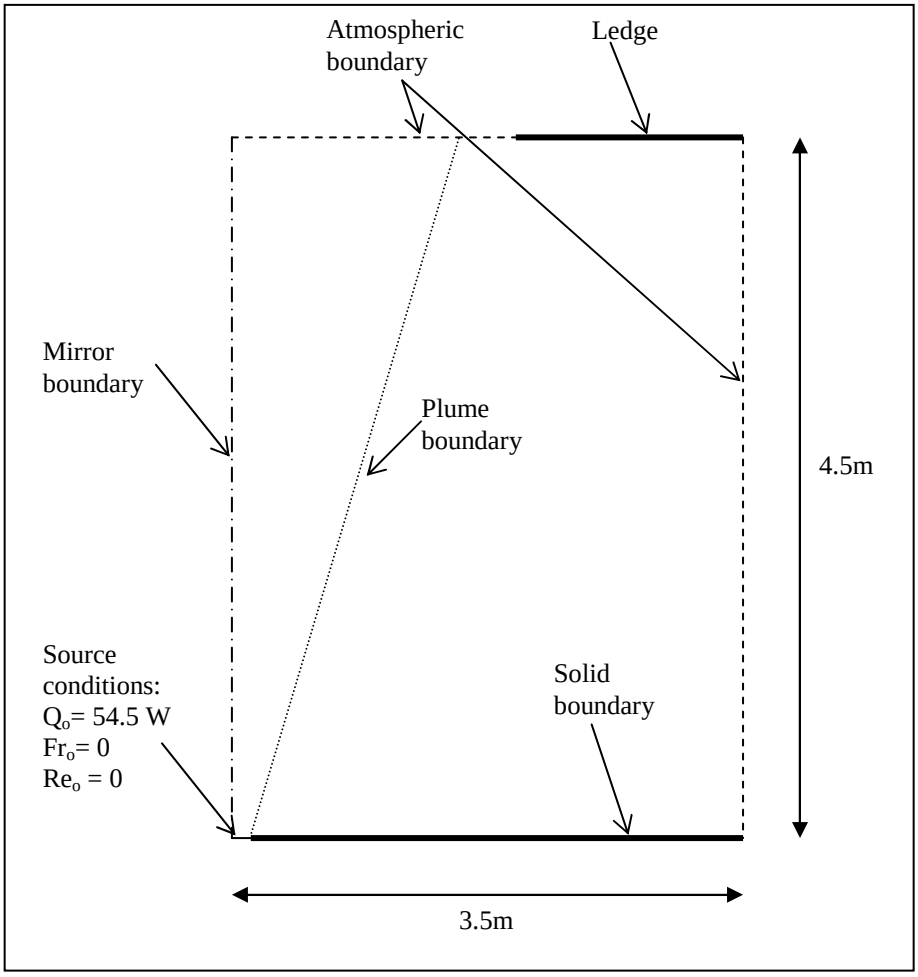

Figure 6-2: Schematic diagram of solution domain of plane pure plume.

6.2.2 Plane Buoyant Jet

Figure 6-3 shows the solution domain and boundary conditions for the plane buoyant jet. This was based on experiments of Ramaprian and Chandrasekhara (1989) (RC). The jet was initiated by heated water exiting into an ambient environment of cooler water. The simulations were truly two-dimensional, whereas the experiments had some depth. The authors stated that the two-dimensionality of the plume was retained in the measurement region; hence, this was a reasonable assumption.

Preliminary simulations were undertaken to assess the dependence of the plume simulations on both the domain size and structure (table 6-4). These simulations found the standard k-ε model to be unstable, it caused spurious velocities at the free boundary. Various tests on the structure of the domain were considered to promote stability. An example of this was to introduce a ceiling to the solution domain in addition to a horizontal ledge in the upper part of the solution domain. This, in effect, caused a ceiling layer to form that exited from the upper part of the vertical free boundary, above the ledge. Results from this simulation are retained for completeness. This structure was not used in any further simulations as limiting the turbulent timescale at the free boundaries was used instead to enforce stability. The turbulent timescale was limited by the laminar viscosity, which prevented spurious values. Simulations on domains of differing size was again undertaken but found to have limited influence; a small difference is seen between the domains of differing size, this is possibly due to the grid quality. Thus, the final dimensions were based on the experiment of RC. A ledge at the upper boundary as explained in section 6.2.1.

A grid independence study was conducted. Figure 6-3 shows the cross-stream profile of velocity for three of the considered grids and table 6-5 shows the spreading rates for three grids. Variation between the coarse and medium density grids is significant but insignificant between the medium and fine density grids. Hence, the medium grid was used for subsequent simulations (appendix C).

The buoyant jet requires inlet boundary conditions to be defined for turbulence, unlike the pure plume. These quantities need to be estimated through intuition since no values are available from the experimental data. Some tests were undertaken to establish the influence of variation in these quantities (table 6-6).

The spreading rate is unaffected by changes in the dissipation term but slightly influenced by changes in the turbulent kinetic energy. However, this influence in small and the inflow boundary conditions for subsequent simulations were based on a 1% turbulent flow with a length scale base on the outlet size.

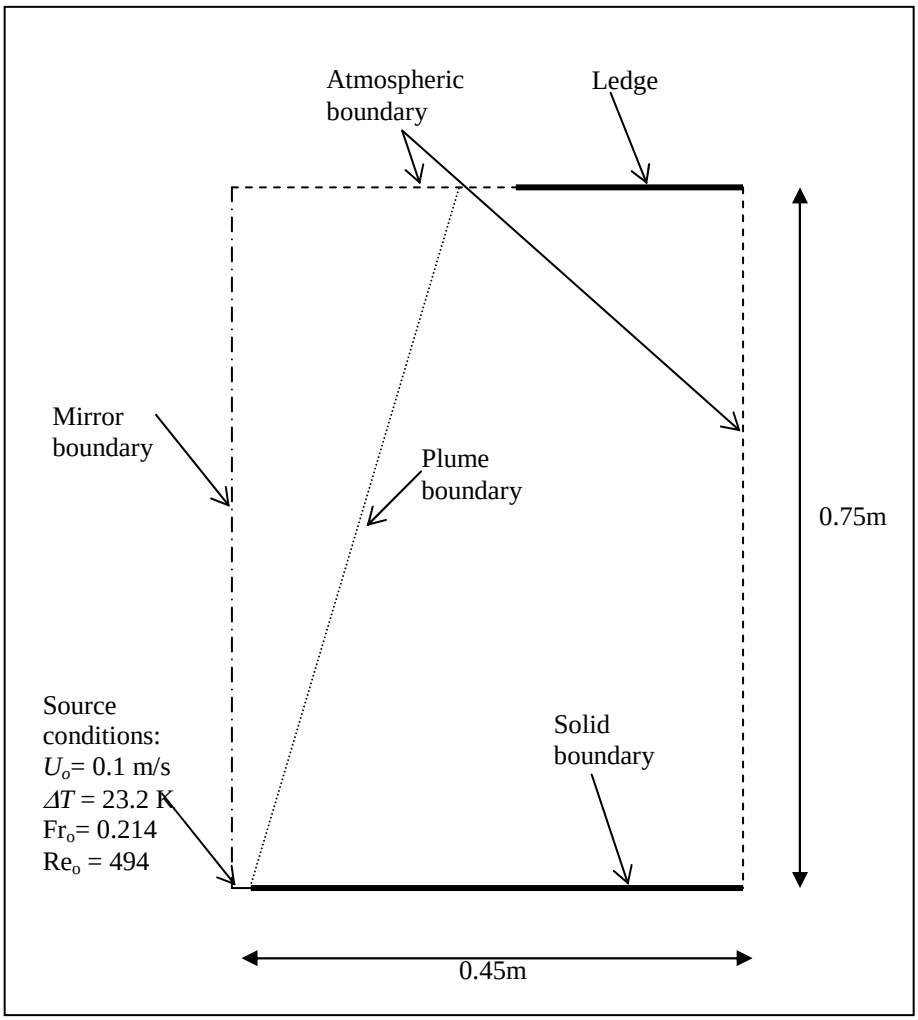

Figure 6-3: Schematic diagram of solution domain of plane buoyant jet.

	Dimensions (width x height (m))	Velocity spreading rate	Temperature spreading rate
Large domain	0.8 x 1.4	0.0825	0.0846
Small domain	0.45 x 0.75	0.08353	0.0872
Small domain with ceiling	0.45 x 0.75	0.08353	0.0860

Table 6-4: Effect of solution domain on spreading rate of plane buoyant jet.

Grid	Grid density (nx x ny)	Velocity spreading rate	Temperature spreading rate
Coarse	42 x 80	0.0808	0.0842
Medium	67 x 100	0.0835	0.0872
Fine	122 x 152	0.0840	0.0876

Table 6-5: Effect of grid density on spreading rate of plane buoyant jet.

Turbulent kinetic energy (m^2/s^2)	Dissipation of turbulent kinetic energy (m^2/s^3)	Velocity spreading rate	Temperature spreading rate
1e-4	0.1	0.0835	0.0872
1e-2	0.1	0.0829	0.0862
1e-4	10	0.0838	0.0876

Table 6-6: Effect of inlet turbulent boundary condition on spreading rate.

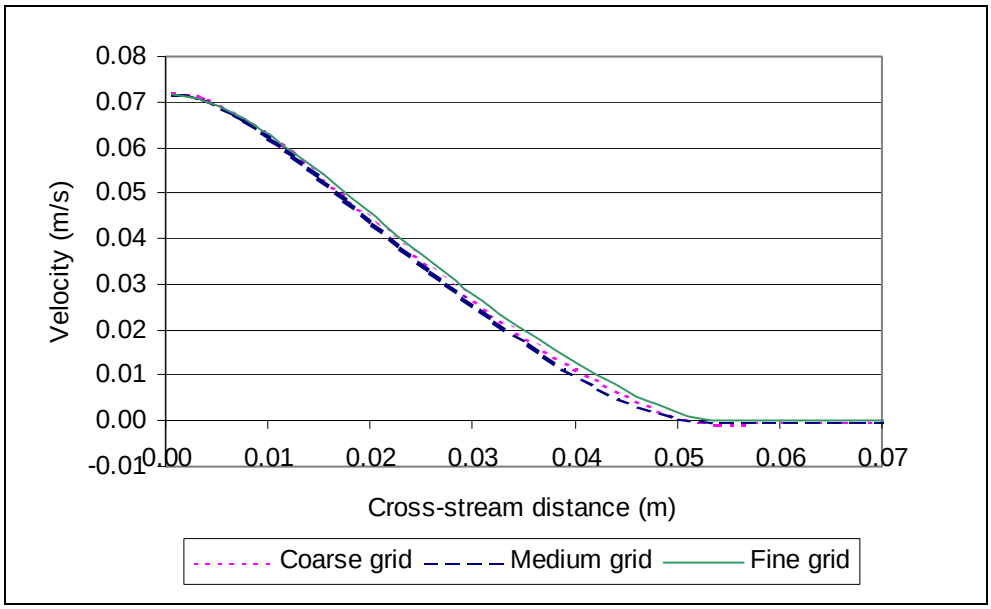

Figure 6-4: Mean velocity cross-stream profiles for plane buoyant jet predicted on grids of different density.

6.2.3 Axisymmetric Buoyant Jet

Figure 6-**6** shows a plane view of the solution domain and boundary conditions for the axisymmetric buoyant jet. The simulation was assumed to be symmetrical enabling only a 1^o segment of the plume to be simulated; the radial boundaries were defined as mirror boundaries. The simulations reported in this section were based on a set of experimental studies by Dai et al (1994, 1995(a), 1995(b) (DTF). The current simulations and the experiments of DTF varied in the jet fluid injected into the ambient environment. The experiments of DTF involved a jet of carbon dioxide being injected into an atmospheric environment. The buoyant force was, therefore, established by the density difference of the fluids. It was convenient, for current work, to consider only a single fluid. That is to have the same fluid injected as that of the ambient environment. The temperature of the incoming jet fluid was thus reduced until the inlet density matched that of the inflowing carbon dioxide plume of DTF's experiments. Hence, the current simulations consider only air: a cold air jet injected into a relatively warm atmospheric environment.

A grid independence study was undertaken as with the other buoyant jets considered in the previous two sections. Typical examples of the results gained from this set of simulations are given in terms of cross-stream profiles (figures 6**.**5) and spreading rate (table 6-7). The fine grid was selected as the most suitable for subsequent simulations. The grid independence study considered finer meshes. These demonstrated slight differences in the spreading rate but inspection of the cross-stream and centreline profiles revealed this difference to be very small.

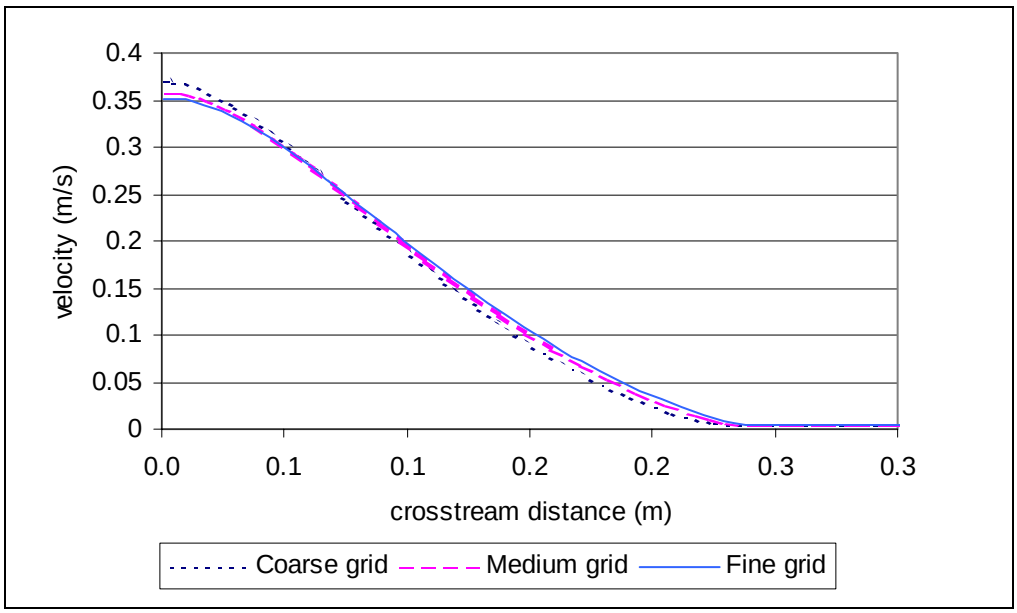

Figure 6-5: Mean velocity cross-stream profile of axisymmetric buoyant jet predicted on different grids.

Grid	Grid density (nx x ny)	Velocity spreading rate	Temperature spreading rate
Coarse	54 x 100	0.0849	0.0804
Medium	74 x 120	0.0887	0.0843
Fine	94 x165	0.0915	0.0872

Table 6-7: Effect of grid density on prediction of spreading rate of axisymmetric buoyant jet.

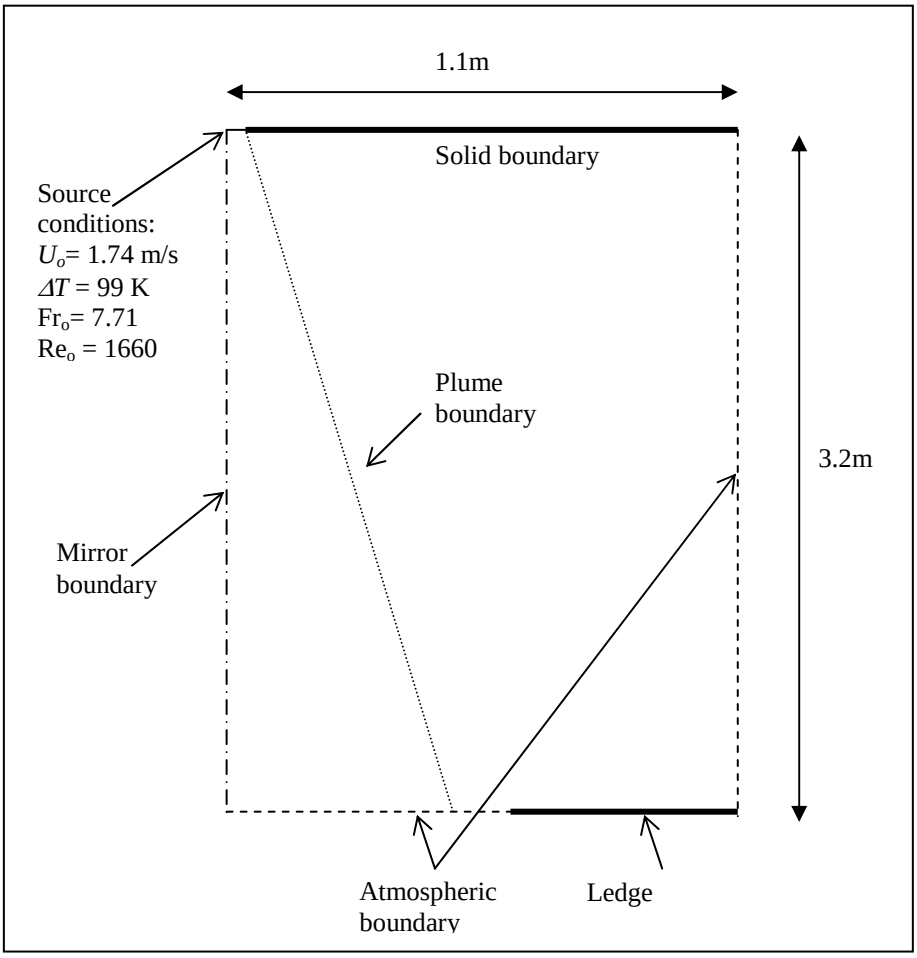

Figure 6-6: Schematic diagram of solution domain of axisymmetric buoyant jet.

6.3 Comparison of Standard k-ε Model Predictions against Experimental Data

In this section, a critical analysis of the experimental data is undertaken with reference to the prediction made with the buoyancy-modified standard k-ε model, this will be referred to as the standard k-ε model. The standard k-ε model is still the most commonly used model and it is useful to use this as a base comparison in addition to experimental studies.

6.3.1 Spreading Rate

The spreading rate was defined in section 2.2; it is a useful first point for comparison as it enables a very general assessment of the quality of the simulation results.

Tables 6-8 and 6-9 compare some of the spreading rates available from numerical and experimental studies in the literature with the predictions made in the current work for axisymmetric buoyant jets and plane buoyant jets, respectively.

The values reported for the current study are roughly equivalent to those reported for simulation of plane plumes and less than those reported for simulation of axisymmetric plumes. The differences between the various studies could have resulted from a number of factors, such as, differences in numerical schemes or additional numerical correction, for example, the Hossain and Rodi simulations use the Rodi centreline correction[2]. Finally, it is not clear whether the spreading rates taken from the literature were derived from truly grid and domain independent solutions.

Despite large variations in the numerical results, all these studies underpredict the spreading rate relative to the experimental data. This underprediction has been regarded as an inherent problem of the standard k-ε model and led to a number of authors to use higher order turbulence models, as discussed in the literature survey. The main reason proffered for this underprediction is the lack of influence from buoyancy in the eddy-viscosity relationship.

Disparity in the spreading rates from experimental studies implies that critical consideration of the data is also important. The numerical study by Riopelle et al (1994) demonstrates the influence of the spreading rate on ambient stratification but few experimental studies take adequate consideration of this. The non-dimensional height at which measurements are taken in the plume also varies greatly between

[2] Rodi's centreline correction (Rodi (1972)) was developed to deal with the characteristic overprediction of the spreading rate of pure jets and was later adopted in plume calculations.

studies, implying that some measurements are not taken within the self-similar region. For the spreading rates of different experiments to be truly comparable, measurements must be within this region.

This disparity is clearly demonstrated in the comparison of the data of Chen and Rodi (1980) with that of Dai et al (1994, 1995(a), 1995(b) (DTF). The large difference in DTF data was associated with measurements being taken well within the self-similar region, unlike previous studies. Comparison of these two datasets with the numerical simulation demonstrates that the older data uphold the common wisdom that the standard k-ε model underpredicts the spreading rate, whereas the recent data of DTF show an overprediction. This is a significant result since the quality of the turbulence model has been always questioned, leading to significant effort directed at the improvement of turbulence models associated with the plume prediction. However, comparison with the DTF results suggests that the experimental data are at fault. This will only be confirmed when data supporting the results of DTF becomes available.

A consistent feature through the various studies is the relative spread of the velocity in the scalar plume. This is a useful comparison, where the absolute values are inconsistent. The experimental values show that the temperature spread is greater than the velocity spread for the plane plume, whereas the velocity spread is greater than the temperature spread for axisymmetric plumes. These trends are accurately represented in all the predictions by the standard k-ε model.

Comparisons between the numerical and experimental spreading rates provide a superficial first comparison of the simulated results. The calculation of the absolute value of spreading rate is subject to some variation in the method of calculation, in particular, whether the value accounts for the virtual origin. Due to these differences, the spreading rate in the current work is used as a rough guide to the quality of the simulations and for comparative assessments, not as a measure of the model accuracy.

The discussion has shown that predictions by the standard k-ε model in SOFIE are comparable with those from other numerical studies. Validation against experimental data initially demonstrated the traditional view that the standard k-ε model underpredicted the spreading rate. However, considering the recent data of DTF, this view is no longer upheld, suggesting that standard k-ε model may have been wrongly accused of inadequacies.

The following section will consider the mean flow and scalar fields in greater detail in order to provide a more detailed view of the quality of the predictions.

Authors	Date	Model	Velocity spreading rate based on half width	Temperature spreading rate based on half width	Velocity spreading rate based on e^{-1} width	Temperature spreading rate based on e^{-1} width
Hossain and Rodi	1982	Standard k-ε	0.100	0.095	x	x
Martynenko Korovkin and Yu	1986	Standard k-ε	0.114	0.1	x	x
Wilks and Hunt	1986	Standard k-ε	0.126	0.1	x	x
Shankar, Davidson and Olsson	1995	Standard k-ε	0.1		x	x
Buoyant jet simulated in current work		Standard k-ε	0.0919	0.0866	x	x
DTF	1994 1995	Experimental	0.0863	0.0745*	0.10	0.09*
Chen and Rodi	1980	Experimental	0.112	0.104	x	x

Table 6-8: Spreading rates of axisymmetric plumes: comparison of published numerical and experimental results with the simulation of axisymmetric buoyant jets undertaken in the current work. *Spreading rate of mixture fraction rather than temperature.

Authors	Date	Model	Velocity spreading rate based on half width	Temperature spreading rate based on half width
Hossain and Rodi	1982	Standard k-ε	0.115	0.119
Sini and Dekeyser	1987	Standard k-ε with functional C_μ	0.10	0133
Bergstrom, Strong and Stubley	1990	Standard k-ε with C_μ=0.109	0.090	0.096
Riopelle, Stubley and Strong	1994	Standard k-ε	0.09	0.09
Riopelle, Stubley and Strong*	1994	Standard k-ε	0.11	0.13-0.06**
Shankar, Davidson and Olsson	1995	Standard k-ε	0.068	x
Yan and Holmstedt	1998	Standard k-ε	0.081	0.080
Pure plume simulated in current work		Standard k-ε	0.0835	0.0872
Buoyant jet simulated in current work		Standard. k-ε	0.0847	0.0870
Chen and Rodi	1980	Experimental	0.12	0.13
Ramaprian and Chandrasekhara	1989	Experimental	0.11	0.133

Table 6-9: Spreading rates of plane plumes: comparison of published numerical and experimental results with the simulations of a plane plume and a buoyant jet undertaken in the current work.*Simulated in an enclosure. **Value decreases with height

6.3.2 Mean Velocity and Scalar Fields

Figures 6-7 and 6-8 shows a general comparative view of temperature and flow fields, respectively, of the three plumes considered. These figures demonstrate the relative size of the different plumes considered. Despite the differences in size, fluid and orientation, the basic flow structure is common between the three scenarios.

6.3.2.1 Centreline Predictions

In the previous section, the importance of ensuring that results of experimental measurements are in a self-similar region was demonstrated. It is also important to demonstrate this for simulated plumes. This can be achieved by utilising the decay laws discussed in section 2.2. Figure 6-9 presents a log-log graph of normalised velocity versus distance and figure 6-10 gives a log-log graph of normalised mixture fraction versus distance, for the axisymmetric plume. The height at which comparisons are made of the numerical results with experiment lies in the region where the plumes have achieved the gradients expected by the decay law. Hence, it is possible to say with confidence that the following profiles considered are well within the self-similar region.

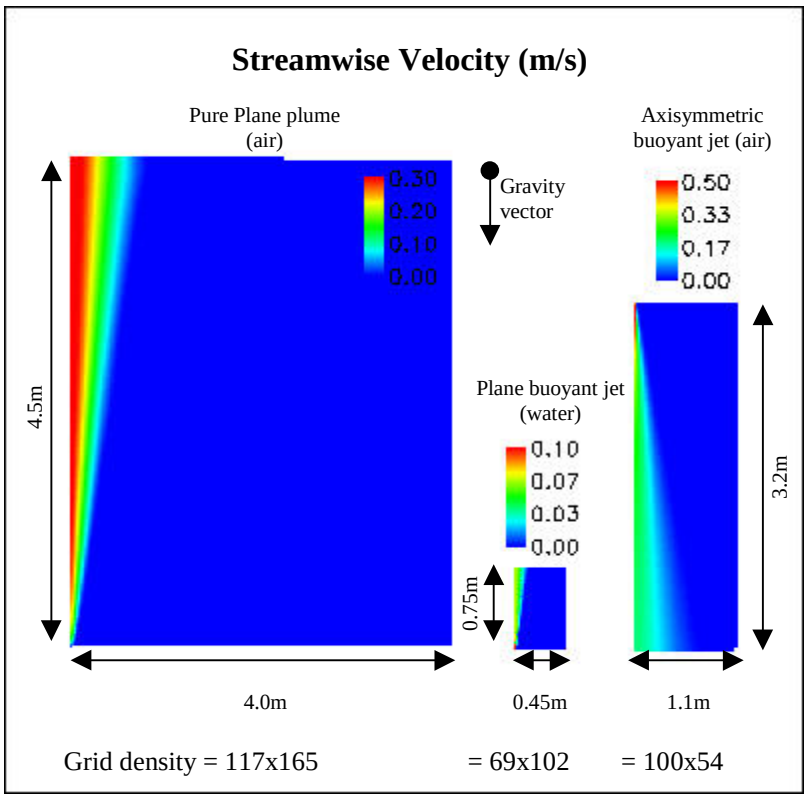

Figure 6-7: Comparison of streamwise velocity field of three considered buoyant jets.

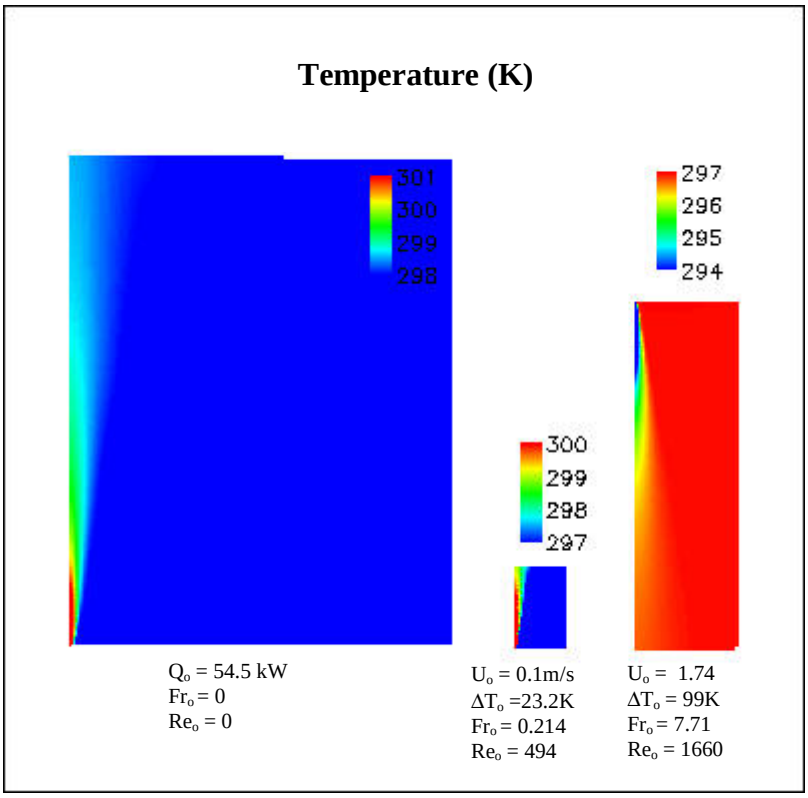

Figure 6-8: Comparison of temperature field of three considered buoyant jets.

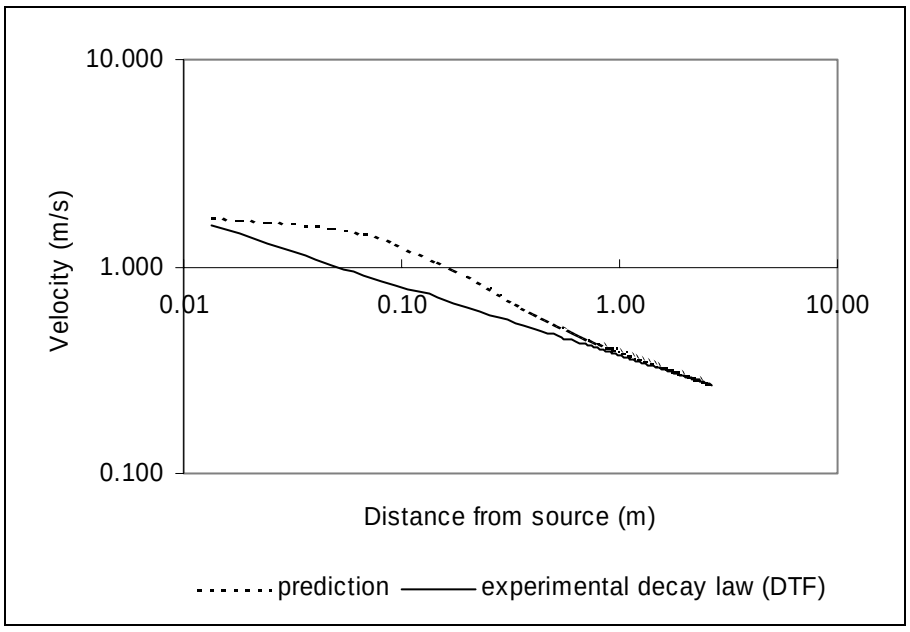

Figure 6-9: Decay of centreline velocity for axisymmetric buoyant jet, comparison between simulations and experimental data of Dai, Tseng and Faeth (1995a).

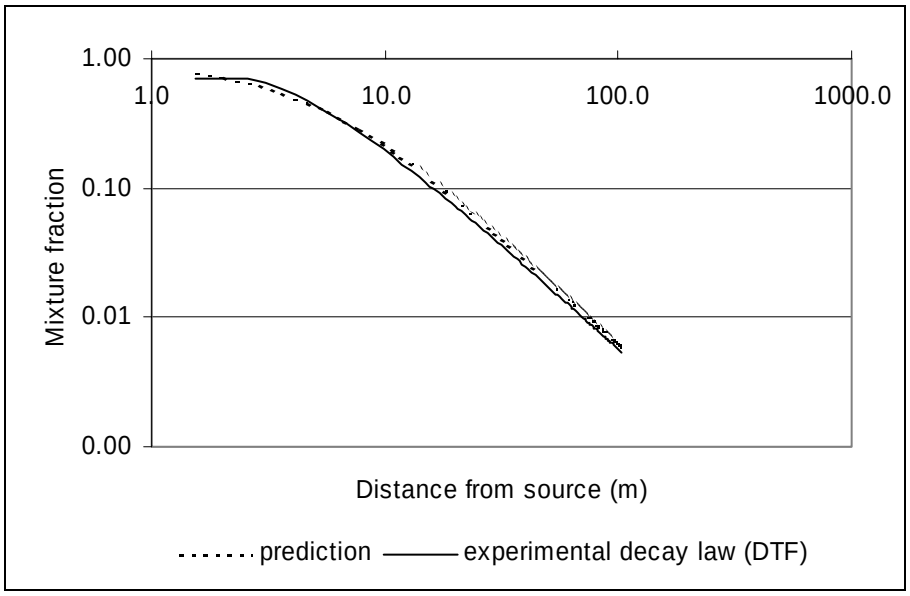

Figure 6-10: Decay of centreline mixture fraction for axisymmetric buoyant jet, comparison between simulations and experimental data Dai, Tseng and Faeth (1994).

6.3.2.2 Pure Plume

Figures 6-11 and 6-12 show normalised profiles for the pure plane plume simulations. This is the format commonly used to present data in the literature. The relevant centreline value is used as the scaling factor for the temperature or velocity. Cross-stream distance is normalised by the height of the profile in the plume. This normalising technique forces unification of the data from experiments and predictions. The technique is useful when dissimilar plumes are being compared but hides the faults under investigation in the CFD predictions.

The profiles do reveal the bad predictions at the edge of the velocity profile. A similar separation of the curves has been observed in a number of other studies. Two reasons have been forwarded for this. Firstly, the experimental data at the edges of the plume are of lower quality due to the low speeds and bi-directional flow (e.g. Malin and Spalding (1984)). Secondly, the solution at the boundary of the flow is sensitive to the type of solver used (e.g. Sini and Dekeyser (1987)). A third reason could be associated with the fitting of the Gaussian curve to the data. The Gaussian fit produces a smoothed curve at the plume boundary that is possibly an exaggeration of the true data.

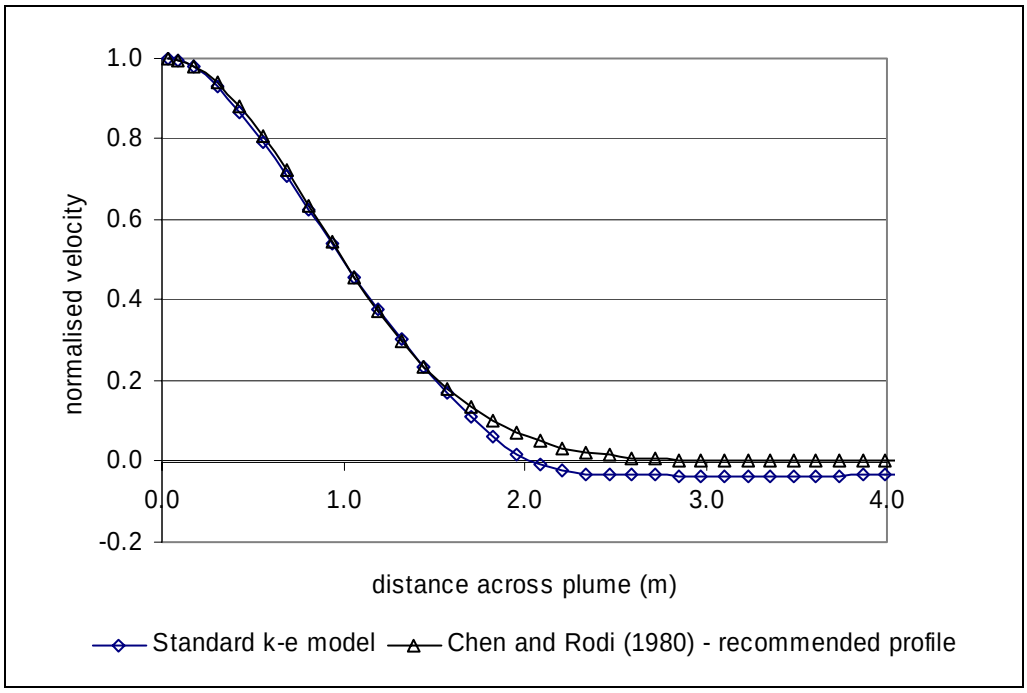

Figure 6-11: Comparison cross-stream profile of normalised velocity profile for the simulation and recommended profile of Chen and Rodi (1980).

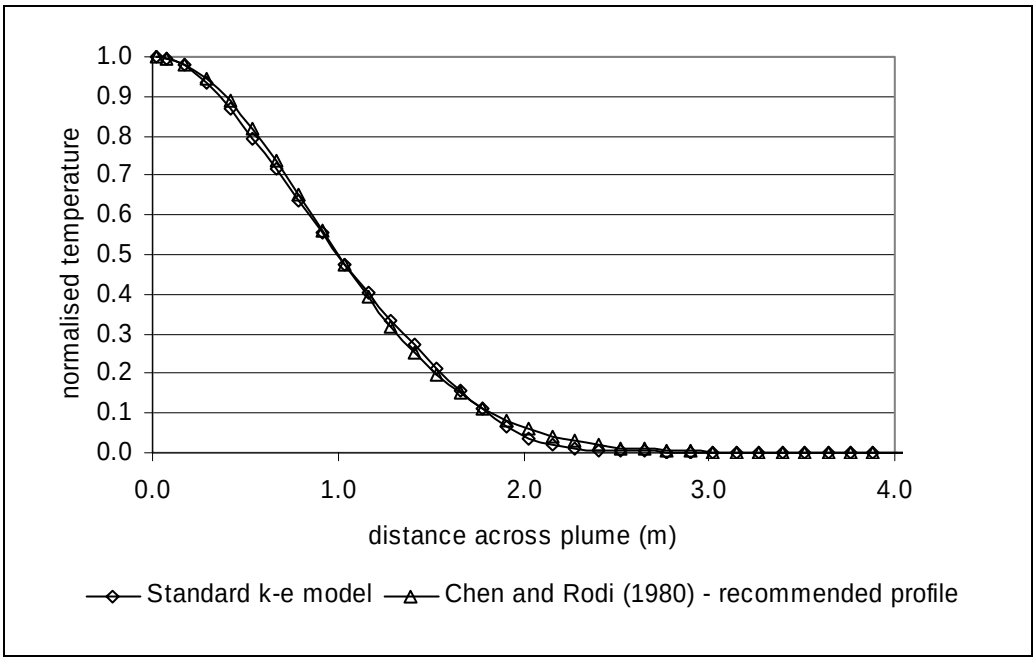

Figure 6-12: Comparison cross-stream profile of normalised temperature profile for the simulation and recommended profile of Chen and Rodi (1980).

6.3.2.3 *Plane Buoyant Jet*

Figures 6-13 and 6-14 show the mean velocity and temperature cross-stream profiles from the predictions and two sets of experimental data. The curves presented for the experimental data are not the true measurements, but rather the values obtained from a Gaussian curve, fitted to the normalised experimental measurements. The Gaussian curves were defined as:

$$\frac{\overline{U}}{U_m} = e^{-0.69\eta_u} \qquad 6.1$$

$$\frac{\Delta\overline{T}}{\Delta T_m} = e^{-0.69\eta_t} \qquad 6.2$$

Where

$$\eta_u = \frac{x}{b_u}; \eta_t = \frac{x}{b_t} \qquad 6.3$$

The experimental temperature and velocity measurements were normalised by the maximum value in a given profile, in the same manner as the results presented for the plane plume. The experimental values of maximum temperature excess and velocity were then fitted to the relationship, defined below, to determine the constants, σ_u and σ_t. These relationships are the decay laws defined, here, in term of buoyant flux rather than the Froude number as given in section 2.2:

$$U_m = \sigma_u B^{1/3} \qquad 6.4$$

$$\Delta T_m = \frac{B^{2/3}}{\beta g \sigma_t (y - y_{ot})} \qquad 6.5$$

Ramaprian and Chandrasekhara (1989) (RC) defined these quantities in a slightly different manner to previous studies, where the initial buoyancy flux (B_o) has been used rather that the local buoyancy flux (B), arguing that it is the heat flux (H) that is unconditionally conserved not the buoyancy flux. The assumption in previous studies that the buoyancy flux is conserved is based on the assumption that the coefficient of thermal expansion is constant. Ramaprian and Chandrasekhara

suggested that this assumption might not be valid due to the rapid change in temperature in the near field of the plume. The buoyancy flux at a given height (y) is defined as:

$$B = \int_{-\infty}^{+\infty} \beta g(\Delta \overline{T}\,\overline{U} + \overline{u'\theta})dx \qquad 6.6$$

$$H = \int_{-\infty}^{+\infty} (\Delta \overline{T}\,\overline{U} + \overline{u'\theta})dx \qquad 6.7$$

The decay relationships for mass (Q) and momentum (M) fluxes are also defined with reference to the local rather than the initial buoyancy flux. Hence:

$$Q = \sigma_Q B^{1/3} y \qquad 6.8$$

$$M = \sigma_M B^{2/3} y \qquad 6.9$$

The universal constants that appear in the decay laws are summarised in table 6-10 for different experimental studies. The data of Rouse et al (1952) were collected on relatively primitive instrumentation, as discussed in the literature survey, and are assumed to contain a large margin of error. The proposed values of Chen and Rodi (1980) were estimated from a review of previously available experimental data.

Figures 6-13 and 6-14 show the results of different interpretations of the experimental data. For Ramaprian and Chandrasekhara, curves are shown that were calculated using the true experimental data and with maximum values for velocity and temperature excess derived from equations 6.4 and 6.5, respectively. The curves for Kotsovinos and List's experimental data show the difference between using the local and initial buoyancy fluxes in the decay laws. Table 6-11 compares the fluxes, the maximum values, and the half widths of the various interpretations of the experimental data.

The fluxes calculated using the local buoyancy flux with Kotsovinos and List (1977) (KL) constants reveals values that were consistently lower than all the fluxes reported for the other cases. This suggests that direct comparison of the constants is inappropriate, unless the differences in the treatment of the buoyancy flux are

accounted for. The differences between the fluxes calculated with the KL data with the initial buoyancy flux and the RC data with local buoyancy flux arise from differences in the experimental measurements.

Heat flux (H) is unconditionally conserved in a plume; hence, the heat flux at any height in a plume should be equal to the initial heat flux. Comparison of the values for heat flux, in table 6-11, show there is considerable disparity between the various cases. Those values estimated as integral fluxes have taken no account of turbulence; Ramaprian and Chandrasekhara estimated this contribution to be $0.18U_m$.

The values of H calculated from the raw experimental data are notably higher than the initial value. The most obvious source of this discrepancy is experimental scatter. Comparison of the values for velocity and temperature excess, in both the tables and the graphs, shows that the experimental values at the height of the measurements are overestimated relative to the other cases.

The sets of data that can be considered the most representative of curves fitted to raw experimental data are the Ramaprian and Chandrasekhara data calculated with the local buoyancy flux (B-RC const.) and the Kotsovinos and List data calculated with initial buoyancy flux (B_o-KL const.). Comparison of the heat flux in these two cases again reveals a considerable disparity. This is confirmed by consideration of the graphs: the sum of the areas under the velocity and temperature excess curves is equal to the heat flux without taking account of the turbulent heat flux. If account is taken of the turbulence in the value of H given in the table, the Ramaprian and Chandrasekhara data appear more accurate. However, this could be misleading since the value of B used in the calculation is taken directly from experimental data that have previously been suggested as having a large margin of error. The Kotsovinos and List data use the initial buoyancy flux that is generally a more reliable measurement.

No conclusive decision can be made with respect to the relative quality of the data in these experimental studies until further data are available for comparison. For this reason the validation of various models in the current work will consider both sets of experimental data, i.e. those of RC and KL.

The predictions by SOFIE are considerably different to the experimental data. Notably, both the velocity and excess temperature predictions for spreading rate are small. The peak velocities lie within experimental error but the peak excess temperature is greatly overpredicted. The heat flux appears to be well predicted, but it cannot necessarily be assumed from this that the velocity and temperature curves are accurate.

The gross differences between the SOFIE predictions and the experimental data are most likely due to differences in the inlet conditions. The Ramaprian and Chandrasekhara paper provides limited information concerning the inlet conditions, including inlet velocity and temperature. These values were used to define the inlet boundary conditions in SOFIE. The inlet velocity was derived from the measurements of mass flow. Since no ambient pressure term has been provided, this has been assumed to be 101325 Pa. It is possible that this would have a slight effect on the density and hence initial mass flux. Comparison of the velocity curve and the mass flux in the table suggests the velocity of the Kotsovinos and List data is closer to the SOFIE prediction than the Ramaprian and Chandrasekhara data. This comparison becomes closer when account is taken of the fact that the mass flux integral is calculated from the area beneath a best fit curve for the SOFIE prediction, whereas the experimental mass flux integral is calculated from the Gaussian curve that tends to overpredict the values at the edge of the curve relative to a mean fit.

If the Kotsovinos and List data are used for the comparison, the spreading rates are underpredicted and the centreline values are overpredicted, this is the same trend observed in previous numerical studies.

	σ_u	σ_t	Velocity spreading rate	Temperature spreading rate
Ramaprian and Chandrasekhara (1989)	2.13	0.39	0.11	0.133
Kotsovinos and List (1977)	1.66	0.42	0.097	0.13
Chen and Rodi (1980)	1.9		0.12	0.13
Rouse, Yih and Humphreys (1952)	1.8	0.385	0.147	0.13

Table 6.10: Comparison of the universal constants and spreading rates achieved in some experimental studies.

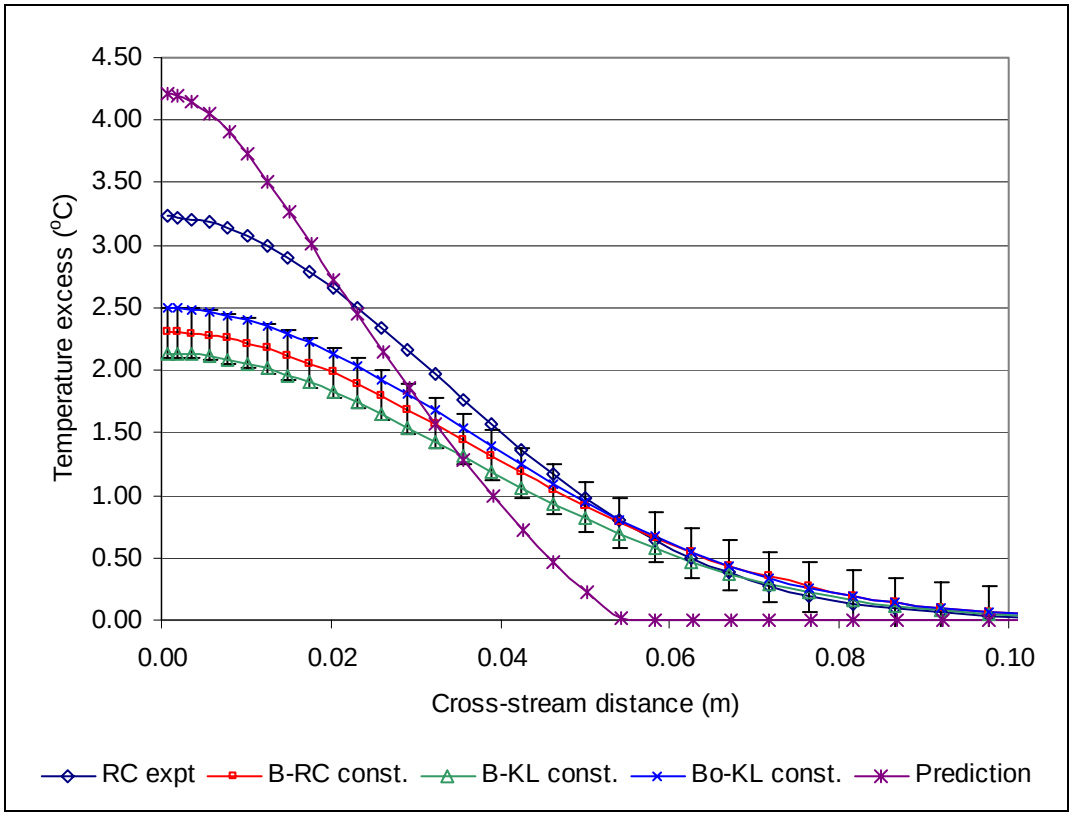

Figure 6-13: Comparison of the mean temperature profile for different interpretation of the experimental data with the prediction of the plane buoyant jet. Refer to table 6-11 for abbreviations.

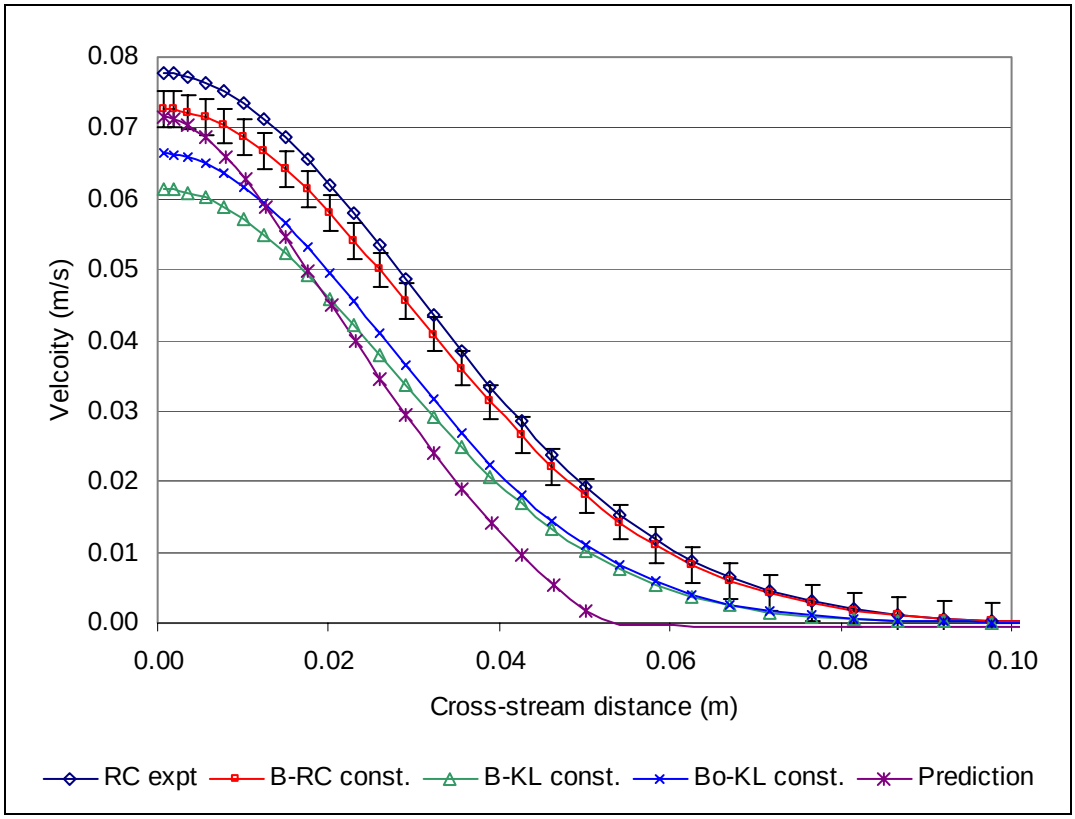

Figure 6-14: Comparison of the streamwise velocity profile for different interpretation of the experimental data with the prediction of the plane buoyant jet. Refer to table 6-11 for summary of abbreviations.

	Initial experimental conditions (RC)	Experimental measurements at nondimensional height of 60	Values calculated with local experimental *B* and RC constants	Values calculated with local experimental *B* and KL constants	Values calculated with experimental value of initial *B* and KL constants	Current predictions
Dataset		RC expt	B – RC const.	B – KL const.	B_o – KL const.	
Momentum flux M (m^3/s^2)	50×10^{-6}	296×10^{-6} 314×10^{-6} *	276×10^{-6} (eq. 6.9) 274×10^{-6} *	172×10^{-6} *	201×10^{-6} *	184×10^{-6} *
Mass flux Q (m^2/s)	5×10^{-4}	53.5×10^{-4}	52.4×10^{-4} (eq. 6.8) 56.2×10^{-4} *	42.0×10^{-4} *	45.4×10^{-4} *	36.5×10^{-4} *
Buoyant flux** B (m^3/s^3)	503×10^{-6}	39.8×10^{-6}	46.5×10^{-5}*	33.0×10^{-5}*	42.2×10^{-5}	x
Heat flux** H ($m^2.{}^oC/s$)	116×10^{-4}	145.8×10^{-4} 135×10^{-4} *	95.4×10^{-4} *	68.4×10^{-4} *	86.5×10^{-4} *	115×10^{-4} *
b_u (m)		3.52×10^{-2}	3.52×10^{-2}	3.10×10^{-2}	3.10×10^{-2}	2.54×10^{-2}
b_t (m)		3.8×10^{-2}	4.32×10^{-2}	4.23×10^{-2}	4.23×10^{-2}	2.65×10^{-2}
U_m (m/s)	10×10^{-2}	7.78×10^{-2}	7.27×10^{-2}	6.15×10^{-2}	6.64×10^{-2}	7.15×10^{-2}
ΔT_m (^oC)	23.4	3.23	2.30	2.14	2.50	4.22

Table 6.11: Comparison of some characteristic parameters for various interpretations of experimental data and the simulations of a plane buoyant plume.

*Values calculated by estimating area under relevant graphs. These values will be referred to as integral fluxes. Since the values are calculated from the mean curves, there is no account of turbulence.

**No account taken of turbulent heat flux except in experimental measurements

6.3.2.4 *Axisymmetric Buoyant Jets*

Figures 6-15 and 6-16 show the velocity and density cross-stream profiles for an axisymmetric buoyant jet. The simulations were based on the data of Dai et al. (1994, 1994a, 1995b) (DTF) but a second set of experimental data have been included for comparison (Shabbir and George (1994) (SG)). These experimental data have been derived from Gaussian curves fitted to the normalised experimental data, as in the case of the plane buoyant jet. The Gaussian curves were normalised with reference to the decay laws, rather than the local maximum values:

$$f = \left(\frac{\pi \mathrm{Fr}_o}{4}\right)^{2/3}\left(\frac{\rho_o}{\rho_a}\right)\left(\frac{(x-x_o)}{d}\right)^{-5/3} \mathrm{F}(0)e^{-\mathrm{k}_f^2(r/(x-x_o))^2} \qquad 6.10$$

$$U = \left(\frac{B_o}{(x-x_o)}\right)^{1/3} \mathrm{U}(0)e^{-\mathrm{k}_u^2(r/(x-x_o))^2} \qquad 6.11$$

Where,

$$\rho = \rho_a/(1-f(1-\rho_a/\rho_o)) \qquad 6.12$$

The constants in these relationships are determined from experimental data, table 6-12 gives the values from two different experimental studies. Considerable variation can be seen between the two studies. DTF state that this is a result of previous studies not taking measurements a large enough distance from the source for the plume to be accurately self-similar. However, the SG paper does display, through consideration of the centreline profiles, that a self-similar state was achieved.

	Constants			
Paper	k_f^2	F(0)	k_u^2	U(0)
DTF	125	12.6	93	4.3
Shabbir and George (1994) (SG)	68	9.4	58	3.4

Table 6.12: Comparison of universal constants from experimental studies on axisymmetric buoyant jets.

Close examinations of the definitions in the DTF paper revealed that the data had been incorrectly compared against previous studies. The claim that the cross-stream

profiles was significantly finer than previous experimental results is true, but the method of normalisation is not consistent with the quoted references. The normalisation velocity utilised the initial buoyancy flux (B_o) and the mixture fraction, the initial Froude number (Fr_o). DTF defined these relationships as:

$$B_o = \frac{\pi}{4} d^2 u_o g \left|\rho_o - \rho_a\right| / \rho_a \qquad 6.13$$

$$\mathrm{Fr}_o = \sqrt{\frac{\rho_a u_o^2}{g\left|\rho_o - \rho_a\right| d}} \qquad 6.14$$

whereas previous authors, including those quoted by DTF (e.g. List (1982)), define these quantities as:

$$B_o = \frac{\pi}{4} d^2 u_o g \left|\rho_o - \rho_a\right| / \rho_o \qquad 6.15$$

$$\mathrm{Fr}_o = \sqrt{\frac{\rho_o u_o^2}{g\left|\rho_o - \rho_a\right| d}} \qquad 6.16$$

The graphs in figures 6-15 and 6-16 show the effect of the different definitions of B_o and Fr_o both sets of experimental data. Figures 6-17 and 6-18 show the two sets of data that are considered the accurate interpretations, compared to the SOFIE prediction.

The comparison of the SOFIE prediction against the different experimental data leads to differing conclusions. Consideration of the DTF data reveals the velocity profile is well predicted as it lies within experimental error, and the profile for density shows an underpredicted peak, with large spreading rate. This result is considerably different to the comparison against the SG data, confirming the result seen in the spreading rate section (section 6.3.1). Comparison against the SG data upholds the traditional view that the standard k-ε model gives inadequate predictions of the plume, where the spreading rate is underpredicted. The large differences between these results suggest it is now necessary to question whether it is the experimental data that are at fault rather than the turbulence model.

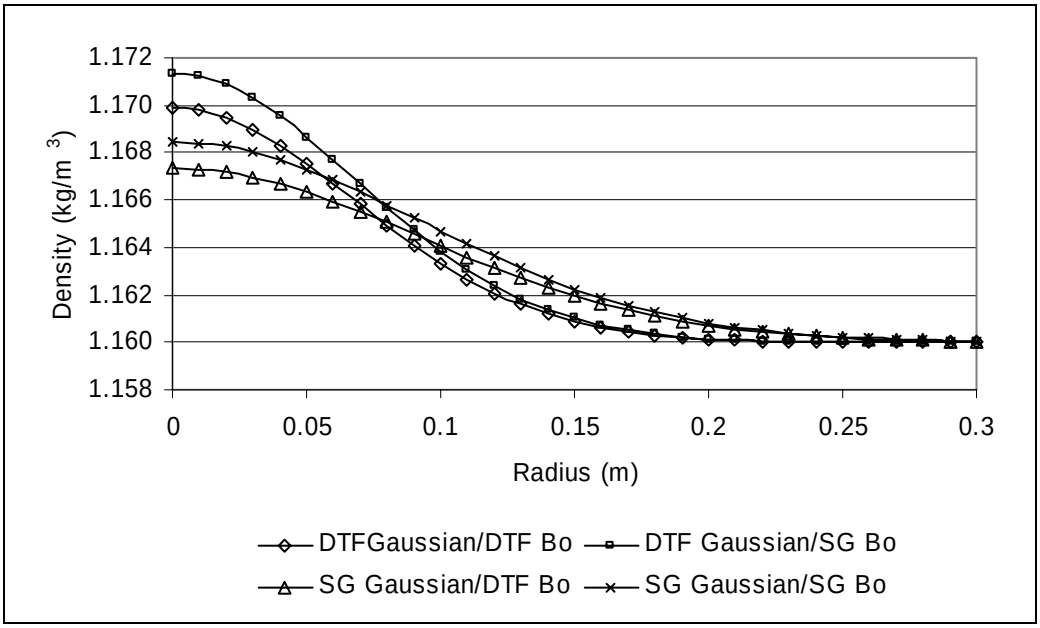

Figure 6-15 Comparison of the density profile for different interpretations of the experimental data: DTF Gaussian/DTF B_o – profile calculated with DTF constants and DTF definition of initial buoyancy; DTF Gaussian/SG B_o - profile calculated with DTF constants and SG definition of initial buoyancy; SG Gaussian/DTF B_o - profile calculated with SG constants and DTF definition of initial buoyancy; SG Gaussian/SG B_o - profile calculated with SG constants and SG definition of initial buoyancy.

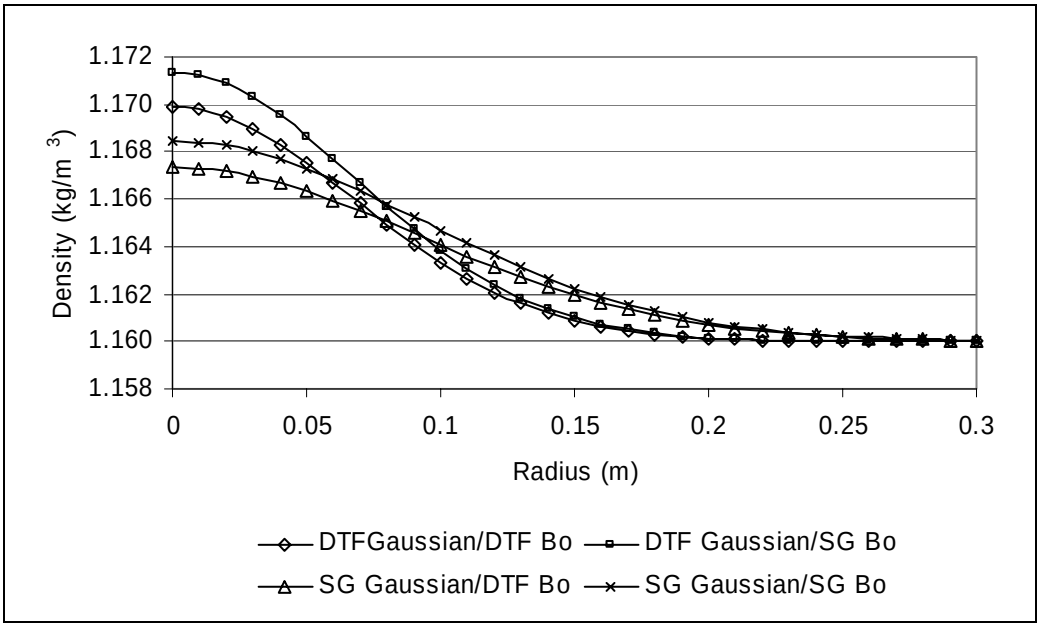

Figure 6-16: Comparison of the streamwise velocity profile for different interpretations of the experimental data with the prediction of the axisymmetric buoyant jet. Refer to figure 6-15 for details of abbreviations.

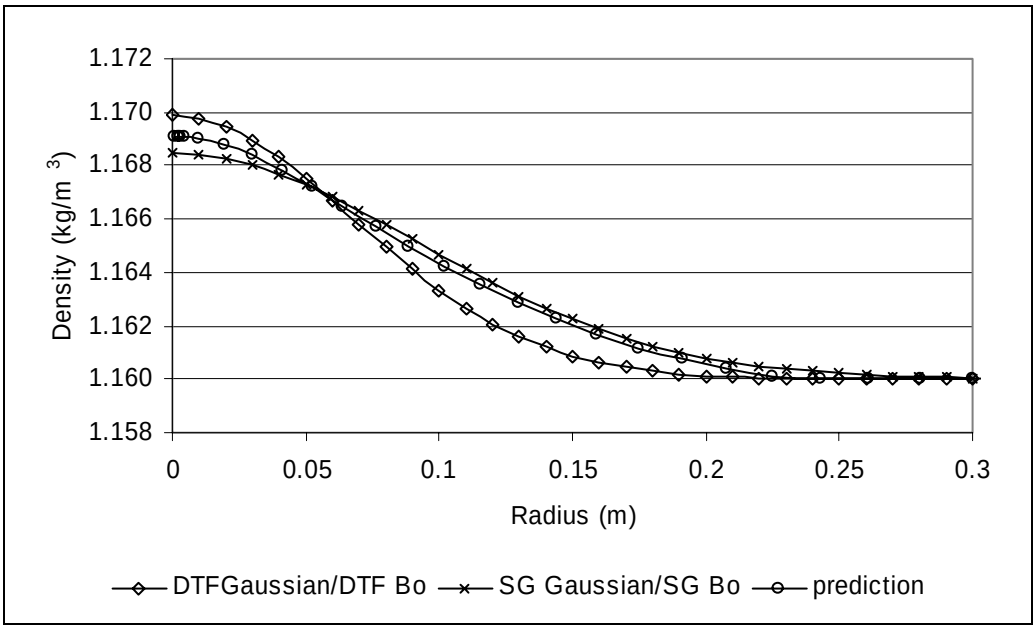

Figure 6-17: Comparison of the density profile for useful interpretations of the experimental data with the prediction of the axisymmetric buoyant jet. Refer to figure 6-15 for details of abbreviations.

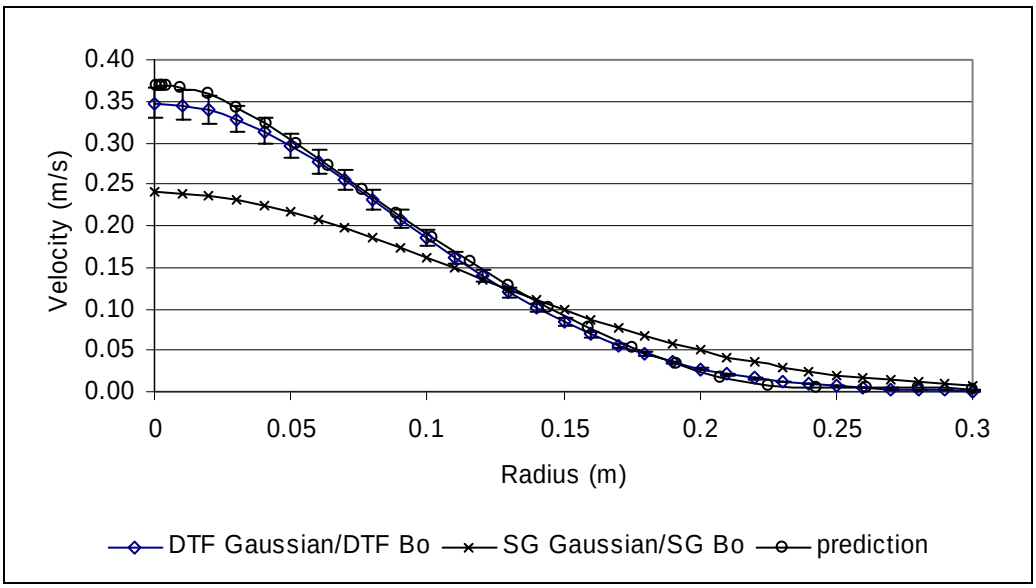

Figure 6-18: Comparison of the streamwise velocity profile for useful interpretation of the experimental data with the prediction of the axisymmetric buoyant jet. . Refer to figure 6-15 for details of abbreviations.

6.3.3 Turbulent Characteristics

Recent experimental studies of buoyant jets have generally included some measurements of velocity and of scalar fluctuations and their correlations. The measurements for plane plumes have not reached a mature state and considerable variation exists between the various studies. The measurements from the axisymmetric buoyant jet studies, however, appear to be more consistent. This section compares the experimental measurements and numerical predictions of the characteristics of axisymmetric buoyant jets. It will be limited to a comparison of the predictions of the turbulent characteristics of the axisymmetric buoyant jet by the standard k-ε model with the experimental measurement of Dai, Tseng and Faeth (1994, 1995a and 1995b) (DTF).

6.3.3.1 *Normalised Velocity Fluctuations*

The graphs of experimental velocity and mixture fraction fluctuations have been reproduced for comparative purposes (Figure 6.19, 6.20, 6.21). The axial region is characterised by a minimum for the velocity fluctuations and a maximum for the mixture fraction fluctuations. Non-buoyant jets are characterised by a minimum for both velocity and scalar fluctuations. The maximum observed for the mixture fraction fluctuations is thus assumed to be a direct result of the buoyancy-turbulence interaction. The minimum observed in the velocity fluctuation measurements is expected, due to a reduction in the turbulent production due to symmetry. A comparison of the graphs for experimental velocity fluctuations reveal the radial and tangential fluctuations are roughly equal over the cross-section of the plume, whereas the streamwise fluctuations are larger near the central region. However, at the edge of the plume all the fluctuations are of a similar magnitude hence isotropic turbulence can be assumed to exist in this region.

Figure 6-22 shows the values of velocity fluctuations calculated from the eddy-viscosity relationship for the axisymmetric plume simulations based on the DTF experiments. It is clearly seen that the anisotropy of the experimental plume is not

well reproduced in the simulations. This is a well-established inadequacy of the eddy-viscosity relationship (equation 3.31). The normal components of fluctuations calculated from this relationship are given below:

$$-\rho\overline{u_1'u_1'} = 2\left(\mu + \frac{\mu_t}{\sigma_t}\right)\frac{\partial \tilde{U}_1}{\partial x_1} - \frac{2}{3}\rho k \qquad 6.17$$

$$-\rho\overline{u_2'u_2'} = 2\left(\mu + \frac{\mu_t}{\sigma_t}\right)\frac{\partial \tilde{U}_2}{\partial x_2} - \frac{2}{3}\rho k \qquad 6.18$$

$$-\rho\overline{u_3'u_3'} = 2\left(\mu + \frac{\mu_t}{\sigma_t}\right)\frac{\partial \tilde{U}_3}{\partial x_3} - \frac{2}{3}\rho k \qquad 6.19$$

The normal component of mean velocity gradient, in the self-similar region of the plume, can be expected to be small; hence, the normal fluctuating components become approximately equal.

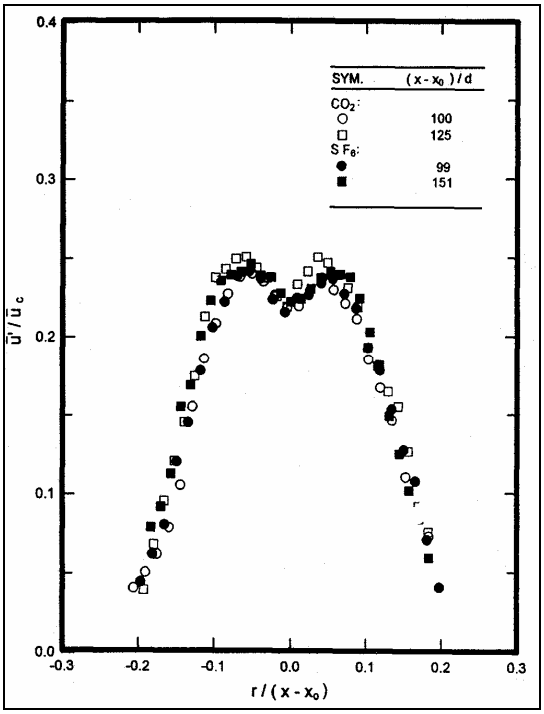

Figure 6-19: Experimental measurements streamwise velocity fluctuation against the normalised velocity reproduced from Dai et al. (1995a). Where $\overline{u}'/\overline{u}_c$ is the velocity fluctuation normalised by the mean centreline velocity; r/(x-x$_o$) is the radius normalised by the height at which the measurements were taken; (x-x$_o$)/d is the height at which the measurements were taken normalised by inlet diameter.

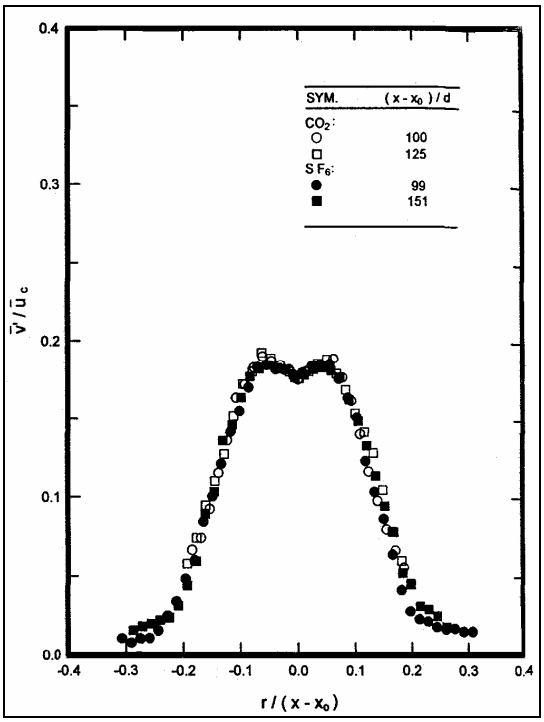

Figure 6-20: Experimental measurements radial velocity fluctuation against the normalised velocity reproduced by Dai et al. (1995a). See figure 6-19 for nomenclature.

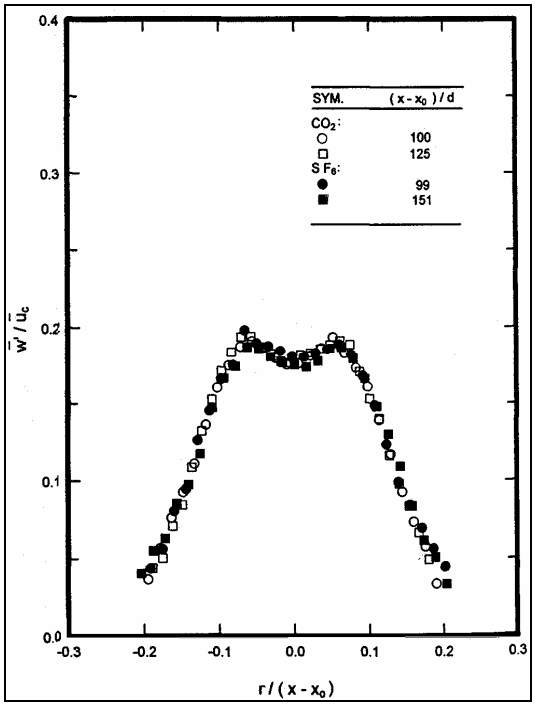

Figure 6-21: Experimental measurements circumferential velocity fluctuation against the normalised velocity reproduced from Dai et al. (1995a). See figure 6-19 for nomenclature.

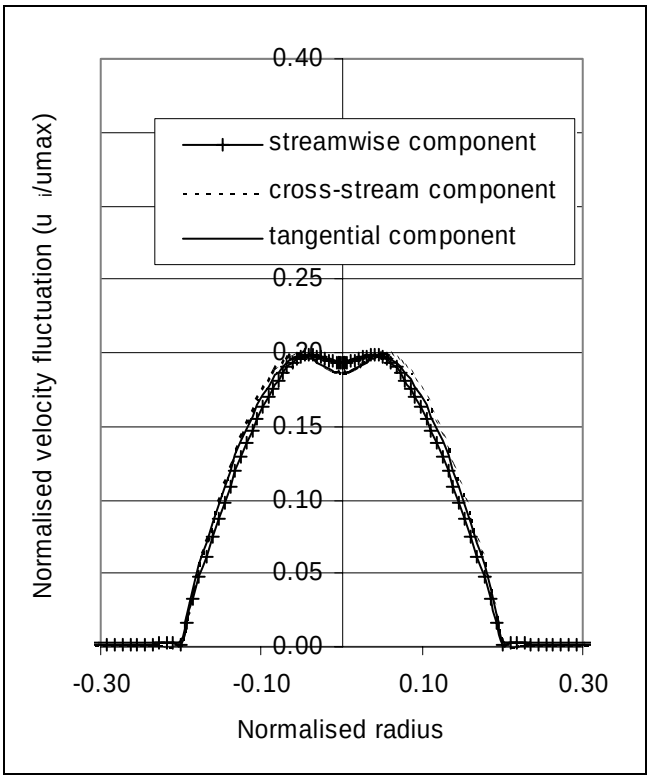

Figure 6-22: Velocity fluctuations of the axisymmetric buoyant jet, predicted with the linear eddy-viscosity model.

6.3.3.2 *Reynolds Stresses*

Figure 6-23 shows the graph reproduced from Dai et al. (1994b) of the experimental measurements for the turbulent shear stress. The consistency of the experimental data was checked against a simplified form of the momentum equations that was found to be:

$$\frac{\overline{u'v'}}{\overline{u_c}^2} = \left(\frac{\mathrm{F}(0)}{2\eta \mathrm{k}_\mathrm{f}^2 \mathrm{U}(0)^2} \right) \left(1 - e^{-\mathrm{k}_\mathrm{f}^2 \eta^2} \right) + \left(\eta + \frac{1}{3\mathrm{k}_\mathrm{u}^2 \eta} \right) e^{-2\mathrm{k}_\mathrm{u}^2 \eta^2} - \frac{1}{\left(3\mathrm{k}_\mathrm{u}^2 \eta\right)^2} - \frac{\overline{u}\,\overline{v}}{\overline{u}_c^2} \qquad 6.20$$

Figure 6-24 shows the prediction of Reynolds shear stress made with the linear eddy-viscosity relationship. Comparison of these two graphs shows the Reynolds shear stress of the plume is reasonably well predicted by this model.

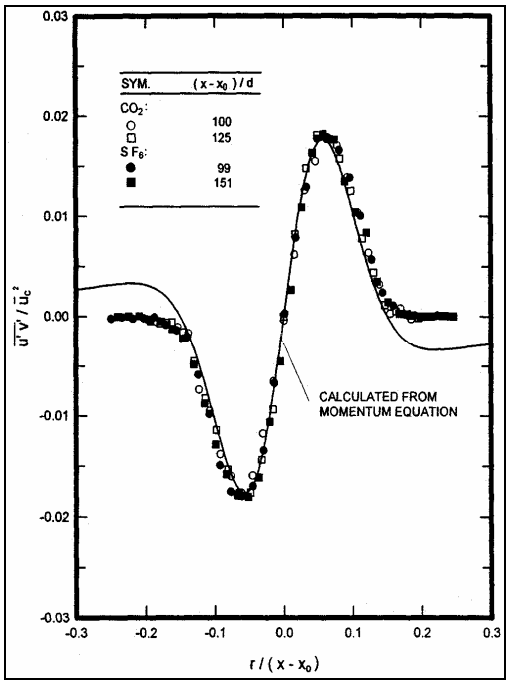

Figure 6-23: Experimental measurements Reynolds shear stress against the normalised radius reproduced from Dai, Tseng and Faeth (1994b). See figure 6-19 for nomenclature.

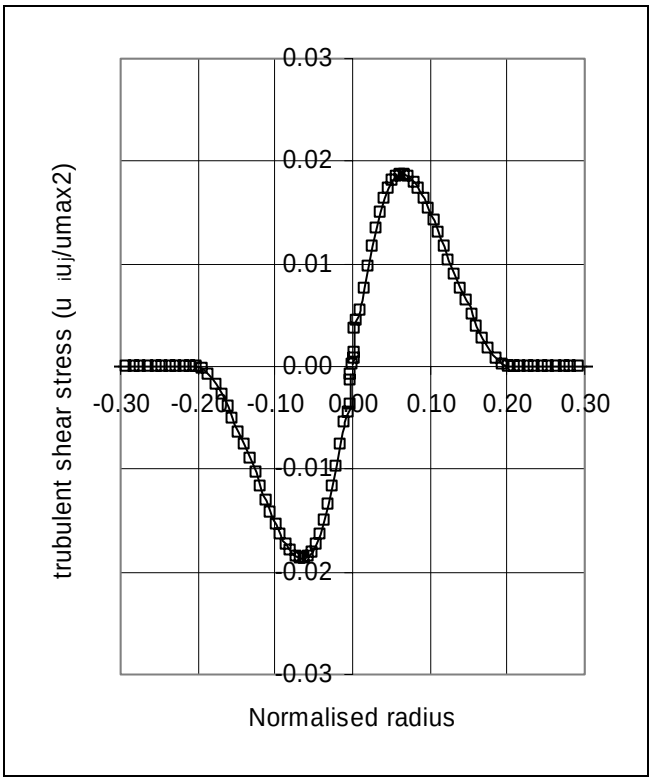

Figure 6-24: Reynolds shear stress for the axisymmetric plume, predicted by the linear eddy-viscosity relationship.

***6.3.3.3** Turbulent Mixture Fraction Flux.*

Figure 6-25 show the reproduced graph of the experimental results for turbulent mixture fraction flux and figure 6-26 gives the predictions made in the current numerical simulations. The predicted values are derived from the eddy-diffusivity relationship. The radial and tangential components are reasonably well predicted. The streamwise component, however, is underpredicted at its peak by an order of magnitude. This underprediction is associated with the eddy-diffusivity model, the streamwise component of which is defined by equation 6.21:

$$\overline{\rho u_1'' f''} = -\Gamma \frac{\partial \tilde{f}}{\partial x} \qquad 6.21$$

This shows the streamwise component of mixture fraction flux to be dependent on the mean streamwise gradient of mixture fraction. In the self-similar region, this term becomes very small and hence producing a poor prediction. Physically, some influence from buoyancy and the cross-stream gradients would be expected.

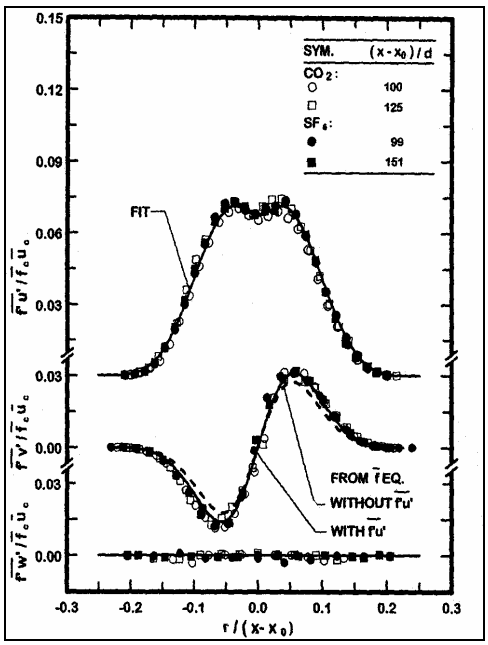

Figure 6-25: Experimental measurements of turbulent scalar flux components reproduced from Dai, Tseng and Faeth (1994b). Where $\overline{f'u'}/\bar{f}\bar{u}_c$, $\overline{f'v'}/\bar{f}\bar{u}_c$, $\overline{f'w'}/\bar{f}\bar{u}_c$ is the streamwise, radial and circumferential turbulent scalar flux, respectively, normalised by the mean centreline velocity and mixture fraction; r/(x-x$_0$) is the radius normalised by the height at which the measurements were taken; (x-x$_0$)/d is the height at which the measurements were taken normalised by inlet diameter

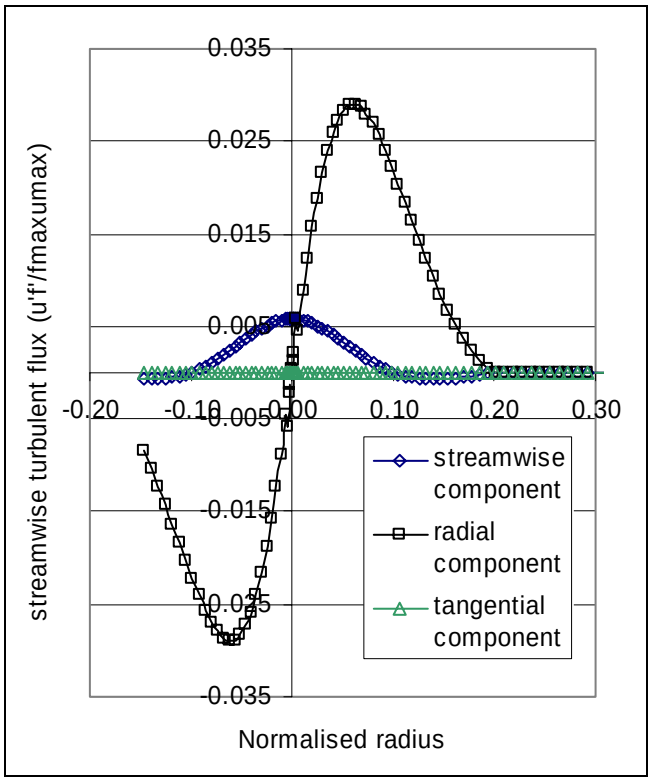

Figure 6-26: Turbulent scalar flux components for axisymmetric buoyant jet predicted by eddy-diffusivity model.

6.3.3.4 Budget of Turbulent Kinetic Energy

Figures 6-27 and 6-28 show the experimental and predicted graphs of the turbulent kinetic energy budget, respectively. The budget estimates the normalised values of the various terms in the relevant transport equation.

Comparison of these graphs reveals a large underprediction of turbulent buoyant production, a significant underprediction in the magnitude of the peak value of dissipation and small underprediction in magnitude of the peak and spread of the diffusion term. A good prediction for the mean property profiles for the axisymmetric buoyant jet, when compared against the DTF experimental data, is possible because the bad prediction in the different terms compensate for one another. That is, the large underprediction in the buoyant production is balanced by less diffusion and dissipation in the plume. Although the actual values for the

various terms are not physically accurate, the resultant sum gives a good estimate of the turbulent kinetic energy.

The buoyant production term for the standard k-ε model is modelled by the eddy-diffusivity relationship. Buoyancy is only of influence along the gravitational component of the flow, which, in the considered flow, is the streamwise component. In the previous section, it was demonstrated that the mean gradient in this component direction is very small, hence the buoyant influence becomes insignificant.

The dissipation term is modelled by a transport equation that is subject to a large number of modelling assumptions, including the modelling of the buoyant influence. The underpredicted peak is off the centre where velocity gradients would be expected to be significant, as in the case of the shear stress production. It is possible that the modelling assumptions have over simplified the influence of the velocity gradients on this term.

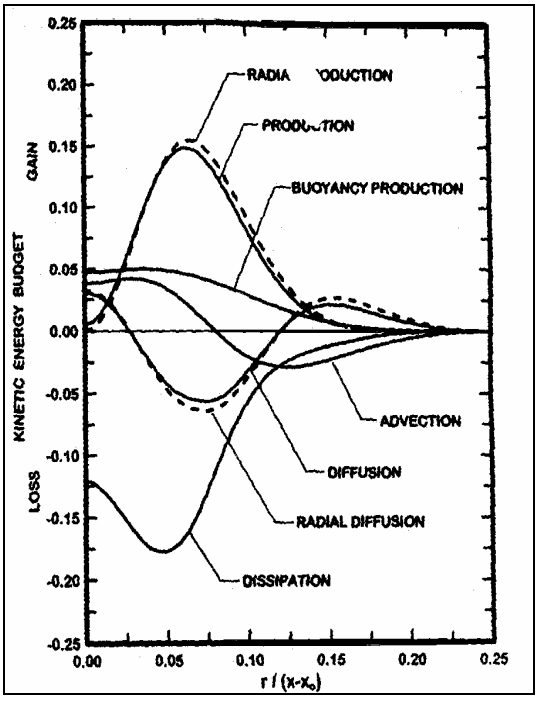

Figure 6-27: Turbulent kinetic energy budget reproduced from Dai Tseng and Faeth (1994b).

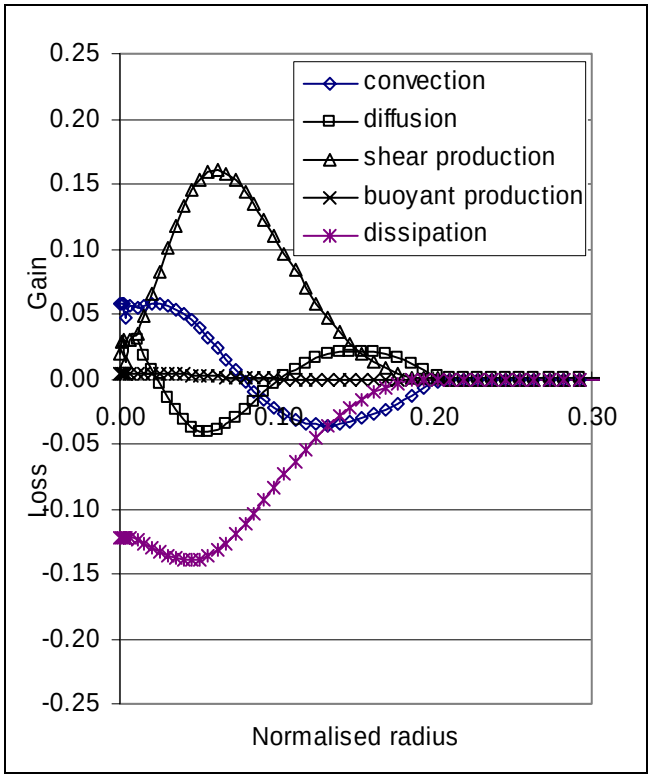

Figure 6-28: Predicted turbulent kinetic energy budget for axisymmetric buoyant jet.

6.4 Closure

This chapter reported the solution achieved for the turbulent buoyant jets with the standard k-ε model combined with the linear eddy-viscosity model. Three turbulent buoyant jets were considered: a plane pure plume, a plane buoyant jet and an axisymmetric buoyant jet. The pure plume was found to be a computationally sensitive flow whereas the simulations of the buoyant jets were more robust.

The simulated plane pure plume was not directly based on an experimental study. The pure plume was thus validated against experimental data through consideration of similarity but this normalised comparison was found to be uninformative. The plane and axisymmetric buoyant jets were based directly on experimental studies and this enabled comparison of absolute values.

A comparison was made of spreading rates from reported experimental data, previous numerical simulations and the numerical simulation results from this study. It was demonstrated that, for plane buoyant jets, the spreading rates predicted in the numerical studies were consistently below that of the experimental studies. However, this comparison of spreading rates for the axisymmetric buoyant jets was dependent on experimental datasets.

A trend in the reported experimental studies has shown that there is a reduction in the spreading rate with more recently published literature. This is a consequence of the increased sophistication of the experimental apparatus that enables measurements at ever-increasing distances from the plume source. The consequence of this has been to refute the view that the standard k-ε model underpredicts the spreading rate of turbulent buoyant jets. It appears that the turbulence models were not inadequate rather the experimental data lacked current sophistication and hence accuracy.

The turbulent characteristics of the axisymmetric buoyant jet, predicted by the standard k-ε model and linear eddy-viscosity model, were compared with the published experimental data to gain a better understanding of the capabilities of this model. This showed the inability of the eddy-viscosity model to predict the anisotropy in the velocity fluctuations and of the eddy-diffusivity model to predict the streamwise turbulent flux.

The budget of the turbulent kinetic energy transport equation demonstrated the poor prediction of turbulent production by buoyancy, and the slight underprediction of the diffusion. The overall good prediction of the turbulent kinetic energy suggested that the inadequacies, shown by this budget, compensated for each other and that the net solution of the resultant flow and thermal field was acceptably accurate.

In summary, this chapter has made a detailed comparison of the prediction of the three considered turbulent buoyant jets and enabled the strengths and weaknesses of the buoyancy-modified standard k-ε model to be identify.

CHAPTER 7

Simulations of Buoyant Jets with Selected Turbulence Models

7.1 Introduction

This chapter reports the application of those models implemented in the current work to the considered turbulent buoyant jets. The quality of the predictions achieved is discussed with reference to the standard k-ε model predictions and existing experimental data.

All the simulations in the current work were undertaken using SOFIE. A hybrid discretisation scheme was adopted with a TDMA solver for the momentum and scalar transport equations. The SIMPLEC algorithm was adopted for the pressure correction scheme and SIP was used for the pressure solver. The convergence criterion was based on a mass residual of 1×10^{-3}.

Section 7.1 presents results from high Reynolds number two-equation models, the transformed k-ε model and the RNG model, that are considered as direct alternatives to the standard k-ε model. Natural convective flows are often characterised by low Reynolds numbers. It was considered appropriate to test the capabilities of two low Reynolds number two-equations models, the Launder and Sharma model and the standard k-ω model. The results gained from the application of these models are reported in section 7.2.

It was found that the buoyant production of turbulent kinetic energy was poorly predicted by the standard k-ε model. Alternative methods for modelling this term are considered in section 7.3. Section 7.4 reports on the effect of the introduction of a more advanced scalar diffusion model. Finally, section 7.5 reports on the application of the nonlinear eddy-viscosity models to the axisymmetric turbulent buoyant jet.

7.2 Alternative Two Equation Models

7.2.1 High Reynolds Number (HRN) Models

Two HRN number models were considered in addition to the standard k-ε model: the RNG k-ε model and the transformed k-ε model. These models were presented in section 3.9 and their implementation was discussed in section 5.7

The following section will discuss the quality of the predictions made by each of these models in comparison to the standard k-ε model and experimental data. The spreading rates calculated from these models are summarised in table 7-1

	Plane buoyant jet		Axisymmetric buoyant jet	
	Velocity spreading rate	Temperature spreading rate	Velocity spreading rate	Temperature spreading rate
RNG k-ε	0.0840	0.0880	0.0931	0.0906
Transformed k-ε	0.0983	0.1030	0.1073	0.1038
Standard k-ε	0.0835	0.0872	0.0907	0.0864
DTF	x	x	0.0863	0.745
RC	0.110	0.1330	x	x

Table 7-1: Comparison of the spreading rate of the buoyant jet predictions by different turbulence models and the experimental data of Dai Tseng and Faeth (1994, 1995a) (DTF) and Ramaprian and Chandrasekhara (1989) (RC).

Transformed Model

The transformed model (Menter (1994)) was developed for application to aerodynamic flows, but has been recently used in a similar form for the prediction of recirculating cavity flows (Peng et al. (1997)). Comparison of the predictions made with this model to the standard k-ε model vary between the plane and axisymmetric plumes; these differences are more exaggerated in the prediction of the scalar spread. Figures 7-1 to 7-3 compare the cross-stream profiles of mean temperature of the standard k-ε and transformed k-ε models for the plane plume, plane buoyant jet and axisymmetric buoyant jet respectively.

The prediction for the plane buoyant jet by the transformed model is comparable with those of the standard k-ε model, although a slight widening of the plume is observed. However, this is not true of the axisymmetric buoyant jet predictions that show a far more significant spread. Figures 7-4 and 7-5 show the centreline prediction of the mixture fraction for the plane and axisymmetric buoyant jets respectively. This confirms the large disparity exhibited between the standard and transformed model prediction of the thermal plume development that is not observed in the plane plume predictions.

Menter's transformed model neglected a viscous cross-diffusion term, which was demonstrated to have negligible effect. This has also been demonstrated in the

validation procedure in the current work, in which the prediction of a 2-dimensional channel flow replicated that of the standard k-ε model (Appendix A). The implemented form of the transformed k-ε equation, with this term included is given in equations 7.1 and 7.2.

$$\frac{\partial(\bar{\rho}k)}{\partial t}+\frac{\partial\left(\bar{\rho}\tilde{U}_j k\right)}{\partial x_j}=\underbrace{\tilde{\tau}_{ij}\frac{\partial\tilde{U}_i}{\partial x_j}}_{P_k}+\frac{\partial}{\partial x_j}\left(\left(\mu+\frac{\mu_t}{\sigma_k}\right)\frac{\partial k}{\partial x_j}\right)+\underbrace{\beta g_i\frac{\mu_t}{\sigma_T}\frac{\partial T}{\partial x_j}}_{G_k}-\bar{\rho}k\omega \qquad 7.1$$

$$\frac{\partial(\bar{\rho}\omega)}{\partial t}+\frac{\partial\left(\bar{\rho}\tilde{U}_i\omega\right)}{\partial x_j}=\frac{\partial}{\partial x_j}\left[\left(\mu+\frac{\mu_t}{\sigma_\varpi}\right)\frac{\partial\omega}{\partial x_j}\right]+C_{\omega 1}\frac{\omega}{k}\left(P_k+G_k\right)$$
$$-C_{\omega 2}\bar{\rho}\omega^2+2\left(\mu+\frac{\mu_t}{\sigma_\varpi}\right)\frac{1}{k}\frac{\partial k}{\partial x_j}\frac{\partial\omega}{\partial x_j} \qquad 7.2$$

The inclusion of this laminar viscous term in the simulations of the axisymmetric plume resulted in the prediction of a laminar plume, demonstrating that it has a non-negligible effect in the simulations of natural convection-type flows

Wilcox (1994) demonstrated that predictions of spreading rate of jets by the standard k-ω model was highly dependent on the free-stream values of the ω, this led to the development of transformed model that has been shown to have no sensitivity to the free-stream value of ω. A series of tests on both the free and inlet turbulent boundary conditions revealed little or no variation in the prediction of the spreading rate.

Analysis of the cross-stream ω-profile revealed a discontinuity at the boundary of the plume. The discontinuity appears to be a characteristic of the plume since it is also apparent, although to a lesser extent, in the ω-profile transformed from the converged solution of the standard k-ε model (figure 7.6). The prediction of turbulent/non-turbulent interfaces is a recognised difficulty in turbulence modelling. Wilcox (1994), in general reference to turbulence modelling, identified such solutions as being weak and characterised by two problems: firstly, multiple solutions are predicted and secondly, it has an adverse effect on the convergence and

the accuracy. For buoyant jet predictions, the second of these problems becomes apparent through the calculation of the gradient of ω that becomes indeterminable by the second order central differencing scheme used. The effect of this discontinuity becomes significant for the axisymmetric plumes since the expanding area of adjacent control volumes in the radial direction exaggerates the effect.

A converged solution with physical characteristics is achieved, despite this discontinuity, for both buoyant jets since the contribution from the cross-diffusion term is limited to the positive contribution only (Menter (1994)).

One possible approach to limit the effect of this cross-diffusion term would be for it to be treated as part of the diffusion term rather than a source term. This would eliminate the need to calculate the gradient of ω explicitly. It would be expected that the ω cross-stream profile would retain the discontinuity at the plume boundary but its gradient would not be calculated hence, the numerical difficulties associated with that calculation would not be relevant.

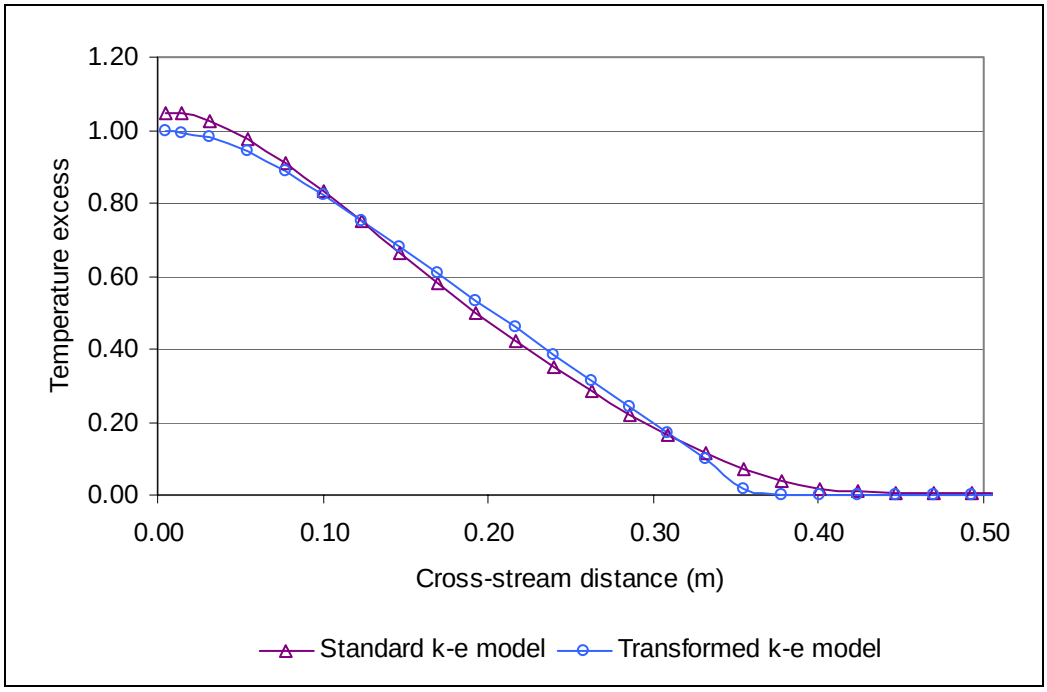

Figure 7-1: Comparison of cross-stream temperature profiles predictions by different turbulence models for a plane pure plume.

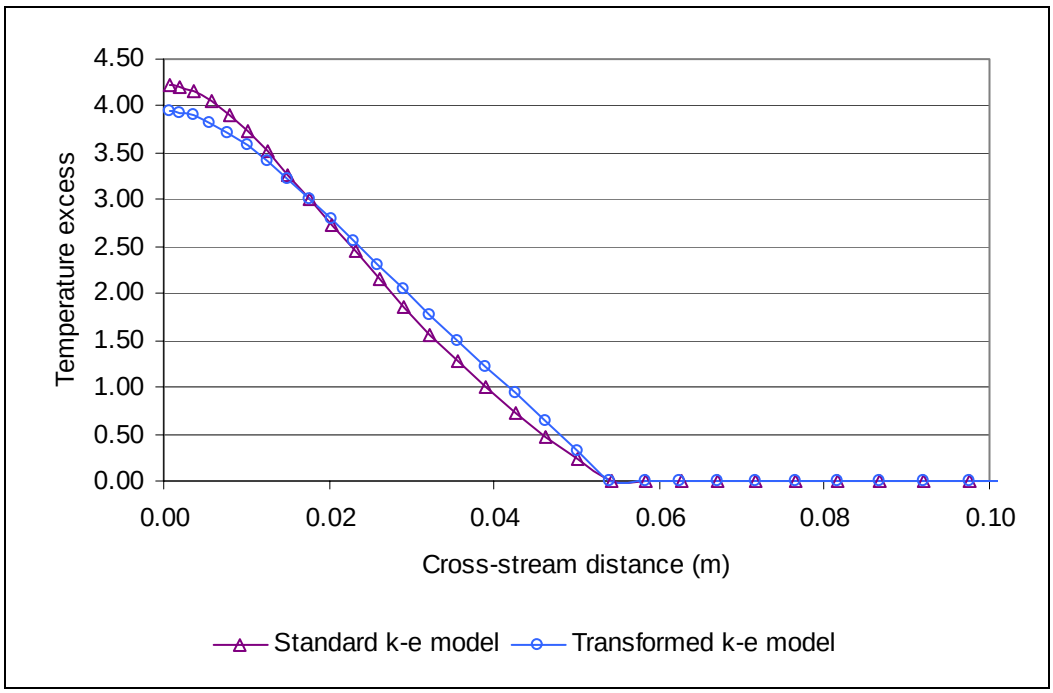

Figure 7-2: Comparison of cross-stream temperature profiles predictions by different turbulence models for a plane buoyant jet.

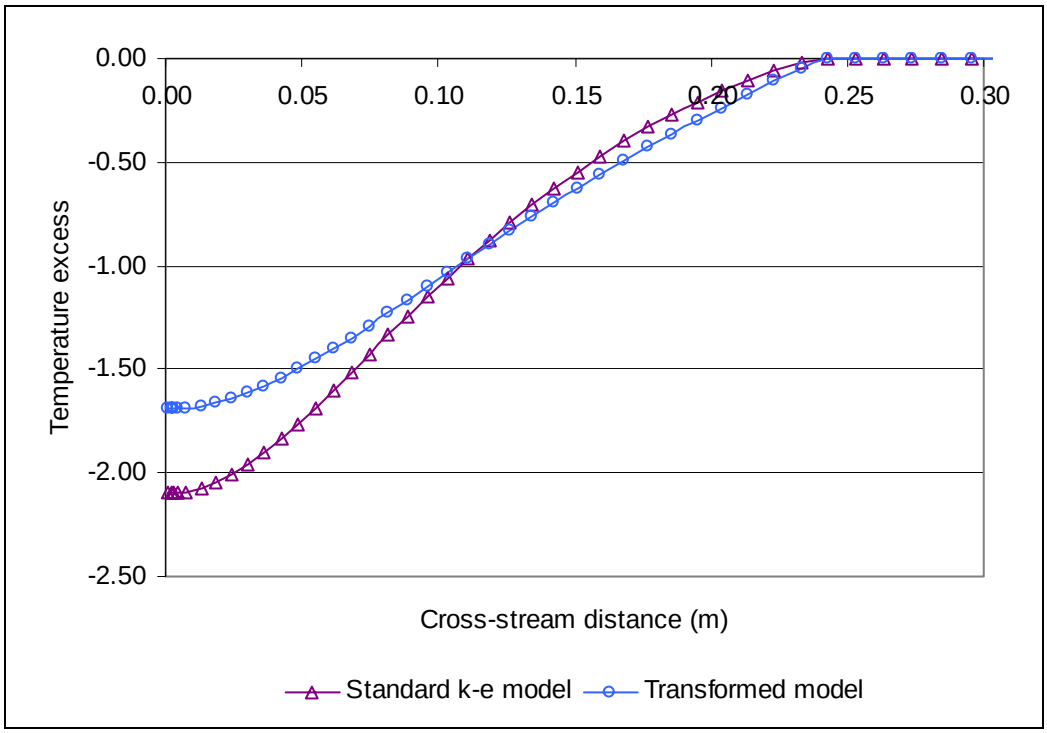

Figure 7-3: Comparison of cross-stream temperature profiles predictions by different turbulence models for an axisymmetric pure buoyant jet.

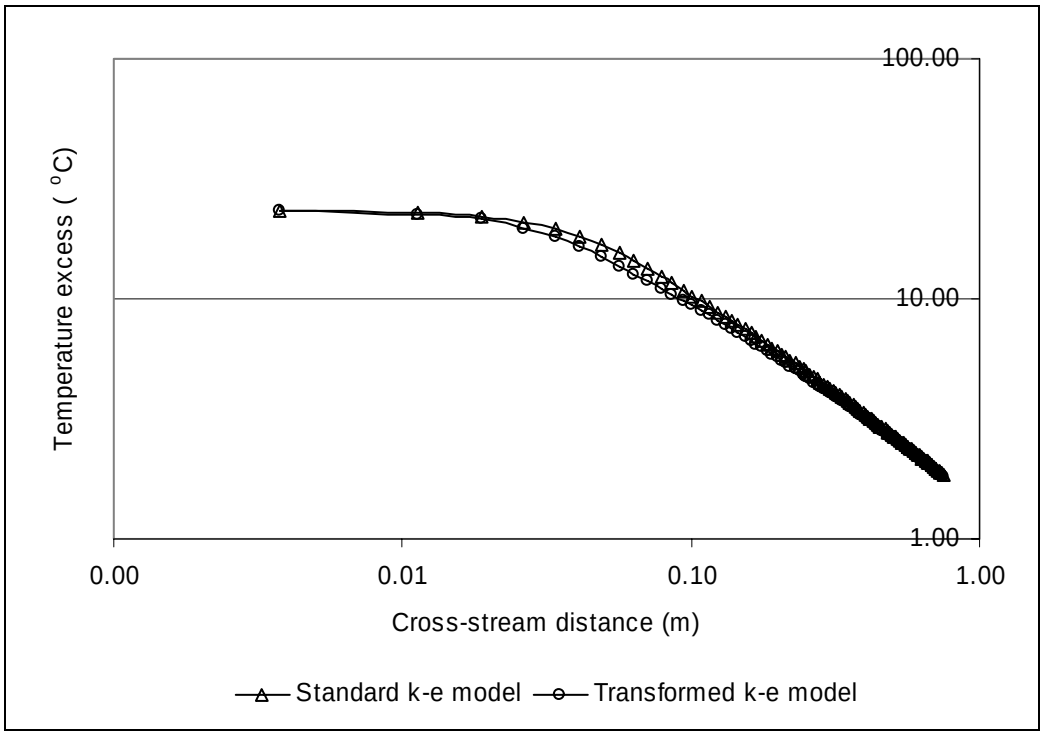

Figure 7-4: Prediction of mean temperature excess along the centreline of the plane buoyant jet by the standard k-ε and transformed models.

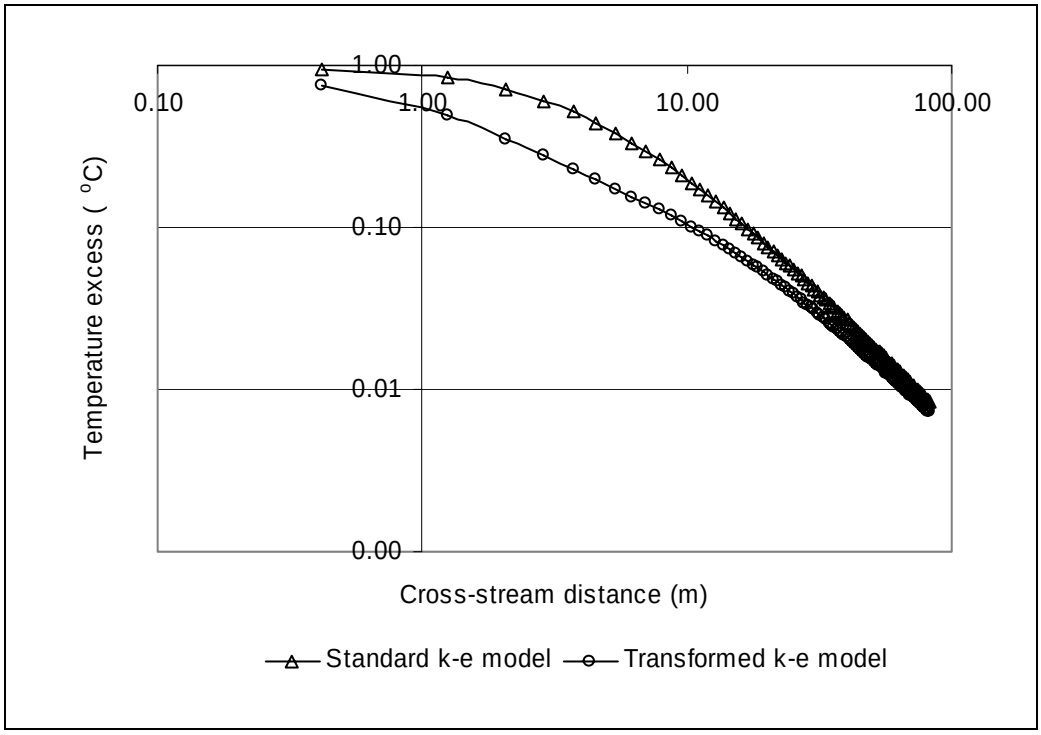

Figure 7-5: Prediction of mean temperature excess along the centreline of the axisymmetric buoyant jet by the standard k-ε and transformed models.

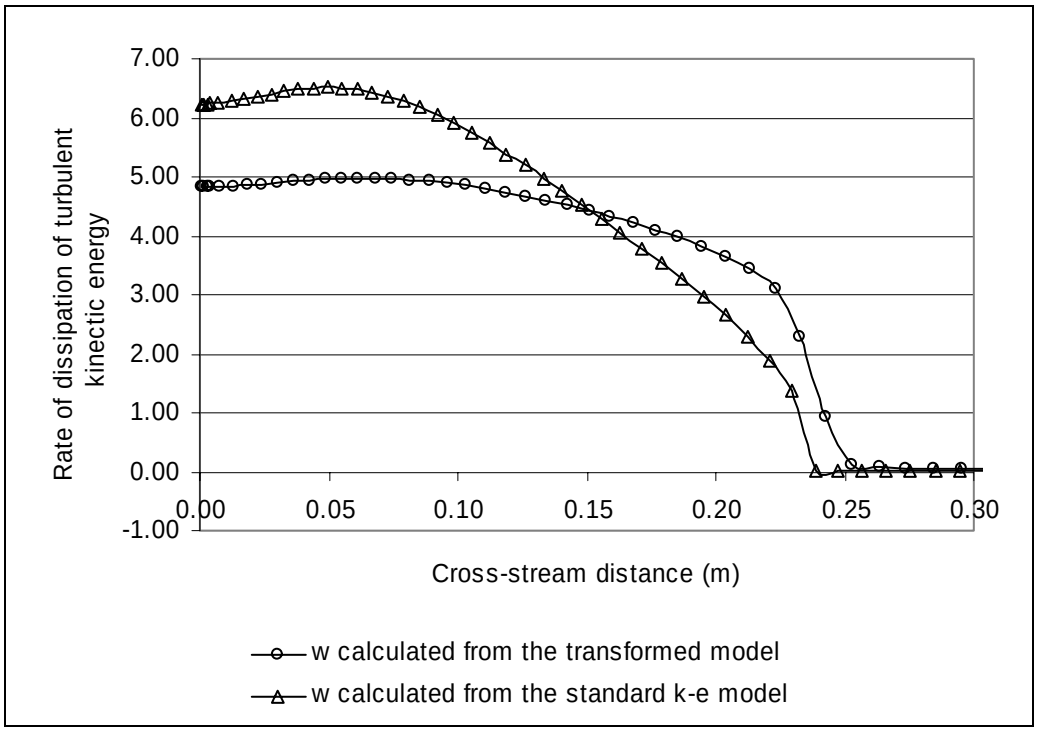

Figure 7-6: Cross-stream profile of ω for the axisymmetric buoyant jet predicted by the transformed and standard *k*-ε models.

RNG Model

Table 7-1 demonstrates that the RNG model slightly increases the spreading rate compared to the standard *k*-ε model. The RNG model has a similar form to the standard *k*-ε model, but with different coefficients and an additional term in the ε-equation. A series of simulations of the axisymmetric plume were undertaken to establish which of these factors had a significant effect on the flow. Figure 7-7 shows the velocity profiles from the set of three simulations: firstly the RNG model, secondly the RNG model with the standard *k*-ε model coefficient, and thirdly the standard *k*-ε model combined with the RNG coefficients. This demonstrates the equal but opposite effect of each feature, the additional term and the coefficients, to the prediction by the RNG model.

The implementation of the RNG model (section 5.7) was such that the additional term introduced by the RNG model to the ε-equation was considered to be a

component of the coefficient to the shear production term. Figure 7-8 shows the value calculated for this coefficient compared to the constant value (1.42) adopted by the standard k-ε model. The sharp variation in the value of the coefficient suggests that a finer grid may be requires for the RNG model compared to the standard k-ε model, to achieve a suitable resolution for the solution of this coefficient.

The resultant effect on k and ε is shown in figure 7-9. The most significant variation between the standard k-ε and RNG models appears in the core region of the plume, the dissipation is seen to reduce and results directly in an increase in the turbulent kinetic energy. The overall increase in the turbulence is considered a positive result since, from consideration of the velocity fluctuations in the experimental data compared to the predictions by the standard k-ε model, it can be deduced that there is a slight underprediction in the turbulent kinetic energy (section 6.3.3). Figure 7-10 shows the budget as predicted by the RNG model, the peak in the dissipation term is less clearly defined than for both the experimental data (figure 6-27) and standard k-ε model.

The RNG model predicts a mean velocity and scalar field similar to those obtained from the standard k-ε model. Distinct differences are observed in the turbulent field but it is unclear whether these amount to an overall improvement to the prediction.

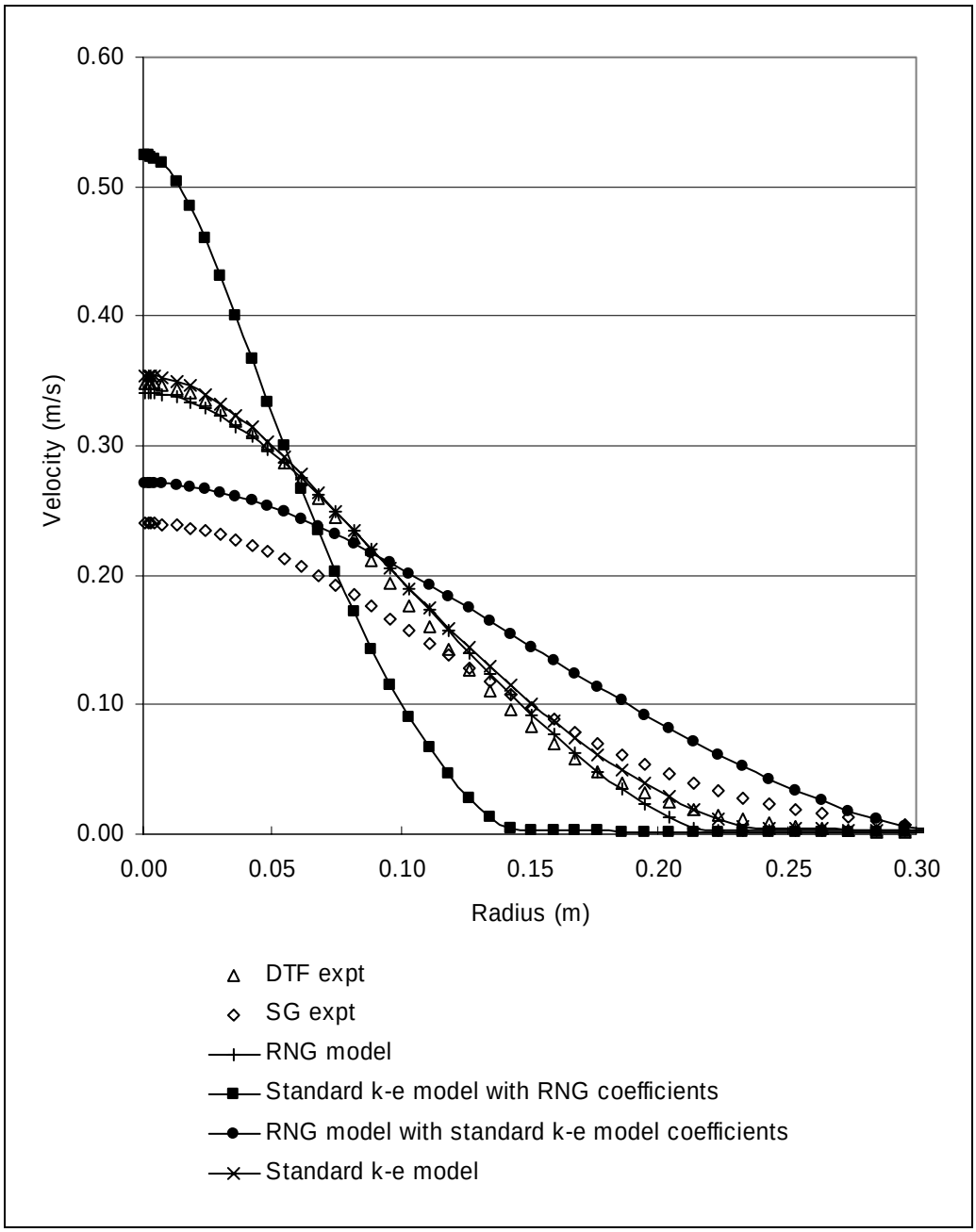

Figure 7-7: Mean velocity profiles predicted by the RNG and standard k-ε model in addition to hybrids of the two models compared to experimental data.

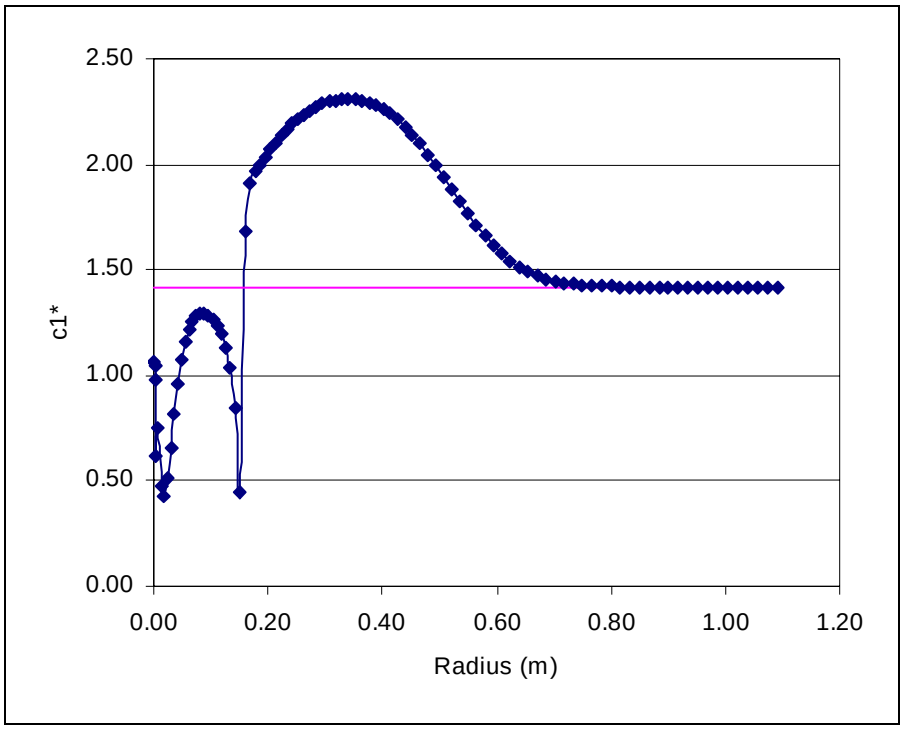

Figure 7-8: Predicted value of coefficient to the production term in the turbulent dissipation equation compared to the constant value of the standard *k-ε* model.

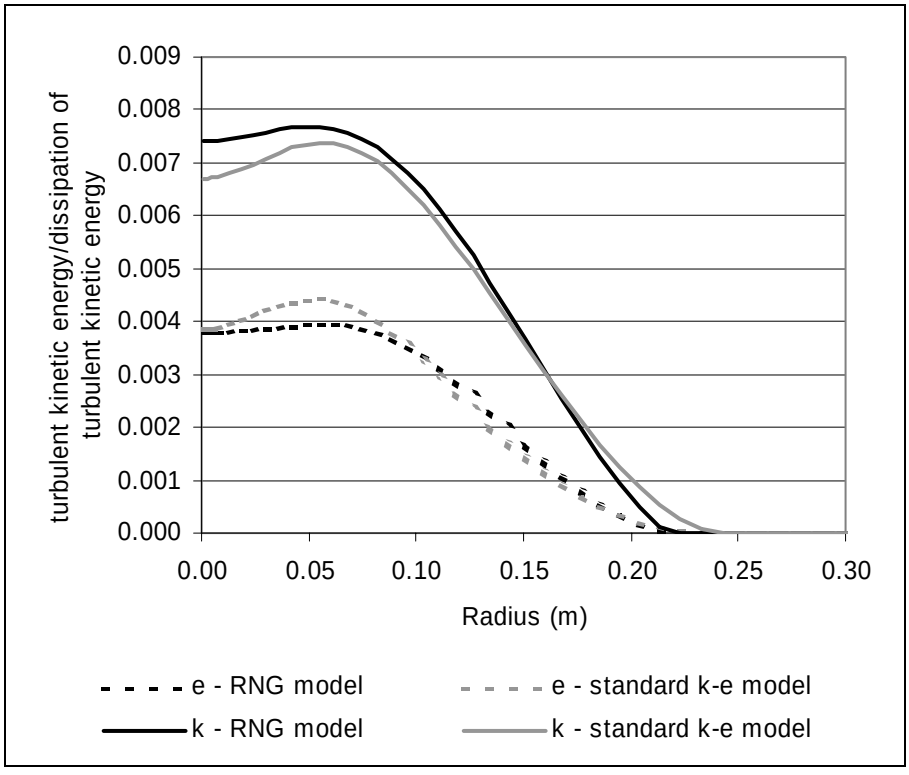

Figure 7-9: Comparison of turbulent kinetic energy (k) and dissipation turbulent kinetic energy (e) as predicted by the standard *k-ε* and RNG turbulent models.

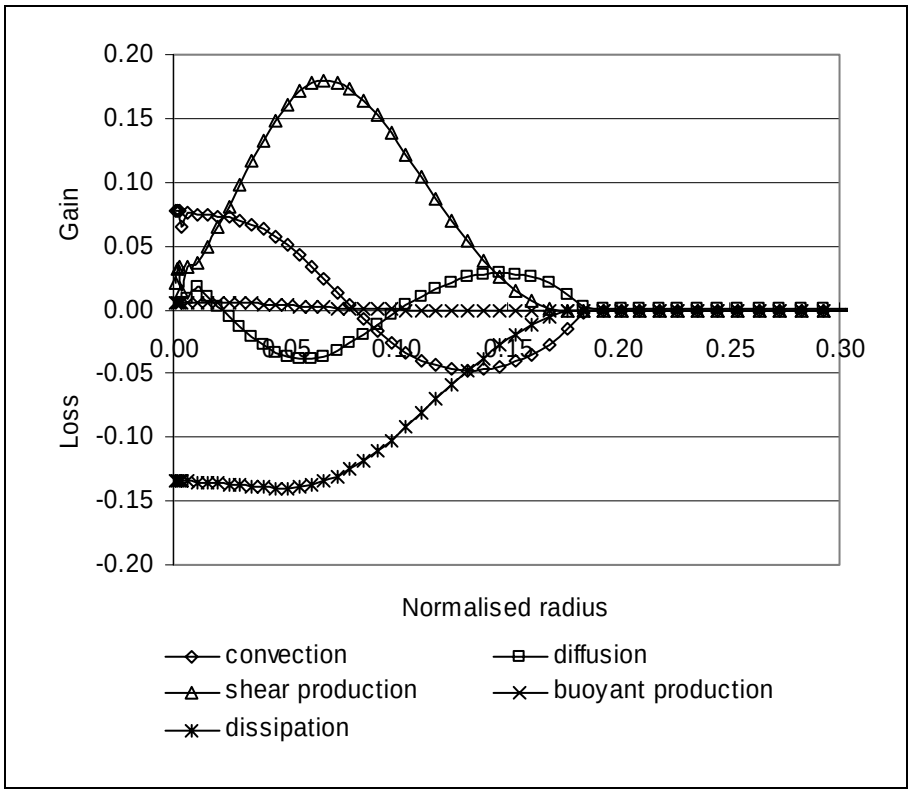

Figure 7-10: Budget of terms in the turbulent kinetic energy transport equations predicted by the RNG turbulence model.

7.2.2 Low Reynolds Number (LRN) Models

Two LRN models were implemented into SOFIE in the current work: Launder and Sharma's (LS) k-ε model (Launder and Sharma (1974)) and the standard k-ω model (Wilcox (1994)). These models were presented in section 3.9 and their implementation was discussed in section 5.7. Validation of these models was undertaken on two-dimensional channels flows to ensure physical results comparable to previous studies were achieved (Appendix A).

The LS LRN model has a similar form to the standard k-ε model, however the coefficients are sensitised to the turbulence in the flow and there is an additional term in both the k and ε equations. The LS LRN model was found to have limited success in the prediction of buoyant jets. A laminar solution resulted from predictions of the plane water plume. Comparative consideration of the various terms in the LS LRN turbulence model revealed a disproportionate contribution

from the 'extra term' (E) in the ε-equation. This term was introduced into the model in order to impart a velocity profile in the boundary layer with the correct shape; it had no physical basis. Figure 7-11 compares the velocity fields of the plane buoyant jet predicted with the LS LRN turbulence model when this term is included and neglected. The modified version of this model predicts a turbulent plume.

	Plane plume		Axisymmetric plume	
	Velocity spreading rate	Temperature spreading rate	Velocity spreading rate	Temperature spreading rate
LS LRN	0.0117	0.0112	0.0779	0.0750
Modified LS LRN	0.0793	0.0846	0.0825	0.0795
Standard k-ε	0.0820	0.086	0.0907	0.0864

Table 7-2: Comparison of the spreading rate of the buoyant jet predictions by different turbulence models.

Figure 7-12 compares the mean velocity profiles of the axisymmetric buoyant jet predicted by the LS LRN model in both its complete and modified forms. For this case it is clear that there is a far smaller difference, in the flow field, predicted by the LS LRN model in its complete and modified forms.

The high dependence of these predictions on the boundary conditions and the variation between the plane and axisymmetric plumes demonstrates this model to be highly sensitive. Hence, further simulation of plumes and convective flows were not undertaken.

Plume predictions by the standard k-ω model were found to be highly unreliable. No results of the quality of the previous models were achieved. In addition, the solutions were found to be highly dependent on initial and boundary conditions.

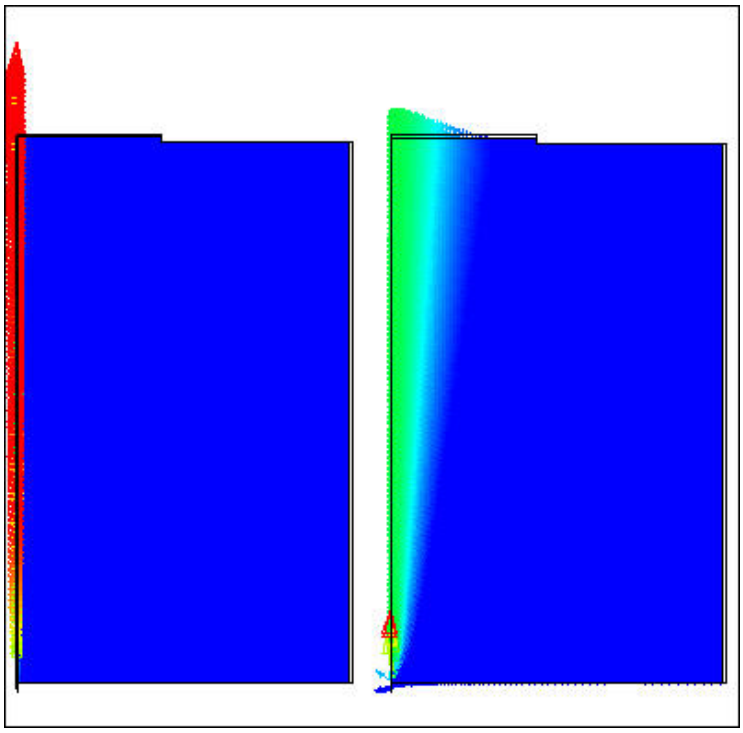

Figure 7-11: Comparison of the velocity flow of the plane buoyant jet as predicted by the LS LRN and modified LS LRN flow turbulence model.

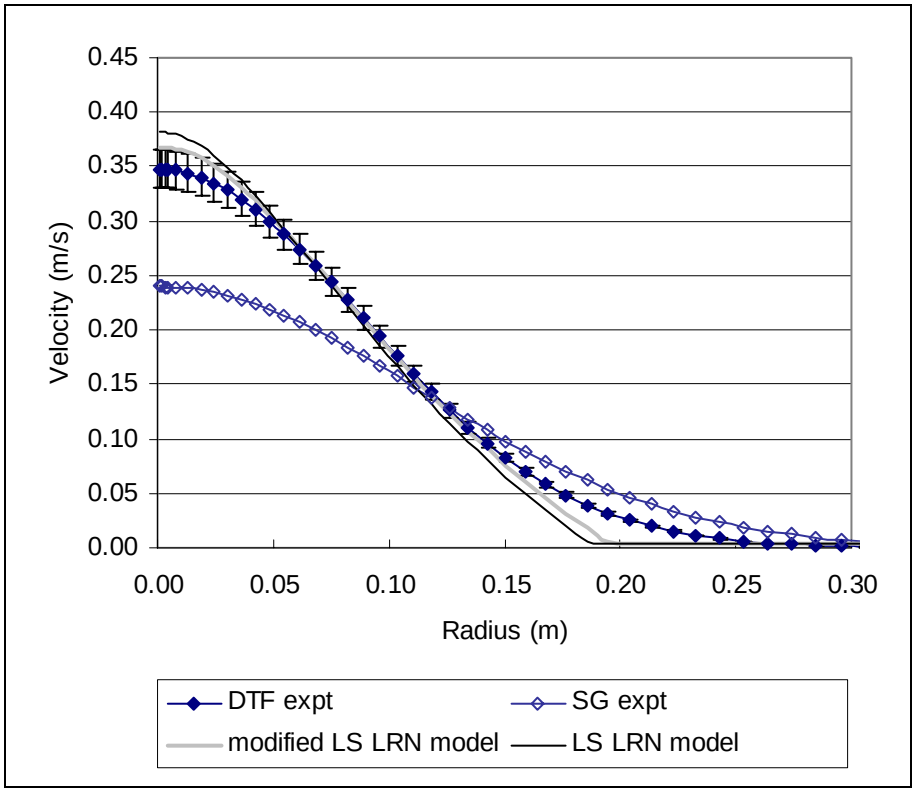

Figure 7-12: Mean velocity profile of the axisymmetric buoyant jet predicted by the LS LRN model and the modified LS LRN model compared to experimental data.

7.3 Turbulent Buoyancy Models

The results presented in the previous sections have all included the standard turbulent buoyancy model based on the eddy-diffusivity model (section 3.6.2). Figure 6.28 showed the budget of terms for the transport equations of turbulent kinetic energy predicted by the standard k-ε model and demonstrated that, in comparison with the other terms, the turbulent buoyant production (G_k) was significantly underpredicted. This inadequacy has been widely reported in the literature and, in this section, the results from a more complex representation of the buoyant turbulent production are presented. In addition, the relative influence of the G_k term's inclusion in the k and ε transport equations is considered.

Previous authors have all demonstrated an increase in spreading rate with the inclusion of a turbulent buoyancy model, however the significance of the effect has varied. The authoritative text of Hossain and Rodi (1982) showed the spreading rate to be increased by the inclusion of the eddy-diffusivity model form of G_k, by an amount comparable to that achieved with the introduction of an ASM model. However, subsequent studies, including the current work, have not shown such a significant effect.

The reasons for poor prediction of turbulent buoyant production by the eddy-diffusivity model are well established and were discussed in section 4.2.4. The GGDH model provided a further improvement to the turbulent buoyant term, as had been demonstrated in other buoyant flows such as differentially heated cavities (Ince and Launder 1989)

The effect of introducing a more complex representation of the Reynolds stresses into the GGDH models was also considered. Here, the linear representation was replaced by a cubic nonlinear relationship. This form of the model increased the spreading rate of the plane buoyant jet and there was a slight decrease in the spread of the axisymmetric jet. The cubic model is discussed in more detail in section 7.5.2.

	Pure plane plume spreading rates		Plane buoyant jet spreading rates		Axisymmetric buoyant jet spreading rates	
	Velocity	Temp.	Velocity	Temp.	Velocity	Temp.
None	x	x	0.0836	0.0873	0.0900	0.0833
Eddy-diffusivity model	0.0847	0.0870	0.0837	0.0873	0.0907	0.0864
GGDH model with linear eddy-viscosity	0.0870	0.0892	0.0855	0.0892	0.0890	0.0847
GGDH model with cubic eddy-viscosity	x	x	0.0884	0.0920	0.0888	0.0846
Experimental	0.112*	0.104*	0.11**	0.133**	0.0863***	0.0745***

Table 7-3 Comparison of the spreading rate of the buoyant jet and plume predictions with different buoyant turbulent production models.

*Chen and Rodi
**Ramaprian and Chandrasekhara
***Dai, Tseng and Faeth

Figure 7-13 demonstrates the improvement in the prediction of the turbulent buoyant production by the GGDH model compared to the eddy-diffusivity model (figure 6.28). A comparative increase is seen in the prediction of the plane buoyant jet[3]. Despite this, the net effect on the spreading rate of the two plumes varies. An increase is seen in the spread of the plane buoyant plume whereas the prediction for the axisymmetric plume decreases. Comparison with the plane pure plume confirms the variation to be a result of geometry rather than fluid or orientation, since the plane pure plume exhibits the same trends in the spreading rate prediction as the plane buoyant jet (table 7-3).

[3] The budget produced in this section has been normalised with velocity half width rather than height, as used in the previous figures of budget. However the relative magnitude of G_k compared to the other terms demonstrates the increase in magnitude.

The work of Rodi and Hossain (1982) compared the cross-stream profiles and the budget of the turbulent kinectic energy for axisymmetric and plane pure plumes and non-buoyant jets. The general form of the turbulent kinetic energy budget of Hossain and Rodi (1982) has been replicated, as can be seen by comparison of figure 7-13 and figure 7-14, although as mentioned a comparable increase in the G_k prediction was not achieved. The work of Hossain and Rodi demonstrated that there was significant variation between the *k*-profile of the plane pure plume and jet but not for the axisymmetric pure plume and jet. The explanation for this was found by examination of the *k*-budgets: 'For the axisymmetric plume, there is again [as with the plane plume] a positive buoyant production in addition to the shear production, but in this case the average total production ($P+G$) is not much larger than the average dissipation, so that convection is not very important in this case and there is no significant difference in the *k*-level between the *k*-level in the axisymmetric jet and the corresponding plume. In contrast, the *k*-level in the plane plume was higher than that of the plane jet, and this is because in that case the total production is higher than the dissipation.' (Hossain and Rodi).

		Plane buoyant jet		Axisymmetric buoyant jet	
		C-D	P+G-ε	C-D	P+G-ε
Eddy-diffusivity model	$C_{\varepsilon 3} = C_{\varepsilon 1}$	-0.274	0.291	-0.000234	0.0000999
	$C_{\varepsilon 3} = 0$	-0.299	0.291	-0.000241	0.0001070
GGDH model	$C_{\varepsilon 3} = C_{\varepsilon 1}$	-0.375	0.293	-0.000216	0.0000922
	$C_{\varepsilon 3} = 0$	-1.05	0.844	-0.000775	0.0003420

Table 7-4: Integral of terms in the turbulent kinectic energy budget of the plane and axisymmetric jets: Convection (C), diffusion (D), shear production (P), buoyant production (G) and dissipation (ε).

Figures 7-15a and 7-15b show the normalised *k*-profiles for the various turbulent buoyancy models for the axisymmetric and plane buoyant jets respectively. Comparison of the eddy-diffusivity and GGDH models, when included in both the *k* and ε equations shows an insignificant variation in the *k*-prediction of the axisymmetric jet, whereas there is a noticeable increase across the *k*-profile of the plane buoyant jet. A rough numerical integration of the terms displayed in the *k*-budgets normalised by maximum cross-stream velocity and velocity half width is

given in table 7-4. This verifies the conclusion of Hossain and Rodi that the production and dissipation terms of an axisymmetric plume exhibit a greater tendency towards local equilibrium that a plane plume. The inclusion of the GGDH model in the axisymmetric plume is shown to have a minimal net effect of the balance term but becomes far more significant for the plane buoyant jet (i.e. comparison of the values in the first and third lines of table 7-4), giving rise to the higher level of k.

7.3.1 Buoyancy Correction in the ε-equation

The form of the turbulent buoyancy production term in the ε-equations varies considerably between studies. The three common approaches are:

- The neglect of the term, the justification for this was that there is no physical basis for its inclusion and the overall effect on the solution from this term was insignificant (Markatos, Malin and Cox (1982))
- The term is multiplied by a coefficient equation equal to that of the shear buoyant production. This was the default method chosen in the current work and is the approach taken unless otherwise stated.
- The term is multiplied by the modified Richardson flux number in addition to a coefficient. Hossain and Rodi (1982) developed this method in order to distinguish between horizontal and vertical shear layers; this approach has been investigated by (Worthy, Rubini and Sanderson (2000)).

The current work considers both the neglect of the G_k term in the ε-equations ($C_{\varepsilon 3}$ = 0) and its inclusion with a coefficient equal to that of the shear production term ($C_{\varepsilon 3}$ = $C_{\varepsilon 1}$). Table 7-5 shows the spreading rates achieved from this series of simulations.

An increase in the spreading rate is observed when the G_k term is neglected in the ε-equations compared to its inclusion in both the k and ε equations. This trend is consistent for both the eddy-diffusivity and GGDH turbulent buoyancy models and for both the plane and axisymmetric buoyant jets; it is more exaggerated for the GGDH model. The increase results from the reduction in the ε through the neglect

of the G_k term. ε is directly coupled to the transport equation for k and a reduction in its value results in a larger value of k. The net effect is an increase in the effective viscosity and hence an increase of the diffusion in the momentum equations, leading directly to a larger spreading rate. The neglect of the GGDH G_k term from the ε-equations in the axisymmetric buoyant jet, results in a large increase in the budget imbalance (table 7-4). Although the differences are small compared to the plane buoyant jet, this result suggests that the turbulent buoyancy correction should be retained in both equations in order that equilibrium is satisfied.

		Plane buoyant jet		Axisymmetric buoyant jet	
		Velocity spreading rate	Temperature spreading rate	Velocity spreading rate	Temperature spreading rate
Eddy-diffusivity model	$C_{\varepsilon 3}=C_{\varepsilon 1}$	0.0820	0.0860	0.0907	0.0864
	$C_{\varepsilon 3}=0$	0.0834	0.0871	0.0917	0.0878
GGDH model	$C_{\varepsilon 3}=C_{\varepsilon 1}$	0.0880	0.0917	0.0890	0.0847
	$C_{\varepsilon 3}=0$	0.11623	0.1193	0.1157	0.1093

Table 7-5: Spreading rate predicted with two different turbulent buoyancy production models where the contribution to the ε-equations has been varied.

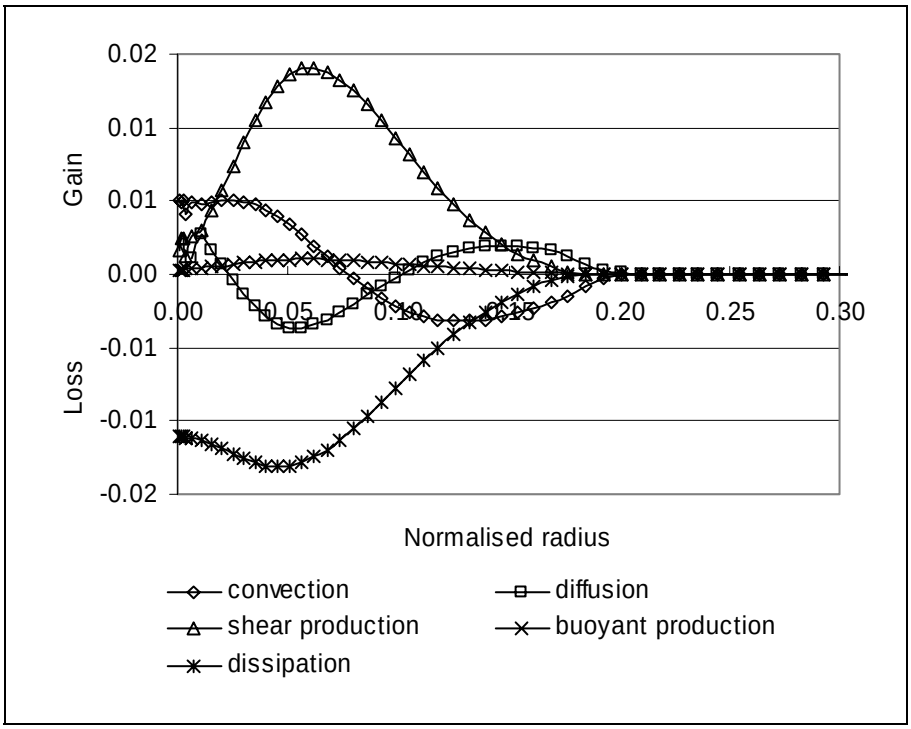

Figure 7-13: Budget of terms in the turbulent kinectic energy equation when predicted with the standard *k*-ε model with a GGDH turbulent buoyancy model.

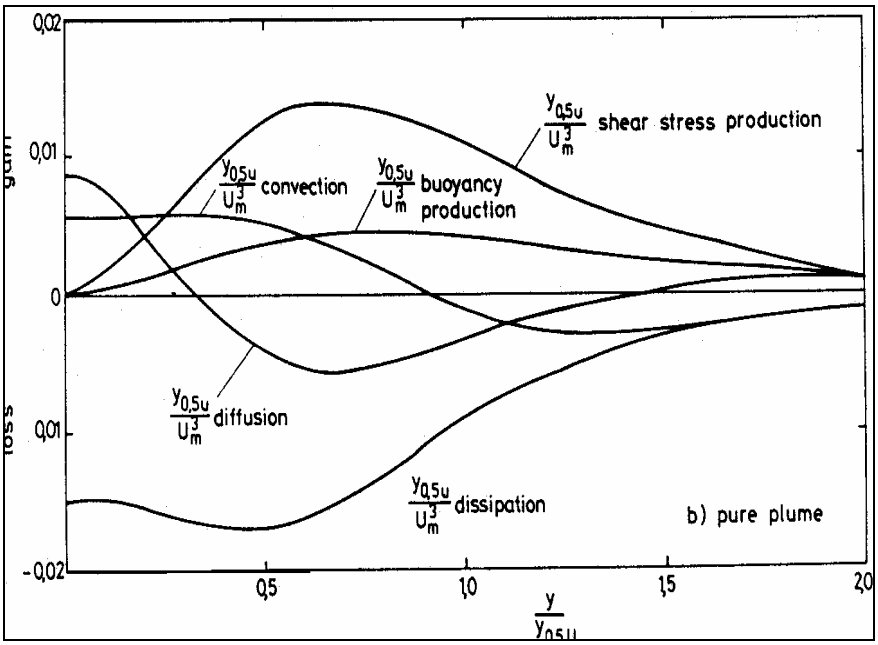

Figure 7-14: Budget of terms in the turbulent kinetic energy equation reproduced from Hossain and Rodi (1982).

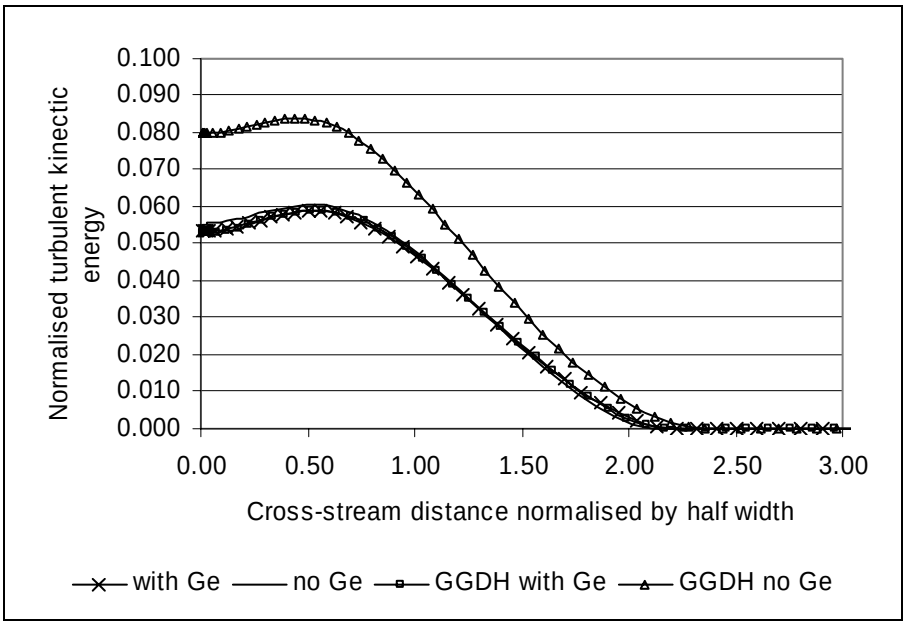

Figure 7-15a: Effect of the implementation of a turbulent buoyancy production term in the dissipation of turbulent kinectic energy transport equation (Ge) on the normalised turbulent kinetic energy for the axisymmetric buoyant jet.

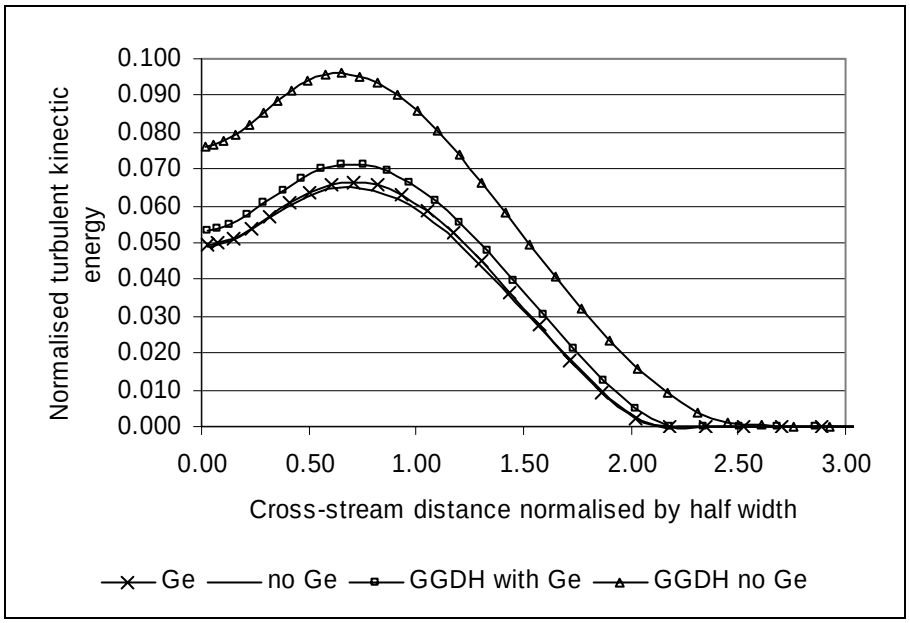

Figure 7-15b: Effect of the implementation of a turbulent buoyancy production term in the dissipation of turbulent kinectic energy transport equation (Ge) on the turbulent kinectic energy budget for the plane buoyant jet.

7.3.2 Ceiling Layers

The GGDH turbulent model is a general improvement to the quality of the turbulent buoyancy model and as such, it should offer improvements in the prediction of both horizontal and vertical buoyant flows. Tests were undertaken in which a ceiling was introduced on the upper boundary of the solution domain of the plane buoyant jet, replacing the ledge in previous simulations. A layer of hot fluid was thus formed under the ceiling, this is known as a ceiling layer. The relative effect of the turbulent buoyancy model on this layer was then assessed.

The ceiling layer is a characteristic of compartment fire flows, where the fire plume impinges on and then spreads along the ceiling. These 2-dimensional simulations provide a preliminary assessment of the expected effect of this model on the ceiling layer region of the 3-dimensional compartment fire simulations.

Figure 7-16 shows the solution domain and flow field predicted by the eddy-diffusivity turbulent buoyancy model. Figure 7-17 shows the vertical velocity

profile taken approximately half way along the domain width. This demonstrates a small difference between the eddy-diffusivity and the GGDH turbulent buoyancy models in the core of the layer, where the latter has slightly greater spread. A more significant variation at the edge of the layer is observed. Figure 7-18 shows the temperature profile at the same position as the velocity profile. The GGDH turbulence model clearly shows a larger hot layer, suggesting this model increases the diffusion of the layer.

A general assumption that the GGDH model will increase the predicted size of the thermal layer cannot be made. However, this exercise clearly demonstrates that difference between the two turbulent buoyancy models considered, although slight, can be expected in the prediction of ceiling layers.

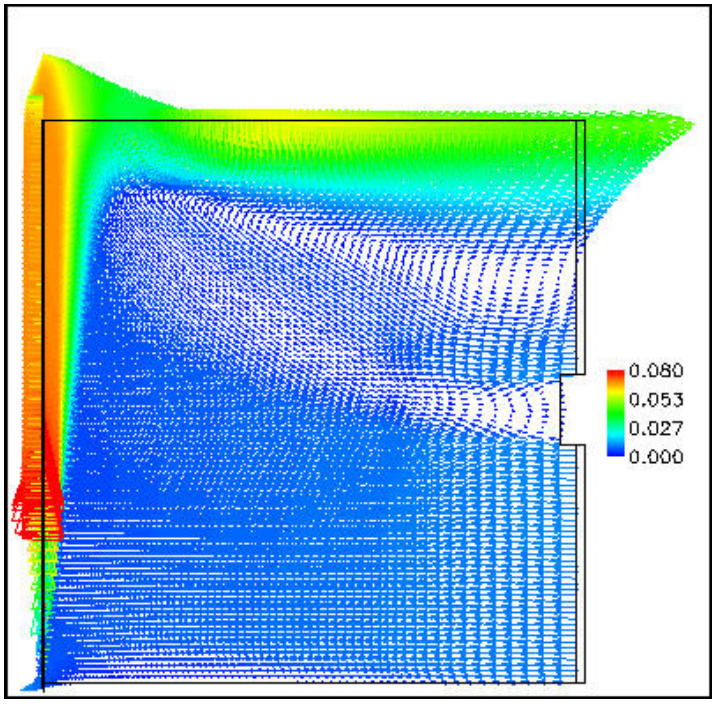

Figure 7-16: Flow field (velocity vectors coloured by velocity magnitude (m/s)) predicted with eddy-diffusivity turbulent buoyancy correction of plane buoyant jet with ceiling defined at top boundary.

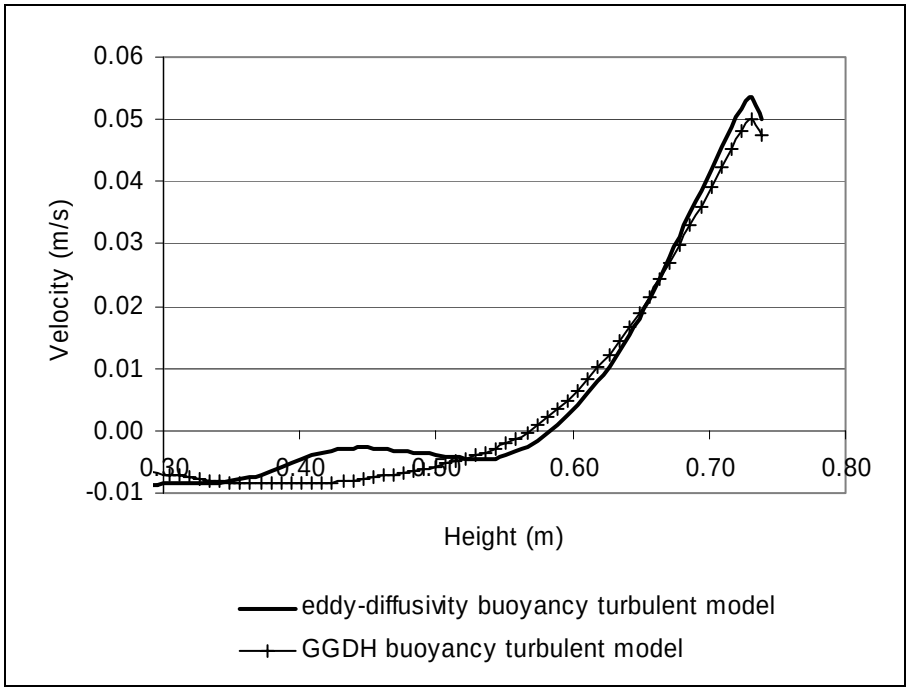

Figure 7-17: Streamwise velocity profile defined approximately at the half the distance of the domain.

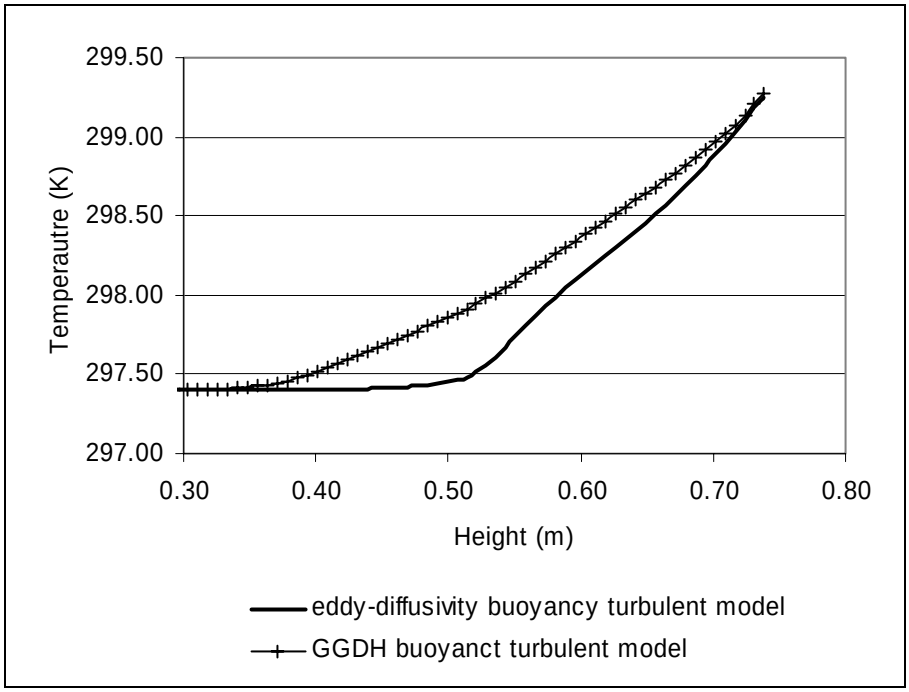

Figure 7-18: Temperature profile defined approximately at the half the distance of the domain.

7.4 Scalar Diffusion Models

The preliminary comparison of the budget of terms in the turbulent kinetic energy transport equation, predicted by the standard k-ε model, for the axisymmetric buoyant jet (figures 6-28 and 6-27) exhibited an underprediction of the diffusion term. The standard model adopted for the prediction of diffusion was the eddy-diffusivity relationship. In this section, the generalised gradient diffusion hypothesis (GGDH) model for turbulent flux has been considered as an alternative to the eddy-diffusivity model (sections 3.**Error! Bookmark not defined.** and 5.8). This model includes a correlation between the Reynolds stresses and the mean scalar gradient. The model was implemented with three possible representations of the Reynolds stresses: the linear eddy-viscosity model, a hybrid of the eddy-viscosity model and ASM and, finally, a cubic eddy-viscosity model. The models will be referred to as linear GGDH, hybrid GGDH and cubic GGDH diffusion models, respectively.

		Spreading rates for plane buoyant jet		Spreading rates for axisymmetric buoyant jet	
		Velocity	Temperature	Velocity	Temperature
	Eddy-diffusivity model	0.082	0.086	0.0907	0.0864
Model included in enthalpy transport equation	Linear GGDH model	0.0.838	0.0889	0.0911	0.0868
	Hybrid GGDH model	0.0856	0.0913	0.0910	0.0866
	Cubic GGDH model	0.0803	0.0784	0.0891	0.0802
Model included in all scalar transport equations	Linear GGDH model	0.0817	0.0860	0.0877	0.0847
	Hybrid GGDH model	0.0883	0.0938	0.0902	0.0858
	Cubic GGDH model	0.0920	0.0876	0.1045	0.0940

Table 7-6: Comparison of spreading rates predicted by different diffusion models.

Table 7-6 gives the spreading rates of velocity and temperature for the various simulations in which the GGDH diffusion models were tested. The GGDH relationship combined with different representations of the Reynolds stresses was first applied to the enthalpy equations only; the eddy-diffusivity relationship was retained to define the diffusion for the other scalar transport equations. Secondly, the GGDH diffusion model was adopted in all the scalar transport equations: turbulent kinetic energy, dissipation of turbulent kinetic energy and enthalpy.

The relative spread between the flow and temperature fields in the two buoyant jets is consistent with experimental data and the standard k-ε model for all the models except for simulation of the plane buoyant jet by the cubic GGDH diffusion model.

Figures 7-19 and 7-20 show the mean velocity profile and the mean mixture fraction profile, respectively, for the axisymmetric buoyant jet modelled by the standard k-ε model with the GGDH representation of the enthalpy diffusion term. The effect on the mean velocity profile was seen to be very small; although examination of the spreading rate shows that for both the plane and axisymmetric buoyant jets there is a slight increase in both the temperature and velocity spreading rate predicted by the linear and hybrid GGDH diffusion models. A more significant difference is seen in the prediction with the cubic GGDH model, which reduces the spreading rate considerably.

The inclusion of the GGDH diffusion model in all the scalar equations has a more notable effect on the overall flow field. A consistent trend is not observed in the prediction of the buoyant jets by the GGDH diffusion model. The cubic GGDH model predicts an increase in the spreading rate of both plumes, the hybrid GGDH model shows an increase in the spread of the plane plume but a decrease of the axisymmetric plume, the linear GGDH model predicts a slight decrease in the prediction of both spreading rate. The complexity of the modelled transport equations and the high level of coupling between the flow, turbulent and scalar fields causes difficulty in discerning the dominant influences. The accuracy of the

implementation, and hence confidence in the quality of the results, can be ascertained by consideration of the calculated Reynolds stresses and the turbulent fluxes with examination of the relevant model equations.

The normalised velocity fluctuations, normalised turbulent shear stress and the normalised turbulent mixture fraction fluxes profiles are given in figure 7-23, 7-25 and 7-24, respectively. The profiles are normalised to enable comparison with the experimental plots given in figures 6-[23] and 6-[25]. Consistency between the results was achieved by calculating the various terms from the same converged flow and temperature field, rather than those predicted by the individual models.

The hybrid representation of the Reynolds stress has no significant effect on the normal component compared to the standard k-ε model, demonstrating that this model is also incapable of modelling the anisotropy of the turbulence near the centreline. However, the average value and spread of the turbulent shear stress was seen to increase. Comparison with the standard model (figure 6-22) suggests that this is a slight departure from the experimental measurements (figures 6-20 to 6-21). Equations 7.1 to 7.3 give the simplified two-dimensional ASM component of the hybrid model of the Reynolds stresses.

$$\overline{u_1 u_1}_{asm} = \frac{k}{\varepsilon}\frac{(1-C_3)}{C_1}\left[\beta g \frac{\Gamma}{\rho}\left(\frac{5}{3}\frac{\partial T}{\partial x_1} - \frac{2}{3}\frac{\partial T}{\partial x_2}\right)\right] \qquad 7.1$$

$$\overline{u_2 u_2}_{asm} = \frac{k}{\varepsilon}\frac{(1-C_3)}{C_1}\left[\beta g \frac{\Gamma}{\rho}\left(\frac{5}{3}\frac{\partial T}{\partial x_2} - \frac{2}{3}\frac{\partial T}{\partial x_1}\right)\right] \qquad 7.2$$

$$\overline{u_1 u_2}_{asm} = \frac{k}{\varepsilon}\frac{(1-C_3)}{C_1}\left[\beta g \frac{\Gamma}{\rho}\left(\frac{\partial T}{\partial x_1} + \frac{\partial T}{\partial x_2}\right)\right] \qquad 7.3$$

In the case of plume flow the mean cross-stream gradient ($\partial T/\partial x_2$) is large compared to the mean streamwise gradient ($\partial T/\partial x_1$). The trends in the Reynolds stresses observed in the simulation results are upheld by consideration of the above equations. The contribution from the ASM component of the hybrid model to the

shear stress term consists of the sum of the two mean gradients, whereas the contribution to the normal stress terms consists of a fractional difference of the two mean gradients. Hence the overall contribution from the ASM component of the model to the hybrid representation is relatively small.

The nonlinear model has a far more significant effect on the normal Reynolds stress compared to the hybrid model, whereas the effect on the turbulent shear stress is comparable to the hybrid model. The effect of the nonlinear terms on the turbulent mixture fraction flux is to increase the streamwise flux by an amount comparable with the hybrid model but to decrease the cross-stream value significantly.

An expanded, simplified form of the GGDH turbulent mixture fraction flux model is presented in equations 7.4 and 7.5 in order to gain some understanding of the processes which produce the variations in the prediction of turbulence.

$$\overline{\rho u_1^{"} f^{"}} = -1.5 \frac{C_\mu}{\sigma_f} \frac{k}{\varepsilon} \left[\overline{\rho u_1^{"} u_1^{"}} \frac{\partial \tilde{f}}{\partial x_1} + \overline{\rho u_1^{"} u_2^{"}} \frac{\partial \tilde{f}}{\partial x_2} \right] \qquad 7.4$$

$$\overline{\rho u_2^{"} f^{"}} = -1.5 \frac{C_\mu}{\sigma_f} \frac{k}{\varepsilon} \left[\overline{\rho u_2^{"} u_1^{"}} \frac{\partial \tilde{f}}{\partial x_1} + \overline{\rho u_2^{"} u_2^{"}} \frac{\partial \tilde{f}}{\partial x_2} \right] \qquad 7.5$$

As mentioned, the dominant gradient is the cross-stream gradient ($\partial f/\partial x_2$). Hence, the shear stress term has a more dominant effect on the streamwise turbulent flux ($\overline{u_1^{"} f^{"}}$), than on the cross-stream turbulent flux ($\overline{u_2^{"} f^{"}}$). The latter is more influenced by the cross-stream Reynolds stress, since it is this term that is multiplied by the cross-stream gradient.

The eddy-diffusivity equations can be rewritten in the form given below:

$$\overline{\rho u_i^{"} f^{"}} = -0.5 \frac{C_\mu}{\sigma_f} \frac{k}{\varepsilon} \left[\overline{\rho u_k^{"} u_k^{"}} \frac{\partial \tilde{f}}{\partial x_2} \right] \qquad 7.6$$

The assumption that the term, $\overline{\rho u_k'' u_k''}$, in equation 7.6 is isotropic[4] results in an equation equal to the first term in equation 7.4 and the second in equation 7.5. This difference in the models is reflected directly in the prediction of the turbulent flux (figure 7-24). The slight increase in cross-stream turbulent flux predicted by the linear and hybrid GGDH models, compared to the eddy-diffusivity relationship, is dependent on the first term in equation 7.5, since the normal Reynolds stress terms, that appear in the second term, were shown to be comparable in figure 7-23. However, the significant drop in the nonlinear GGDH prediction is a direct result of the large drop in the normal streamwise Reynolds stress. The consistently large increase in the prediction of the streamwise turbulent flux by all the GGDH models is a result of the second term in equation 7.4, which does not appear in the eddy-diffusivity model. The insignificant difference between the nonlinear and hybrid GGDH predictions of the turbulent flux demonstrates the minor effect of variations in the normal streamwise Reynolds stress.

The Reynolds stress predictions for the nonlinear model, calculated from the converged flow field predicted by this model, exhibit an unphysical discontinuity at the edge of the plume. This affected the mean velocity profile for the simulations which included the cubic GGDH model in all the scalar equations, as shown in figure 7-26, and was a consistent effect for the plane and axisymmetric buoyant jets. Consideration of the various terms contributing to this model (section 3.5) identified the cubic term multiplied by the C_4 coefficient as the cause of the discontinuity. Figure 7-26 shows the mean flow profile from simulations both including and neglecting this term; demonstrating that the kink is not apparent in the profile of latter case. The spreading rate for the cubic GGDH model in all scalar equations presented in table 7-1 included the C_4 coefficient, providing an explanation for the unphysical comparative spread of the velocity and temperature plumes by this model. This phenomenon will be considered in more detail in the next section that

[4] This is not an accurate assumption for a plume-type flow, but it is useful approximation for the explanation of observed trends.

considers application of the nonlinear eddy-viscosity model to the diffusion model of the velocity transport equations and the turbulent shear production.

The inclusion of the GGDH diffusion model in the enthalpy transport equation only, resulted in a small increase in the spreading rate for both the plane and axisymmetric buoyant jets. The influence of the GGDH diffusion model in the enthalpy transport equation only is coupled to the momentum equation through the gravitational term and to the turbulence equations through the buoyancy production term. The net effect of these influences is to increase the spreading rates.

The inclusion of the GGDH model in all the scalar transport equations tended to reduce the spreading rates compared to the eddy-diffusivity model. The reduction in the spread rate was initially a disappointing result since it was hoped that this model might improve the underprediction observed in the diffusion of the turbulent kinetic energy predicted with the standard k–ε model. However, examination of the contributing terms of the model demonstrated that the predicted reduction in the spread of the plume was not an unexpected result. The expanded form of the GGDH model showed the contribution of the additional terms introduced in this improved model. Both these terms, by their nature will be negative and hence reduce the overall value of the turbulent flux. The multiplying coefficient in the GGDH was consistent between all the different transport equations for the current work. It may be appropriate to tune these to the relevant transport equations.

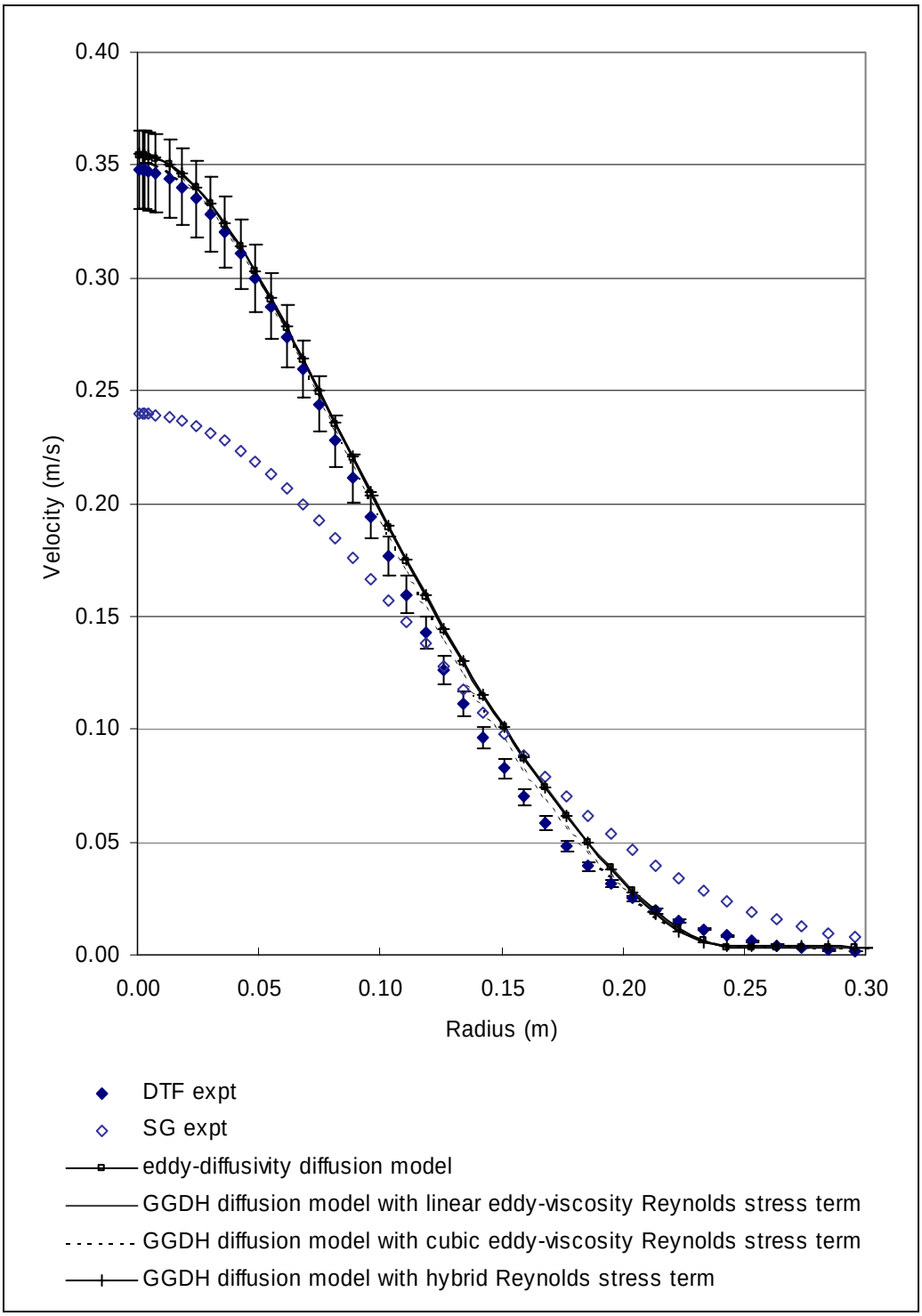

Figure 7-19: Mean velocity profiles of the axisymmetric buoyant jet predicted with different models of the diffusion term in the enthalpy equations and compared to experimental data.

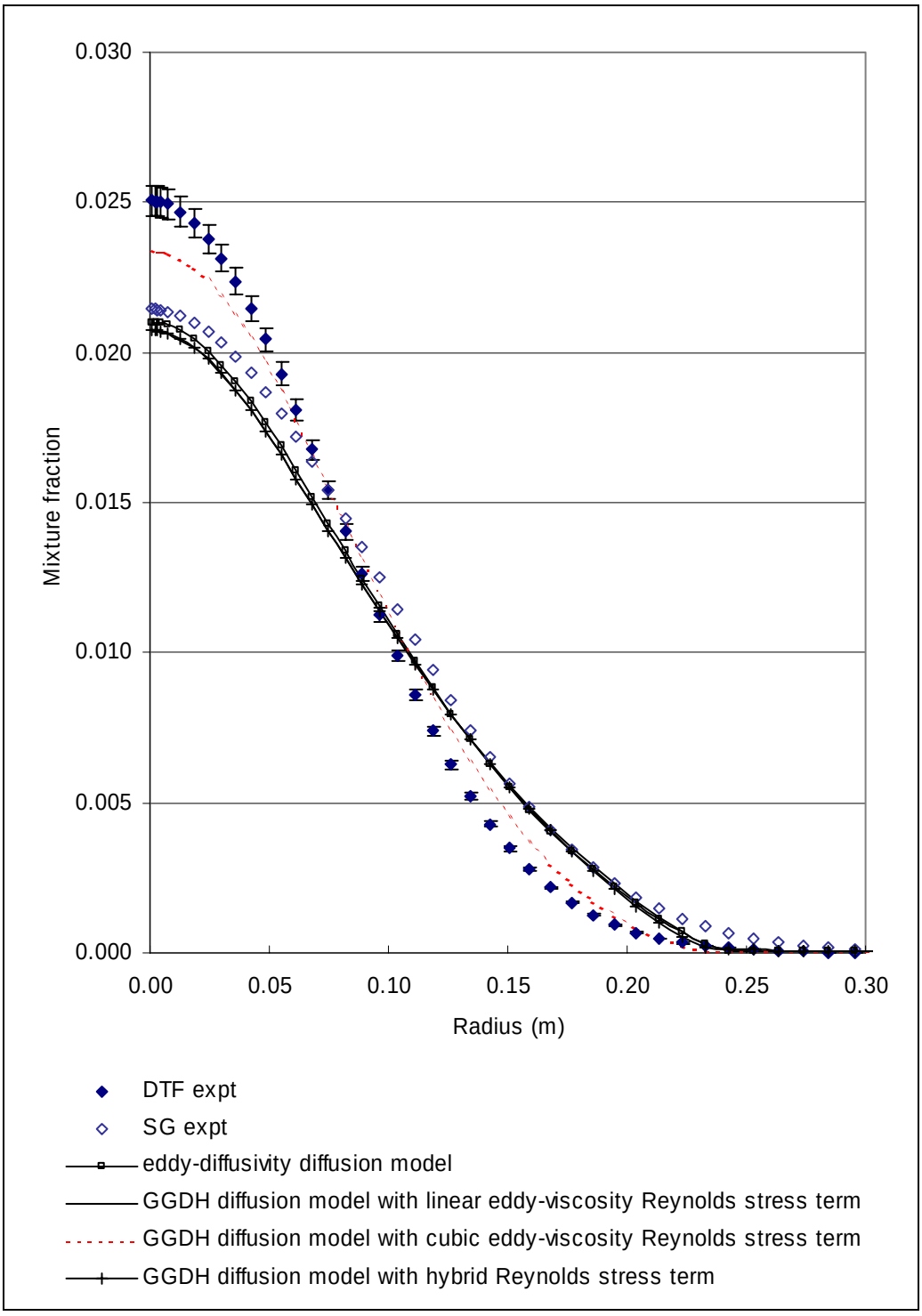

Figure 7-20: Mean mixture fraction profiles of the axisymmetric buoyant jet predicted with different models of the diffusion term in the enthalpy equations and compared to experimental data.

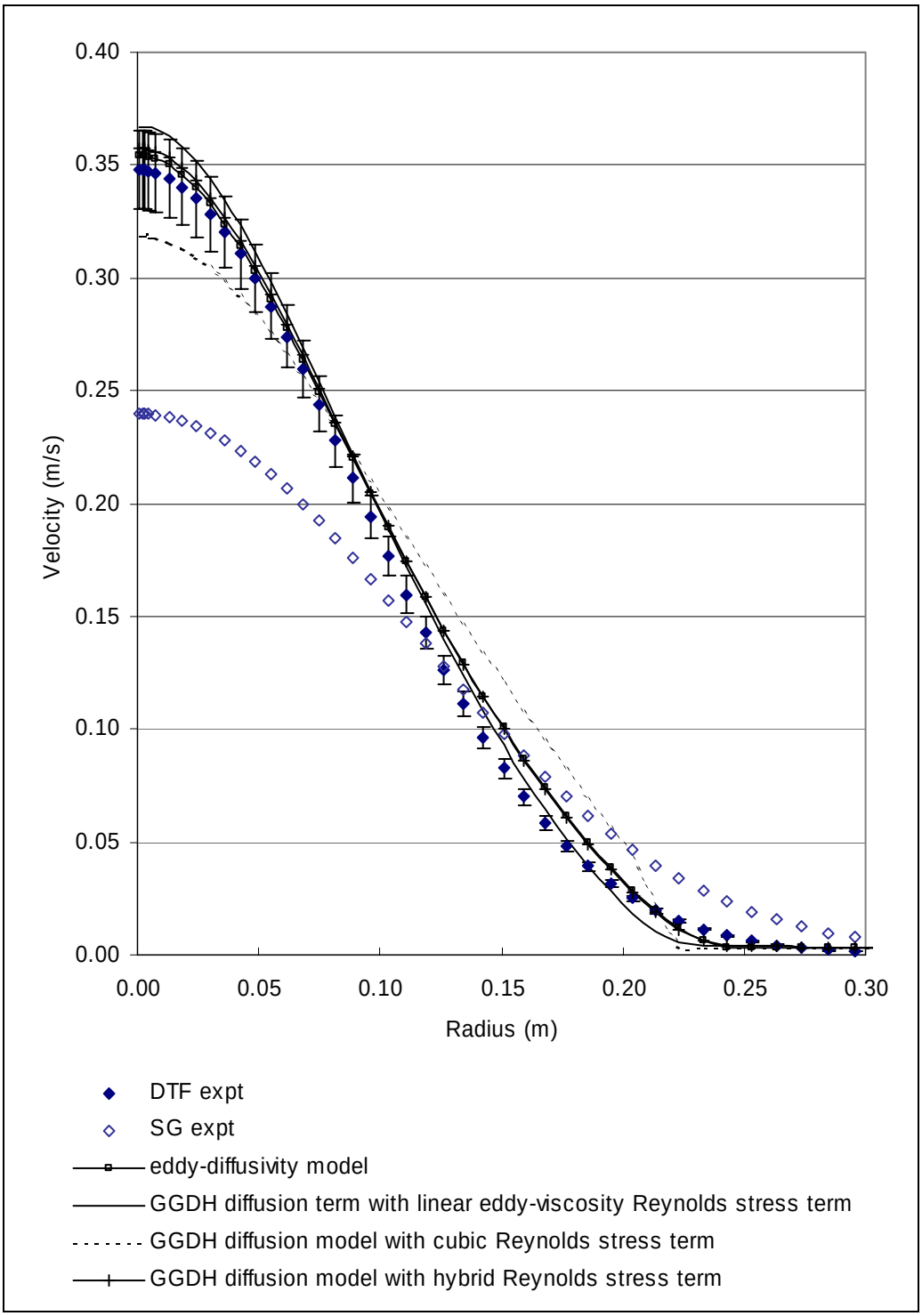

Figure 7-21: Mean velocity profiles of the axisymmetric buoyant jet predicted with different models of the diffusion term in all the scalar equations and compared to experimental data.

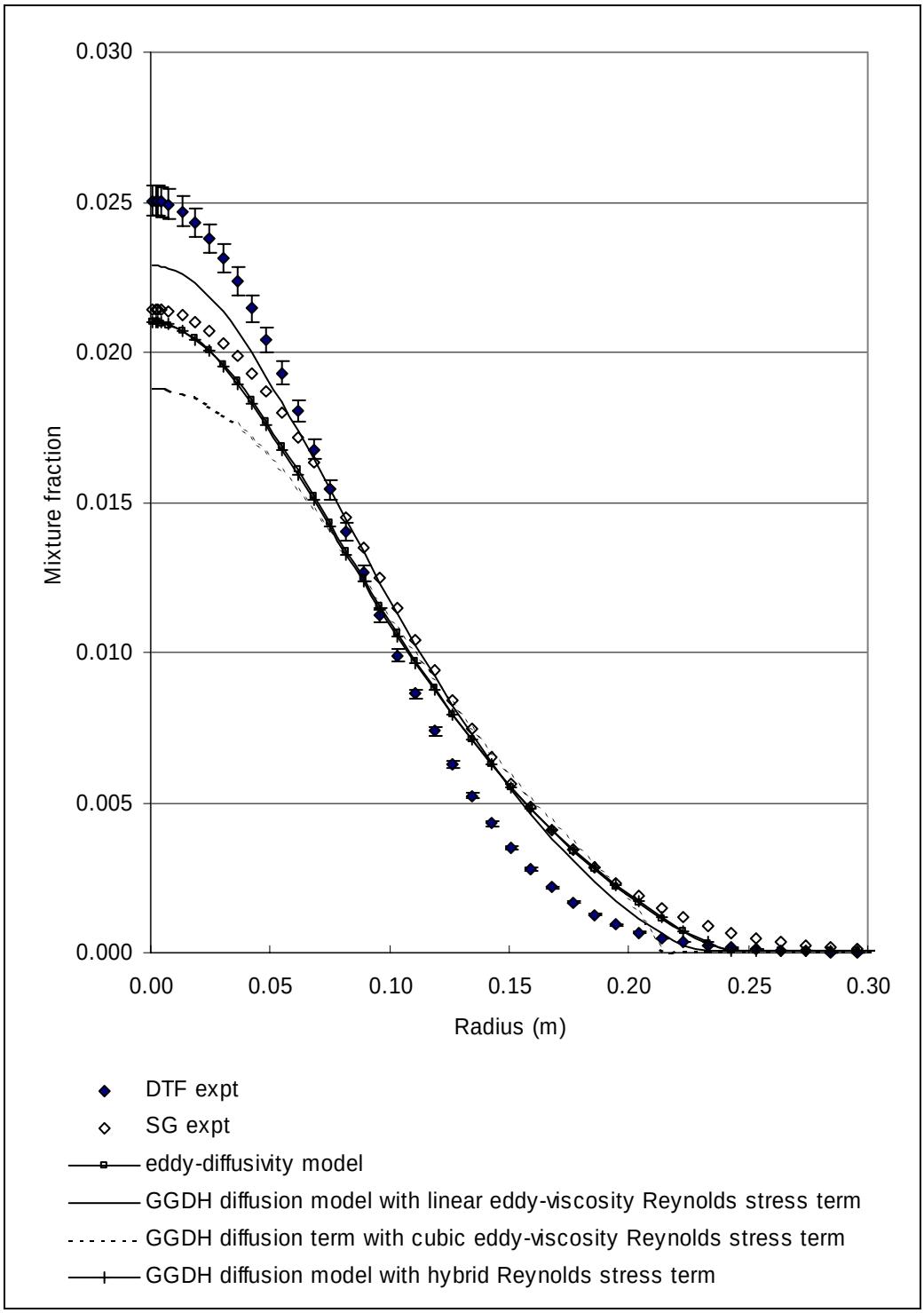

Figure 7-22: Mean mixture fraction profiles of the axisymmetric buoyant jet predicted with different models of the diffusion term in the enthalpy equations and compared to experimental data.

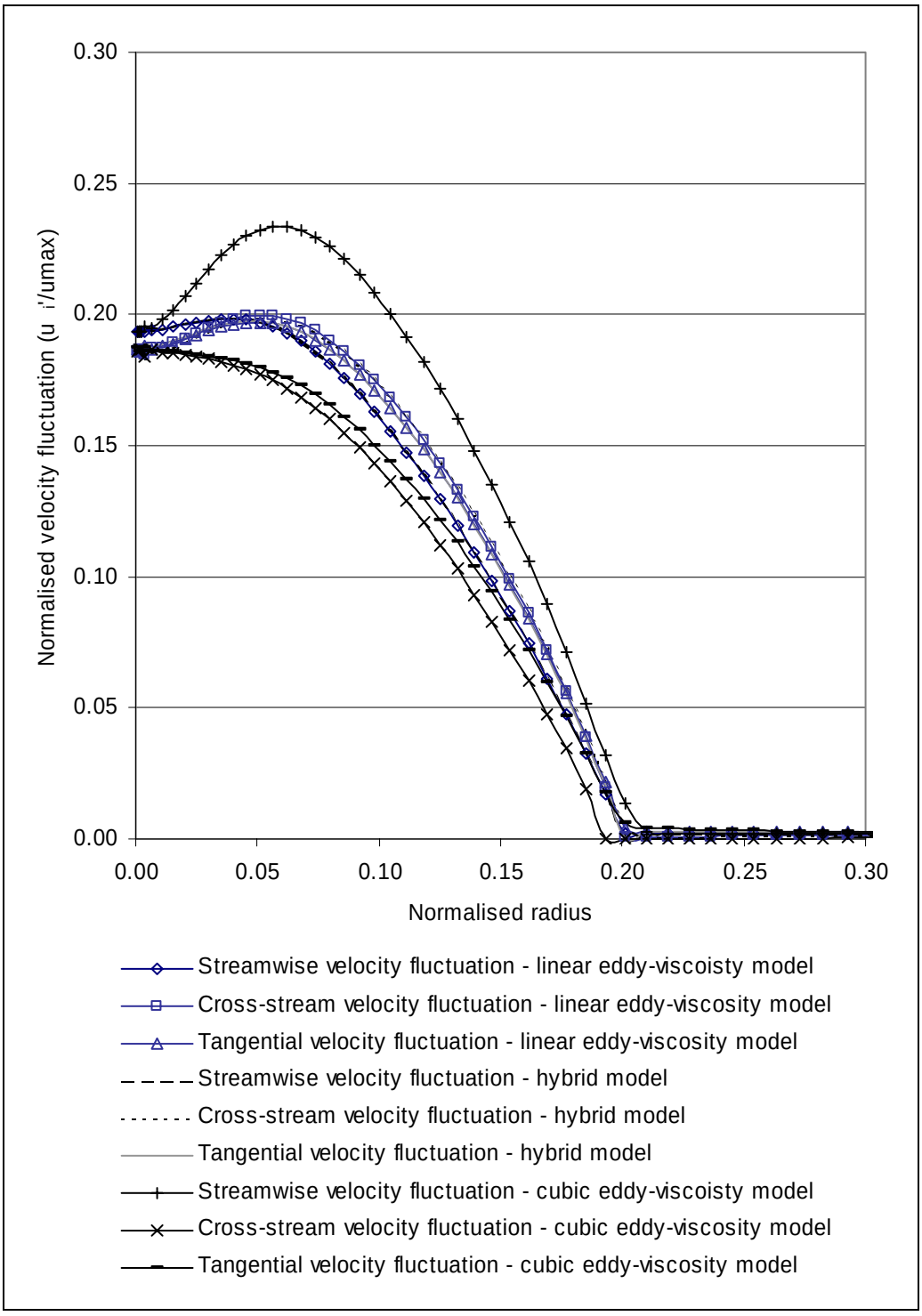

Figure 7-23: Normalised velocity fluctuation calculated by the linear eddy-viscosity, the cubic eddy-viscosity and the hybrid model.

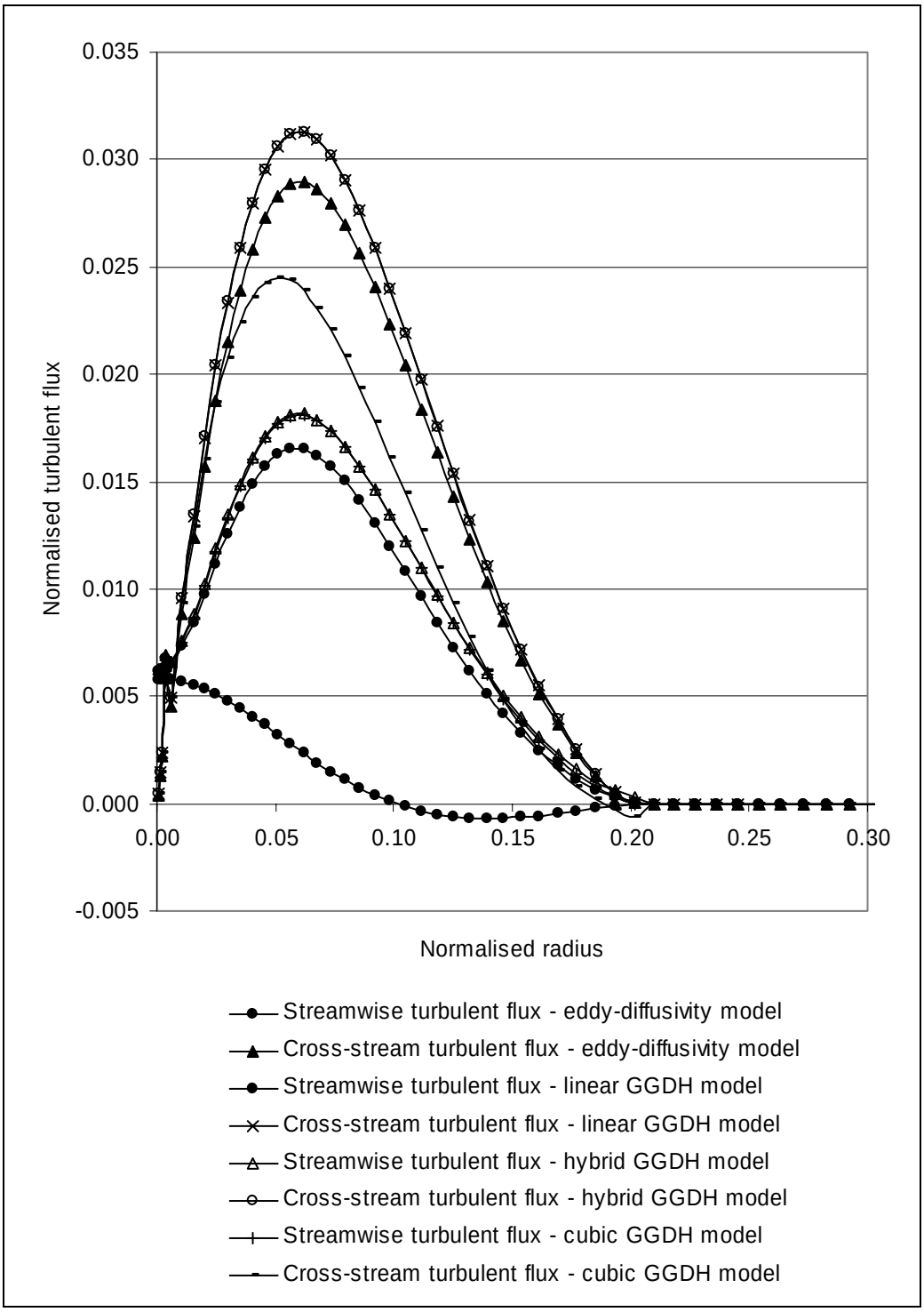

Figure 7-24: Turbulent mixture fraction flux calculated by the various GGDH diffusion models considered in this section.

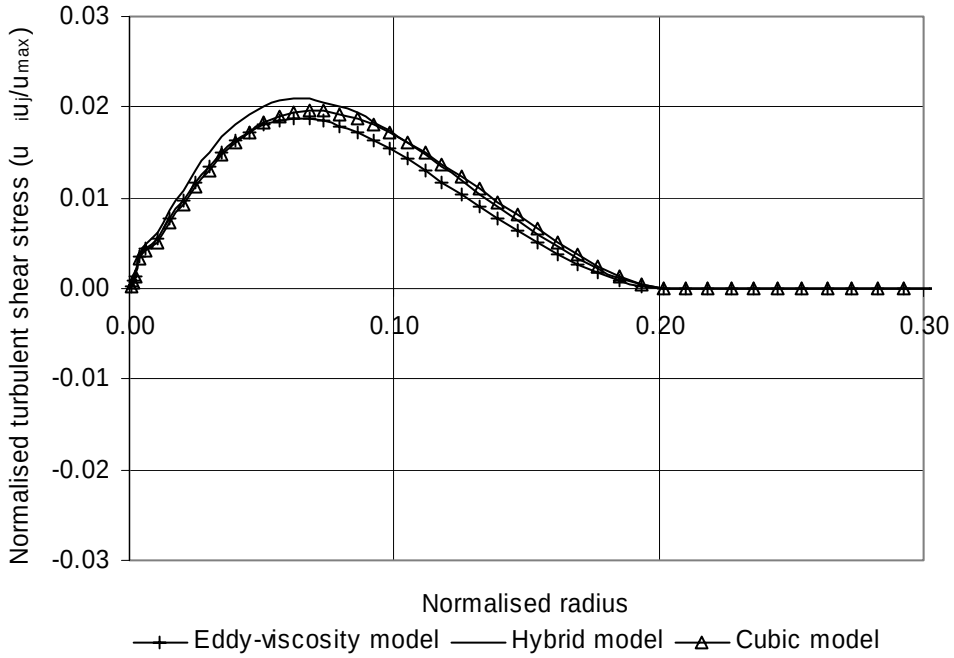

Figure 7-25: Turbulent shear stress calculated by the linear eddy-viscosity, the cubic eddy-viscosity and the hybrid model.

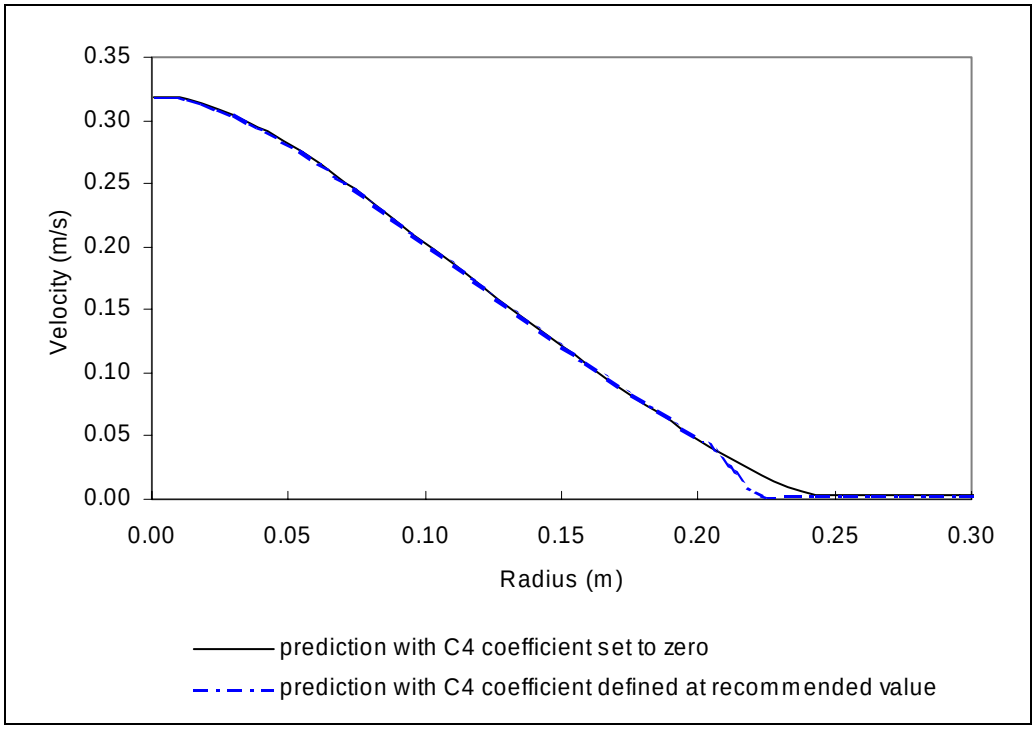

Figure 7-26: Mean velocity profile of the axisymmetric buoyant jet predicted by the GGDH diffusion model with the cubic eddy-viscosity model, comparing the prediction where the terms multiplied by the C_4 coefficient in the cubic eddy-viscosity model are included and neglected.

7.5 Nonlinear Eddy-Viscosity Models

This section presents results of simulations of the axisymmetric buoyant jet with the two nonlinear eddy-viscosity model: Speziale's quadratic model (Speziale (1987)) and Craft's cubic model (Craft, Launder and Suga (1993)). The nonlinear eddy-viscosity relationship is used in the modelling of both the diffusion term in the momentum equations and in the shear production of turbulent kinetic energy. The experimental data for the velocity fluctuations were presented in section 6.3.3 and demonstrated the anisotropy of the turbulence in the plume. The comparison of these data with the prediction of the standard k-ε model, which adopts a linear representation of the eddy viscosity, showed the inability of this model to represent this anisotropy. Comparison of the computational and experimental budget of the terms, in the turbulent kinetic energy equation, showed there is a slight overprediction in this term.

The nonlinear eddy-viscosity models were presented in section 3.5 and the implementations of the models were discussed in section 5.9. The implementation of these models was of particular importance in the promotion of stability. The models were validated by consideration of a 3-dimensional square channel flow (Appendix A). The form of the cubic model implemented in the current work for plumes did not adopt the functional C_μ coefficient. This was found to be inappropriate for plume-type free shear flow, since the exponential component became unrealistic.

Comparison of the results from these nonlinear eddy viscosity models showed considerable variance, an explanation for which is provided through consideration of the expanded, simplified form of the equations.

7.5.1 Speziale's Quadratic Model

Figures 7-27 and 7-28 show the cross-stream profiles of mean streamwise velocity and mean mixture fraction, respectively. Table 7-7 gives the velocity and temperature spreading rate predicted by the quadratic eddy-viscosity compared to that of the linear eddy-viscosity and experimental values.

	Velocity spreading rate	Temperature spreading rate
Experimental (Dai et al. (1994))	0.0863	0.0745
Standard k-ε with linear eddy-viscosity	0.09076	0.08644
Standard k-ε with quadratic eddy-viscosity	0.09715	0.09296

Table 7-7: Comparison of spreading rates predicted by nonlinear eddy-viscosity models and experiment.

Consideration of these figures and the spreading rate demonstrates that the plume predicted with the quadratic eddy-viscosity spreads more quickly than that of the linear model, with lower centreline values.

Figure 7-29 shows the budget of the terms in the transport equations for the turbulent kinetic energy transport equations. Comparison of this with the equivalent budget of the standard k-ε model and the experimental data, figures 6-27 and 6-28 respectively, reveals a slight improvement in the prediction of the shear production term and this is the only term the nonlinear model directly influences in the k-transport equation. An equivalent reduction is seen in the dissipation term but this is a result of the equilibrium of the production and dissipation terms being satisfied. The large underprediction in the dissipation is associated with the poor prediction of the turbulent buoyant production rather than the eddy-viscosity model.

Figure 7-30 shows a comparison of the predicted velocity fluctuations and the turbulent shear stress by the linear and quadratic eddy-viscosity models. This comparison demonstrates the direct effect of the more complex model on the

solution; in addition, comparison with the experimental data in figure 6-19 to 6-21 allow for an assessment of the model.

Significant anisotropy in the Reynolds stresses has been predicted by the quadratic eddy-viscosity model (figure 7-30), which is beyond the capabilities of the linear eddy-viscosity model. Comparison with the experimental data reveals that the trends in the predictions are accurate: the streamwise normal velocity fluctuation has a larger off centreline peak than the cross-stream fluctuation. The difference in the peak values (approx. 0.6) is close to that observed in the experimental data. However, the absolute values for both the velocity fluctuations and the turbulent shear stress are overpredicted. Since the relative prediction of the velocity fluctuations is good, it can be inferred that the model produces an improvement in the prediction of the Reynolds stresses. However, the coefficient multiplying the nonlinear terms is likely to be inappropriate since its value was deduced from consideration of a channel flow.

Equations 7-3 to 7-5 show the expanded form of the equations for a two-dimensional plume-type flow. The crossed terms are those that make a relatively small contribution to the final value. In addition, the w_{21} term (the gradient of cross-stream velocity in the streamwise direction) is small compared to the w_{12} term (the gradient of the streamwise velocity in the cross-stream direction).

$$-\overline{\rho u_1'' u_1''} = \cancel{2\mu_t w_{11}} - 2\rho k/3 + C(\cancel{-w_{11}w_{11}} - 0.75w_{12}w_{12} + 0.25w_{21}w_{21} - 0.5w_{12}w_{21} - s_{kl}s_{kl} - s_{kk}) \quad 7.3$$

$$-\overline{\rho u_2'' u_2''} = \cancel{2\mu_t w_{22}} - 2\rho k/3 + C(\cancel{-w_{22}w_{22}} - 0.75w_{21}w_{21} + 0.25w_{12}w_{12} - 0.5w_{12}w_{21} - s_{kl}s_{kl} - s_{kk}) \quad 7.4$$

$$-\overline{\rho u_1'' u_2''} = \mu_t(w_{12}+w_{21}) + C(\cancel{-w_{11}w_{21}} - \cancel{w_{22}w_{12}}) \quad 7.5$$

Where:

$C = 6.72 C_\mu \mu_t k/\varepsilon$

$s_{kl}s_{kl} = (\cancel{w_{11}w_{11}} \cancel{+ w_{22}w_{22}} + 0.5(w_{12}w_{12} + w_{21}w_{21} + 2w_{12}w_{21}))/3$

$s_{kk} = (- \cancel{2w_{11}w_{11}} \cancel{- 2w_{22}w_{22}})/3$

Comparison of the normal Reynolds stress terms show that the nonlinear contribution to the streamwise component will be larger than for the cross-stream component. That is, the most significant term ($w_{12}w_{12}$) is multiplied by a larger number for the streamwise Reynolds stress. This is reflected in figure 7-30, where a more significant difference is seen between the linear and quadratic prediction of the streamwise velocity fluctuation than the cross-stream velocity fluctuation. Equation 7.5 demonstrates that the nonlinear contribution to the shear stress is expected to be small, as reflected in figure 7-30.

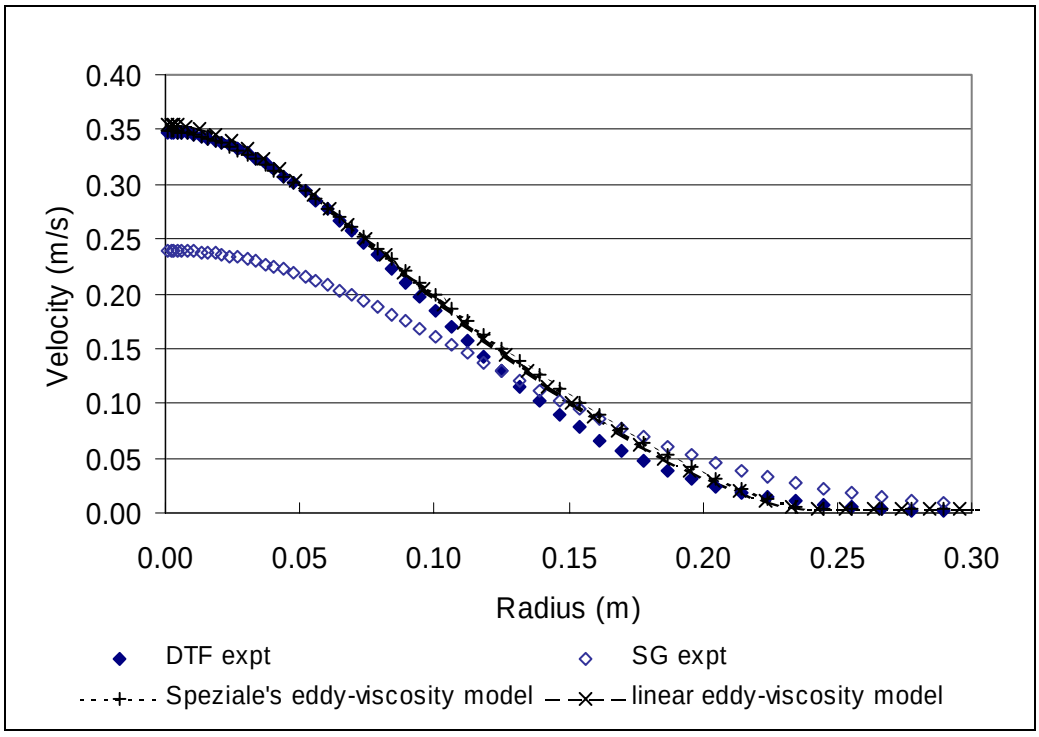

Figure 7-27: Mean velocity profile of the axisymmetric buoyant jet predicted with the linear and quadratic eddy-viscosity model and compared to experimental data.

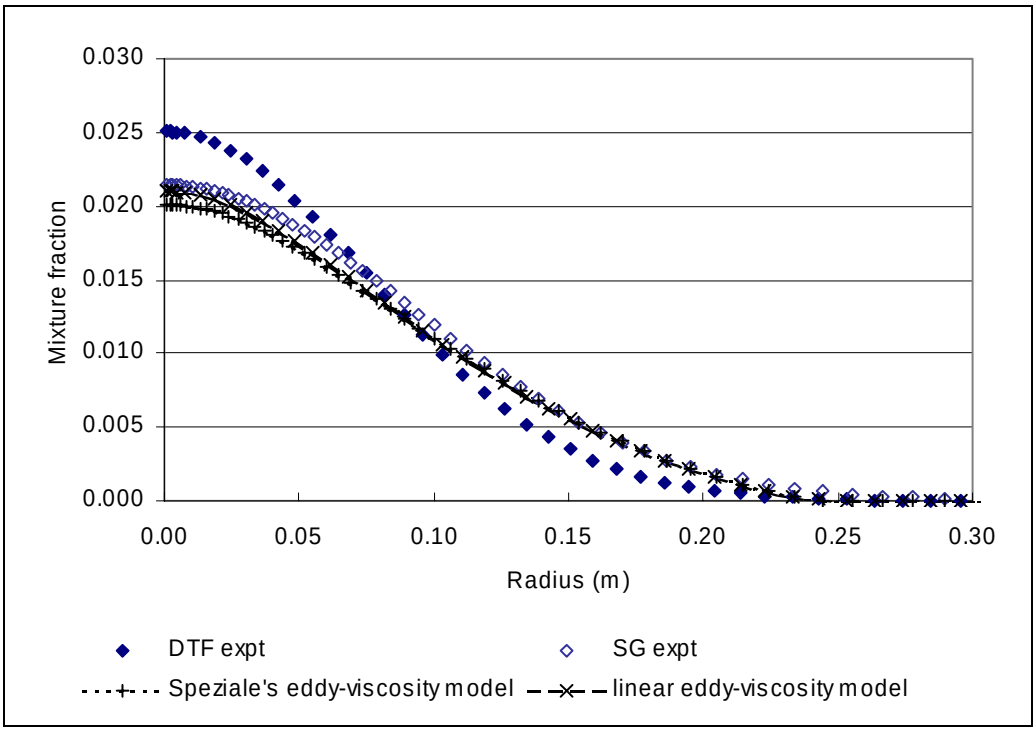

Figure 7-28: Mean mixture fraction profile of the axisymmetric buoyant jet predicted with the linear and quadratic eddy-viscosity model and compared to experimental data.

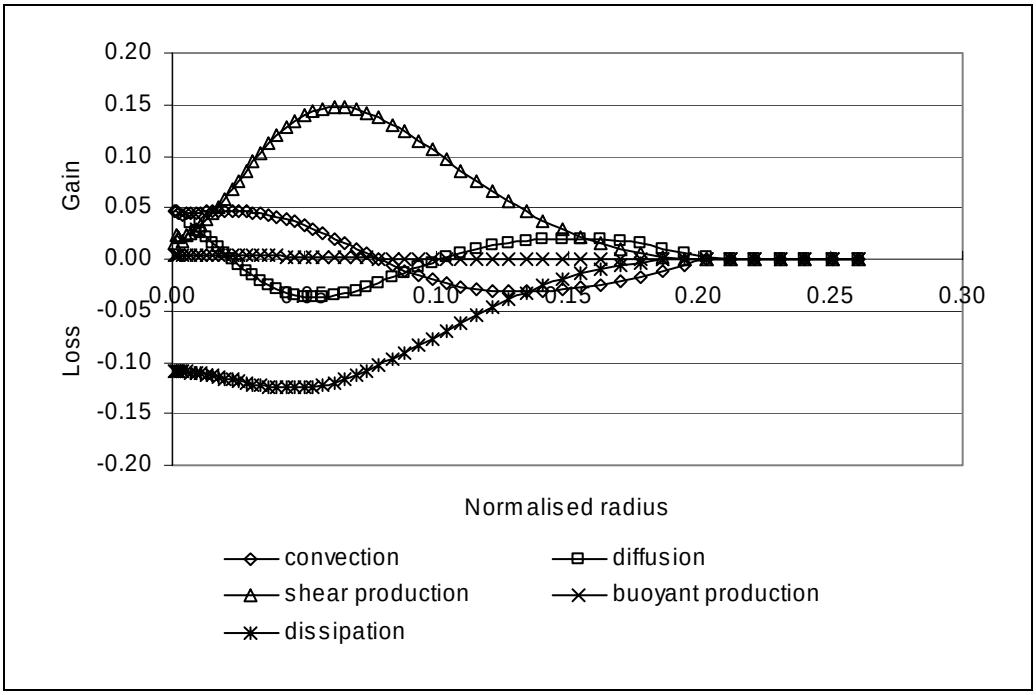

Figure 7-29: Budget of terms in the turbulent kinetic energy transport equation as predicted with the quadratic eddy-viscosity model.

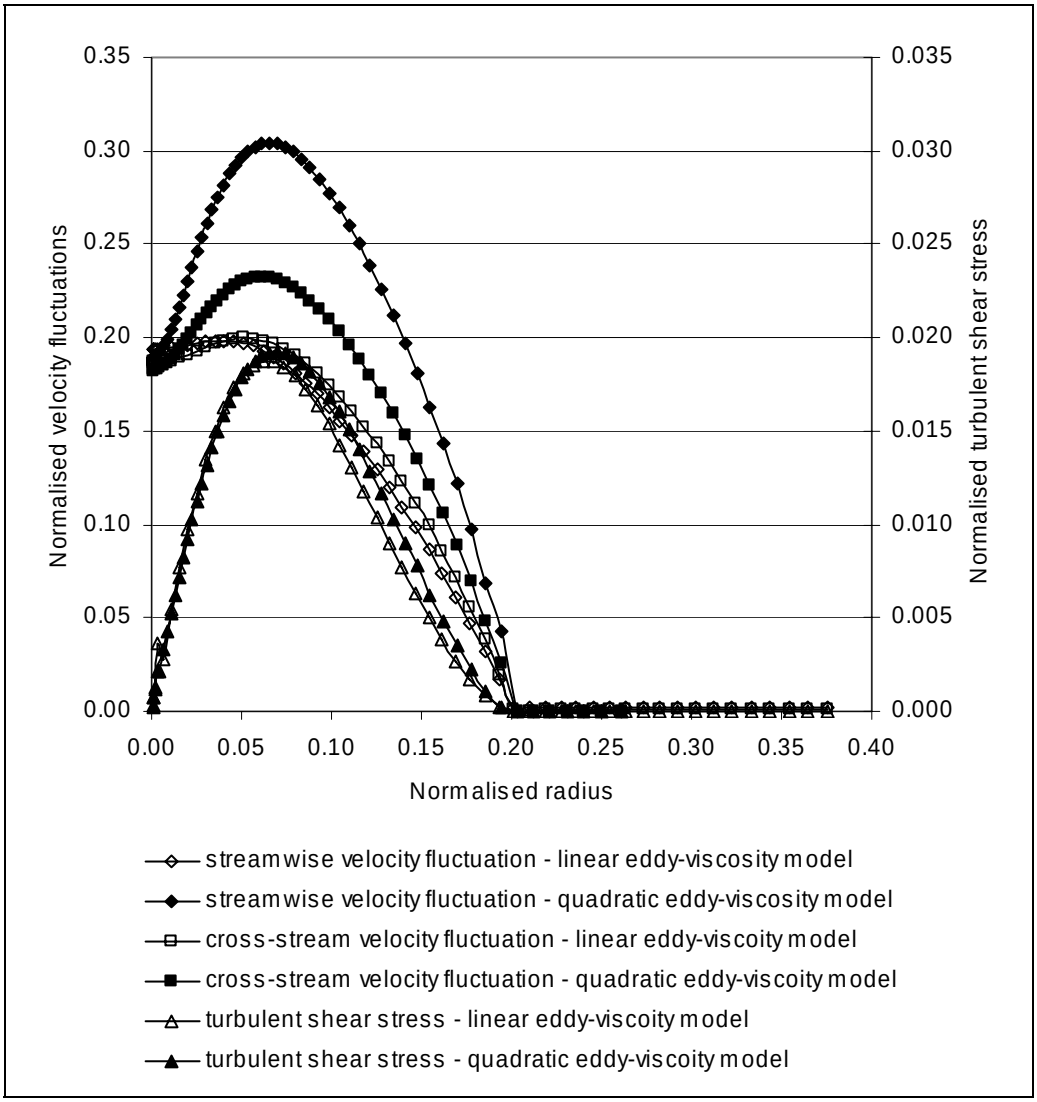

Figure 7-30: Comparison of the Reynolds stresses predicted by the linear and quadratic eddy-viscosity models.

7.5.2 Craft's Cubic Eddy-viscosity Model

This section details predictions of the axisymmetric buoyant jet with a cubic eddy-viscosity model based upon Craft's model. Craft's model presented in section 3.**5**, was found to be highly unstable in the prediction of these flows, despite its implementation to minimise such difficulties. The applied model neglected the C_4 term that was found to be the cause of the instabilities; this term was also the cause of the unphysical prediction observed with the cubic GGDH diffusion model

(section 7.4). This will be shown to be a reasonable assumption through consideration of the contributions of each of the terms to the solution.

Figure 7-31 shows cross-stream profile for the mean velocity predicted by Craft's cubic model including both the cubic and quadratic terms and including only the quadratic terms, in addition to the prediction by the linear eddy-viscosity model and experimental data. It can be seen that there is no discernible difference between the results from the various models. The same was also observed in the mixture fraction predictions. A significant difference is, however, observed in the prediction of velocity fluctuations (figure 7-32). Comparison of these with the experimental data shows a significant improvement in the prediction of streamwise velocity fluctuations, but a worsening in the cross-stream predictions. This is unlike the quadratic model of Speziale that produced an improvement in relative predictions of velocity fluctuations. The lack of an overall change in the predictions of the mean profiles of the cubic model compared to the standard model is associated with the differences in Reynolds stresses cancelling each other.

Figures 7-33 to 7-35 show the contribution from each of the terms in the cubic model to the Reynolds stresses, calculated from the converged flow field, predicted by the standard k-ε model with linear eddy-viscosity. Equations 7.6 to 7.27 show the 2-dimensional expanded form of the cubic eddy-viscosity. The nonlinear terms are grouped by the multiplying coefficient. The crossed terms are those that are relatively small for plume-type flows, the w_{12} term (the gradient of streamwise velocity in the cross-stream direction) can be considered large compared to the w_{21} term (the gradient of cross-stream velocity in the streamwise direction).

The cubic terms only carry a significant influence with the shear stress terms, as demonstrated in figure 7-35, however the contribution from the terms multiplied by the C_4 coefficient on all the Reynolds stresses is seen to be small. The other cubic terms, those multiplied by C_6 and C_7, both have a significant effect but these are found to cancel each other. Examination of equations 7.24 and 7.27 demonstrates

that the significant terms are identical. The coefficients for C_6 and C_7 are equal and opposite, so any influence from these terms is lost.

The reduction of the value of the cross-stream normal Reynolds stress appears to be predominantly a result of the term multiplied by the C_2 coefficient, clearly demonstrated in figure 7-34. Hence the inclusion of the C_1 coefficients introduces a slight decrease in the overall value of the term, the further inclusion of the terms multiplied by the C_2 coefficient leads to a significant reduction in the term with the shape of the curve approaching linear. The addition of C_3 terms produces some improvement, increasing the value of the term and regaining some of the expected shape of the curve. The C_4 coefficient terms are seen to have a small influence, while the effects of the C_6 and C_7 coefficient terms again cancel each other.

Examination of the relative contribution to the normal Reynolds stresses from the terms associated with the C_2 coefficient reveal the contribution is equal and opposite; hence the overall value of the streamwise Reynolds stress increases with a concurrent increase in the off centreline peak, whereas, as mentioned above, the opposite is true for the cross-stream Reynolds stress.

The contribution from the C_3 coefficient terms is the same for both normal Reynolds stresses and this is reflected in the figures 7-33 to 7-35.

The above discussion demonstrates the expected result from examination of the model equations and is reflected in the predicted result. The C_4 term is shown to have a negligible effect on all the Reynolds stress components, providing legitimacy for its neglect from the calculations. The overall contribution from the C_6 and C_7 terms is small, as their sum is negligible. Comparison of the quadratic terms in this and Speziale's model reveals that the same significant terms exist in both but there is a significant difference in the magnitude and sign of the components, leading to different predictions from the two models.

$$-\overline{\rho u_1'' u_1''} = \cancel{2\mu_t w_{11}} - 2\rho k/3$$
$$- \mu_t k/\varepsilon \left(c1_{11} + c2_{11} + c3_{11} - c1.s_{kl}s_{kl} - c3.m_{kl}m_{kl}\right)$$
$$- \mu_t C_\mu^2 (k/\varepsilon)^2 \left(c4_{11} + c6_{11} + c7_{11} \right)) \quad 7.6$$

$$-\overline{\rho u_2'' u_2''} = \cancel{2\mu_t w_{22}} - 2\rho k/3$$
$$- \mu_t k/\varepsilon \left(c1_{22} + c2_{22} + c3_{22} - c1.s_{kl}s_{kl} - c3.m_{kl}m_{kl}\right)$$
$$- \mu_t C_\mu^2 (k/\varepsilon)^2 \left(c4_{22} + c6_{22} + c7_{22} \right)) \quad 7.7$$

$$-\overline{\rho u_1'' u_2''} = \cancel{2\mu_t w_{12}}$$
$$- \mu_t k/\varepsilon \left(c1_{12} + c2_{12} + c3_{12} \right)$$
$$- \mu_t C_\mu^2 (k/\varepsilon)^2 \left(c4_{12} + c6_{12} + c7_{12} \right)) \quad 7.8$$

Where:

$$s_{kl}s_{kl} = 2(\cancel{2w_{11}w_{11} + 2w_{22}w_{22}} + w_{12}w_{12} + w_{21}w_{21} + 2w_{12}w_{21})/3 \quad 7.9$$

$$m_{kl}m_{kl} = 2(w_{12}w_{12} + w_{21}w_{21} - 2w_{12}w_{21})/3 \quad 7.10$$

$$c1_{11} = C_1(\cancel{w_{11}(w_{11}+w_{11})} + w_{12}(w_{12}+w_{21}) + \cancel{w_{11}(w_{11}+w_{11})} + w_{21}(w_{12}+w_{21})) \quad 7.11$$

$$c1_{22} = C_1 (w_{21}(w_{21}+w_{12}) + \cancel{w_{22}(w_{22}+w_{22})} + w_{12}(w_{21}+w_{12}) + \cancel{w_{22}(w_{22}+w_{22})}) \quad 7.12$$

$$c1_{12} = C_1 (w_{11}(w_{21}+w_{12}) + \cancel{w_{12}(w_{22}+w_{22})} + w_{11}(w_{21}+w_{12}) + \cancel{w_{21}(w_{22}+w_{22})}) \quad 7.13$$

$$c2_{11} = C_2 (2(w_{12}w_{12} - w_{21}w_{21})) \quad 7.14$$

$$c2_{22} = C_2 (2(w_{21}w_{21} - w_{12}w_{12})) \quad 7.15$$

$$c2_{12} = C_2 (2(\cancel{w_{11}w_{21}} + w_{22}w_{12} - \cancel{w_{12}w_{11}} - w_{22}w_{21})) \quad 7.16$$

$$c3_{11} = C_3 (w_{12}w_{12} + w_{21}w_{21} - 2w_{12}w_{21}) \quad 7.17$$

$$c3_{22} = C_3 (w_{21}w_{21} + w_{12}w_{12} - 2w_{21}w_{12}) \quad 7.18$$

$$c4_{11} = C_4 (\cancel{4w_{11}w_{11}w_{11} + 2w_{11}s_{12}(2w_{21}-w_{12}) + 4w_{22}(w_{21}w_{21}-w_{12}w_{12})}$$
$$\cancel{- w_{11}(4w_{11}w_{11} + 2w_{12}w_{12} + 2w_{12}w_{21})}) \quad 7.19$$

$$c4_{22} = C_4 (\cancel{4w_{22}w_{22}w_{22} + 2w_{22}s_{12}(2w_{12}-w_{21}) + 4w_{11}(w_{12}w_{12}-w_{21}w_{21})}$$
$$\cancel{- w_{22}(2w_{21}w_{21} + 2w_{21}w_{12} + 4w_{22}w_{22})}) \quad 7.20$$

$$c4_{12} = C_4 (\cancel{4w_{11}w_{11}(w_{12}-w_{21}) + 4w_{22}w_{22}w_{21}} + 2s_{12}w_{12}w_{21}$$

$$- w_{12}(2w_{21}w_{21} + 2w_{21}w_{12} + \cancel{4w_{22}w_{22}})) \quad 7.21$$

$$c6_{11} = 6.C_6 (\cancel{w_{11}s_{kl}s_{kl}}) \quad 7.22$$

$$c6_{22} = 6.C_6 (\cancel{w_{22}s_{kl}s_{kl}}) \quad 7.23$$

$$c6_{12} = 3.C_6 (w_{12}+w_{21})\, s_{kl}s_{kl} \quad 7.24$$

$$c7_{11} = 6.C_7 (\cancel{w_{11}m_{kl}m_{kl}}) \quad 7.25$$

$$c7_{22} = 6.C_7 (\cancel{w_{22}m_{kl}m_{kl}}) \quad 7.26$$

$$c7_{12} = 3.C_7 (w_{12}+w_{21})\, m_{kl}m_{kl} \quad 7.27$$

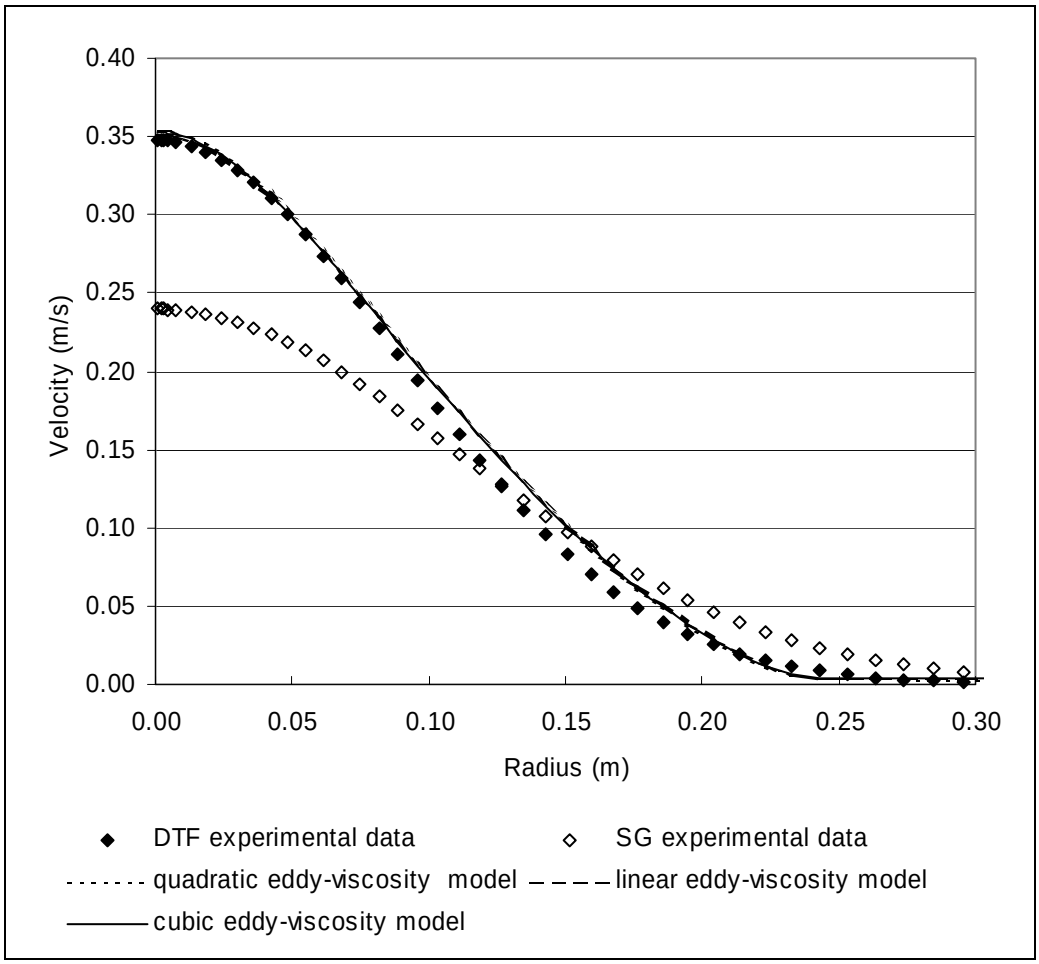

Figure 7-31: Mean velocity profile of the axisymmetric buoyant jet predicted with the linear eddy-viscosity model and Craft's nonlinear eddy-viscosity model either including both the quadratic and cubic terms or only the quadratic terms.

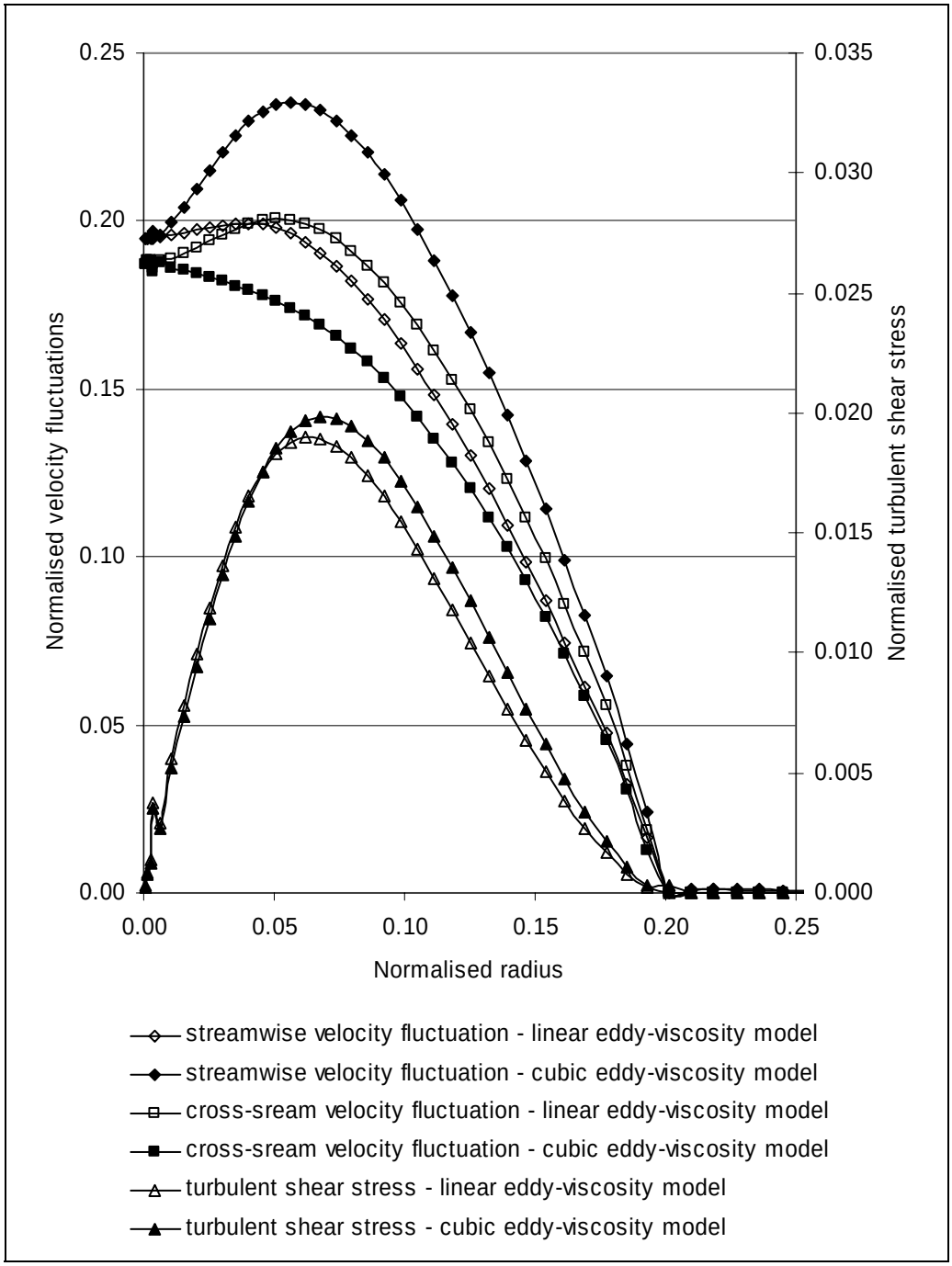

Figure 7-32: Reynolds stresses prediction by the linear and cubic eddy-viscosity models.

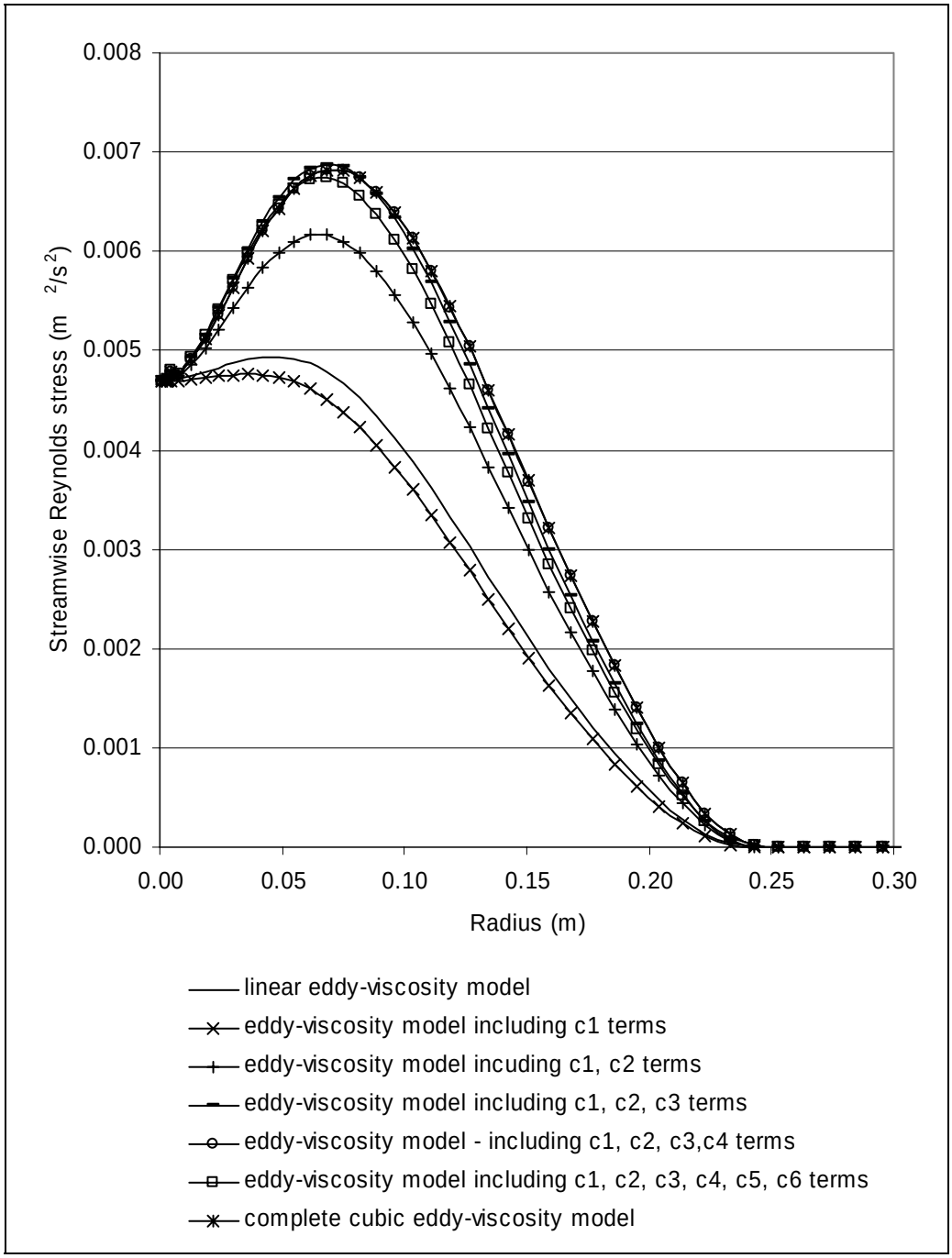

Figure 7-33: Comparison of the contribution to the streamwise Reynolds stress by the various terms in the cubic model.

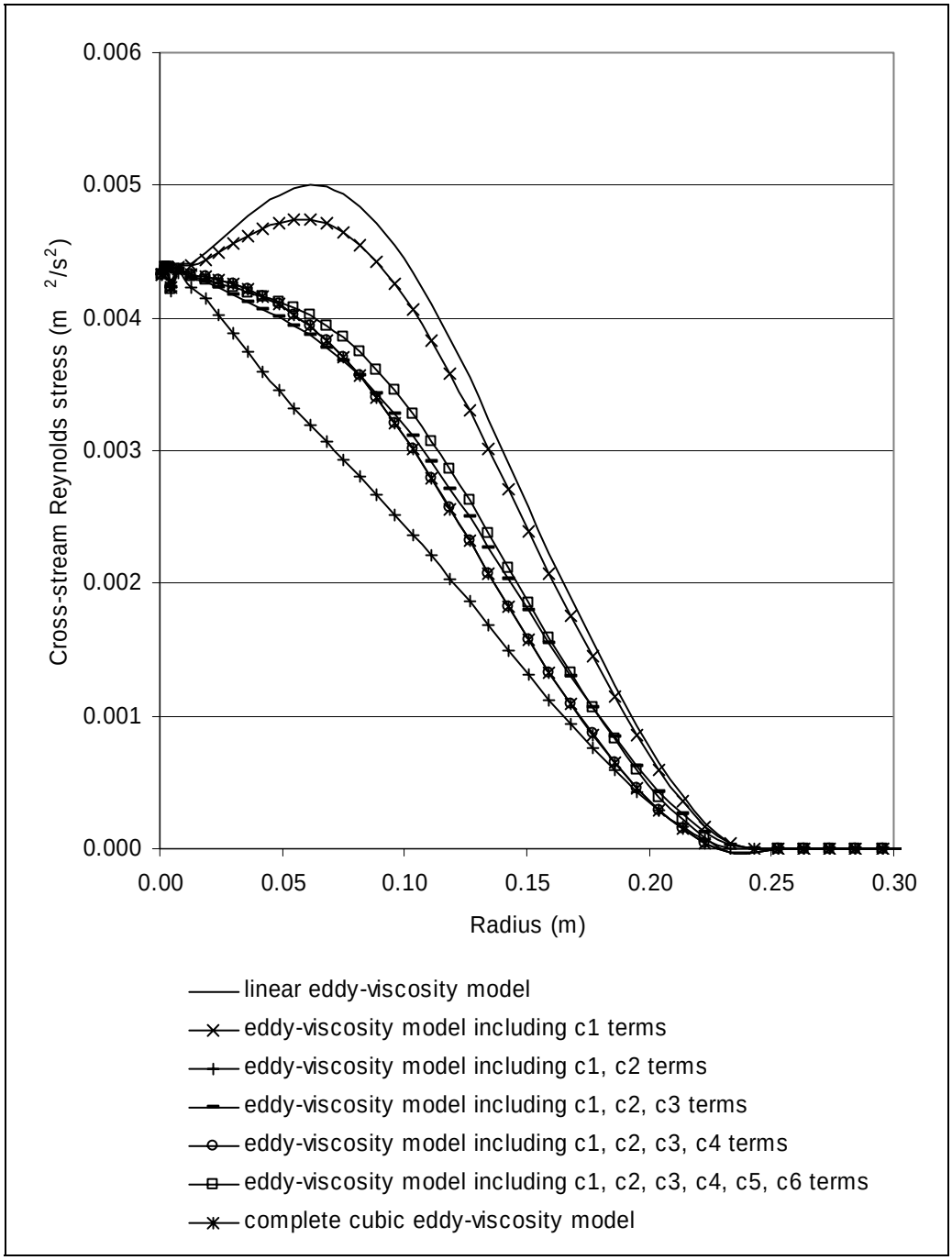

Figure 7-34: Comparison of the contribution to the cross-stream Reynolds stress by the various terms in the cubic model.

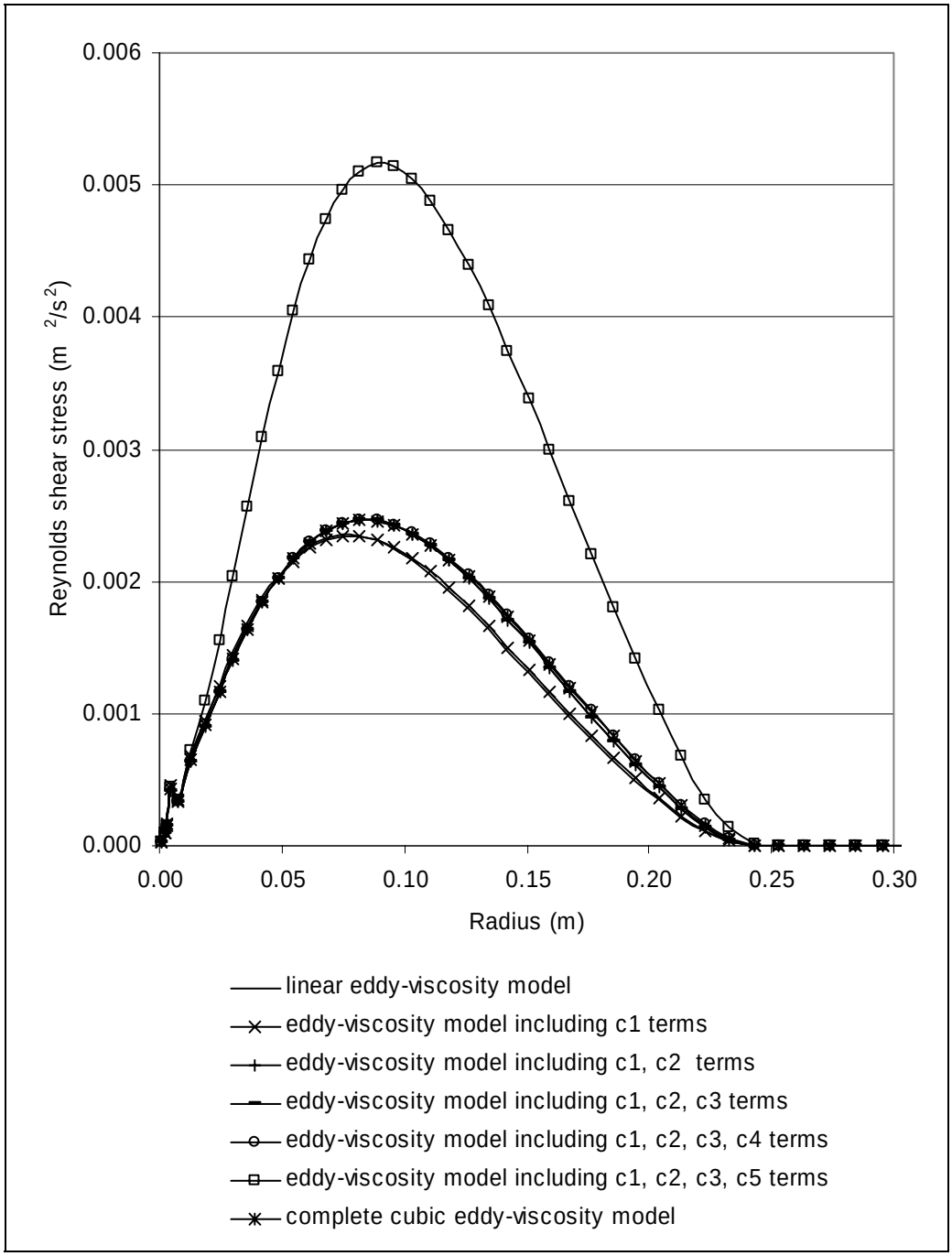

Figure 7-35: Comparison of the contribution to the shear Reynolds stress by the various terms in the cubic model.

7.6 Closure

This chapter has reported on the results achieved in the simulations of turbulent buoyant jets using a variety of turbulence models. The purpose was to investigate whether an improvement in the quality of the prediction of turbulent buoyant jets made with the standard k-ε model combined with the linear eddy-viscosity and with the eddy-diffusivity models could be achieved.

The transformed and RNG models were adopted as direct alternatives to the standard k-ε model. Comparison of the standard k-ε model and the transformed model found the latter increased the spreading rate. An irregularity was observed in the ω-profile that caused some numerical difficulties. These became apparent in the simulations of the axisymmetric turbulent buoyant jet. The RNG model, compared to the standard k-ε model, also produced a slight increase in the spreading rate and a more significant variation in the turbulence characteristics. The RNG model tends to flatten the profile near the centreline that was a departure from the experimentally observed profile. The functional coefficient introduced in the ε-equation of the RNG model was found to vary considerably over the width of the plume and may require a finer mesh to capture the detail.

Two low-Reynolds number models were also considered, the Launder and Sharma model and the standard k-ω model. The Launder and Sharma model showed limited success, but both models were found to be highly sensitive to boundary conditions.

The buoyant production of turbulence term was considered with respect to the model used and the inclusion of the term in the ε-equation of the standard k-ε model. Comparison of the eddy-diffusivity model and the GGDH model, in the description of this term, showed that the GGDH model increased the buoyant production of turbulence. This was an improvement in comparison with the experimental data. The net effect on the mean flow was dependent on the initial geometry of the buoyant jets. The value of turbulent kinetic energy in the plane buoyant jet is affected, to a larger extent, by the improvement of the turbulent buoyancy model

than is the axisymmetric buoyant jet, since this plume does not exhibit equilibrium of turbulent kinetic energy.

The neglect of the buoyant production of turbulence term from the ε-equations was found to increase the spreading rate; this effect was more significant with the GGDH model. A reduction in the value of ε resulted from the neglect of this term causing an increase in the turbulent viscosity and hence diffusion.

The GGDH model was also introduced into the diffusion term of the scalar equations. The model was combined with different representations of the Reynolds stresses. The inclusion of this model in the enthalpy transport equations only, resulted in a consistent increase in all the spreading rates, but its inclusion in all the scalar equations led to varying results. The cubic GGDH model was found to be unreliable.

Nonlinear eddy-viscosity models were considered as an alternative to the linear model for the momentum diffusion and the shear production of turbulence. A quadratic and a cubic model were considered with limited success. The quadratic model was found to improve the trend in the anisotropy of predicted turbulence, although the absolute values were overpredicted. The cubic model suffered from considerable instabilities and was modified from the original model. The predictions of the mean field made by this model showed very little difference from the linear model. However, components of the turbulence field predictions were considerably worse which could be associated with inappropriate values of the model coefficients.

CHAPTER 8

Numerical modelling of compartment fires

8.1 Introduction

Compartment fires, or fires enclosed within a building, can pose a serious threat to life and property. Figure 8-1 shows Home Office statistics (Watson (1999)) for fire related injuries. This demonstrates clearly that the smoke or fumes produced pose the largest threat to human life, within the category of fire related injures. The ability to predict real life fires and their spread over interiors and furnishing is beyond current modelling capabilities. However, the prediction of a stationary fire and the resultant temperature and flow field has been well reported in the literature, a brief summary of some studies is given in section 4.3

The predictive capabilities offered by the application of CFD methods to compartment fires, provides a tool for both forensic examination in the aftermath of a fire and during the design of a building to meet fire safety regulations.

This chapter will present the results of simulations of compartment fires using the CFD code SOFIE (Simulation of Fires In Enclosures) combined with the models newly implemented and applied to the simulation of turbulent buoyant jets described in the previous chapters. Section 8.2 details the results of simulations of the Steckler compartment fire and section 8.3 reports on a theoretical atrium-type compartment, based on the Steckler compartment.

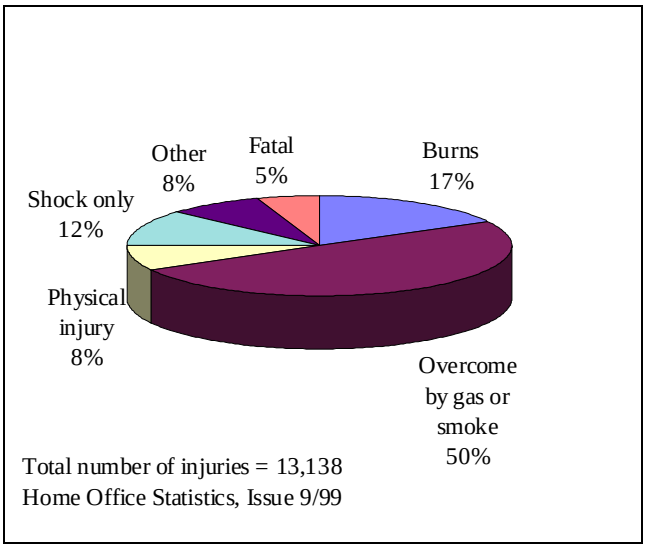

Figure 8-1: Home office statistics for fire related injures.

8.2 Steckler Compartment

Figure 8-2 shows a schematic drawing of the Steckler compartment. The experimental rig consisted of a compartment measuring 2.8 x 2.8m plane and with a height of 2.18m, a door was positioned centrally in a wall and had a height of 1.83 m and width 0.74 m. The walls were 0.1m thick and the walls and ceiling were lined with a lightweight ceramic fibre insulation board. A circular burner, central in the compartment, was supplied with light commercial grade methane at a fixed rate, sufficient to produce a heat output of 62.9kW. Temperature measurements were taken in the compartment opening and at the opening-side corner of the compartment. Velocity measurements were also taken in the doorway.

The numerical simulations were based on these experiments, however the physical structure of the domain was varied slightly for computational ease. The walls of the compartment were assumed to consist entirely of the lightweight ceramic rather than this just being a lining. The burner was assumed rectangular enabling ease of spatial definition in a Cartesian grid. The width of the burner was based on the experimental burner diameter and the inlet velocity was adjusted to ensure an accurate heat release. The symmetry of the compartment enabled simplification of the computational domain to half the room cut along the line of symmetry, as shown in figure 8-2. An external corridor was included in the computational domain to enable a better representation of the solution boundary conditions.

Previous experience in the simulation of this compartment fire has lead to the computational domain being confidently defined by a 100,000 cell grid (Sanderson et al. (1999)), with the eddy-break-up sub-model used in the prediction of combustion (Lewis et al. (1997)) and thermal radiation simulated using the deterministic ray tracing technique (DTRM) with gaseous optical properties described by a weight sum of grey gases (WSGG) model (Rubini and Moss (1997)). The hybrid-differencing scheme was used for the discretisation of the convective and diffusive term and the SIP solver was used for the solution of the pressure and the TDMA was applied to the momentum and scalars. The combination of these sub-models and numerical techniques with the standard k-ε model gives a reasonable prediction of the temperature and velocity field at the door of the compartment. However, there has been a general consensus in the modelling of fire plumes, as with thermal plumes, that the entrainment into the plume is underpredicted. Those turbulence models found to be most successful in the current plume simulations were applied to the simulation of the Steckler cavity, in order to assess whether comparable effects were observed. This assessment of the considered models will enable a confident recommendation of the most appropriate turbulence model for application to these complex flows with current computational ability.

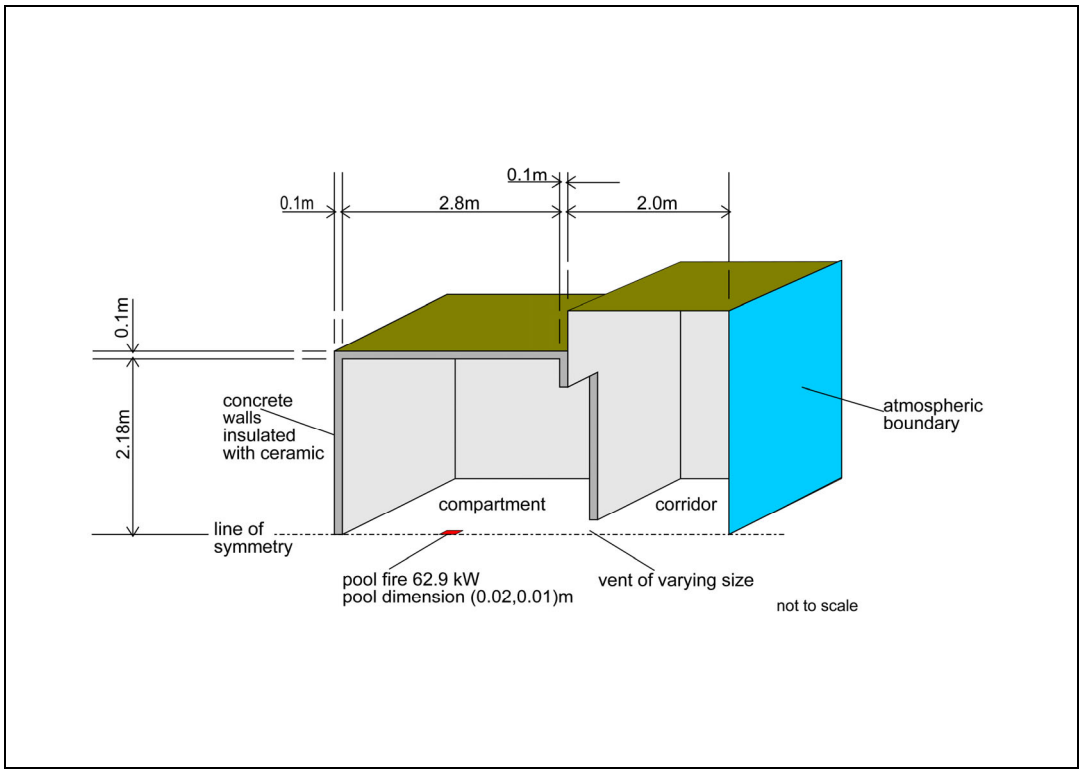

Figure 8-2: Schematic drawing of the Steckler compartment fire.

The quality of the predictions, made by each model, was assessed by comparison of the predicted and measured vertical temperature and velocity profiles at the centreline of the doorway and the vertical temperature profile in the corner of the room adjacent to the doorway. Variations between the considered models were further evaluated by comparison of the flow statistics, in addition to a visual comparison of the flow and thermal fields in the compartment.

Figures 8-3 and 8-4 show a comparison between the simulation results and the experimental measurements of temperature and velocity, respectively, at the door centreline for the standard k-ε, transformed k-ε and RNG model. The three models were combined with the GGDH turbulence buoyancy model. Figure 8-5 shows this comparison of the models for the vertical temperature profile in the corner of the room. Only a slight difference between the models is observed at the door centreline.

Table 8-1 compares the inlet mass flow statistics for the simulations undertaken. Comparison of the standard k-ε model with the GGDH turbulence buoyancy term and the RNG and transformed models reveals that the latter models predicted a smaller mass flow of air into the room. It is assumed that the mass flow of air into the room is a direct measure of the air entrained into the plume. This reduction in entrained air results in the hotter upper layer, since the hot plume is less diluted, which is seen in both the door centreline temperature profile (figure 8-3) and the thermal/flow field picture (figures 8-6, 8-7 and 8-8). The significant difference in the internal flow structure (figures 8-6, 8-7 and 8-8) is reflected in the corner temperature profiles (figure 8-5). The mixing between the upper and lower layers is greater with the standard model with the internal layer hieght at the corner being notably lower. The generally lower temperature of the upper layer in the standard model prediction would result in a smaller upward buoyancy force to retain the higher layer height. Comparison of the corner temperature profiles (figure 8-5) show that the RNG model gives a better prediction of the layer height whereas the standard model returns the best prediction of the upper layer temperature. The transformed model appears to predict a more diffusive plume resulting in lower velocities in much of the domain. The plume prediction with the transformed model was shown to have a lower level of ω than would be calculated by the standard model (section 7.2.1). This would lead directly to a larger turbulent viscosity and hence increase the diffusion.

The inclusion of a turbulence buoyancy model and the type of model used was considered. Two turbulence buoyancy models were considered in conjunction with the standard k-ε model: the standard turbulent buoyancy model and the GGDH turbulent buoyancy model. Figures 8-12, 8-13 and 8-14 show the thermal and flow fields within the room. Figures 8-9 and 8-10 compare the experimental measurements with the predicted vertical profiles of temperature and velocity at the door centreline. Figure 8-14 shows the experimental measurements and predictions of vertical profile of temperature in the corner of the room adjacent to the doorway. The structure of the internal flow field for the three considered models is fairly

similar. However, the flow statistics (table 8-1) show the inclusion of a turbulence buoyancy model and the subsequent improvement of the model, from the standard model to the GGDH model, leads to successive increases in the amount of fluid entrained. The temperature predicted within the cavity with no turbulent buoyancy model is markedly higher than those in which a model was included. The lack of turbulent buoyancy production term results in a comparatively smaller value of turbulent kinetic energy, hence the predicted turbulent viscosity and consequently the thermal diffusion would be less. The physical effect of this is to have a thermal flow more highly influenced by the flow field. Comparison against the experimental data shows that the inclusion of a buoyant turbulent model provides a significant improvement in the temperature and fluid predictions. The expected improvement with GGDH model is not apparent in this validation against experimental data as the development of the plume is so limited by the height of the compartment and the large ceiling layer. The next section considers a theoretical atrium based on this Steckler compartment but three times the height; in this case a greater height for the plume to develop is available.

The GGDH diffusion model was adopted for a series of simulations: firstly the linear and hybrid GGDH models were included in the enthalpy equations only, then the hybrid GGDH models were applied to all the diffusion term in all the solved scalar transport equations. Figures 8-18, 8-19 and 8-20 show the thermal and flow fields within the room. Figures 8-15 and 8-16 compare the experimental measurements with the predicted vertical profiles of temperature and velocity at the door centreline. Figure 8-17 shows the experimental measurements and predictions of vertical profile of temperature in the corner of the room adjacent to the doorway. The trend in the entrainment into the compartment correspond to those observed in the axisymmetric buoyant jet prediction, that is, there is a slight increase where the GGDH model is included in the enthalpy equation only and a slight decrease where it is included in all the scalar transport equations.

Model	Flow into compartment
Transformed model with GGDH turbulent buoyancy model	0.2944
RNG model with GGDH turbulent buoyancy model	0.2794
Standard k-ε model with no turbulent buoyancy model	0.2938
Standard k-ε model with standard turbulent buoyancy model	0.2941
Standard k-ε model with GGDH turbulent buoyancy model	0.3045
Standard k-ε model with GGDH turbulent buoyancy model and linear GGDH diffusion model in the enthalpy equation	0.3048
Standard k-ε model with GGDH turbulent buoyancy model and hybrid GGDH diffusion model in the enthalpy equation	0.3111
Standard k-ε model with GGDH turbulent buoyancy model and hybrid GGDH diffusion model in the all scalar equations	0.3044

Table 8-1: Total flow entering and leaving compartment predicted by considered models and maximum predicted temperature in the solution domain.

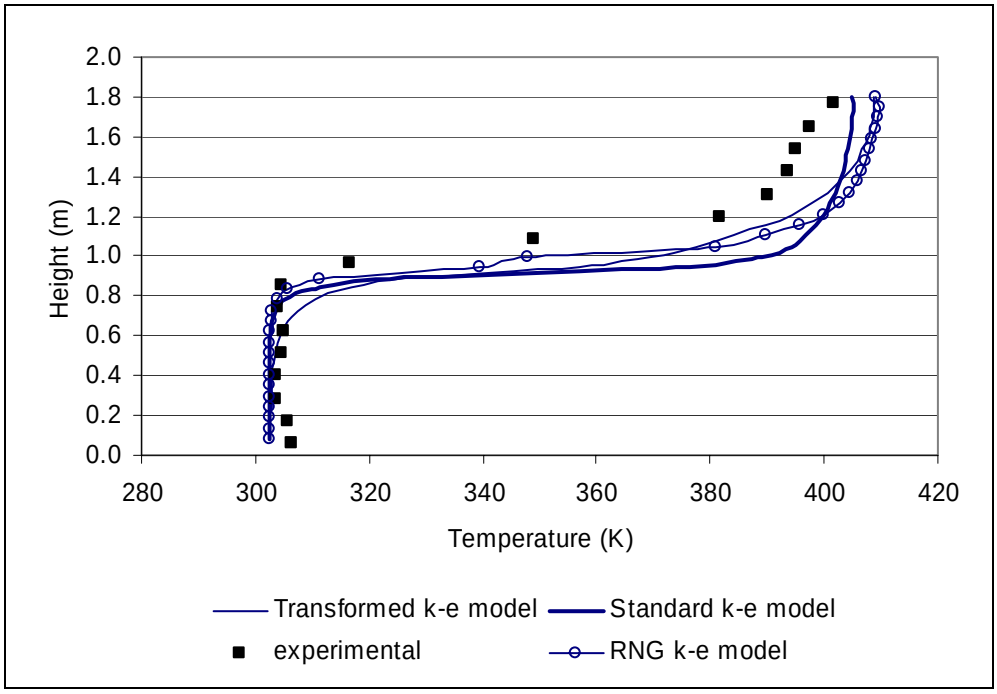

Figure 8-3: Temperature profile at the centreline of the doorway of the Steckler compartment. Comparison between standard k-ε model, transformed k-ε model, RNG k-ε model all with the GGDH turbulent buoyancy model and the experimental data.

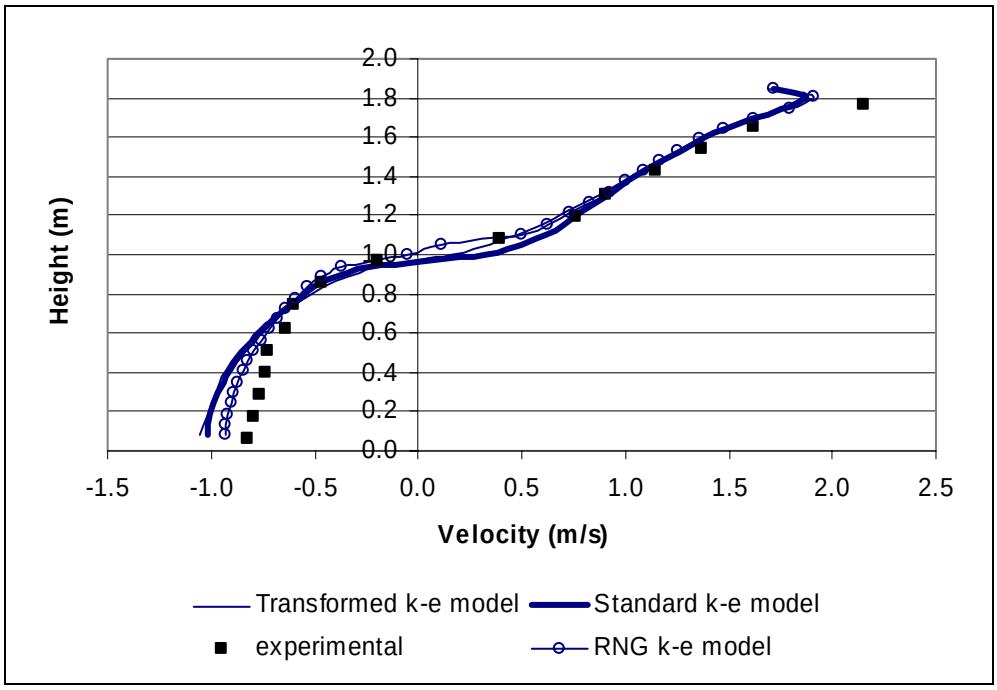

Figure 8-4: Velocity profile at the centreline of the doorway of the Steckler compartment. Comparison between standard *k*-ε model, transformed *k*-ε model, RNG *k*-ε model all with the GGDH turbulent buoyancy model and the experimental data.

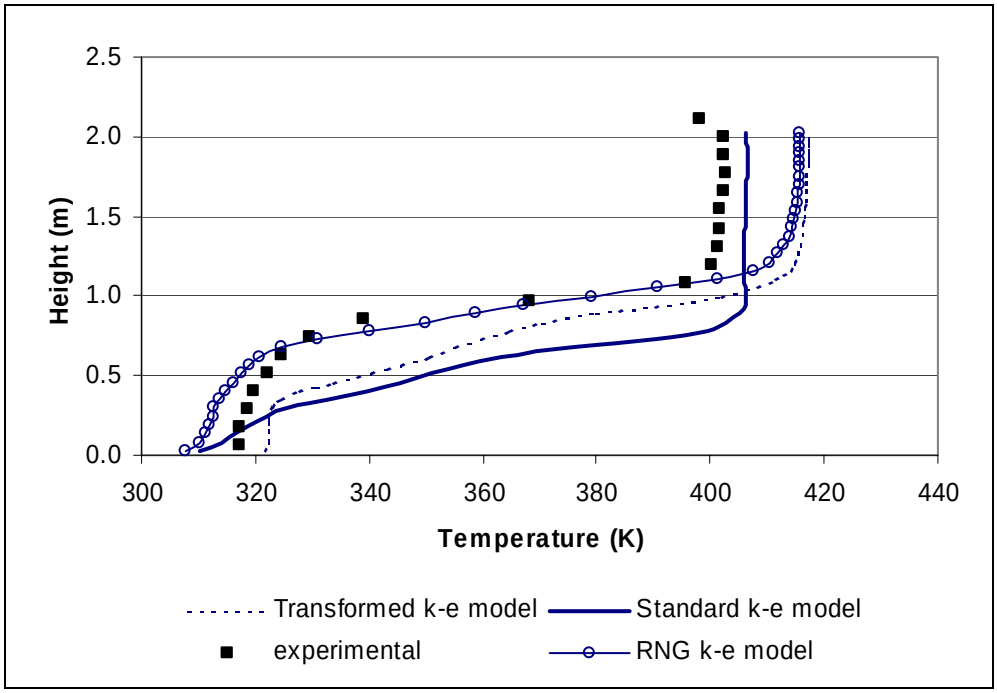

Figure 8-5: Vertical temperature profile in corner of Steckler compartment adjacent to the doorway. Comparison between standard *k*-ε model, transformed *k*-ε model, RNG *k*-ε model all with the GGDH turbulent buoyancy model and the experimental data.

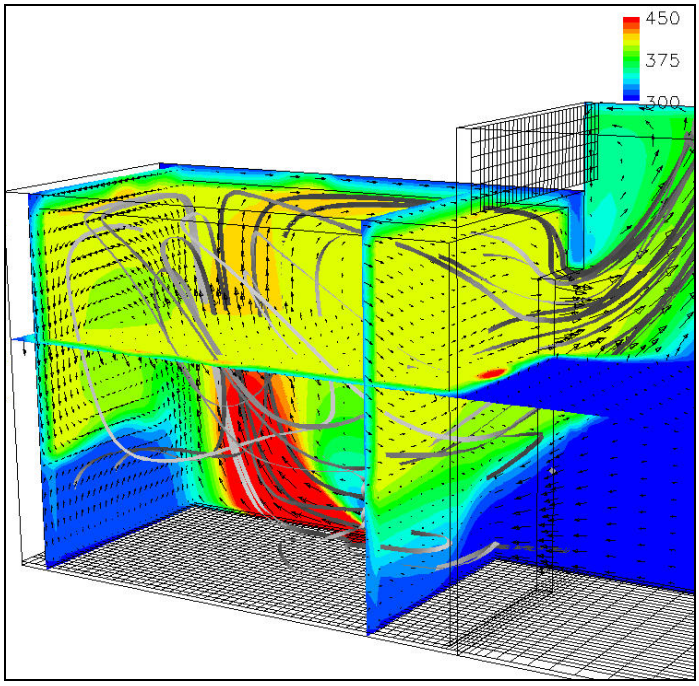

Figure 8-6: Picture of solution domain predicted with the standard k-ε model combined with the GGDH turbulence buoyancy model. The temperature field overlaid by velocity vectors is shown with streamlines.

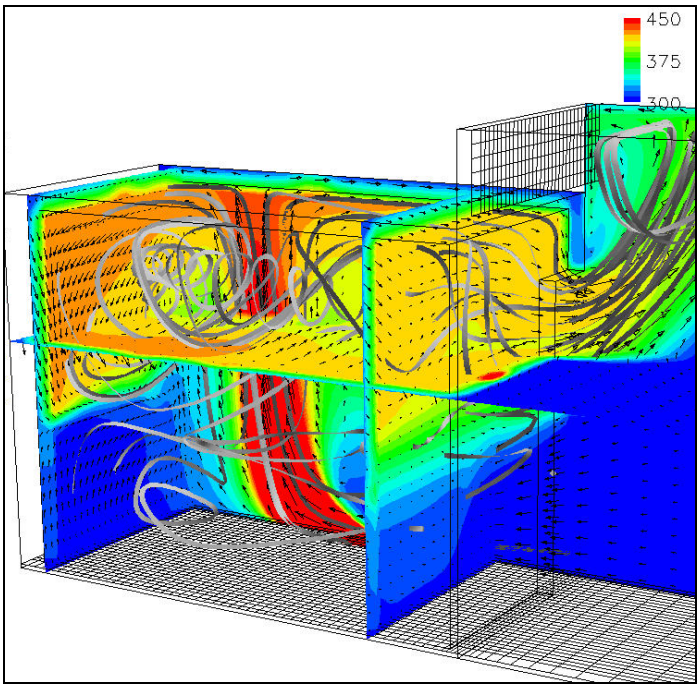

Figure 8-7: Picture of solution domain predicted with the RNG k-ε model combined with the GGDH turbulence buoyancy model. The temperature field overlaid by velocity vectors is shown with streamlines.

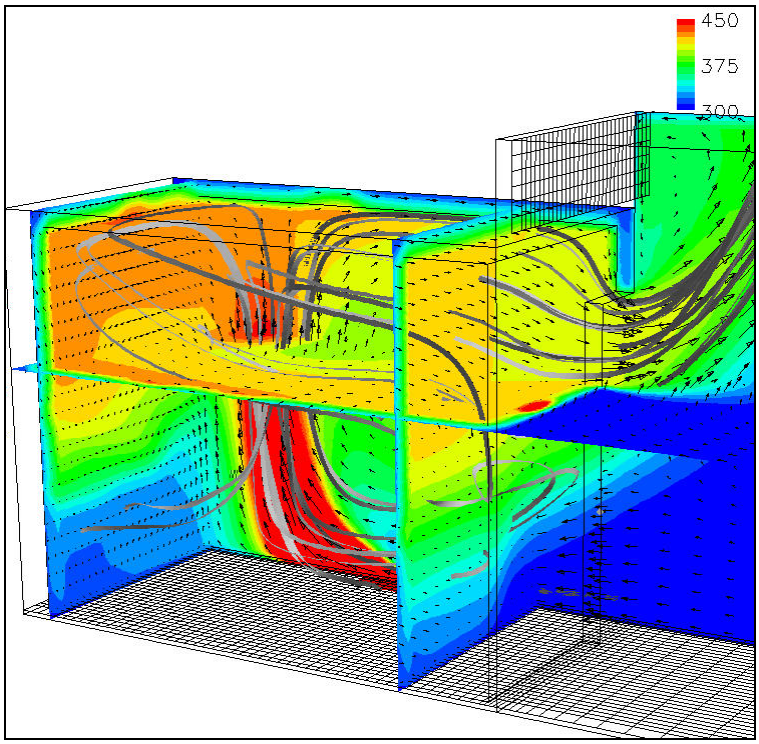

Figure 8-8: Picture of solution domain predicted with the transformed *k*-ε model combined with the GGDH turbulence buoyancy model. The temperature field overlaid by velocity vectors is shown with streamlines.

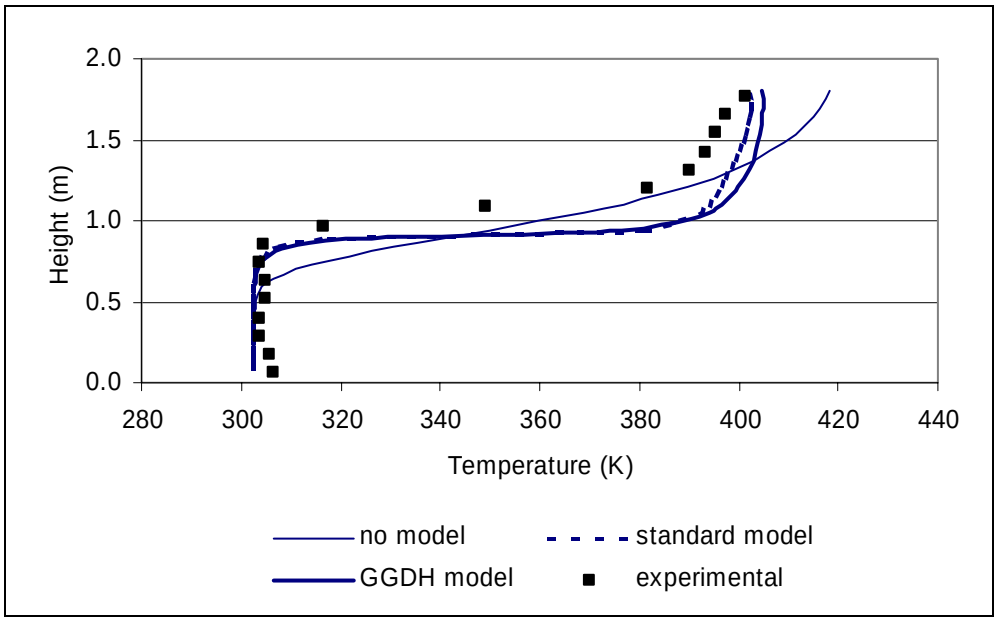

Figure 8-9: Temperature profile at the centreline of the doorway of the Steckler compartment. Comparison between standard *k*-ε model with no turbulent buoyancy model, the standard turbulence buoyancy model and the GGDH turbulent buoyancy model and the experimental data.

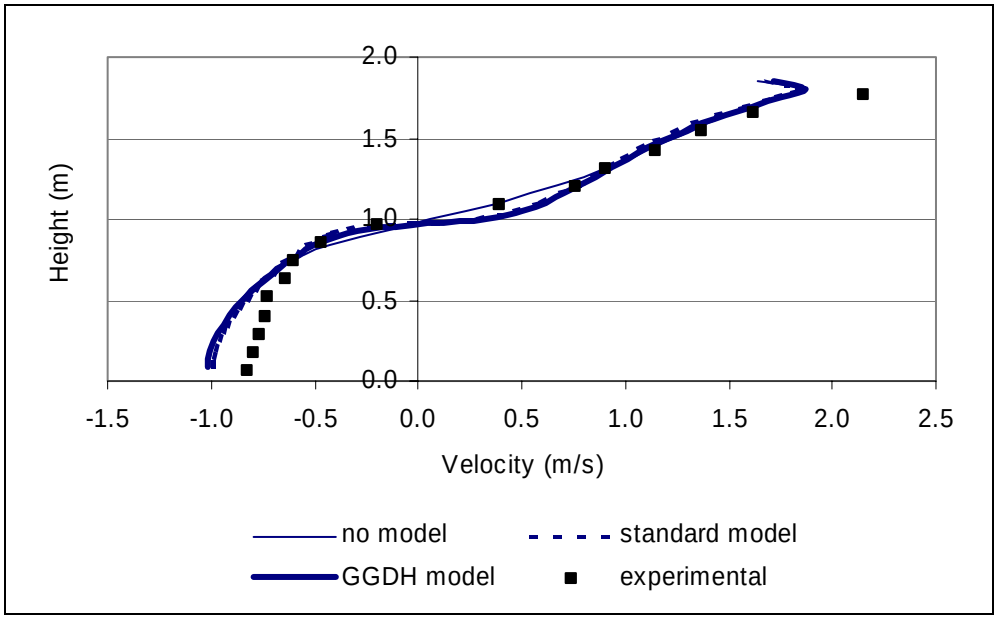

Figure 8-10: Velocity profile at the centreline of the doorway of the Steckler compartment. Comparison between standard *k-ε* model with no turbulent buoyancy model, the standard turbulence buoyancy model and the GGDH turbulent buoyancy model and the experimental data.

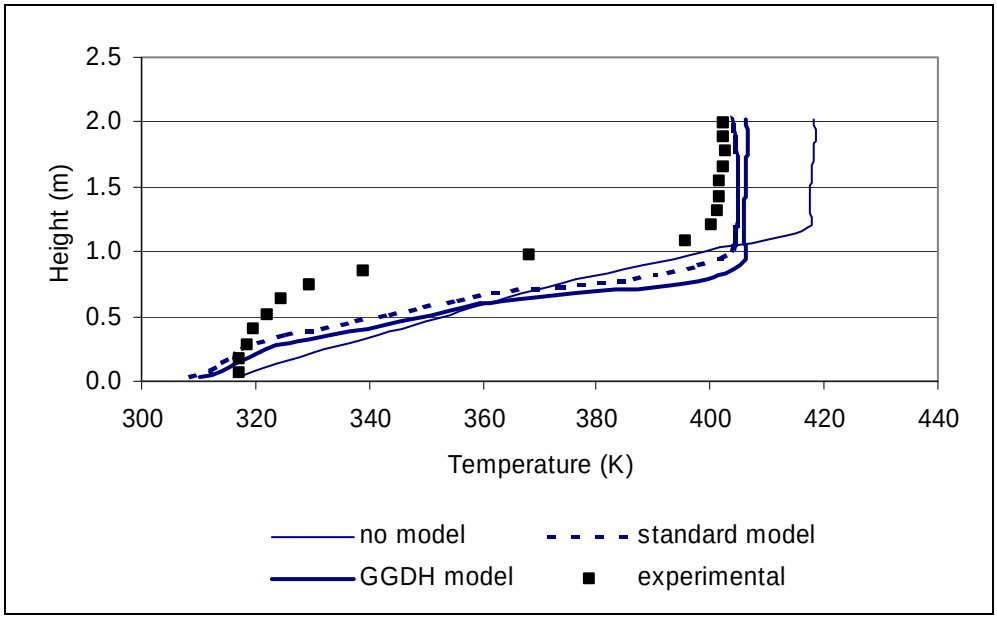

Figure 8-11: Vertical temperature profile in corner of Steckler compartment adjacent to the doorway. Comparison between standard *k-ε* model with no turbulent buoyancy model, the standard turbulence buoyancy model and the GGDH turbulent buoyancy model and the experimental data.

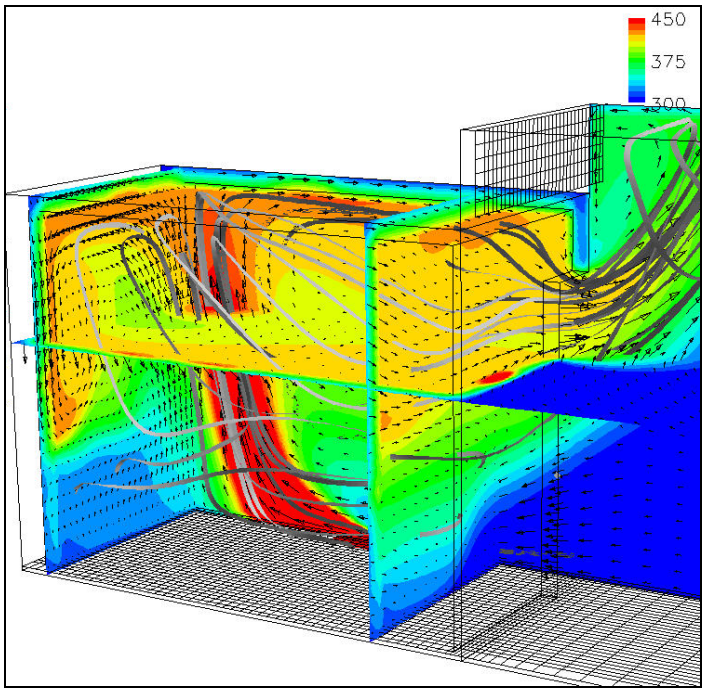

Figure 8-12: Picture of solution domain predicted with the standard *k*-ε with no turbulence buoyancy model. The temperature field overlaid by velocity vectors is shown with streamlines.

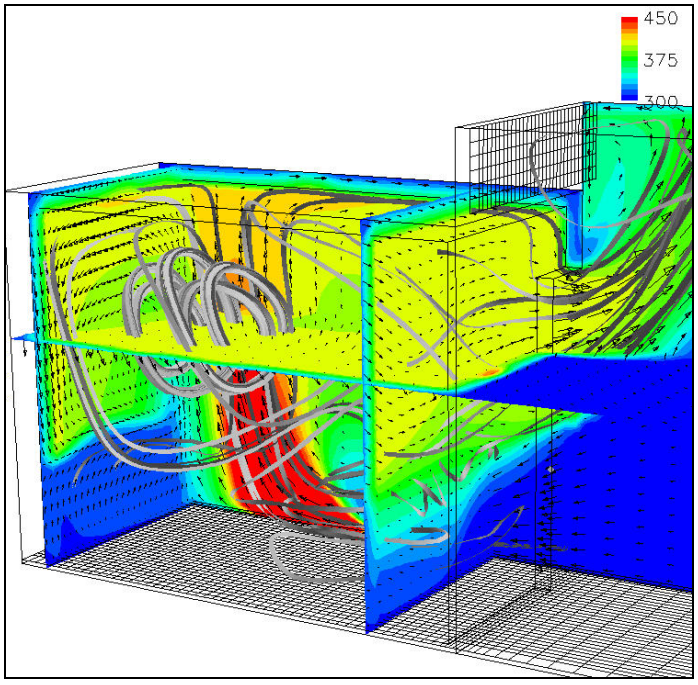

Figure 8-13: Picture of solution domain predicted with the standard *k*-ε with the standard turbulence buoyancy model. The temperature field overlaid by velocity vectors is shown with streamlines.

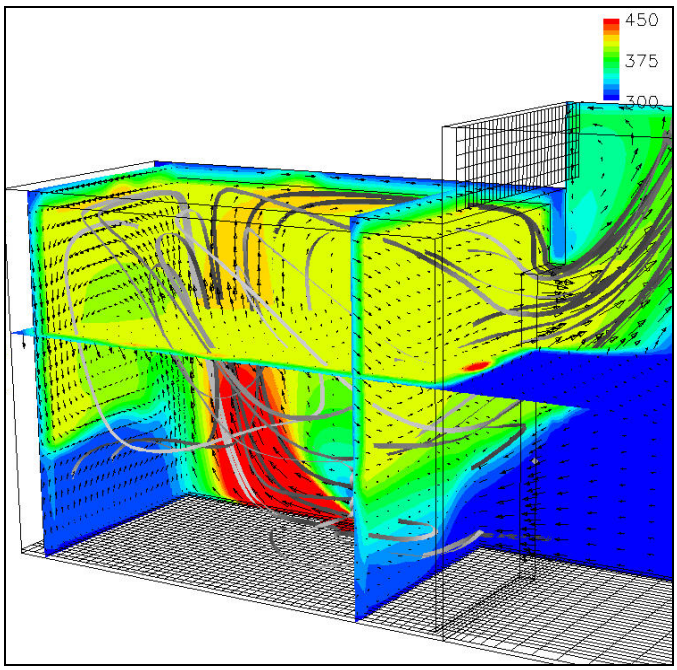

Figure 8-14: Picture of solution domain predicted with the standard *k*-ε with the GGDH turbulence buoyancy model. The temperature field overlaid by velocity vectors is shown with streamlines.

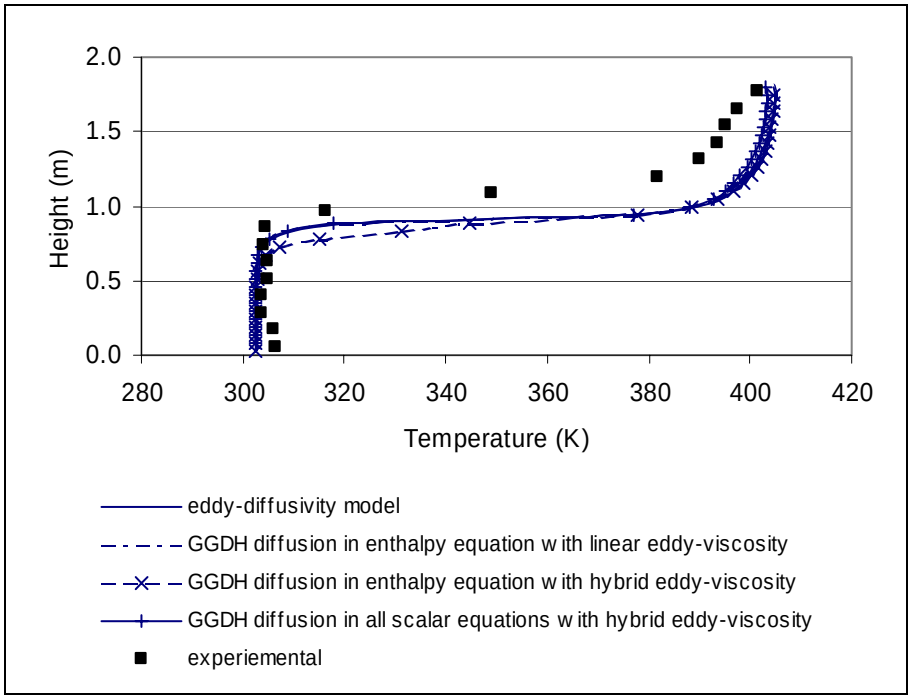

Figure 8-15: Temperature profile at the centreline of the doorway of the Steckler compartment. Comparison between diffusion models and experimental data. The compared diffusion models were: the eddy diffusivity model in all the scalar equations; the linear GGDH model in the enthalpy equation and the eddy-diffusivity in the remaining scalar equations; the hybrid GGDH model in the enthalpy equation and the eddy-diffusivity in the remaining scalar equations; the hybrid GGDH model in the all the scalar equations.

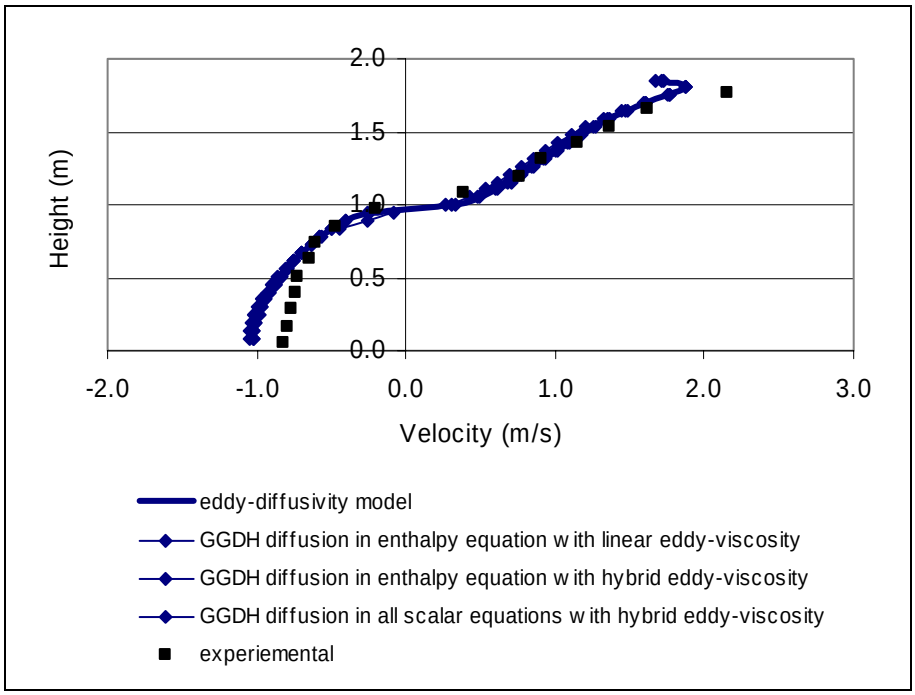

Figure 8-16: Velocity profile at the centreline of the doorway of the Steckler compartment. Comparison between diffusion models and experimental data. The compared diffusion models were: the eddy diffusivity model in all the scalar equations; the linear GGDH model in the enthalpy equation and the eddy-diffusivity in the remaining scalar equations; the hybrid GGDH model in the enthalpy equation and the eddy-diffusivity in the remaining scalar equations; the hybrid GGDH model in the all the scalar equations.

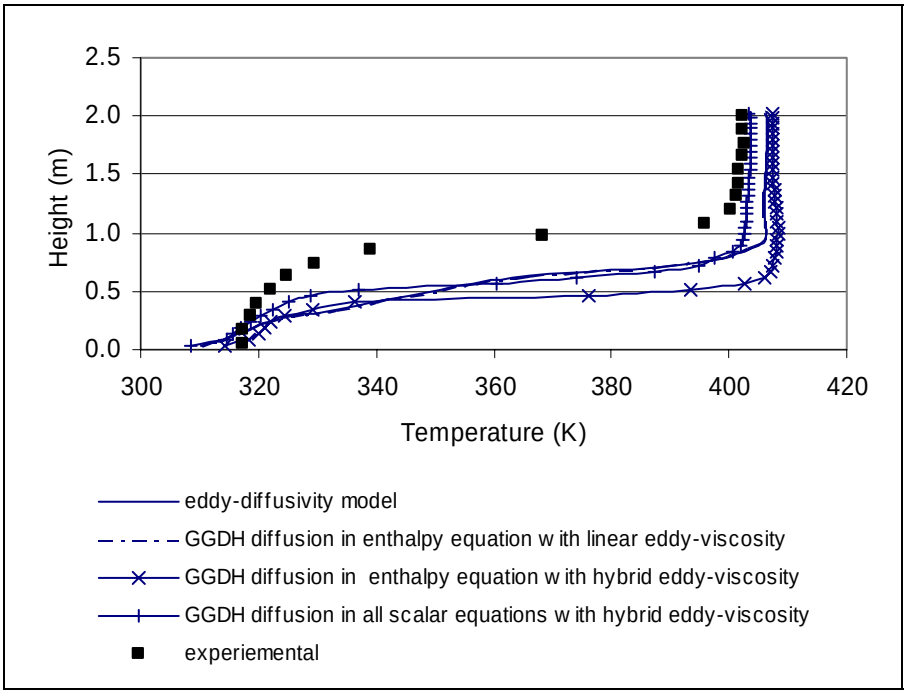

Figure 8-17: Vertical temperature profile in corner of Steckler compartment adjacent to the doorway.. Comparison between diffusion models and experimental data. The compared diffusion models were: the eddy diffusivity model in all the scalar equations; the linear GGDH

model in the enthalpy equation and the eddy-diffusivity in the remaining scalar equations; the hybrid GGDH model in the enthalpy equation and the eddy-diffusivity in the remaining scalar equations; the hybrid GGDH model in the all the scalar equations.

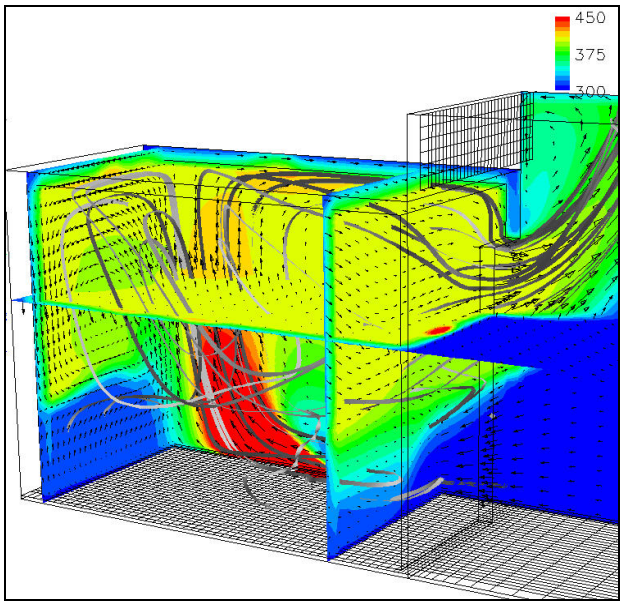

Figure 8-18: Picture of solution domain predicted with the standard *k*-ε with the GGDH turbulence buoyancy model and the diffusion term in the enthalpy equation modelled by the GGDH model with a eddy-viscosity model for the Reynolds stress. The temperature field overlaid by velocity vectors is shown with streamlines.

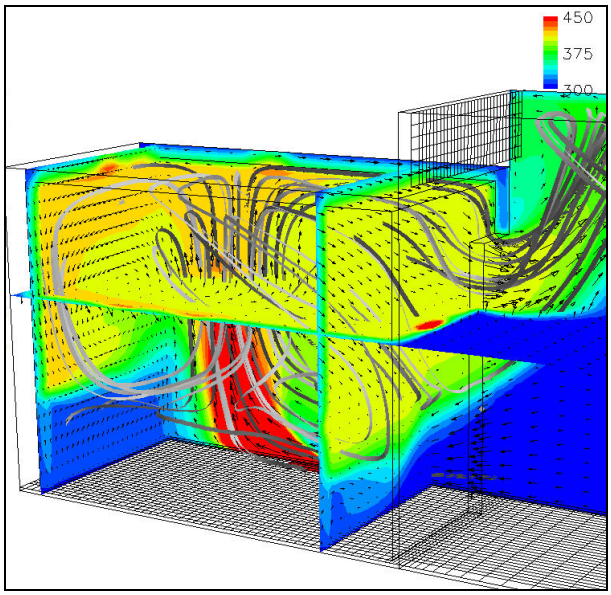

Figure 8-19: Picture of solution domain predicted with the standard *k*-ε with the GGDH turbulence buoyancy model and the diffusion term in the enthalpy equation modelled by the GGDH model with a hybrid model for the Reynolds stress. The temperature field overlaid by velocity vectors is shown with streamlines.

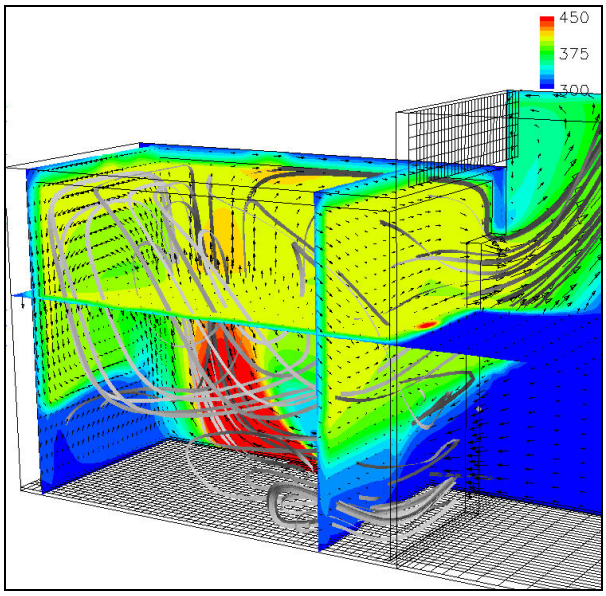

Figure 8-20: Picture of solution domain predicted with the standard *k-ε* with the GGDH turbulence buoyancy model and the diffusion term in the all scalar equations modelled by the GGDH model with a hybrid model for the Reynolds stress. The temperature field overlaid by velocity vectors is shown with streamlines.

8.3 Atrium

A theoretical atrium based on the Steckler compartment was considered. The plan dimensions of the atrium were consistent with those of the Steckler compartment but the atrium height is three times that of the Steckler compartment. The compartment door is retained but a second opening, which represents a doorway on the third floor, was introduced. The fire location and power is also unchanged from the Steckler compartment calculations. This scenario is theoretical and there is no useful experimental data available but as the atrium has become a common feature in many commercial buildings, such as offices and shopping centres it deserves investigation. The simulations reported in this section are intended to be a demonstration of the increased effect of the turbulence buoyancy model on the predicted field within a larger development region and contribute to the understanding of fires in such spaces.

The complexity of the simulations is reduced, compared to the Steckler compartment, through the neglect of the radiation model and conjugate heat transfer.

The lack of any experimental data renders the absolute values of the flow and the thermal field of less importance than the comparative trends of the considered models. The neglect of the radiation model substantially reduced the computational time required to gain a converged solution. A comparison was made between solutions with and without a combustion model to assess whether this was having a substantial effect on the considered turbulence models.

The domain was described by a mesh of 203,252 density. The numerical models used were the same as those in the Steckler compartment simulations.

Table 8-2 shows the mass flow into the atrium calculated at the doorway. In addition, the positive vertical mass flow through a horizontal plane at a height of 3m is calculated. The mass flow rate is seen to increase initially with the inclusion of a turbulent buoyancy model and then, again, with the added complexity of the model from the standard model to the GGDH model. The increase in mass flow can be physically interpreted as an increase in the entrainment into the plume. This trend is consistent between the combusting and non-combusting solutions.

Figure 8-21 to 8-26 shows the thermal and flow fields for each of the models considered. A comparison of the combusting thermal/flow field for the three cases where the turbulence buoyancy model is neglected, or the standard or GGDH model is included (figures 8-21 to 8-23), demonstrates a trend with the increased complexity of the model. In all cases the plume is forced over by the momentum of the incoming flow. However the extent to which this incoming cold flow penetrates the upward motion of the hot fluid is reduced with the increased complexity of the model. The cold inflow impinges on the rear wall where the turbulence buoyancy model is neglected. The increasing complexity of the model is reflected in the fluid plane adjacent to this wall getting hotter as the flow is associated more with the rising fire fluids rather than the incoming cold ambient air.

The inclusion of the hybrid GGDH diffusion model in all the scalar equations leads to a more notably different solution than was observed in the Steckler compartment. The entrainment is reduced and the diffusion between the hot and cold regions appears to reduce, compared to the standard diffusion model. This result is consistent with that observed in the plume simulations, in which the spreading rate of the axisymmetric buoyant jet was reduced by this model.

Model		Mass flow into atrium (kg/s)	Positive vertical mass flow through a plane height 3.0m (kg/s)
Combusting solution using standard k-ε model	no turbulent buoyancy model	0.777	1.056
	Standard turbulent buoyancy model	0.902	1.222
	GGDH turbulent buoyancy model	0.913	1.761
	GGDH turbulent buoyancy model with GGDH diffusion model	0.897	1.3252
Non-combusting solution	Standard turbulent buoyancy model	0.892	1.284
	GGDH turbulent buoyancy model	0.903	1.8904

Table 8-2: Flow statistic calculated from numerically predicted flow field for atrium.

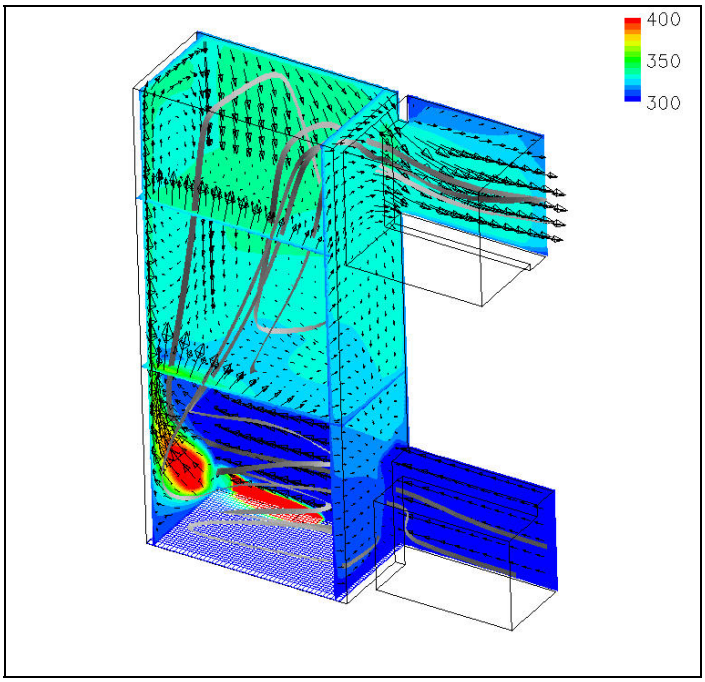

Figure 8-21: Picture of thermal field overlaid with vectors and showing streamlines. Predicted with the standard *k*-ε model and no turbulence buoyancy model.

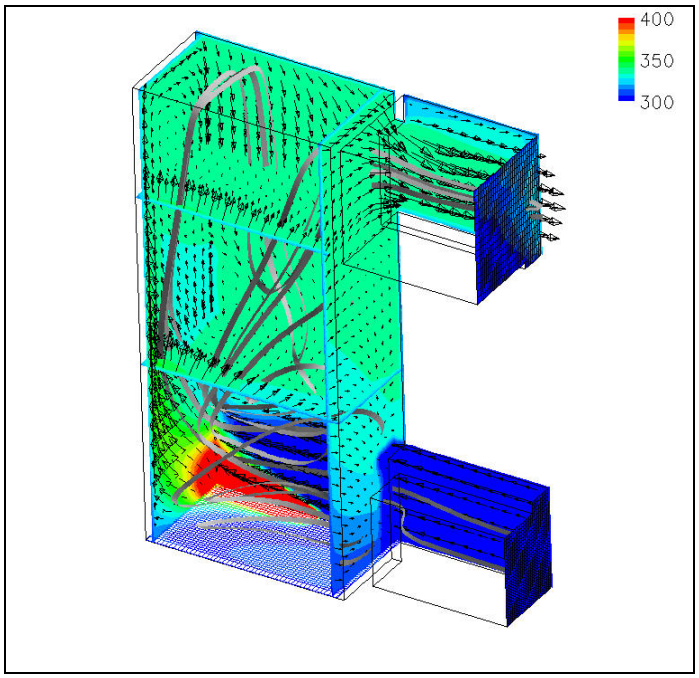

Figure 8-22: Picture of thermal field overlaid with vectors and showing streamlines. Predicted with the standard *k*-ε model combined with the standard turbulence buoyancy model.

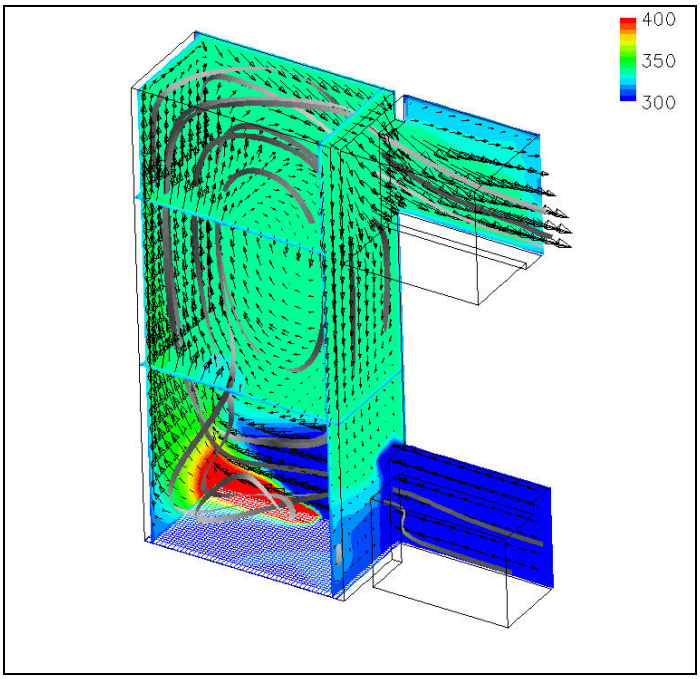

Figure 8-23: Picture of thermal field overlaid with vectors and showing streamlines. Predicted with the standard *k*-ε model and no turbulence buoyancy model.

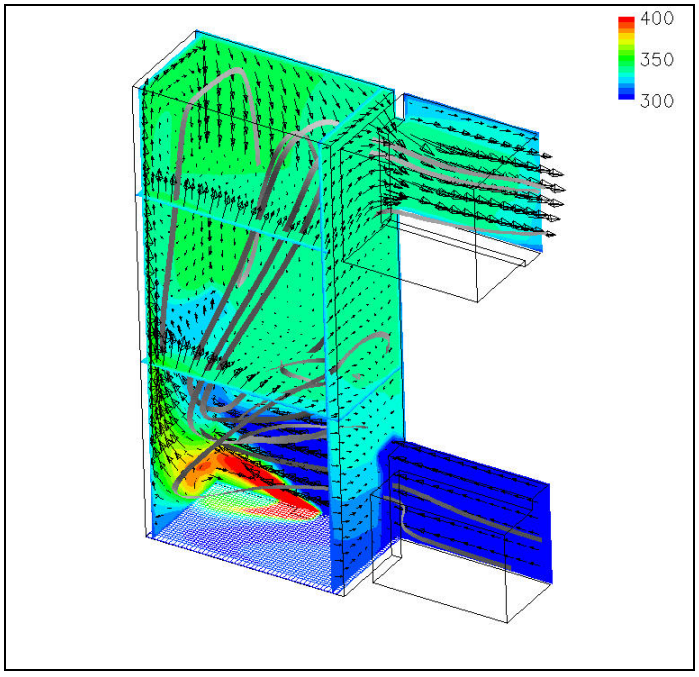

Figure 8-24: Picture of thermal field overlaid with vectors and showing streamlines. Predicted with the standard *k*-ε model with GGDH turbulence buoyancy model.

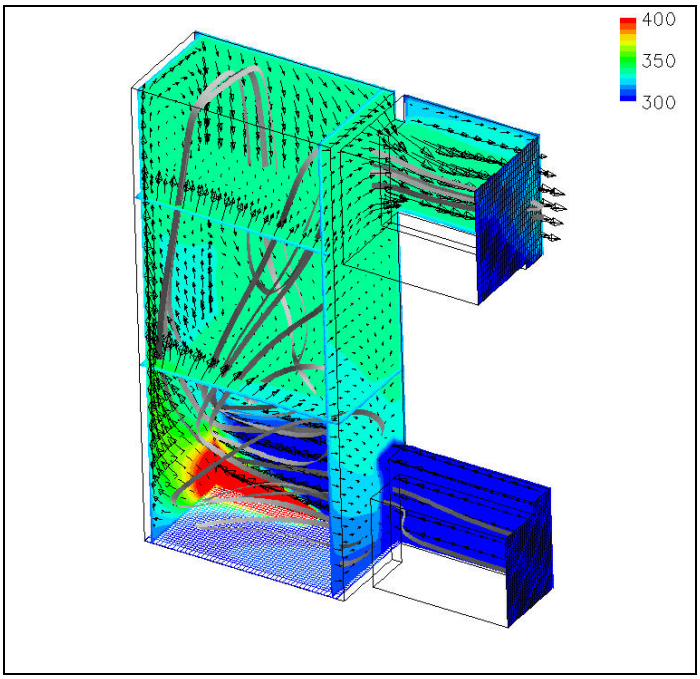

Figure 8-25: Picture of thermal field overlaid with vectors and showing streamlines. Predicted with the standard k-ε model with SGDH turbulence buoyancy model and enthalpy source term to represent the heat input.

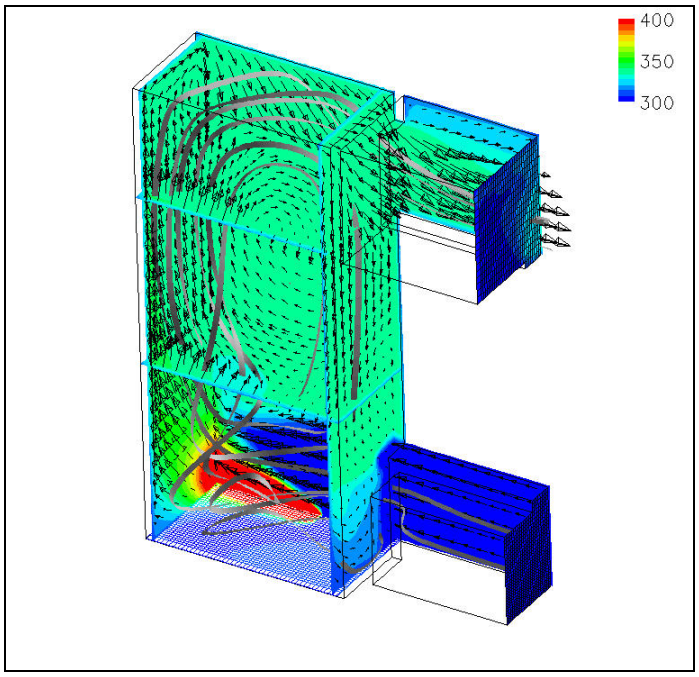

Figure 8-26: Picture of thermal field overlaid with vectors and showing streamlines. Predicted with the standard k-ε model with GGDH turbulence buoyancy model and an enthalpy source term to represent the heat input.

8.4 Closure

This chapter has reported on simulations of compartment fires with a variety turbulence models, turbulent buoyant production models and diffusion models. Two compartment fires were modelled: the Steckler compartment fire based on an experiment; and an atrium fire that was based on the Steckler compartment, for which no experimental data exists.

Three two-equation turbulence models were applied to the Steckler compartment. These were the standard k-ε model, the transformed model and the RNG model. The latter two reduced the entrainment into the compartment resulting in a far hotter upper layer than those predicted by the standard k-ε model, which was a departure from the experimental data.

The introduction of a buoyant production term in the k and ε equations of the turbulence models provided a significant improvement in the temperature profile prediction at the door of the Steckler compartment. The introduction of the GGDH model, compared to the standard model, resulted in an increase in entrainment for both the Steckler compartment and the atrium. The overall effect was more significant in the atrium with a notably different internal flow field.

Application of the GGDH diffusion models to the enthalpy equations gave results consistent with the turbulent buoyant jet predictions in which the entrainment was increased. The GGDH diffusion model, when applied to all the scalar diffusion terms, led to a reduction in the entrainment and this characteristic was more emphasised in the atrium than in the Steckler compartment.

A clear trend in the results from the compartment fire simulations is not immediately apparent. However, the knowledge gained from the simulations reported in the current thesis would lead to the recommendation that the k-ε turbulence model coupled with the linear eddy-viscosity model is still the most reliable approach to modelling compartment fire simulations. The turbulent scalar flux in the turbulent

buoyancy production term and the turbulent diffusion term in the enthalpy equation should be modelled by the GGDH model as standard, since this provides an improved prediction at little computational cost. The modelling of all the scalar diffusion terms by the GGDH model is considered an overall improvement, but has not been found to be as stable as the eddy-diffusivity model.

CHAPTER 9

Conclusions and further work

9.1 Conclusions

The work presented in this thesis has been concerned with the numerical simulation of turbulent buoyant jets and compartment fires. The influence of selected turbulence models on the prediction of turbulent buoyant jets was investigated, both through a literature review and through numerical simulation. These simulations were undertaken using the research-based CFD code SOFIE (Simulation Of Fires In Enclosures). The standard k-ε model existed within SOFIE and the implementation of alternative models was undertaken as an integral part of the work.

The experience gained from the comparative study of turbulence models for buoyant jets was applied to the simulation of compartment fires. The flow in a compartment fire is complex compared to that of turbulent buoyant jets but is still driven by the entrainment of fluid into the plume. The consequence of this is that the results associated with the buoyant jet simulations are broadly applicable to compartment fires.

Three turbulent buoyant jets were considered: a plane pure plume, a plane buoyant jet and an axisymmetric buoyant jet. The validation of the theoretical plane pure plume against experimental data, generalised by similarity laws, was possible through the normalisation of the data. The normalisation, however, disguises differences between the results and rendered the comparison uninformative. The plane and axisymmetric buoyant jets considered were based on published experiments, therefore absolute comparisons of the resulting data could be made.

For each turbulent buoyant jet, a comparison was made of the solutions achieved with the standard k-ε model, the experimental data and previous numerical studies. A recurring conclusion in published numerical studies of turbulent buoyant jets, that had adopted the standard k-ε model, was that the spreading rate was underpredicted when compared to experimental data. The prediction of the spreading rate for the plane buoyant jet in the current work also found the spreading rate to be underpredicted compared to the experimental data. However, for the axisymmetric buoyant jet, the spreading rate was underpredicted when compared to all but the most recent experimental study, which revealed it to be slightly overpredicted. A literature review of the available experimental studies on buoyant jets revealed considerable disparity. It appears that the increased sophistication of recent experimental methods and apparatus has enabled accurate measurements to be taken at greater distances from the source. This has resulted in more recent studies quoting smaller values of spreading rate at a given normalised distance from the source and suggests that, in earlier experimental studies, measurements were not taken in the self-similar region of the buoyant jet.

The consequence of the overprediction of the spreading rate observed in the current work has been to contradict the established wisdom that the standard k-ε model, combined with the eddy-viscosity relationship, is inadequate for the prediction of turbulence buoyant jets. The underprediction s observed in the early work has led to considerable research into the application of more complex turbulence models. Assessment of the quality of the standard k-ε model and the linear eddy-viscosity

models was undertaken by validating the turbulent characteristics of the axisymmetric buoyant jet against recent experimental measurements. These models do not predict the anisotropy of the turbulence at the centreline of the buoyant jet and thus the peak value of the streamwise velocity fluctuations is underpredicted. This is a recognised inadequacy of the linear eddy-viscosity model in thermal flows where the normal velocity gradients are small. The streamwise turbulent flux was also greatly underpredicted due to the inadequacy of the eddy-diffusivity model in its application to this flow. This led directly to a large underprediction of the buoyant production of turbulence in the standard k-ε model. Good reproduction of the turbulent shear stress and cross-stream turbulent scalar flux was observed at this level of modelling.

Several alternatives to the standard k-ε model were implemented and applied to the buoyant jets. None of these offered a great advantage over the standard k-ε model. The low-Reynolds number models considered were found to be sensitive to boundary conditions. Application of the alternative two-equation models to the compartment fire simulations predicted less entrainment compared to the standard k-ε model.

The standard model for buoyant production of turbulence uses the eddy-diffusivity relationship. The inadequacy of this for the prediction of turbulent buoyant jets has been well established. Alternatives to this were adopted in the form of the GGDH model. This model provided a significant improvement to the prediction of this term. The influence on the solution was found to be dependent on the geometric type of the turbulent buoyant jet and on the coefficient of the turbulent buoyant production term in the ε-equation. The axisymmetric jet exhibits local equilibrium of turbulence that is not apparent in the plane buoyant jet. The effect of the improved buoyancy model is less for the axisymmetric jet since any increase in turbulent production is compensated for by an equivalent increase in dissipation. The consequence is the net effect on the turbulent kinetic energy is small. The neglect of the buoyancy term from the ε-equations causes a loss of equilibrium in

the turbulent kinetic energy of the axisymmetric case. This results in a more notable influence on the spreading rate. The inclusion of a buoyant turbulent production term in the k and ε-equations gives a significant improvement to the temperature prediction of compartment fires. The entrainment into the compartment is seen to increase with the increased complexity of the model from the eddy-diffusivity to the GGDH model.

The GGDH model was also applied to the scalar diffusion term. The accuracy of the implementation was ensured through examination of the predicted results against simplified model equations. The inclusion of the model in the enthalpy equation resulted in a small increase in the spreading rates and also a slight increase of the entrainment of the compartment fire. However, the modelling of all the scalar diffusion terms with this model resulted in varying effects on the spread of the turbulent buoyant jets. The application to the compartment fires resulted in a clear reduction of entrainment and the diffusion of flow and thermal fields. The stability of this model was also found to be less reliable than that of the eddy-diffusivity model.

Two nonlinear eddy-viscosity models were implemented to address the lack of anisotropy predicted by the linear model. Both these models were found to be relatively unstable and suffered from numerical difficulties. These problems were addressed through the methods used in their implementation. The solutions achieved by these two nonlinear eddy-viscosity models for the axisymmetric buoyant jet varied greatly. The quadratic model of Speziale was found to be most successful in improving the relative prediction of the velocity fluctuations, although the absolute values were overpredicted. The coefficients in both models were found to be inappropriate to the application of turbulent buoyant jets. The development of general coefficients is beyond the scope of the current work and the development of coefficients specific to buoyant jets would be limiting and would offer little advantage to the complex flow of a compartment fire. The mean flow predictions were found to be only slightly effected by the variation in normal Reynolds stresses.

That suggested that the additional complexity of the nonlinear model is unnecessary if only the mean flow and mean scalar fields are of interest. Due to their instability, these models were not applied to compartment fires.

The main conclusions from the simulations undertaken in this work are summarised below.

- An informative comparison between numerical simulation and experimental studies of buoyant jets is best made in absolute terms.
- There is a large variation in the spreading rates of buoyant jets measured in experimental studies.
- The prediction of spreading rate with the standard k-ε model, when compared to the most recent experimental data, shows a slight underprediction rather than an overprediction.
- The two-equation models considered as alternatives to the standard k-ε model show no notable advantage in the prediction of turbulent buoyant jets and compartment fires.
- There was an improvement in the prediction of the buoyant production of turbulent kinetic energy by the GGDH model over the eddy-diffusivity model. The overall effect on the mean flow field was dependent on the source geometry and its influence in the ε-equation.
- The application of the GGDH to model the buoyant production of turbulent kinetic energy in the compartment fire simulations increased the entrainment into the room. The influence was more emphasised in atrium than the room.
- The GGDH model was successfully used to describe the turbulent scalar diffusion in both turbulent buoyant jet and compartment fire simulations, although the stability was less reliable than the eddy-diffusivity model.
- Large variations were seen in the predictions of buoyant jets by the two nonlinear eddy-viscosity models as a result of the coefficients used in the definition. Speziale's quadratic model compared better with the experimental data. These models were found to suffer from considerable instability and numerical difficulties.

From this work, there are two main recommendations. Firstly, that the standard k-ε turbulence model, combined with the linear eddy-viscosity model, is still the most effective approach to modelling turbulence where the mean flow field of a turbulent buoyant plume is the main concern. Secondly, the standard model for the turbulent scalar flux should be improved. This work has shown that the GGDH model provides greater sophistication at little computational cost compared to the eddy-diffusivity model.

9.2 Further Work

The work undertaken in this study has resulted in a recommendation for a effective turbulence model to achieve a good prediction of mean flow field for turbulent buoyant jets and compartment fires. The continuation of the work could progress through further consideration of those models implemented for this thesis and by expanding the field to consider the need for more advanced models.

The further work required, in relation to those models that have been considered, in this study should include the following points.

- Further consideration of those two-equation models that, theoretically, should offer some advantage over the standard k-ε model.
    - An alternative implementation of the cross-diffusion term in the transformed model, such that the spatial velocity derivative is not being explicitly discretised. This would eliminate the need to discretise the velocity derivation over a discontinuity and the associated numerical difficulties.
    - Further consideration of the RNG model should be made to assess the influence of the functional coefficient in detail.
- The implementation of the GGDH diffusion models should be improved to optimise its stability and performance.
- The nonlinear models have shown limited success this is due to two major issues:

- The stability and convergence of these models is poor in comparison to the linear eddy-viscosity models.
- Coefficients applicable to buoyant driven flows should be established.

Continuations of the general field of turbulence modelling of buoyancy driven flows must first identify the importance of the accuracy of the turbulent field. At the current level of modelling, a good prediction of the flow field is achieved. The introduction of the GGDH model for the turbulent scalar fluxes results in a good prediction of the scalar field. If the turbulence field becomes of greater importance, possibly due to the dependence of sub-models, then investigation in to higher order model should be undertaken. A substantial amount of literature has been published on the application of ASM to buoyant driven flows and there is considerable variation in the models of different studies. An assessment of whether the continuing development of ASM is constructive, or whether the increased complexity of an RSM would be a more effective approach, should be made.

APPENDIX A

Validation

A.1 Introduction

Several of the turbulence models considered in this work have an established record in the prediction of simple flows. The correct implementation of the model was ensured through a validation procedure that compared published experimental data and numerical simulations with results achieved in the current work. In demonstrating that a model is capable of replicating published results, confidence in the implementation of a model is attained.

Section A.2 reports on the validation of both high and low-Reynolds number two-equation turbulence models with a two-dimensional channel flows. The simulations were based on the well-established dataset of Laufer (1952) that has been used for the validation in previous studies.

Section A.3 reports on the validation of the two nonlinear eddy-viscosity models. Both models were initially tested in a 3-dimensional channel to demonstrate the capabilities in predicting the secondary recirculations. The cubic eddy-viscosity

model was then tested on an experimental impinging jet. This case had been by used the model developer Suga (1995)).

A.2 Channel flow simulations by two-equation turbulence models

The base case for comparing all the two-equation turbulence models was a 2-dimensional channel flow based on the experiments of Laufer (1952). These consisted of a channel of width 127mm with a Reynolds number (based on the half width of the channel and the maximum velocity) of 12,300. This provided a simple well-tested flow against which the models could be validated.

The simulations were all run with SOFIE, the only variation being in the choice of the turbulence model. The SIMPLEC pressure-correction method was used with the SIP solver (Stone (1968)). The momentum and scalar transport equations were discretised using the hybrid scheme and were solved by the TDMA. Advantage was taken of the symmetry of the flow by simulating only half the channel with a mirror boundary defined along the line of symmetry.

High Reynolds Number (HRN) Models

Three high Reynolds number models were considered in this thesis, the standard k-ε model, the RNG model and the transformed model. High Reynolds number models were coupled with wall functions for the description of the near wall flow. The wall functions provide an algebraic description of the boundary layer. Therefore, the validation of these models is more concerned with the accuracy of the bulk fluid flow, not the boundary layer prediction.

The simulations were undertaken on a range of mesh densities varying from 10 to 100 cross-sectional cells. Figure A-1 show the log-law predicted by a mesh with 10 cross-sectional cells. This demonstrates the quality of the near-wall flow prediction that is possible with a coarse mesh when the wall functions are adopted. Figures A-

2 and A-3 show the bulk flow predicted by this coarse mesh and finer meshes respectively. The bulk flow is well predicted by the finer meshes for all the HRN turbulence models considered.

The results demonstrate that all these models reproduce a simple channel flow in a consistent manner. This is the desired conclusion since none of these models should offer an advantage in such a flow; the differences between the models become apparent in more complex flows. For example, the standard and transformed k-ε models are theoretically identical. The advantage of the transformed k-ε model is that the solution of the ω-equation, rather than the ε-equation, is more stable since ω has a significant value at low Reynolds numbers.

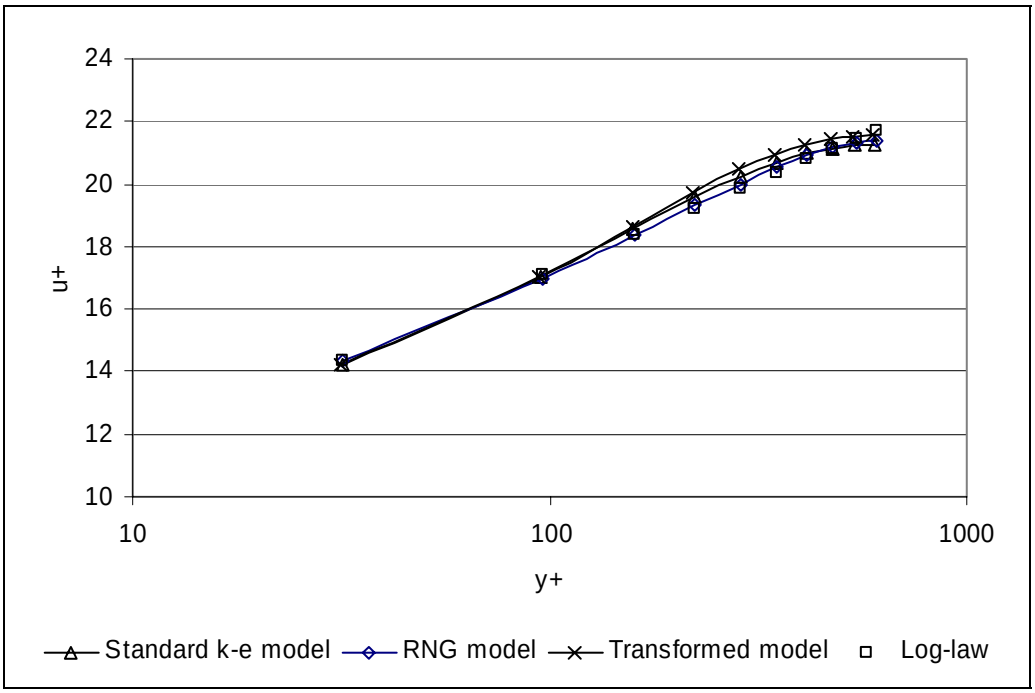

Figure A-1 Log law predicted by three HRN turbulence model simulated on a coarse grid with 10 cross-stream nodes.

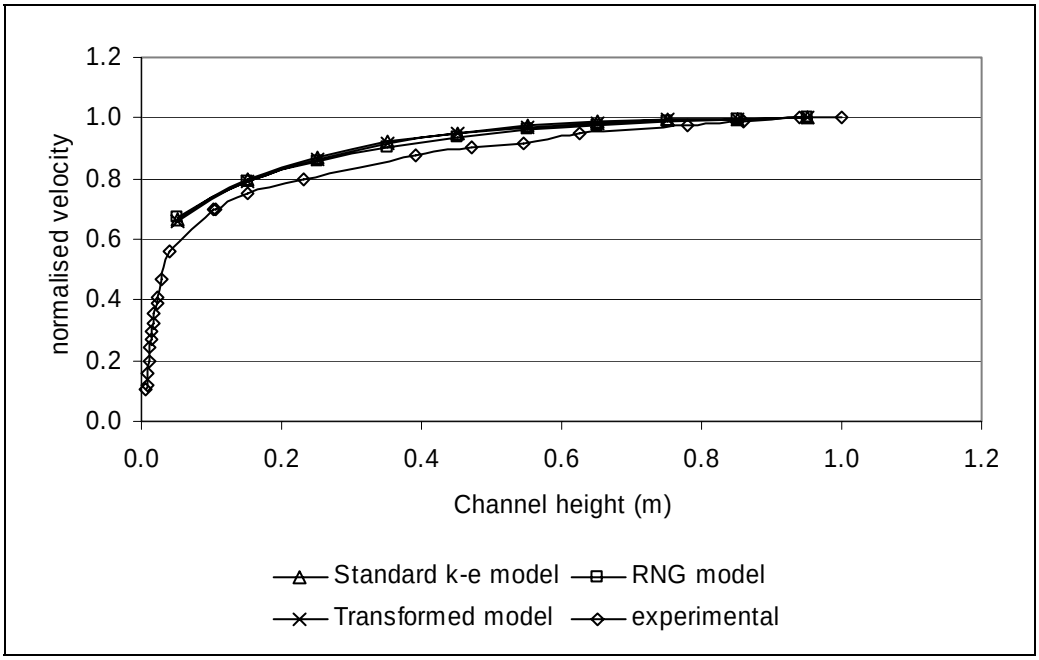

Figure A-2: Velocity field of 2-dimensional-channel flow predicted on coarse mesh with 10-cross-stream nodes.

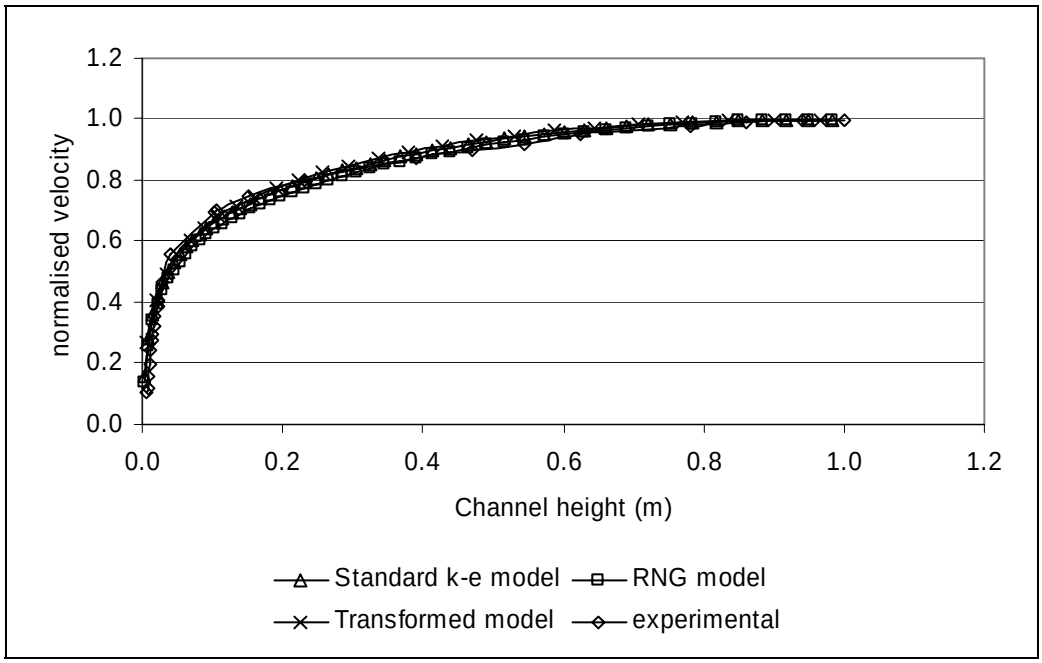

Figure A-2: Velocity field of 2-dimensional-channel flow predicted on fine mesh with 50-cross-stream nodes.

Low Reynolds Number (LRN) Model

Low Reynolds number models have generally been developed to solve the boundary layer region of a flow as discussed in section 4.2.2. These models have been widely tested on simple channel flow as a validation exercise by a number of authors, for example Patel, Rodi and Scheuerer (1985). A feature of LRN models is the requirement for the near wall mesh to be fine in order that the detail of the flow can be captured. A large number of simulations were undertaken in which both the number of cross-sectional nodes and stretch of the mesh near the wall boundary were considered. A range of these grids will be considered in this section to demonstrate the capability of the model.

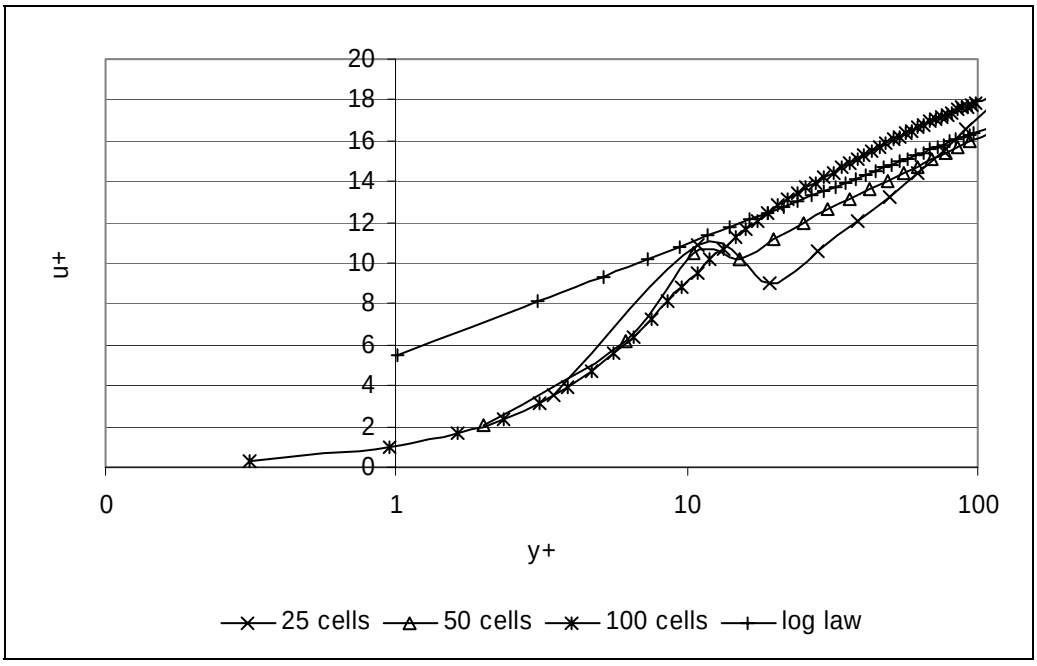

Figure A-1: Log law predicted by the Launder and Sharma LRN k-ε model. Comparison between grid with a differing number of cross-stream cells.

Predictions of the log-law from the Launder and Sharma (1974) (LS) k-ε model are given in figure A-1. The sensitivity of this model to the near wall grid density is demonstrated. The finest of the displayed grids has approximately 35 nodes under a y+ of 50 hence a grid of comparable refinement to that of Launder and Sharma when testing channel flows is not achieved here. However, the characteristic of the

overprediction of the log-law, observed in the well-regarded paper Patel, Rodi and Scheuerer (1985), has been repeated.

Nonlinear Models

Two nonlinear models were considered in the current thesis. The quadratic model of Speziale (1987) and the cubic model of Suga (1995).

The work of Speziale (1987) demonstrated the capability of nonlinear eddy-viscosity models to predict the secondary flows in a three-dimensional channel. This was chosen to be the primary case with which to validate the implementation of both nonlinear eddy-viscosity models.

The square channel had a dimension of 10mm plan and a length of 0.5m. A mesh density of 12,000 defined the domain consisting of a quarter of the true channel. Mirror symmetry boundaries defined two adjacent boundaries and the remaining two were defined as solid walls. The flow was simulated with the standard k-ε turbulence model, combined with the linear eddy-viscosity model, in addition to both nonlinear eddy-viscosity models in order to provide a comparison. The SIMPLEC algorithm was adopted for the pressure correction. The momentum and scalar equations were discretised with a hybrid scheme and solved using TDMA.

Figure A-2 shows the typical results gained for both nonlinear eddy-viscosity models (right) compared to the linear solution (left). The figures display the secondary velocity vectors in a plan view of the channel. This clearly shows the secondary flow predicted by the nonlinear eddy-viscosity model. The ability of the model to capture the anisotropy of the flow is demonstrated.

The cubic nonlinear model was validated on an axisymmetric impinging jet flow. This example was adopted in the model development by Suga (1995). Figure A-3 shows the solution domain of the impinging jet. The circumferential symmetry of

the problem enabled a sector of the domain to be modelled through the definition of mirror symmetry boundaries along the radial planes.

Figure A-5 shows the result of the linear and cubic eddy-viscosity models in the prediction of the impinging jet by SOFIE. The numerical models adopted for these simulations were the same as those used for the channel flow simulations. The comparative trends of the two models are similar to those reported by Suga (1995). Suga demonstrates the peaks of the velocity profiles, predicted by the cubic eddy-viscosity model, increased compared to that predicted by the linear eddy-viscosity model. Differences were apparent between the absolute values achieved in this and Suga's study but this could be associated with the turbulence model. The current work solved the standard k-ε model whereas the previous work adopted a LRN turbulence model. Additional simulations were undertaken considering the influence on the functional C_μ. It was found that it was this rather than the nonlinear terms that had the dominant effect on the velocity predictions.

A.3 Closure

This appendix has summarised the validation simulations undertaken to provide confidence in the turbulence models implemented in this work. A two-dimensional channel for which experimental data existed was used to validate the two-equation models. It was shown that all the models reproduced the experimental data with reasonable quality. The nonlinear eddy-viscosity models were tested on a 3-dimensional channel and both models successfully demonstrated the capability to predict the secondary flows. The cubic nonlinear model was then applied to an impinging jet. The trends observed in the prediction of this jet were comparable to those observed in earlier studies.

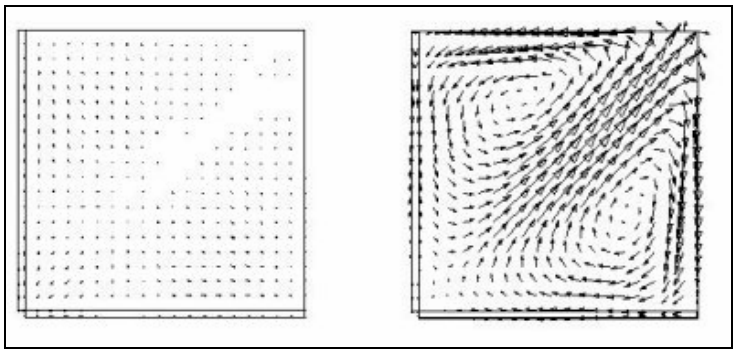

Figure A-2: Plan view of 3-dimensional channel flow showing secondary velocity vectors

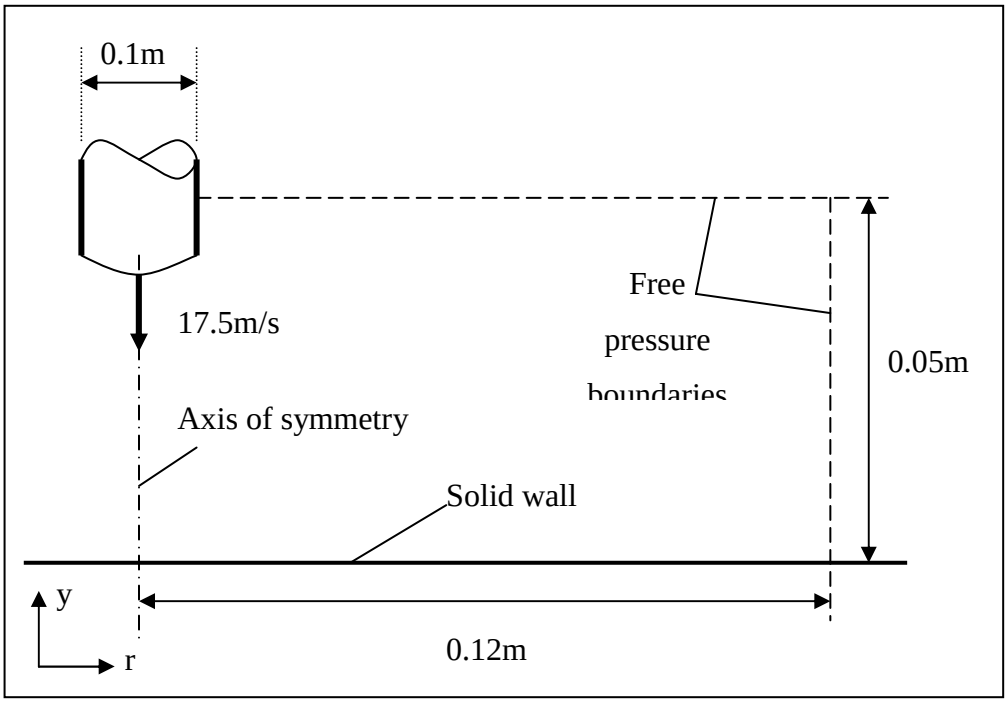

Figure A-3: Solution domain for impinging jet

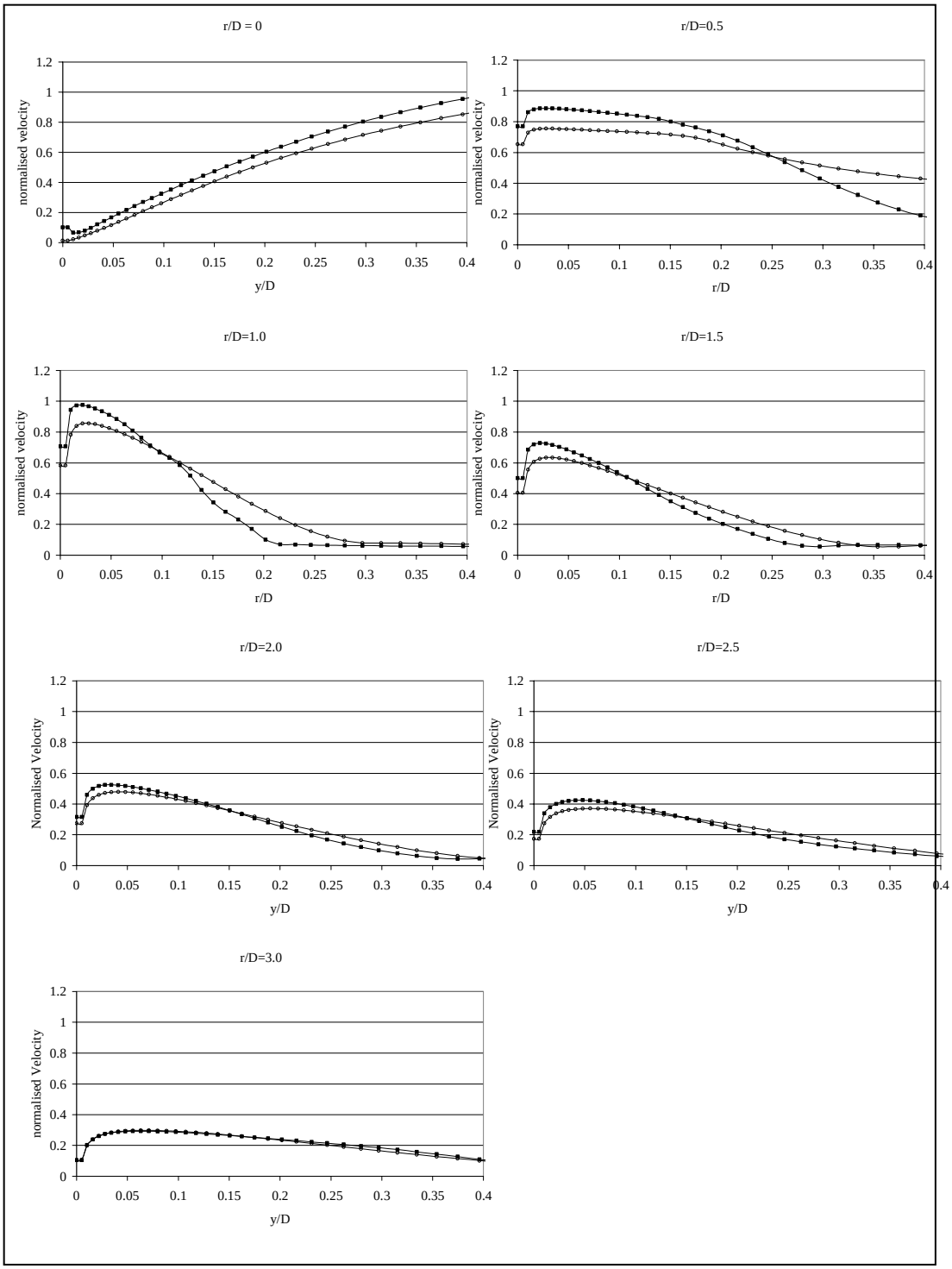

Figure A-4: Normalised velocity of impinging jet and at a number of prescribed distances from the centreline of the jet. Hollow circles represent solution with linear eddy-viscosity solution and square represent solution with cubic eddy-viscosity model.

APPENDIX B

Computational Grids

Figure B-1 to B-3 show figures of the grids used in the simulations of each buoyant jet. Table B-1 summarises the grid densities.

	Domain dimension (m)	Grid density	Cells across inlet
Plane plume	3.52 x 4.5	117 x 165	2
Plane Buoyant jet	0.4525 x 0.75	67 x 100	2
Axisymmetric buoyant jet	1.1047635 x 3.2	94 x 150	4

Table B-1: Computational grid density.

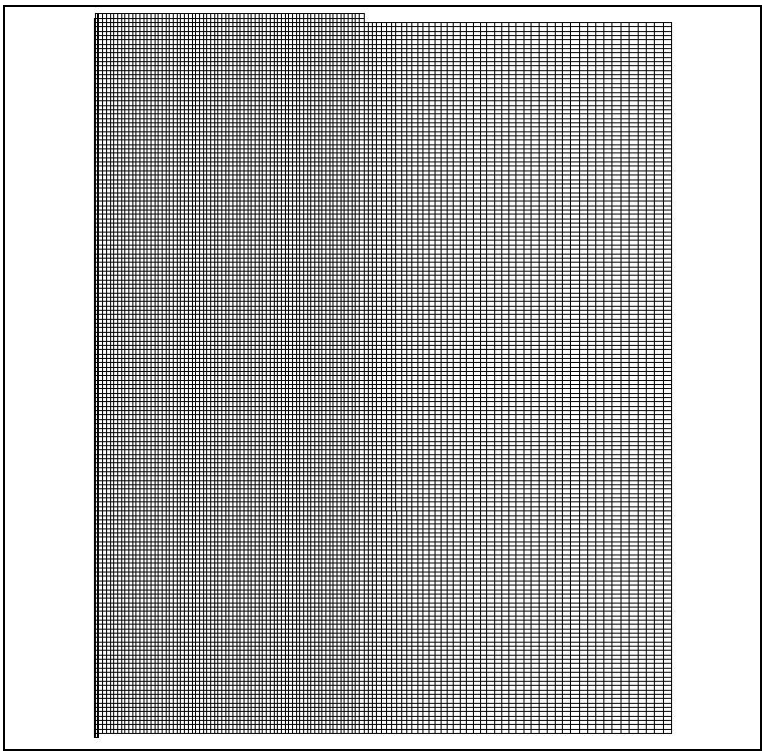

Figure B-1: Computational grid used for simulations of plane pure plume

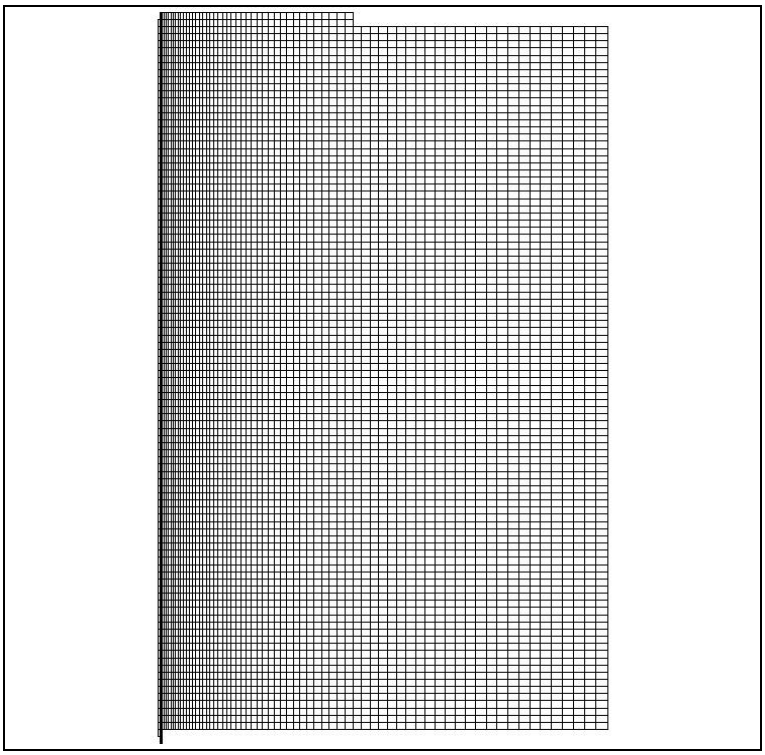

Figure B-2: Computational grid used in simulations of plane buoyant jets.

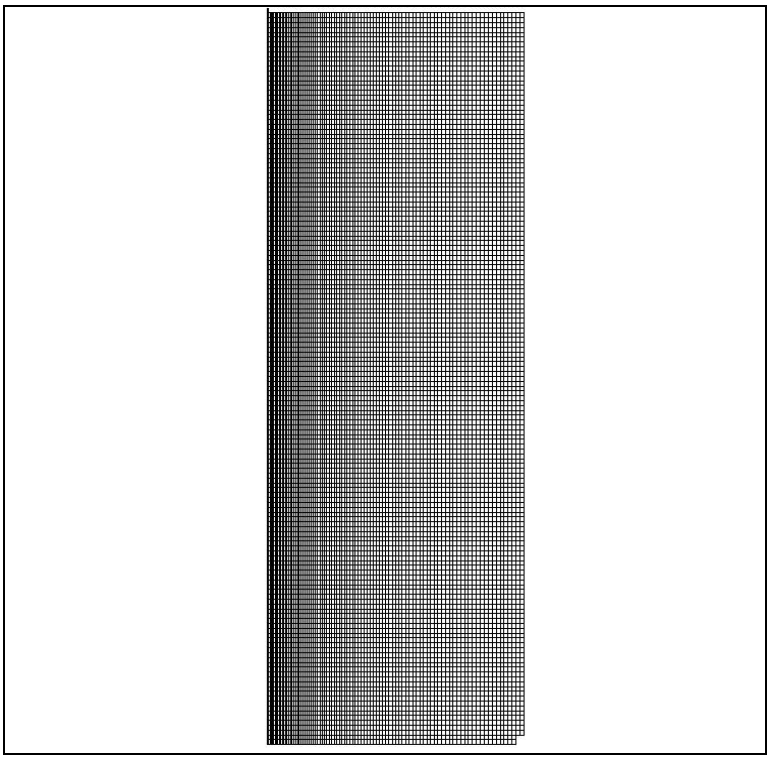

Figure B.3: Computational grid used in simulations of axisymmetric buoyant jet.

APPENDIX C

Influence of 'ledge' on flow field

A ledge was introduced on the exiting boundary of the domain, to promote stability. This was found to have a minimal effect on the flow region of interest, as will be demonstrated in this appendix. Figure C-1 shows the streamwise velocity profile of the plane buoyant jet at approximately half the height of the domain. It is clearly seen that the influence of the ledge on flow field in this region of interest in minimal.

Figures C-1 to C-2 show the flow field for the three domains with ledges of varying size. The ledge is seen to influence the ambient flow in the upper region of the domain. A recirculation is seen to form under the largest of the ledges. The smaller two are characterised by an inflow on the exiting boundary. The ledge of middle size was used in the plane buoyant jet simulations. This was seen to provide the least disturbance at the upper boundary.

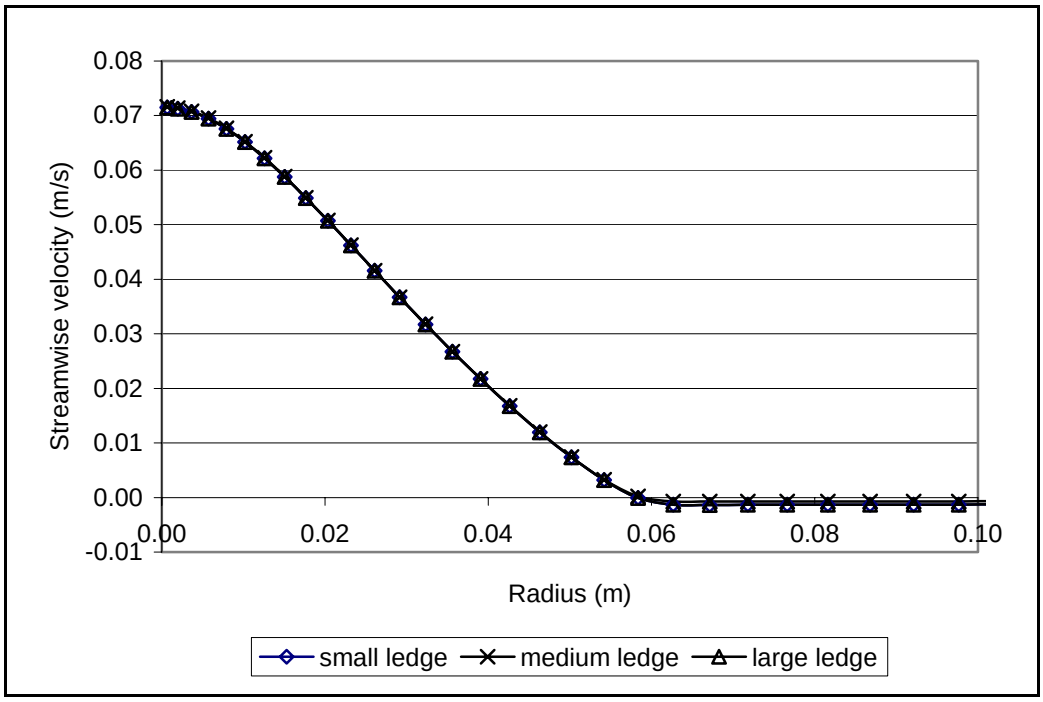

Figure C-1: Streamwise velocity profiles for solution domains with upper boundary ledges of varying size.

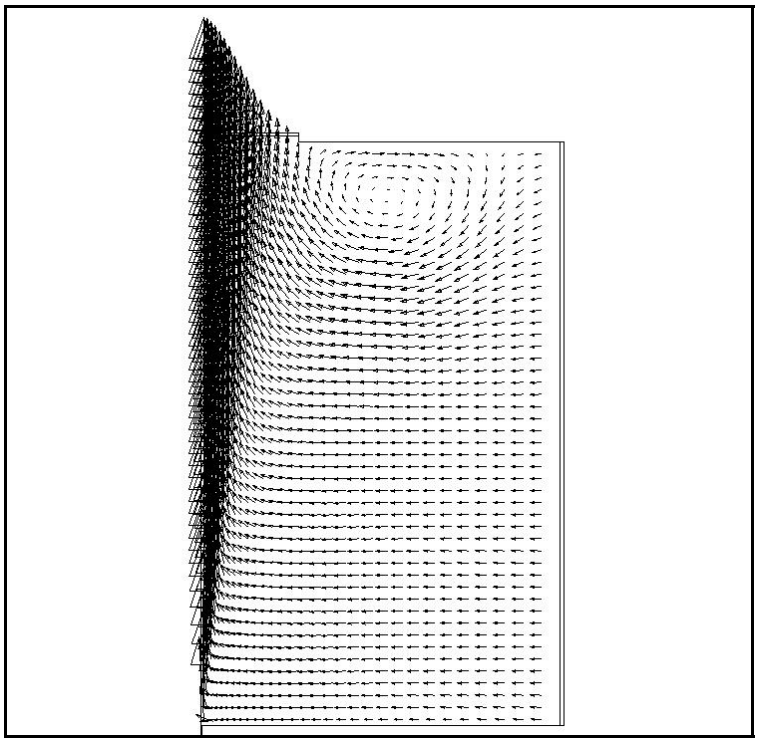

Figure C-2: Flow field of plane buoyant jet with large upper boundary ledge

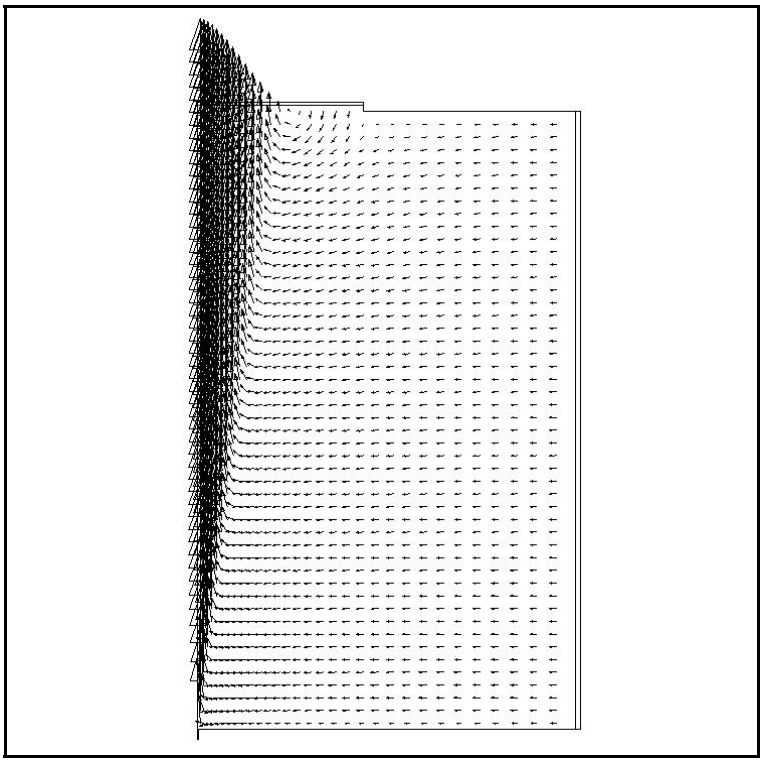

Figure C-3: Flow field of plane buoyant jet with medium upper boundary ledge

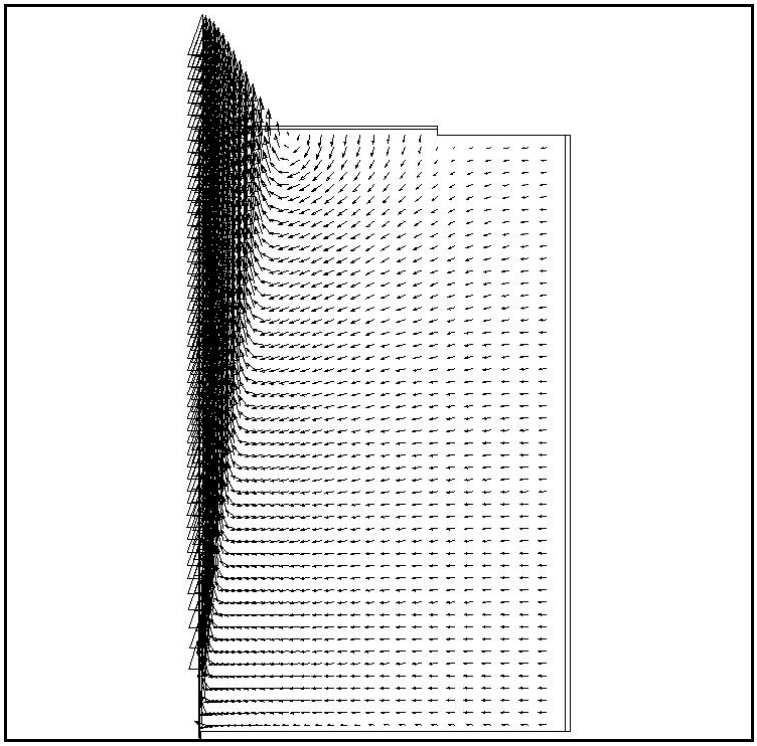

Figure C-4: Flow field of plane buoyant jet with small upper boundary ledge

REFERENCES

Abib, A.H. and Jaluria, Y., Turbulent penetrative and recirculating flow in a compartment fire, *ASME J. Fluids Eng.*, 117, 1995. 927-936.

Ashworth, A., A renormalisation group turbulence model for three-dimensional wall bounded flows, *DRA/AS/LBA/TR94008/1*, 1994.

Aspley, D.D. & Leschziner, M.A., A new low-Reynolds-number nonlinear two-equation turbulence model for complex flows, *Int. J. Heat Fluid Flow*, 19(3), 1998. 209-222.

Barton, M.J., Rubinstein, R. & Kirtley, K.R., Nonlinear Reynolds stress model for turbulent shear flows, *AIAA 91-0609*, 1991.

Baum, H.R. and McGrattan, K.B., Simulation of oil tank fire, *8th International Interflam Conference 1999, Edinburgh, Scotland*, June 1999. 1117–1128.

Bergstrom, D.J., Strong, A.B. and Stubley, G.D., Algebraic stress model prediction of a plane vertical plume, *Num. Heat Trans., Part A*, 18, 1990. 263–281.

Betts, P.L. & Dafa'Alla, A.A., Turbulent buoyant air flow in a tall rectangular cavity, *Proc. ASME Meeting, HTD*, 60, 1986. 59.

Beuther, P.D., An experimental investigation of turbulent buoyant plume, *PhD, Buffalo, NY*, 1980.

Beuther, P.D. & George, W.K., The turbulent buoyant plume in a stratified environment, *Proc. Natl. Congr. Theor. And Appl. Mech., Cornell University, Ithaca, NY*,1982.

Boussinesq, J., Théorie de l'Écoulement Tourbillant, *Mem. Présentés par Divers Savants Acad. Sci. Inst. Fr.*, 23, 1877. 46-50.

Brodowicz, K & Kierkus, W.T., Experimental investigation of laminar free convection flow in air above horizontal wire with constant heat flux, *Int. J. Heat Mass Transfer*, 9, 1966. 81-96.

Chen, C.J. & Chen, C.H., On predictions and unified correlations of vertical buoyant jets, *J. Heat Trans. - ASME*, 101, 1979. 533-584.

Chen, J.C. & Rodi, W., A mathematical model for stratified turbulent flows and its application to buoyant jets, *Proc. 16th Congress, IAHR, Sao Paulo, Brasil*, 1975.

Chen, J.C. & Rodi, W., Vertical turbulent buoyant jets: a review of experimental data, *Pergamon*, 1980. 1-58.

Chen, Q. and Chao, N-T., Comparing turbulence models for buoyant plume and displacement ventilation simulations, *Indoor Built Environ.*, 6, 1997. 140 –147.

Chen, Q., Comparison of different *k-e* models for indoor airflow computations, *Numerical Heat Transfer, Part B*, 28, 1995. 353-369.

Chen, Q., Prediction of room air motion by Reynolds-stress models, *Building and Environment*, 31(3), 1996. 233-244.

Chien, K-Y., Prediction of channel and boundary layer flows with a low-Reynolds number two equation model of turbulence., *AIAA 80-0134*, 1980.

Chow, W.K., Numerical studies on the transient behaviour of a fire plume and ceiling jet, *Mathl. Comput. Modelling*, 17(9), 1993. 71-79.

Chow, W.K., A comparison of the use of fire zone and field models for simulating atrium smoke-filling processes, *Fire Safety Journal*, 25, 1995a. 337-353.

Chow, W.K., Use of computational fluid dynamics for simulating enclosure fires, *Journal of Fire Sciences*, 13, 1995b. 300-333.

Chow, W.K., & Yin, R., Free boundary conditions for simulating air movement in a big hall induced by a 'bare cabin' fire, *Journal of Fire Sciences*, 17, 1999. 111-147.

Collins, D.C. & Williams, M.J., Free convection of heat from fine wires, *Aeronautical Research Laboratories, Aeronautical Notes* 140, 1954.

Cox, C., The challenge of fire modelling, *Fire Safety Journal*, 23, 1994. 127-132.

Craft, T.J., Launder, B.E. & Suga, K., Extending the applicability of eddy-viscosity model through the use of deformation invarients and non-linear elements, *Proc. 5th Int. Symp. Refined flow modelling and turbulence measurements, Paris*, 1993.

Craft, T.J., Launder, B.E. & Suga, K., Development and application of a cubic eddy-viscosity model of turbulence, *Int. J. Heat Mass Transfer*, 17(2), 1996. 8-115.

Craig, K.J., De Kock, D.J. and Snyman, J.A., Using CFD and Mathematical optimisation to investigate air pollution due to stacks, *Int. J. Numer. Meth. Engng*., 44, 1999. 551-565.

Dai, Z., Tseng, L.K & Faeth, G.M., Structure of round, fully-developed, buoyant plumes, *J. Heat Transfer - ASME*, 116(2), 1994. 409-417.

Dai, Z., Tseng, L.K. & Faeth, G. M., Velocity statistics of round fully developed buoyant turbulent plumes, *J. Heat Transfer - ASME*, 117, Nov 1995a. 138-145.

Dai, Z., Tseng, L.K. & Faeth, G. M., Velocity/mixture fraction statistics of round, self preserving buoyant turbulent plumes, *J. Heat Transfer - ASME*, 117, Nov 1995b. 918-926.

Dai, Z. & Faeth, G.M., Measurements of the structure of self preserving round buoyant turbulent plumes, *J. Heat Transfer - ASME*, 118, May 1996. 493.

Daly, B.J. & Harlow, F.H., Transport equations in turbulence, *The Physics of Fluids*, 13(11), 1970. 2634-2649.

Davidson, L., Second-order correction of the k-e model to account for non-isotropic effect due to buoyancy, *Int. J. Heat Mass Transfer*, 33(12), 1990. 2599-2608.

Dol, H.S., Hanjalic, K. & Kenjeres, S., A comparative assessment of the second moment differential and algebraic models in turbulent natural convection, *Int. J. Heat Mass Transfer*, 18, 1997. 4-14.

Ewer, J.A.C., Galea, E.R., Patel, M.K. & Knight, B., The development and application of group solvers in the Smartfire fire field model, *8th International Interflam Conference, Edinburgh*, 1999, 939.

Forstrom, R.J. & Sparrow, E.M., Experiments on the buoyant plume above a heated horizontal wire, *Int. J. Heat Mass Transfer*, 10, 1967. 321-331.

George, K.G., Alpert, R.I. & Tamanini, F., Turbulence measurements in an axisymmetric buoyant plume, *Int. J. Heat Mass Transfer*, 20, 1977. 1145-1154.

George, W.K. & Capp, S.P., A theory for natural convection turbulent boundary layers next to heat vertical surfaces, *Int. J. Heat Mass Transfer*, 22, 1979. 813-826.

Gibson, M.M. & Launder, B.E., On the calculation of horizontal, turbulent, free shear flows under gravitational influence, *J. Heat Trans. - ASME*, 98, 1976. 81-87.

Gibson, M.M. & Launder, B.E., Ground effects on pressure fluctuations in the atmospheric boundary layer, *J. Fluid Mech.*, 86(3), 1978. 491-511.

Hadjisophocleous, G.V. & Cacambouras, M. Computer modelling of compartment fires, *Journal of Fire Protection Engineering*, 5(2), 1993. 39-52.

Hagglund, B., Comparing fire models with experimental data, *FOA report C20864-2.4 National Defence Research Establishment, Sweden, 1992.*

Hanjalic, K., Achievements & Limitations of modelling and computation of buoyant turbulent flows and heat transfer, *Proc. 10th Int. Heat Transfer Conf., Brighton*, 1, 1994. 1-18.

Hanjalic, K., Kenjeres, S. & Durst, F., Natural Convection in partitioned two-dimensional enclosures at high Raleigh numbers, *Int. J. Heat Mass Transfer*, 39(7), 1996. 1407-1427.

Hanjalic, K. & Launder, B.E., A Reynolds stress model of turbulence and its applications to thin shear flows, *J. Fluid Mech.*, 52(4), 1972. 609-638.

Hanjalic, K. & Vasic, S., Some further exploration of turbulence models for buoyancy driven flows, *Turbulent Shear Flows 8, Springer Verlag, Berlin*, 1993. 319-341.

Hanjalic, K. and Vasić, S., Computation of turbulent natural convection in rectangular enclosures with an algebraic flux model, Int. J. Heat Mass Transfer, 36(14), 1993. 3603-3624.

Harlow, F.H. & Nakayama, P.I., Transport of turbulence energy rate, *Los Alamos Sci. Lab., University of California Report LA-3854*, 1968.

Haroutunian, V. & Launder, B.E., Second moment modelling of turbulent buoyant shear flows with elliptic solvers, *Significant questions in buoyancy affected enclosure of cavity flows, ASME HTD*, 60, 1986, 93-103.

Heindel, T.J, Ramadyani, S. & Incorpera, E.P, Assessment of turbulent models for natural convection in enclosures, *Numerical Heat Trans - Part B - Fundamentals*, 26(2), 1994. 147-172.

Henkes, R. A, W. M. & Hoogendoorn, C. J., Comparison of turbulence models for the natural convection boundary layer along a heated vertical plate, *Int. J. Heat Mass Transfer*, 32(1), 1989. 157-169

Henkes, R.A.W.M. and Hoogendoorn, C.J. (editors), Turbulent natural convection in enclosures, a computational and experimental benchmark study, *Proc. of Eurotherm Seminar no. 22, Delft, The Netherlands*, March 25-27, 1992.

Henkes, R.A.W.M. & Hoogendoorn, C.J., Numerical determination of wall functions for the turbulent natural convection boundary layer, 1990, Int. J. Heat Mass Transfer, 33, 1996. 1087-1097.

Henkes, R.A.W.M., Van Der Vlugt, F.F. and Hoogendoorn, C.J., Natural-convection flow in a square cavity calculated with low-Reynolds number turbulence models, *Int. J. Heat Mass Trans.*, 34(2), 1991. 377-388.

Hossain, M. S. & Rodi, W. (ed: Rodi, W.), A turbulent model for buoyant flows and its application to buoyant jets. (In: Turbulent buoyant jets and plumes), *Pergamon*, 1982. 121-178.

Hwang, C.B. & Lin, C.A., A low Reynolds number two equation model to predict thermal fields, *Int. J. Heat Mass Trans.*, 42, 1999, 3217-3230.

Hwang, C.C., Zhu, G., Massoudi, M. & Ekmann, J.M., A comparison of the linear and nonlinear k-ε turbulence models in combustors, *J. Fluids Eng.*,115(1), 1993. 93-102.

Ince, N.Z. & Launder, B.E., Three-dimensional and heat-loss effects on turbulent flow in nominally two-dimensional cavity, *Int. J. Heat Fluid Flow*, 16, 1995. 171-177.

Ince, N.Z. and Launder, B.E., On computation of buoyancy-driven turbulent flows in rectangular enclosures, *Int. J. Heat Fluid Flow*, 10(2), 1989. 110-117.

Jaluria, Y. & Gebhart, B., On transition mechanisms in vertical natural convection flow, *J. Fluid Mech.*, 66, 1974. 309-337.

Jones, W.P. & Launder, B.E., The prediction of laminarisatioin with a two-equation model of turbulence, *Int. J. Heat Mass Transfer*, 15, 1972. 301-314.

Jones, W.P. & Launder, B.E., The calculation of low-Reynolds number phenomena with a two-equation model of turbulence, *Int. J. Heat Mass Trans., 16, 1973, 1119-1130.*

Kerrison, L., Galea, E.R., Hoffmann, N. & Patel, M.K., A comparison of a FLOW3S based fire field model with experimental room fire data, *Fire Safety Journal*, 23, 1994. 387-411.

Kolmogorov, A.N., Equations of turbulence motion of an incompressible fluid, *Izvestia Academy of Sciences, USSR, Physics*, 6(1,2), 1942. 56-58.

Kotsovinos, N.E. & List, E.J., Plane turbulent buoyant jet, part 1, integral properties, *J. Fluid Mech.*, 81, 1977. 25-44.

Kotsovinos, N.E., Plane turbulent buoyant jet, part 2, turbulence structure, *J. Fluid Mech.*, 81, 1977. 45-62.

Kumer, S., Mathematical modelling of natural convection in fire – a state of the art review of the field modelling of the variable density turbulence flow, *Fire and Materitials*, 7(1), 1983. 1-24.

Lam, C.K.G. & Bremhorst, K., A modified form of the k-e model for predicting wall turbulence, *J. Fluids Eng. - ASME*, 103, 1981. 456-460.

Laufer, J., Investigation of turbulent flow in a two-dimensional channel, *NACA-TN-2123*, 1952.

Launder, B.E. & Sharma, B.I., Application of the energy-dissipation model of turbulence to the calculation of flow near a spinning disc, *Letter in heat and Mass Transfer*, 1, 1974. 131-137.

Launder, B.E. & Spalding, D.B., Lectures in mathematical models of turbulence, *Academic Press,* 1972.

Launder, B.E. & Spalding, D.B., The numerical computation of turbulence flow, *Comp. Meth. Appl. Mech. and Eng.*, 3, 1974. 269.

Launder, B.E., An introduction to single point closure, *Simulation and Modelling of turbulent flows.* Edited by Gatski, T.B. Hussaini, M.H. & Lumley, J.L. *ICASE/LaRC Series in Computational Sci. and Eng.*, 1996. 243-310.

Lee, S.L. & Emmons, H.W., A study of the natural convection above a line fire , *J. Fluid Mech.*, 11, 1961. 353-368.

Lewis, M.J., Moss, J.B. & Rubini, P.A., CFD modelling of combustion and heat transfer in compartment fires, *Fifth International Symposium on Fire Safety Science, Melbourne,* 1997.

Li, J.D. & Bilger, R.W., Diffusion of conserved and reactive scalars behind line sources in homogeneous turbulence, *Journal of Fluid Mechanics*, 318, 1996. 339-372.

Lien, F.S. & Leschziner, M.A., Assessment of turbulent-transport models including non-linear RNG eddy-viscosity formulation and second moment closure for flow over a backwards-facing step, *Computer Fluids*, 23(8):, 1994. 83-1004.

List, E.J, Turbulent jets and plumes, *Annual Review of Fluid Dynamics,* 14, 1982. 189-212.

Lui, F. and Wen, J.X., CFD simulation of a buoyant diffusion flame with a buoyancy modified turbulence model, *8th International Interflam Conference*, 1999. 963-976.

Lui, F. and Wen, J.X., Development and validation of an advanced turbulent model for buoyancy driven flows in enclosures, *Int. J. Heat Mass Transfer, 1999*

Luo, M. & Beck, V., The fire environment in a multi-room building – comparison of predicted and experimental results, *Fire Safety Journal*, 23, 1994. 413-438.

Luo, M., Yaping, H. & Beck, V., Application of field model and two-zone model to flashover fire in a full-scale multi-room single level building, *Fire Safety Journal*, 29, 1997. 1-25.

Malin, M.R. & Spalding, D.B., The prediction of turbulence jets and plumes by use of the k-W model of turbulence, *PCH PhysicoChemical Hydrodymamics*, 5(2), 1984. 153-198.

Malin, M.R. & Younis, B.A., Calculation of turbulent buoyant plumes with Reynolds stress and heat flux transport closure, *Int. J. Heat Mass Transfer,* 33, 1990. 2247-2264.

Markatos, N. C., Malin, M. R. & Cox, G., Mathematical modelling of buoyant-induced smoke flow in enclosures, *Int. J. Heat Mass Transfer*, 25, 1982. 63.

Markatos, N.C. & Pericleous, K.A., Laminar and turbulent natural convection in an enclosed cavity, *Int. J. Heat Mass Transfer*, 27, 1984. 755-772.

Martynenko, O.G. & Korovkin, V.N., Numerical investigation of turbulent plane and buoyant jets, *Int. J. Heat Mass Transfer* 5(3), 1992. 635-639.

Martynenko, O.G. and Korovkin, V.N., Flow and heat transfer in round vertical buoyant jets, *Int. J. Heat Mass Trans*., 37(1), 1994. 51-58.

Mawhinney, R.N., Galea, E.R., Hoffman, N., A critical comparison of a PHOENICS based fire field model with experimental room fire data, *J. Fire Prot. Eng.*, 6(4), 1994

McComb, W.D., Renormalisation group methods applied to numerical simulation of fluid turbulence, Theoretical Approaches to turbulence, edited by Dwoyer, Hussaini & Voigt, 8, 1984. 187-208.

McGrattan, K.B., Baum, H.R. & Rehm, R.G., Large eddy simulations of smoke movement, *Fire Safety Journal*, 30, 1998. 161-178

Menter, F.R., Improved two-equation k-w model for aerodynamic flows, *NASA TM-103975*, 1992.

Menter, F.R., Two-equation eddy-viscosity turbulence model for engineering applications, *AIAA Journal*, 332(8), 1994. 1598-1605

Mompean, G., Numerical simulation of a turbulence flow near a right-angled corner using the Speziale non-linear model with RNG k-ε equations, *Computers & Fluids*, 27(7), 1998. 847-859.

Morton, B.R., Taylor, G.I. & Turner, J.S., Turbulent gravitational convection from maintained and instantaneous sources, *Proc. Roy. Soc. Ser. A*, 234, 1956.1-23.

Moses, B.O., Sini, J.F. & Dekeyser, I., k-ε model simulation of vertical buoyant jets and plumes in atmospheric environments, *20-23 Sept 1990, 4th Int. Symp. on Refined flow modelling and turbulent measurement, Wuhan, China, Flow Modeling and turbulence measurements*, 92, 1992. 404-411.

Murakami, S., Kato, S. & Ooka, R., Comparison of the numerical predictions of horizontal non-isothermal jet in a room with turbulence models-k-e EVM, ASM and DSM, *ASHRAE Trans*., 100(2), 1994.

Murakami, S., Kato, S., Chikamoto, T., Laurence, D., Blay, D., New low-Reynolds-number k- epsilon model including damping effect due to buoyancy in a stratified flow field, *Int. J. Heat Mass Transfer*, 39(16), 1996. 3483-3496.

Myong, H.K. & Kasagi, N., Prediction of Anisotropy of the near-wall turbulence with an anisotropic low-Reynolds-number k-ε turbulence model, *J. Fluid Eng.*, 112, 1990. 521-524.

Nakagome, H. & Hirata, M., The structure of turbulent diffusion in an axisymmetrical thermal plume, *Proc. of 1976 ICHMT Seminar on turbulent buoyant convection, Hemisphere., 1976.* 361-372.

Nakaya, I., Tanaka. T. & Yoshida, M., Doorway flow induced by fire in a compartment, *Fire Safety J., 10*, 1986. 185-195.

Nam, N. & Bill, R. G., Numerical simulation of thermal plumes, *Fire Safety Journal*, 21, 1993. 231-256.

Noto, K, Swaying motion in thermal plumes above a horizontal line heat source, *J. Thermophysics*, 3(4), 1989. 428-434.

Ozoe, H., Mouri, A. Hiramitsu, M. Churchill, S.W. & Lior, N., Numerical calculation of three-dimensional turbulent natural convection in a cubical enclosure using a two-equation model for turbulence, *J. Heat Transfer - ASME*, 108. 1986. 806-813.

Papanicolaou, P.N. & List, E.J., Investigations of round vertical turbulent buoyant jets, *J. Fluid Mech.*, 195, 1988. 341-391.

Park, T.S. & Sung, H.J., A nonlinear low-Reynolds-number k-ε model for turbulent separated and reattachment flows - 1. Flow field computations, *Int. J. Heat Mass Transfer*, 38(14), 1995. 2657-2666.

Patel, V. C., Rodi, R. & Scheuerer, G., Turbulence models for near-wall an low Reynolds number flows: a review, *AIAA J.*, 23(9), 1985. 1308-1319.

Patankar, S.V., Numerical heat transfer and fluid flow, *Hemisphere publishing, McGraw Hill*, 1980

Peeter, T.W.J. and Henkes, R.A.W.M., The Reynolds-stress model of turbulence applied to the natural-convection boundary layer along a heated vertical plate, *Int. J. Heat Mass Trans*, 35(2), 1992. 403-420.

Peng, S-H., Davidson, L. and Holmberg, S., A two-equation turbulence k-ε model applied to recirculating ventilation flows, *Chamers Univiersity of Technology, Dept. Thermo and Fluid Dynamics*, 96/13, 1996.

Peng, S-H., Davidson, L. and Holmberg, S., A modified low-Reynolds-number k-ε models for recirculating flows, *ASME J. Fluid Eng.*, 119, 1997.

Peng, S-H. & Davidson, L., Computation of turbulent buoyant flows in enclosures with low-Reynolds-number k-ε models, *Int. J. Heat Fluid Flow*, 20, 1999. 172-184.

Pereira, J.C.F. and Rocha, J.M.P., Numerical computation of convective dispersion in turbulence buoyant jets, *Num. Heat Trans., Part A*, 23, 1993. 399-414.

Peric, M., A finite volume method for the prediction of three-dimensional fluid flow in complex ducts, *PhD Thesis, Imperial College, London*, 1985.

Pope, S.B., A more general effective-viscosity hypothesis, *J. Fluid Mech*., 72(2), 1975. 331-340.

Prandtl, L., Uber die ausgebildete Turbulenz, *ZAMM*, 5, 1925, 136-139.

Prandtl, L., Uber ein neues Formelsystem fur die ausgebildete Turbulenz, *Nacr. Akad. Wiss. Gottingen, Math-Phys. Kl.* 1945, 6-19.

Ramaprian, B.R. & Chandrasekhara, M.S., Study of vertical plane jets and plumes, *Iowa Inst. Hydraulic Research, IIHR Repp* , 1983. 257.

Ramaprian, B.R. & Chandrasekhara, M.S., LDA measurements in plane turbulent jets, ASME *J. Fluid Eng*, 107, 1985. 267-271.

Ramaprian, B.R. & Chandrasekhara, M.S., Measurements in vertical plane turbulent plumes, *J. Fluids Eng.*, 111, 1989. 69-77.

Rho, J.S. & Ryou, H.S., A numerical study of atrium fires using derterministic models, *Fire Safety J.*, 33, 1999. 213-229.

Riopelle, G., Stubley, G.D. and Strong, A.B., Numerical Study of the influence of the ambient pressure field on free plane turbulent vertical jets and plumes, *Num. Heat. Trans., Part A*, 26, 1994. 273-286.

Rodi, W., The prediction of free turbulent boundary layers by use of a two-equation model of turbulence, *Ph.D. Thesis, University of London*, 1972.

Rodi, W., Turbulence models and their application in hydraulics: a state of the art review, *IAHT/AIRH Monograph series, A.A. Balkema, Rotterdam, Brookfield, 3rd edition, 1993.*

Rodi, W., Influence of buoyancy and rotation on equations for the turbulent length scale, *2nd Symposium on turbulent Shear flows, London, 1979.*

Rouse, H., Yih, C.S. & Humphreys, H.W., Gravitational convection from a boundary source, *Tellus*, 4, 1952. 201-210.

Rubini, P., SOFIE (Simulation of Fires in Enclosures) Version 3.0, *Cranfield University, School of Mechanical Enginnering*, 1999

Rubini, P.A. & Moss, J.B., Coupled soot and radiation calculations in compartment fires, *Proceedings of 5th international symposium on fire safety science, Melbource, Australia*, March 1997.

Rubinstein, R. & Barton, J.M., Nonlinear Reynolds stress models and the Renormalisation group, *Physic Fluids A-Fluid Dynamics*, 2(8), 1990. 1472-1476.

Sanderson, V.E., Rubini, P.A. & Moss, J.B., The effect of vent size on a compartment fire: numerical simulations and validation, *8th International Interflam Conference, Edinburgh,* 1999.

Sangras, R., Dai, Z. & Faeth, G.M., Mixing structure of plane self-preserving buoyant turbulent plumes, *J. Heat Trans.*, 120, 1998. 1033-1041.

Saunders, J. P. H., Sarh, B., Gokalp, I., Variable density effects in axisymmetric isothermal turbulent jets: a comparison between a first- and second-order turbulence model, *Int. J. Heat Mass Transfer*, 40(4), 1997. 823-842.

Schmidt, W., Turbulente Ausbreitung eines Stromes erhitzter Luft, *Z. angew. Math Mech*, 21(6), 1941. 351-363.

Schorr, A.W. & Gebhart, B., An experimental investigation of natural convection wake above a line heat source, *Int. J. Heat Mass Transfer*, 13, 1970. 557-571.

Shabbir, A. & George, W.K., Experiments on a round turbulent buoyant plume, *J. Fluid Mech.*, 275, 1994. 1-32.

Shabbir, A. & Taulbee, D. B., Evaluation of turbulence models for predicting buoyant flows, *J. Heat Transfer - ASME*, 112, Nov. 1990. 945-951.

Shabbir, A. and Taulbee, D.B., Experimental balances for the second moments for a buoyant plume and their implications on turbulence modelling, *Int. J. Heat Mass Trans.*, 43, 2000. 1777-1790.

Shankar, V., Davidson, L. and Olsson, E., Numerical Investigation of Turbulent plumes in both ambient and stratified environments, *Indoor Air*, 5, 1995. 136-146.

Shih, T.H., Zhu, J. & Lumley, J.L., Calculation of wall-bounded complex flows and free shear flows, *Int. J. Numerical Methods in Fluids*, 23, 1996. 1133-1144.

Sinai, Y.L., Comments on the role of leakages in the field of modelling of under-ventilated compartment fires, *Fire Safety Journal*, 33, 1999. 11-20.

Sini, J. F. & Dekeyser, I., Numerical prediction of turbulent plane buoyant jets discharging in a stratified stagnant or flowing ocean, *Numerical Heat Transfer, Part A*, 16, 1989. 371-387.

Sini, J.F. & Dekeyser, I., Numerical prediction of turbulent plane jets and forced plumes by use of k-e model of turbulence, *Int. J. Heat Mass Transfer*, 39(9), 1987. 1787-1801.

Sneck, H.J. and Brown, D.H., Plume rise from large thermal source such as dry cooling towers, *ASME J. Fluids Eng.*, May 1974

Snider, D.M. and Andrews, M.J., The simulation of mixing layers driven by compound buoyancy and shear, *ASME J. Fluids Eng.*, 118, 1996. 370-376.

Someya, T. Advanced combustion science, ,*Springer – Verlag*, 1993.

Speziale, C.G., On nonlinear K-l and K-e models of turbulence, *J. Fluid Mechanics*, 178, 1987. 459-475.

Steckler, K.D., Quintiere, J.G. & Rinkinen, W.J., Flow induced by fire in a compartment, *NSBIR 82-2520*, 1982.

Stokes, G.G., On the effect of the internal friction of fluids on the motion of pendulums, *Cambridge Philosophical Society Transactions*, 9, 1851. 8-106.

Stone, H.L., Iterative solution of implicit approximations of multi-dimensional partial differential equations, *SIAM J. Num. Anal.*, 5, 1968. 530.

Suga, K., Development and application of a non-linear eddy-viscosity model sensitized to stress and strain invarients, *PhD. Thesis, UMIST*, 1995.

Tamanini, F., The effect of buoyancy on the turbulence structure of vertical round jets, *J. Heat Trans.*, 100, 1978. 659-664.

Tannous, A.G., Ahmadi, G. & Valentine, D.T., Two-equation thermodynamical model for turbulent buoyant flows. Part 1: theory, *Appl. Math. Modelling,* 13, 1978. 194-202.

Tannous, A.G., Valentine, D.T. & Ahmadi, G., Two-equation thermodynamical model for turbulent buoyant flows. Part 2: numerical experiments, *Appl. Math. Modelling*, 14, 1989. 576-587.

Thangam, S. & Speziale, C.G., Turbulent flow past a backward-facing step - a critical evaluation of 2-equation model, *AIAA J*., 30(5), 1992. 1314-1320.

To, W.M. & Humphrey, J.A.C., Numerical simulation of buoyant turbulent flow - 1. Free convection along a heated vertical plate, *Int. J. Heat Mass Transfer*, 29(4), 1986. 573-592.

Turner, J.S., Buoyancy effects in fluids, *Cambridge University Press*, 1973.

Verripoulos, P. A. & Papailou, D. D., Structure of the turbulent temperature field of a two-dimensional fire plume, In *AIAA applied aerodynamics conference, Colorado Springs*, June 20-22 1994.

Versteeg, H.K. & Malalasekera, W., An introduction to computational fluid dynamics, the finite volume method, *Longmann Scientific & Technical,* 1995

Watson, L., Fire statistics, estimates UK 1998, *Home office publication, Issue 9/99 (http://www.homeoffice.gov.uk/rds/pdfs/hosb999.pdf)*, 1999.

Wilcox, D.C., A half century historical review of the k-ω model. *AIAA-91-0615*, 1991.

Wilcox, D.C., Turbulence modelling for CFD, *DCW Industries, Inc, La Canada, California,* Nov. 1994.

Wilks, G. & Hunt, R., The axisymmetric buoyant jet – numerical solution for a semi-empirical theory, *Numerical Heat Transfer*, 9, 1986. 495-509.

Worthy, J., Sanderson, V. & Rubini, P., A comparison of modifed k-ε turbulence models for buoyant plumes, *Numerical Heat Transfer Part B*, 29(2), 2001. 101-125

Xin, S. & Le Quéré, P., Direct numerical simulations of two-dimensional chaotic natural convection in a differentially heated cavity, *J. Fluid Mech.* 304, 1995. 87-118.

Yakhot, V. & Orzag, S.A., Renormalisation Group Analysis of turbulence 1. Basic Theory, *J. Sci. Comput*, 1(1), 1986. 3-51.

Yakhot, V. & Orszag, A., Renormalisation group analysis of turbulence, *J. Sci. Comp*, 1, 1989. 3.

Yakhot, V. & Smith, L.M., The renormalisation group, the ε expansion and derivation of the turbulence models, *J. Sci. Comput*., 7, 1992. 35

Yan, Z. & Holmstedt, G., A two-equation turbulence model and its application to a buoyant diffusion flame, *Int. J. Heat Mass Trans*., 1998.

Yoshizawa, A. , Statistical analysis of the deviation of the Reynolds stress from its eddy-viscosity representation, *Phys. Fluids*, 27(6), 1984. 1377-1387.

Yosinobu, H., Onishi, Y., Amano, S,. Enyo, S. & Wakitani, S., Experimental study on instability of a natural convection flow above a horizontal line heat source, *J. Phy. Soc. Japan*, 47(1), 1979. 312-319.

Zeldovich, Y.B., Limiting laws of freely rising convection currents, *Zh. Eskp. Teoret. Fiz*., 7(12), 1937. 1463-1465.

Zhou, Y., McComb, W.D. & Vahala, G., Renormalization group (RG) in turbulence: Historical and comparative perspective, *NASA CN-NAS1-19480*, 1997.